Novel Methods for Monitoring and Mitigation of Thermally Induced Fracturing in Water Injection Wells

<Misfer Jarallah Almarri>

Submitted for the degree of Doctor of Philosophy

Heriot-Watt University
School of Energy Geoscience Infrastructure and Society
Institute of Petroleum Engineering

May, 2018

Abstract

Waterflooding is a common recovery method used to maintain reservoir pressure and improve reservoir oil sweep efficiency. However, injecting cold water into a reservoir alters the state of the in-situ formation stress and can result in the formation fracturing. In other words, it can result in the initiation and growth of Thermally Induced Fractures (TIFs) even when the original fracture propagation pressure is not exceeded. Consequently, TIFs can cause highly non-uniform distribution of the injected water flow in the wellbores, reduction in the sweep efficiency, and early water breakthrough in the nearby production wells. These reservoir management challenges caused by TIFs need to be addressed with the decisions informed by the appropriate monitoring and modelling of TIF development.

This work describes methods to detect the onset and characterise TIFs followed by an example of evaluation of TIFs' impact on the well and reservoir performance. Then, the performance and potential of Advanced Well Completions in horizontal wells in the presence of TIFs were investigated.

The TIF characterisation problem was addressed by developing monitoring workflow that integrated and adapted several available analytical and semianalytical models previously developed for well performance analysis. The application of the workflow was illustrated and verified by reservoir geomechanical and fluid flow simulation. It was subsequently applied to real field data. Further, the effectiveness of an Advanced Well Completion to mitigate the negative effects of TIF was evaluated using a dynamic thermal reservoir model coupled with a TIF model, a geomechanical model and a detailed wellbore model. A history matched real field sector model was used for this study.

The proposed methods proved to be efficient in detecting and monitoring TIFs as well as evaluating the metrics describing waterflood performance. These included flood efficiency, inter-well communication and pressure maintenance. Furthermore, the added value of advanced completions was quantified and shown to be effective in controlling TIF initiation and propagation as well as in improving the wellbore flow performance. TIFs surveillance and mitigation methods proposed in this thesis are novel and strongly contribute to the research aimed at improving waterflood performance in oil fields.

DEDICATION

"In memory of my father, to my mother who has waited, and to my wife who has sacrificed"

"And your Lord has decreed that you worship none but Him. And that you be dutiful to your parents. If one of them or both of them attain old age in your life, say not to them a word of disrespect, nor shout at them but address them in terms of honour."
(Quran 17:23)

Acknowledgement

In the Name of Allah, the Most Gracious, the Most Merciful

All praise to Allah

First and foremost, I would like to acknowledge my supervisors (Professor David Davies and Dr Khafiz Muradov) for their continuous support and encouragement throughout my PhD study.

I would also like to thank all sponsors of VAWE project for the data provided for my study as well as all valuable discussions and suggestions during the JIP meetings. I am also thankful to Petex and Schlumberger for allowing access to their software.

I extend my thanks to my colleagues: Eltazy Khalid, Abdulati Araibi, Ehsan Nikjoo, Bona Prakasa, Dr Morteza Haghighat, and Dada Akindolu for their fruitful discussions and helpful support.

Thanks to the staff at the Institute of Petroleum Engineering at Heriot-Watt University and my friends at Heriot-Watt University and Edinburgh.

I would like to appreciate all the support and encouragement that I received from my brothers and sisters (Abdulhadi, Saleh, Hamad, Oudah, and Mohammad).

My final and deepest gratitude to my mother (Norah), wife (Duhamah) and children (Norah, Jarallah, and Naji) for their prayers, moral support and patience.

Table of Contents

Chapter 1 Introduction and Motivation 1

1.1 Introduction 1

1.2 Thesis Objectives 3

1.3 Thesis Layout 5

Chapter 2 Literature Review and Background 7

2.1 Thermally Induced Fracturing (TIF) 7

2.1.1 Introduction 7

2.1.2 Rock Mechanics of TIF 10

2.1.3 Simplified Physical Description 13

2.1.4 The effect of temperature and pressure changes on Poro-elastic and thermo-elastic stresses 15

2.1.5 TIFs initiation and growth 17

2.2 Real fields experience with TIF 19

2.2.1 TIF in Waterflooding applications 20

2.2.2 TIF in non-Waterflooding applications 30

2.2.3 Sand Production 37

2.3 Advanced Well Completions 39

2.3.1 Introduction 39

2.3.2 Advanced Well Completion Components 41

2.3.3 Inflow Control Devises (ICDs) 42

2.3.4 Inflow Control Valve (ICVs) 53

2.3.5 Autonomous Flow control Devices (AFCDs) 55

2.3.6 Annular Flow Isolation (AFI) 56

2.4 ICDs Applications in Injection Wells 58

2.4.1 Heel-to-Toe Effect (HTE) and Reservoir heterogeneity (RH) 58

2.4.2 Wormhole Channels and Natural Fractures 60

2.4.3 SAGD injection wells 63

2.5 Potential ICD application with TIF 64

Chapter 3 Modelling of Thermally Induced Fractures 65

3.1 Introduction 65

3.2 Historical Background and modelling development 66

3.3 Analytical TIF Modelling 67

3.4 Pseudo Three-Dimensional TIF Modelling 68

3.5 Fully 3 Dimensional TIF Modelling 70

3.6 Thermally Induced Fracture Modelling Methodology used 71

3.6.1 Introduction and Underlying Assumptions 71

3.6.2 Elasticity Equation 74

3.6.3 Fluid Flow Equation 76

3.6.4 Geomechanical Equations 77

3.6.5 TIF propagation criterion 79

3.6.6 Solution method 80

3.6.7 Implementation Workflow 80

3.6.8 General Thermally Induced Fractures Modelling Notes 81

Chapter 4 Identification and Characterization of Thermally Induced Fractures by Integrating Analytical and Semi-analytical Techniques 83

4.1 Introduction 83

4.2 Methodology 84

4.3 Conventional TIF Diagnostics Techniques 85

4.3.1 Hall Integral 85

4.3.2 The Injectivity index (II) and Reflectivity of Injectivity Index (RII) 88

4.3.3 Other methods 89

4.4 Recent Analytical Methods 91

4.4.1 Fracturing Index (FI) model 92

4.4.2 Modified Hall Integral 94

4.5 Semi-Analytical Method 96

4.5.1 Capacitance Resistance Model (CRM) 96

4.6 Synthetic Case Histories 98

4.6.1 Synthetic Case 1 Histories 99

4.6.2 Synthetic Case 2 Histories 104

4.7 Real Field Case History 105

4.8 Summary 113

Chapter 5 History Matching a Sector Model of (N) Field Using Reservoir Simulation Coupled with Thermally Induced Fracturing and Geomechanical Models 115

5.1 Introduction 115

5.2 Problem Statement and Solution Approach 116

5.3 Previously Reported History Matching Studies with Thermally Induced Fracturing 117

5.4 Methodology 121

5.5 Sector Model Description, Import, and Verification 122

5.5.1 "N" Field Sector Model Description 122

5.5.2 Importing the Eclipse Model into REVEAL Reservoir Simulator 124

5.5.3 Imported Model Verification 124

5.6 Converting the Isothermal Reservoir Model to the Thermal One 126

5.7 History Matching the REVEAL "N" Field Sector Model without TIF 129

5.8 In Situ Stress 131

5.8.1 Estimation of the Vertical Stress 131

5.8.2 Magnitude of the Minimum Horizontal Stress 133

5.8.3 Magnitude of the Maximum Horizontal Stress 135

5.8.4 Orientation of the Minimum Horizontal Stress 136

5.9 Rock Mechanical Properties 137

5.9.1 Young's Modulus & Poisson's Ratio 137

5.9.2 Fracture toughness 139

5.9.3 Biot's coefficient 140

5.10 Uncertainty Analysis 140

5.10.1 Reservoir Pressure 141

5.10.2 Wellbore Modelling 142

5.10.3 Type and Surface Temperature of the Injection Water 143

5.11 History Matching with TIF Modelling Workflow 143

5.11.1 Global History matching 145

5.11.2 Local History matching 146

5.12 Final Matching with TIF modelling 149

5.12.1 Injected water temperature 149

5.12.2 Geomechanical and thermal properties 150

5.12.3 TIF Growth Dynamics 152

5.13 Summary 153

Chapter 6 Evaluation of Inflow Control Device Effectiveness to Mitigate Thermally Induced Fractures in Water Injection Wells 155

6.1 Introduction 155

6.2 Problem Statement and Solution Approach 156

6.3 Methodology 157

6.4 Model Setup 158

6.5 Well Constraints and Pair Specifications 160

6.6 Well Completion Types and Design 161

6.7 ICD, wellbore, and annulus flow modelling options and related problems ... 162

6.7.1 Well Segmentation and reservoir gridding 162

6.7.2 Horizontal well trajectory 163

6.8 Isothermal and Thermal Models Comparison 163

6.9 Impact of different completions installed in the injection well modelled with TIF 166

6.9.1 Transverse TIFs (T-TIF) 166

6.9.2 Longitudinal TIFs (L-TIF) 177

6.10 Summary 185

Chapter 7 Conclusions and Future work 188

7.1 Conclusion 188

7.2 Future work 190

Appendices 192

Appendix A-Pseudo-Steady State approximation for Pressure inside a Water Bank 192

Appendix B- Evaluation of Pseudoskin 193

Appendix C-Methods using the Analytic and Numeric Derivative of Hall Integral 194

Appendix D- Capacitance Resistance Model for Injector and Producer (CRMIP) .. 197

Appendix E- Synthetic Case 2 Figures 199

Appendix F- PVT Tables for Thermal Model 201

References 205

List of Tables

Table 2-1: Current types of ICDs; differences and similarity [49] 51

Table 2-2 : Comparison of ICV and ICD applications [70, 71] 55

Table 2-3: Annular Flow Impact [2] 57

Table 2-4: Comparison of available AFIs [49] 58

Table 2-5: Injector design evaluation for an ICD injection Urd field [81] 59

Table 2-6: Summary of Published ICD Applications in injection wells 63

Table 4-1: Reservoir and Geomechanical Parameters for Cases 1 and 2 98

Table 5-1: Coefficients for the Vazques-Beggs correlations [130] 127

Table 5-2: The isothermal fluid PVT properties 129

Table 5-3: Average reservoir pressure measured by long-term fall off tests for well NI6 142

Table 5-4: Difference between measured test data and calculated values using PROSPER 148

Table 5-5: Initial and final matched Geomechanical and thermal properties 152

Table 6-1: Summary of isothermal and thermal modelling of SAS and 1.6 mm ICD (No-TIF) 186

Table 6-2: Summary of SAS and thermal modelling with/without L-TIF and T-TIF .. 187

Table 6-3: Summary of ICD in injector only vs. SAS in producer (T-TIF and L-TIF) 187

Table 6-4: Summary ICD in both wells vs. SAS with T-TIF and L-TIF 187

List of Figures

Figure 1-1: TIFs impact oil recovery, injectvity, well integrity, and well spacing in waterflooded reserviros [1] 1

Figure 1-2: Main Components of Advanced Well Completions [2] 2

Figure 1-3: Illustration of the effect of (A) Heel-to-Toe effect (B) reservoir heterogeneity [3] 3

Figure 1-4: Illustration of the impact high permeability thief zone [4] 3

Figure 2-1:Temperature evolution around a vertical water injector [8] 7

Figure 2-2: Stress evolution around a vertical water injector [8] 8

Figure 2-3: Impact of temperature on the fracture gradient for the Prudhoe bay field [11] 8

Figure 2-4: Components of stress in three dimensions [14] 10

Figure 2-5: Extentional strain (tesnional stress), shortening (comperssion stress) and shear strain (shaer stress)[15] 11

Figure 2-6: Ideal elastic stress/strain curve 12

Figure 2-7: Three material responses as displayed in a tension test [16] 13

Figure 2-8: Three principal stresses at deep reservoirs where the maximum principal stress is vertical [19] 14

Figure 2-9: Predicted total stress resulting from temperature and pressure changes computed from a reservoir simulation model [8, 23]. 17

Figure 2-10: Schematic showing the direction of the three Principal stresses 18

Figure 2-11: The three modes of fracture [25]. 18

Figure 2-12: Direction of TIF in a horizontal plane [27] 19

Figure 2-13: Location of the Prudhoe Bay oil field on the north slope of Alaska [11]. . 20

Figure 2-14: Prudhoe Bay oil field waterflood area [28] 20

Figure 2-15:Comparison of one of the injector temperature profile before and after fracturing [28] 21

Figure 2-16: Performance plot for one of the injectors showing SW and PW injection periods [29] 22

Figure 2-17: Voidage replacement ratios (VRRs) for the Prudhoe Bay field [29] 22

Figure 2-18: Temperature survey for one of the injector with SW and PW[29] 23

Figure 2-19: Effect of azimuth and deviation on intercept pressure [29] 24

Figure 2-20: Injection data for a high-rate injector in the Ula field [7] 25

Figure 2-21: Flow profile and permeability for one of the injector [29] 26

Figure 2-22: The injectivity index of one of the injector in the Alwyn field during short term injection test [5] 27

Figure 2-23: The measured BHP of one of the injector in the Alwyn field during short term injection test [5] 27

Figure 2-24: The measured BHT of one of the injector in the Alwyn field during short term injection test [5] 28

Figure 2-25: Historical BHP,WHP, and injection rate for one of the injection in the field [9] 29

Figure 2-26: Temperature log in one of the injection well in the field ; at two different times [9] 29

Figure 2-27: Interpretation of SRT for one injection well [30] 31

Figure 2-28: Injection history (WHP and injection rate) for one injection well [30] 31

Figure 2-29: Production log shows > 80 % injection into the top intervals [30] 32

Figure 2-30: First Air-cooler system installed to reduce the PW temperature for steam emissions reduction [27] 33

Figure 2-31: TIF impact on disposal wells in the Villano field in 2012 after installing Air-cooler system [27] 33

Figure 2-32: Additional Air-cooler system installed to reduce the PW temperature for injectivity improvment [27] 34

Figure 2-33: TIF impact on disposal wells in the Villano field in 2013 after installing additional Air-cooler system [27] 34

Figure 2-34: Historical plot of the injectivty index [27] 35

Figure 2-35: Illustration of the concept of GCS [31] 35

Figure 2-36: One injection well (31F-1) and two observation wells (31F-2 and 31F-3)[32] 36

Figure 2-37: Measured BHP and BHT from observation well (32F-2)[32] 37

Figure 2-38: Measured injection BHP and BHT in the injection well (31F-1)[32, 33] .. 37

Figure 2-39: Change in formation strength as a function of temperature for the Forestal Field [43] 38

Figure 2-40: Critical Drawdown Pressure (CDP) during flow back as a function of temperature for the Forestal Field [43] 39

Figure 2-41: An example of a multi-zone, AWC [48] 40

Figure 2-42 :(A) ICD and AFI wellbore placement [49] 40

Figure 2-43: Advanced well completion business drivers to the Norwegian oil industry [50] 41

Figure 2-44: Types of FCDs including new developments [2] 42

Figure 2-45: Higher drawdown and flow rate the heel of the well due to HTE (Courtesy of Halliburton) 43

Figure 2-46:Water breakthrough at the heel of the well (Courtesy of Schlumberger) ... 43

Figure 2-47: Variable perforation density design [49] 44

Figure 2-48: A passive stinger completion [49] 44

Figure 2-49: Schematic of proposed Inflow Control Device 45

Figure 2-50: Fluid flow path from the reservoir to the base pipe [49] 46

Figure 2-51: Labyrinth Channel-type ICD [49] 46

Figure 2-52: A helical channel-type ICD [53] 47

Figure 2-53: Fixed Slot-type ICD 48

Figure 2-54: Adjustable slot-type 48

Figure 2-55: A diagram and actual Tube-type ICD [49] 49

Figure 2-56: A nozzle Type ICD (Courtesy of Schlumberger) 49

Figure 2-57: Nozzle-type ICD for injectors [63] 50

Figure 2-58: Orifice-type ICD 50

Figure 2-59: Inflow Control Valve (ICV) 53

Figure 2-60: ICD and ICV comparsion framework [49] 54

Figure 2-61: Packers (AFIs) installed between joints for annular flow elimination [74] 56

Figure 2-62: Injection log run at 5 bpm injection rate in the ICD completed injector ... 60

Figure 2-63: Modelled injection profile for a liner completion and an ICD completion in one of the injectos in the field 61

Figure 2-64: Injection Pofile for the considered injection well before and after ICD installation 62

Figure 2-65: Horzoitnal well pair in SAGD application[90] 64

Figure 3-1: Fracture geometry models: (a) and (b) 2D models, (c) P3D model, (d) and (e) 3D models [96] 66

Figure 3-2: A two-winged vertical fracture oriented perpendicular to the plane of the minimum horizontal in-situ stress [23] 67

Figure 3-3: The concept of P3D model formulation [105] 69

Figure 3-4: Example of 3D finite element fracture [99] 70

Figure 3-5: A vertical FE TIF model coupled to FD reservoir model and a detailed model of an injection well 72

Figure 3-6: Shape of the TIF in x-direction [107] 72

Figure 3-7: Various relationships invloved in the TIF model [8] 73

Figure 3-8: Workflow coupling among the reservoir model, the geomechanical solution and the TIF model. 81

Figure 3-9: Solution methods used for each element of the coupled models 81

Figure 4-1: Integrating analytical and semi-analytical models workflow 85

Figure 4-2: Overview of HI showing trends of various well injection conditions 88

Figure 4-3: SRTs conducted in one of the injection wells in the Shell Eider field show the variation of fracture pressures with injection water temperature [118] 91

Figure 4-4: Interpretation of FI and II (vertical axis) w.r.t. Cumulative Water Injection Volume (horizontal axis) for TIF Evaluation [27] 94

Figure 4-5: Modified Hall Integral analysis [124] 96

Figure 4-6: CRMIP Model of Flow between an Injection and a Production Well [127] 97

Figure 4-7: The synthetic Model with Well Locations for Cases 1 and 2 99

Figure 4-8: TIF growing from injector 1 (I1) in the x-direction towards producer 1 (P1) 100

Figure 4-9: Case 1: Cold Water Injection reduces the Reservoir Temperature 100

Figure 4-10: Case 1: BHP and Fracture Half Length vs. Time for I1 100

Figure 4-11: Case 1: MHI Plot for I1 with a Downward Separation of the Derivatives, indicating TIF 101

Figure 4-12: Case 1: Pseudo-Skin Evolution vs. Time for I1 shows a significant reduction after 155 and 200 Days 101

Figure 4-13: Case 1: Log-Log plot of FI and II vs Injected Volume for I1 Monitors TIF Initiation and Propagation 102

Figure 4-14: Case 1: Rapid Response of Reservoir Pressure after TIF initiation at 155 days observed in injector I1 102

Figure 4-15: Case 1: Pre-TIF comparison of Production Rate and CRM Calculations for P1 and P2 103

Figure 4-16: Connectivity of I1 and gain of P1 and P2 for Case 2 pre-TIF and Post-TIF 104

Figure 4-17: TIF growing from injector 1 (I1) in the y-direction towards producer 2 (P2) 104

Figure 4-18: Connectivity of I1 and gain of P1 and P2 for Case 2, Pre- and Post-TIF 105

Figure 4-19: No-TIF case has the highest recovery factor indicating the impact of TIF on Cases 1 and 2 105

Figure 4-20: Locations of injectors NI4, NI6 with respect to producer NP4 106

Figure 4-21: Injection Rate and BHP history for injector NI6 106

Figure 4-22: Wellhead Water Temperature and Injection Rate appear to be correlated for Injector NI6 107

Figure 4-23: II and RII for for injector NI6 108

Figure 4-24: Voidage Replacement Ratio (VRR) for the selected sector reservoir 108

Figure 4-25: MHI plot for Injector NI6 shows a downward separation of derivatives implying TIF 109

Figure 4-26: Well NI6's Skin value significantly reduces after 690 days and increases between 870 and 1185 days 109

Figure 4-27: Log-log plot of FI and II of Injection Well NI6 confirms TIF Initiation and Propagation 110

Figure 4-28: Advance of Water Bank and Pressure of Water/Oil Interface for Injector NI6 110

Figure 4-29: Pre- and Post-TIF Connectivity of Well NP4 with NI6 and NI5 111

Figure 4-30: left: connectivity pre-TIF, right: connectivity post-TIF 111

Figure 4-31:FMI image from one of well in the field with tensile fractures (supplied by the operator) 112

Figure 4-32: History Data for Injection Well NI6 and Production Well NP4 112

Figure 5-1: General history matching strategy [129] 116

Figure 5-2: History match assuming radial flow for well A [9] 118

Figure 5-3: History match improves assuming a vertically confined TIF between 30 and 60 days for well A [9] 119

Figure 5-4: TIF dimensions and reservoir permeability in the final history match for well A [9] 120

Figure 5-5: Final history match assuming an unconfined TIF after 60 days for well A [9] 120

Figure 5-6: The 3D reservoir grids system for the "N"field sector model and the well locations 122

Figure 5-7: Porosity distribution histogram for the "N" field sector reservoir model 122

Figure 5-8: Horzointal permeablitiy distribution forthe "N" field sector reservoir model 123

Figure 5-9: The vertical saturation map of the "N" field reservoir (at the start of production) 123

Figure 5-10: Locations of injectors NI6, NI5_H, and NI5_T with respect to producer NP4 124

Figure 5-11: REVEAL and Eclipse model predictions for producer "NP4" BHP 125

Figure 5-12: REVEAL and Eclipse model predictions for injector “NI6” BHP 125

Figure 5-13: REVEAL and Eclipse model predictions for injector “NI5_H” BHP 126

Figure 5-14: Simulation run versus the history for injector NI6 130

Figure 5-15: The historical injection rates and BHPs for injector NI6 130

Figure 5-16: Well N-8 relative location to injector NI6 (supplied by the operator) 131

Figure 5-17:The bulk density (ρb) recorded by the log of Well N-8 (Blue Line) (supplied by the operator) 133

Figure 5-18: Leak off test at 824 m TVD for well N-8 (supplied by the operator) 134

Figure 5-19: Leak off test at 2678 m TVD for well N-8 (supplied by the operator) 135

Figure 5-20: Possible range of σ_{Hmax} for normal faulting regime at depth of 2678 m (8786 ft) TVD 136

Figure 5-21: FMI image from Well N-20 with tensile fractures 137

Figure 5-22: Well N-8 Compressional (Vp) and Shear Wave (Vs) Velocities 139

Figure 5-23: Simulation run with & without TIF modelled versus injector CW6 history data 141

Figure 5-24: Calculated vs. fall off reservoir pressure around well NI6 142

Figure 5-25: Well NI6 calculated (+TIF) simulated reservoir vs history data 142

Figure 5-26: Surface water temperature for injector NI6 143

Figure 5-27: History matching workflow without TIF modelling 144

Figure 5-28: History matching workflow with TIF modelling 145

Figure 5-29: Matching simulated reservoir pressure to fall-off tests around well NI6. 146

Figure 5-30: Well NI6 Completion Schematic 147

Figure 5-31: Injection test for well NI6 148

Figure 5-32: Simulated and History matched BHP for well NI6 149

Figure 5-33: Surface water injection temperature and injection rate are correlated after 690 days 150

Figure 5-34: Simulated injection and history data without TIF after matching reservoir pressure and BHP to reliable data 151

Figure 5-35: Final matched injection rate with TIF modelling after modifying geomechanical and thermal properties 151

Figure 5-36: Geometry of TIF around Well NI6 after 690 days 153

Figure 5-37: Evolving TIF half-length the whole injection period. 153

Figure 6-1: Examples of drainage challenges in horizontal wells [48] 155

Figure 6-2: Conventional injector vs. ICD injector [81] 156

Figure 6-3: Wormhole channels formed between well pair due to sand mobilisation [84] 156

Figure 6-4: 4757 ft long injector and producer wells added to the history matched, "N" sector reservoir simulation model. 158

Figure 6-5: Transverse TIF configuration [134] 160

Figure 6-6: Longitudinal TIF configuration [134] 160

Figure 6-7: Prevention of cross flow in the annulus by packers 161

Figure 6-8: Conceptual ICD completion design with ICD/joint and 4 joints / compartment defined by the packers 161

Figure 6-9: Reservoir grids and packer placement 162

Figure 6-10: Visualisation of reservoir grids and well horizontal section as initially modelled 163

Figure 6-11: Visualisation of reservoir grids and well horizontal section as finally modelled 163

Figure 6-12: shows temperature variation after 3000 days of SAS completion; A) thermal case, B) isothermal case 164

Figure 6-13: Viscosity variation for SAS completion after 3000 days; A) thermal case, B) isothermal case 164

Figure 6-14: Injectivity index for both isothermal and thermal modelling of injector SAS 165

Figure 6-15: BHP required for both isothermal and thermal constant injection rate into SAS completed well 165

Figure 6-16: Cumulative oil production for both isothermal and thermal modelling of SAS completed wells 166

Figure 6-17: Cumulative oil production of both isothermal and thermal case for ICD completed wells.....166

Figure 6-18: Extent of T-TIF propagation at last time step for SAS completed injector where coloring and numbers represent reservoir regions 167

Figure 6-19: Oil Recovery for SAS with and without T-TIF.....167

Figure 6-20: Oil recovery for different regions for SAS with and without T-TIF modelling 168

Figure 6-21: Water injected and BHP for both SAS with and without T-TIF.....168

Figure 6-22: Injection Efficency for both SAS with and without T-TIF 169

Figure 6-23: water outflow from the injector for SAS, ICD-2.5, and ICD-1.6 at early time step when T-TIF injection is not important 170

Figure 6-24: T-TIF frequency and length toward the producer for SAS, ICD-2.5, and ICD-1.6 at last time step.....170

Figure 6-25: Half-length of first initiated T-TIFs for SAS, ICD-2.5, and ICD-1.6 at last time step 170

Figure 6-26: Average reservoir pressure around the injector for SAS, ICD-2.5, and ICD-1.6 mm 171

Figure 6-27: Oil Recovery for SAS, ICD-2.5, and ICD-1.6 171

Figure 6-28: Water Oil Ratio for SAS, ICD-2.5, and ICD-1.6 completions for T-TIF 172

Figure 6-29: Water injection rate and BHP for SAS, ICD-2.5, and ICD-1.6 completions for T- TIF 173

Figure 6-30: Injection efficency for SAS, ICD-2.5, and ICD-1.6 completions for T- TIF 173

Figure 6-31: Time and half length of the first and last initiated T-TIFs for ICD-1.6 in both wells and in injector only.....174

Figure 6-32: Oil inflow rate for ICD-1.6 in both wells and in injector only at early time step when T-TIFs are not important.....174

Figure 6-33: Oil Reovery for SAS, ICD-1.6 in both wells, and in injector only.....175

Figure 6-34: Oil Recovery for SAS, ICD-2.5 mm in both wells and in injector only .176

Figure 6-35: Injection efficiency for SAS, ICD-2.5 mm, and ICD-1.6 mm in both wells 176

Figure 6-36: Production well FBHP for SAS, ICD-2.5 mm and ICD-1.6 mm in both wells 176

Figure 6-37: shows L-TIF propagation after 20 years for SAS completion 177

Figure 6-38: Oil Recovery for SAS with T-TIF, L-TIF and no-TIF..... 177

Figure 6-39: Injection Efficiency for SAS with T-TIF, L-TIF and no-TIF 178

Figure 6-40: Oil recovery per region for SAS with and without L-TIF..... 178

Figure 6-41: Water injection rate and BHP for both SAS with and without L-TIF..... 179

Figure 6-42: L-TIF frequency and distribution toward the producer for SAS, ICD-2.5, and ICD-1.6 mm completion in injection well after 20 years..... 179

Figure 6-43: The time and half-length for the first initiated L-TIF for injection well for SAS, ICD-2.5, and ICD-1.6 mm 180

Figure 6-44: Oil Recovery SAS, ICD-2.5, and ICD-1.6 for L-TIF 181

Figure 6-45: Injection Efficiency for SAS, ICD-2.5, and ICD-1.6 for L-TIF 181

Figure 6-46: Producer water oil ratio for SAS, ICD-2.5, and ICD-1.6 for L-TIF 181

Figure 6-47: Water injection rate and BHP for SAS, ICD-2.5, and ICD-1.6 completions for L-TIF 182

Figure 6-48: Growth of first and last initiated L-TIFs for both ICD-1.6 mm completed well and ICD completed injector only 183

Figure 6-49: Oil Recovery for SAS, Both wells and injector only with ICD-1.6 mm . 184

Figure 6-50: Oil Recovery for SAS, Both wells and injector only with ICD-2.5 mm . 184

Figure 6-51: Producer's FBHP for Both wells SAS, ICD-2.5, and and 1.6 mm 184

Nomenclature

σ_{hmin}	Minimum horizontal stress
σ_e	Effective stress
$\sigma_{T,min}$	Total minimum horizontal stress
P_p	Pore fluid pressure
$\sigma_{hmin,i}$	Initial minimum horizontal stress
$\sigma_{\Delta T}$	Thermo-elastic stress
$\sigma_{\Delta P}$	Poro-elastic stress
α	Coefficient of thermal expansion
E	Young's modulus
ν	Poisson's ratio
β	Shape factor for the cooled region
ΔT	Initial temperature of the reservoir minus the new temperature
ΔP	BHP minus reservoir pressure
C_{gr}	Grain compressibility
σ_{Hmax}	Maximum horizontal stress
σ_v	Vertical Stress
D	Darcy
mD	Millie Darcy
t/d	Tonne (water mass) per day
B	Formation volume factor
ρ_{cal}	Density of calibration fluid (water)
μ_{cal}	Viscosity of calibration fluid (water)
C_d	Discharge coefficient for nozzle or orifice
C_u	Unit conversion factor: $8/\pi^2$ in SI units
l_{ICD}	Length of the ICD joint
ΔP_{ICD}	Pressure drop occurs in ICD
ρ	Density of produced or injected fluid
μ	Viscosity of produce or injected fluid
d	Nozzle or orifice diameter
K_{IC}	Critical stress intensity factor

w_f	Width
G	G
Kr_{ip}	Relative permeability of injected fluid
μ_{ip}	Viscosity of injected fluid
$\Delta\sigma_y$	Minimum horizontal stress due to temperature and pressure changes
K_I	The stress intensity factor
P_{wf}	The bottomhole injection pressure
K	Permeability
h	Reservoir thickness
r_e	Reservoir effective radius
r_w	Wellbore radius
S	Skin
w_i	Cumulative volume of water injected
K_W	Reservoir permeability to water
P_e	Effective reservoir pressure
B_W	Water formation volume factor
i_w	Water injection rate
GOR	Produced Gas Oil Ratio
Q_O	Oil production rate
Q_w	Water production rate
B_W	Oil formation volume factor
B_g	Gas formation volume factor
μ_w	Injected viscosity
L_f	TIF half length
H	TIF height
φ	Porosity
D_{HI}	Analytic derivative of Hall integral
D_{HIn}	Numeric derivative of Hall integral

m	Semilog slope
S^*	Pseudoskin
S_{or}	Residual oil saturation
Δt_{sup}	Summation term in superposition
f_{ij}	fraction of injection from injector i flows to producer j
N_i	Total number of injection wells
N_p	Total number of producer wells
J_{ij}	Productivity index of a producer pair
γ_g	Dissolved gas relative density (air=1)
γ_o	Stock-tank oil relative density (water=1)
P_b	Bubble-point pressure
R_S	Solution gas-oil ratio
T	Absolute temperature
μ_{od}	Dead oil viscosity

Subscripts and superscripts

i	injector index
j	producer index
k	time-step index
ij	injector-producer pair index

Abbreviations

AFI	Annular Flow Isolation
AWC	Advanced Well Completions
BHP	Bottom Hole Pressure
BHT	bottom hole temperature
BWPD	Barrels of water per day
CF	Connection Factor
EOR	Enhanced Oil Recovery
FD	Finite Difference
FE	Finite Element
FI	Fracturing Index
GCS	Geologic CO2 Sequestration
HF	Hydraulic Fracturing
HI	The Hall Integral
HTE	Heel-to-Toe Effect
II	The Injectivity Index
IW	Intelligent Well
LEFM	Linear Elastic Fracture Mechanics
LGR	Local Grid Refinement
MHI	Modified Hall Integral
MRC	Maximum Reservoir Contact
NPV	Net Present Value
P3D	Pseudo 3 Dimensional
PFO	Pressure Fall-Off
PKN	Perkins-Kern-Nordgren
PW	Reinjected Produced Water
RH	Reservoir Heterogeneity
RII	Reflectivity of Injectivity Index
SAGD	Steam Assisted Gravity Drainage
SW	Sea Water
TIFs	Thermally Induced Fractures
TVD	True Vertical Depth
VRR	Voidage Replacement Ratio

WHP	Well Head Pressure
WOR	Water-Oil Ratio

Chapter 1 Introduction and Motivation

1.1 Introduction

Waterflooding is the most common improved oil recovery method used in the oil industry. Waterflooding normally involves the injection of cold water in a warm reservoir. This process results in the alteration of the stress distribution in subsurface formations. During the cooling of the rocks nearby the wellbore, the in situ stress within the cooled zone tend to decrees due to temperature decrease. This results in water injection wells being fractured at bottomhole injection pressure (BHIP) values significantly lower than the original, minimum compressive horizontal stress. These fractures are referred to as Thermally Induced Fractures (TIFs) in the oil industry. Understanding TIFs is important since their existence will impact the oil recovery potential, well injectivity, injection well integrity, and injector-producer well spacing in reservoirs under waterflooding (Figure 2-1). Identifying and characterising dynamic TIF growth is thus a critical step when defining field development strategies and making day - to - day reservoir management decisions.

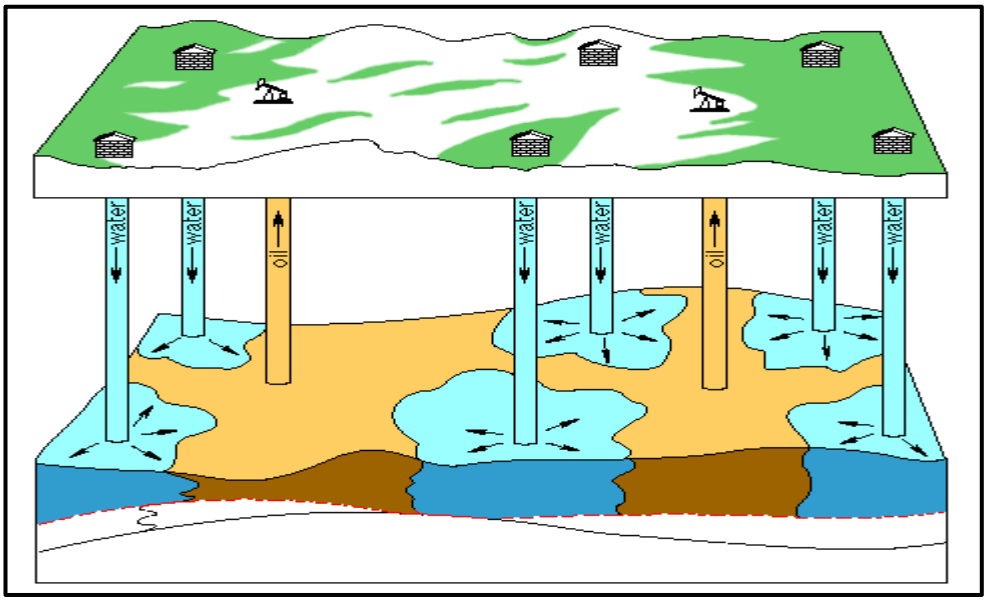

Figure 1-1: TIFs impact oil recovery, injectvity, well integrity, and well spacing in waterflooded reserviros [1]

One of the major documented negative impacts of TIFs is the advance of injection fluids at different rates through the reservoir, thereby reducing the overall sweep efficiency of a flooding operation. The solutions of this problem can be either by maintaining the water injection pressure below the fracturing (breakdown) pressure of the formation or by flexibly controlling the fluid injection profile, namely by distributing the

injected fluid uniformly throughout the reservoir. The first solution can be difficult to maintain technically due to the dynamic, local changes in the reservoir because of the cooling effect. Furthermore, limiting the injection pressure reduces the well injection rate which may result in failure to achieve the required reservoir management objectives. The second solution can be achieved by employing Advanced Well Completions (AWCs).

Advanced well completions consisting of Downhole Flow Control (DFC) technology such as Inflow Control Devices (ICDs), Interval Control Valves (ICVs) and/or Autonomous Flow Control Devices (AFCDs) (Figure 1-2), are developed to deliver practical solutions to problems with production/injection constraints and reservoir description uncertainty related challenges. Production/injection constraints challenges include, but are not limited to, uneven injection/production profile or pressure drawdown, sand production, well clean up, and well stimulation. Reservoir description and geology challenges include but limited to geological structures e.g. uncertain faults, variation in reservoir pressure in different layers and regions, and variation of reservoir properties e.g. permeability crossed by the wellbore.

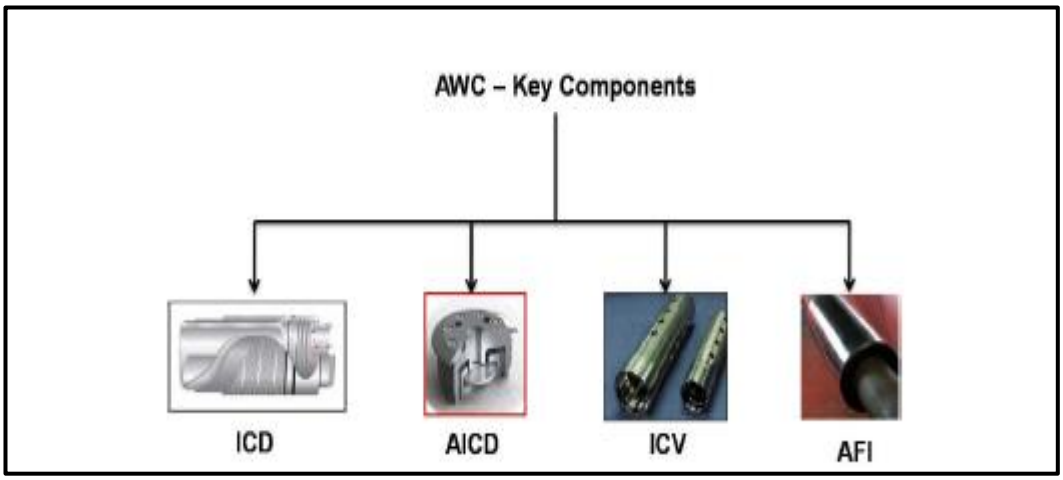

Figure 1-2: Main Components of Advanced Well Completions [2]

ICDs are passive devices with fixed restriction that cannot be changed after installation. These devices provide the inflow/outflow control from/into the reservoir by applying extra pressure drop at different sections along the wellbore. The aim of ICDs is normally to make the well's inflow/outflow profile more uniform. ICDs are a proven technology to enhance the performance of production wells. In addition to ICDs' application in production wells, ICDs have been applied in injection wells with various configurations in different fields around the world. The installation of ICDs in injection wells proved to provide solutions for problems associated with complex reservoirs and well topologies. ICDs have been used to minimise Heel-to-Toe effect (HTE) and flow

heterogeneity effect in production and injection wells (Figure 1-3). Another added value of ICDs in injection wells is the ability to provide optimal pressure support and a more uniform injection profile in fractured reservoirs and reservoirs with thief zones (Figure 1-4).

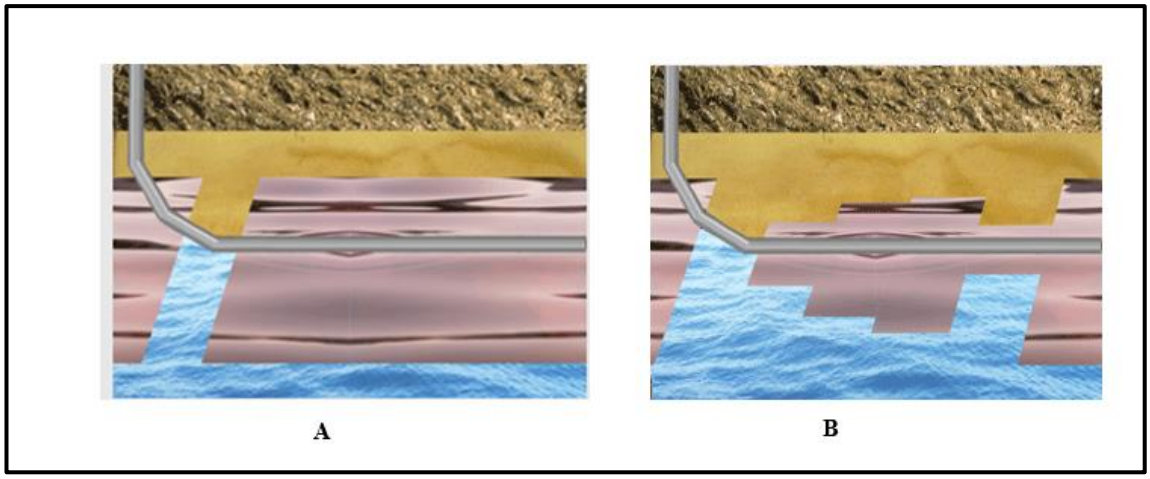

Figure 1-3: Illustration of the effect of (A) Heel-to-Toe effect (B) reservoir heterogeneity [3]

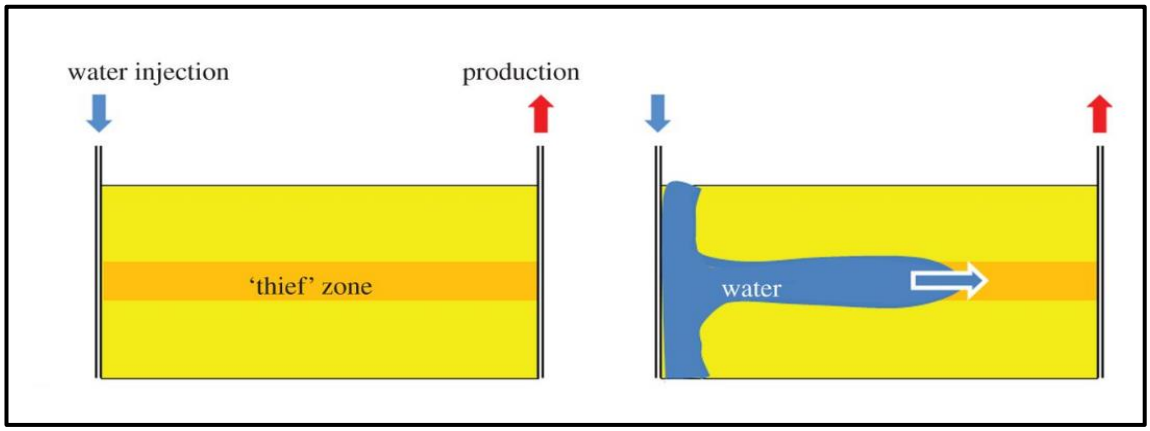

Figure 1-4: Illustration of the impact high permeability thief zone [4]

The above-listed successful applications of ICDs in different reservoir and well conditions was the main driver for this study. The overall objective of this thesis is to develop methods and workflows to identify and characterise TIFs, as well as, investigate the performance of ICD completion in horizontal wells when TIFs are expected.

1.2 Thesis Objectives

The thesis focuses on the Inflow Control Device (ICD) applications and their performance when applied to horizontal wells with the expected occurrence of TIFs. TIFs development in the reservoir alter the outflow profile and affect the sweep efficiency as well as oil recovery. Preventing TIFs from occurring is a difficult task due the complex

interaction between reservoir flow and geomechanical processes. Therefore, controlling and mitigating TIFs by using ICDs can be a potential solution.

Despite the many technical reports and published papers that discuss the details of ICDs' positive impact and applications in different reservoir management challenges, their applications in TIFs prone environments have not been studied in depth.

The thesis addresses the following points and novel methods in relation with TIFs and ICD technology:

1. Developing a workflow that integrates recently developed analytical, well monitoring models with a semi-analytical one to identify the onset of TIF, its propagation properties, direction and impact during reservoir dynamic events occurring at different levels. This workflow is required to:
    a. Provide high resolution detection of TIF and minimise the fluctuations resulted from the measured rates and pressures
    b. Identify subtle, short-term changes on a daily/weekly basis
    c. Evaluation of the impact of TIF at different levels i.e. field-level and producer/injector pair-level
    d. Identification of the likely TIF propagation direction.
2. Developing history matching workflows using a 3D reservoir flow simulation coupled with a 2D finite element TIF model and a geomechanical reservoir model. These workflows are required to:
    a. Take the dynamic nature of the TIF problem into consideration
    b. Improve and validate the reservoir and geomechanical models
    c. Identify and confirm TIF onset and propagation periods
    d. Provide a history matched sector model with defined rock mechanical properties, thermal properties and stress gradients that can be used with confidence for subsequent studies.
3. Evaluation of Inflow Control Device effectiveness to mitigate Thermally Induced Fractures in water injection wells. This will cover the following areas
    a. Understanding the impact of thermal and isothermal reservoir modelling options
    b. Appreciating the importance of taking TIF into consideration during field development planning by comparing Stand-alone Screen (SAS) completion with and without TIF modelling

c. Investigating the impact of different completions installed in the injection well in ‘injector only’ or both the injector and producer on TIFs growth.
d. Studying the impact of wells orientation with respect to the maximum horizontal stress on TIFs initiation and propagation.

The aim of this thesis is to improve the surveillance methods of TIFs as well as to quantify the added value of advanced wells completion employing ICD when TIFs are expected. The surveillance and mitigation methods of TIFs are the two main areas to add to the state-of-the-art research.

1.3 Thesis Layout

The above objectives are addressed throughout the study. The organisation of this thesis can be summarised as follows:

Chapter 2 provides an introduction to Thermally Induced Fractures (TIFs) phenomenon as well as to Advanced Well Completions (AWCs) technology. It describes various reservoir and geomechanical processes related to TIFs in deep reservoirs. The chapter covers real fields experiencing TIFs and their impact in both waterflooding applications and non-waterflooding applications. Various AWCs types are discussed in terms of their capabilities, their objectives, and their reported field applications with special focus on ICDs. The applications, capabilities, and advantages of ICDs in injection wells are reviewed in different fields under various reservoir and well conditions.

Chapter 3 focuses on the modelling of Thermally Induced Fractures. It describes the history of modelling TIFs and their evolution from 2D simple models to complex fully 3D models. The chapter also describes the modelling methodology used in this thesis. It provides the underlying assumptions as well as details governing equations on the TIF model being used for TIFs analysis. The implementation workflow involving coupling 3D reservoir simulation with TIF and geomechanical models is described as well.

Chapter 4 introduces a workflow that integrates recently developed analytical, wellbore injectivity and reservoir flow monitoring models with a semi-analytical one to identify the onset of TIF, its propagation properties, direction and impact during reservoir dynamic events occurring at different levels. The practicality of the proposed workflow is tested using synthetic data and its robustness confirmed by the analysis of data from a real field.

Chapter 5 focuses on history matching a sector model of a field (N-field) using reservoir simulation coupled with Thermally Induced Fracturing and geomechanical models. The

chapter describes the methods of determining in-situ stresses as well as the rock mechanical properties. The finalisation of the history matching process after rectifying uncertainty parameters and modifying geomechanical and thermal properties is described.

Chapter 6 builds on the history matched model from Chapter 5 to evaluate the Inflow Control Device (ICD) performance in injection wells with thermally Induced Fractures (TIFs). It discusses the impact of thermal and isothermal reservoir modelling options as well as comparing their performance with SAS and ICD completions. The chapter also compares the behaviour of TIFs growth under different completions installed in an injection well only and in both injector and producer. The effect of wells orientation with respect to the maximum horizontal stress on TIFs initiation and propagation is included in this chapter as well.

Chapter 7 summarises the conclusions of this study and provides recommendations for future research.

Chapter 2 Literature Review and Background

2.1 Thermally Induced Fracturing (TIF)

2.1.1 Introduction

It is well established in the oil industry that a large proportion of water injection wells are fractured at some time over their extended life [5, 6]. This includes injection wells that are injecting initially at a Bottom hole Pressure (BHP) lower than the original Minimum Horizontal Stress (σ_{hmin}) [7]. When a cold fluid is injected into hot reservoirs, rocks undergo contraction because of the injected fluid temperature being significantly cooler than the reservoir temperature. This contrast in temperatures causes the in-situ stress to reduce considerably. A numerical illustration of the temperature and stress evolution around the injection wellbore is shown Figure 2-1 and Figure 2-2 for a square shape reservoir that includes a horizontal producer and a vertical water injector [8]. Figure 2-2 illustrates that the Minimum Horizontal Stress (σ_{hmin}) is reduced around the injection well due to reduction in temperature. It can also be noted from the same figure that the (σ_{hmin}) decreases with depth. When the Minimum Horizontal Stress (σ_{hmin}) falls below BHP due to temperature changes, fractures may initiate and/or propagate [9, 10, 7]. This applies to both vertical and horizontal wells [6] . Fractures initiation and/or propagation resulted from thermal processes is referred as Thermally Induced Fractures (TIFs).

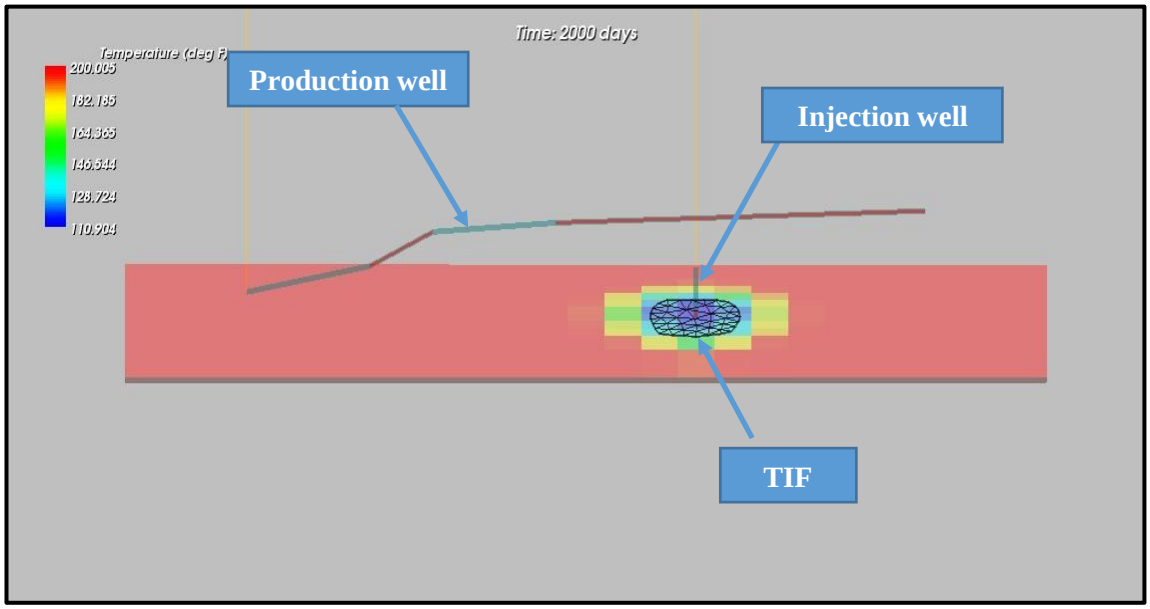

Figure 2-1:Temperature evolution around a vertical water injector [8]

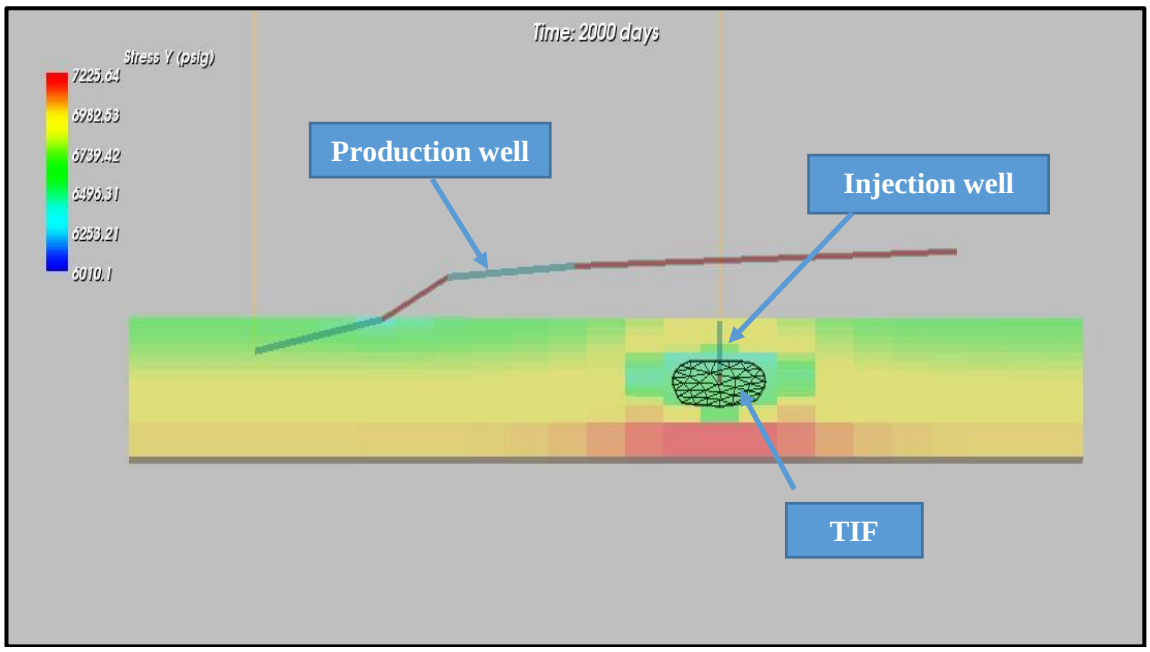

Figure 2-2: Stress evolution around a vertical water injector [8]

A real field example illustrating these thermal phenomena is shown in Figure 2-3 [11]. The fracture gradient reduction is directly proportional to higher temperature difference between the formation and the injected water temperature in Prudhoe bay field for a number of step-rate tests [11]. This shows the significant impact of temperature difference between the formation and the injected fluid on stress reduction and hence on TIF initiation and/or propagation

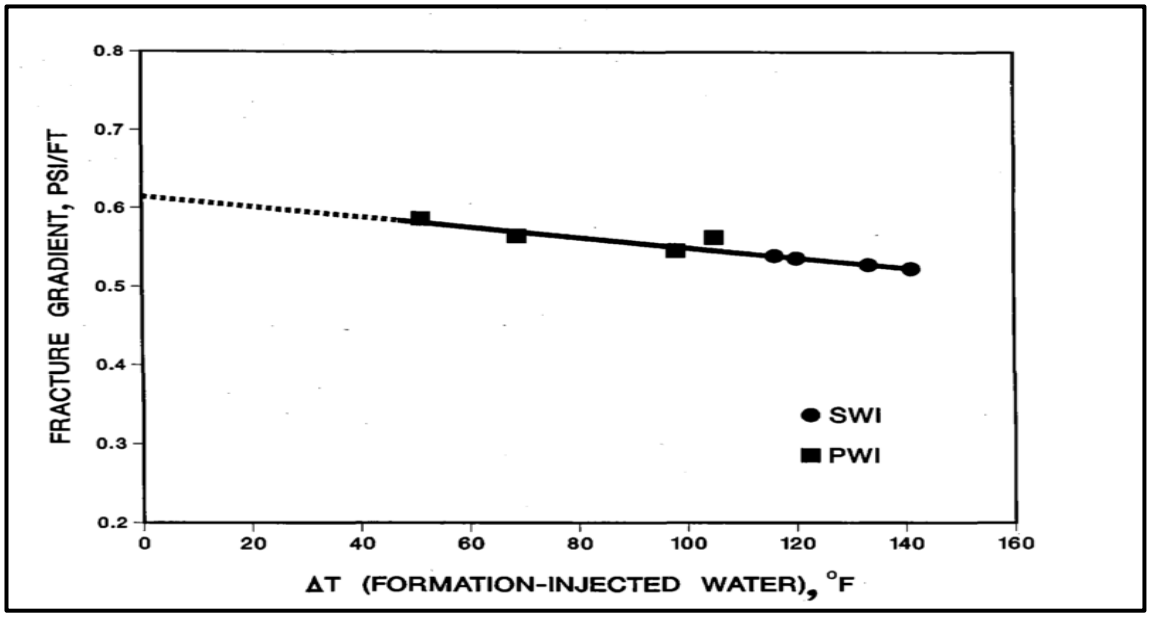

Figure 2-3: Impact of temperature on the fracture gradient for the Prudhoe bay field [11]

Horizontal and vertical injection wells often suffer from the risk of creating thermally induced fractures. The following can result from TIF developments in injection wells in waterflooding and non-waterflooding applications.

I. Non uniform outflow of the injected water from the well into the reservoir. Literature showed that most of the injected water can be accepted by a small zone. This causes poor sweep efficiency and non-uniform pressure support.
II. TIFs can grow out of net payzone which causes the injected water to be lost to the formation above or below the target zone. This results in an inefficient waterflood processes and reduce the oil recovery.
III. Sand production may take place earlier than predicted due to the cooling reducing the temperature and the rocks strength. Sand production may be observed during the back-production of injection wells and during well shut-ins.
IV. TIF can have a positive impact on water treatment facilities. Water-quality specifications can be relaxed because of the influence of TIF.
V. TIF can significantly improve the injectivity in disposal and geologic CO_2 Sequestration (GCS) applications, allowing economic injection rates to be achieved. Avoiding out-of-zone TIF and contamination of fresh water remains a challenge.

In this thesis, the negative impact of TIF during waterflooding operations is the point of interest. Some of the technical issues related to TIF in water injection wells is the poor sweep efficiency, non-uniform pressure support, early water breakthrough and reduced oil recovery. These challenges can lead to early abandonment of unwept portions of the reservoir because of the increased operational costs involved in producing, workover, and reinjecting produced water.

Remedial measures have been suggested in the literature to address the TIF technical issues. These measures include the following:

I. Reduction of injection pressure [12]: This can be done to ensure that Bottom Hole pressures are below the new fracture pressure to prevent TIF formation. This, however, could result in sever under injection that affect the injection wells' performance.
I. Installation Blank Pipe [13]: employment of blank pipes across the TIF. This option even though is cheap and common, it has the following drawbacks:
    a. It will not allow isolating any more TIFs

b. It will decrease the flow area

c. It will create some possible accessibility issues for logging and coil tubing operations in the future.

II. Installation of ICD: This option was a practical solution to highly fractured reservoir and proved the added value [13].

Since ICD is a proven technology in highly fractured reservoirs as well as in other applications, it will be investigated further with TIF in this thesis.

2.1.2 Rock Mechanics of TIF

The basic concepts of rock mechanics includes stress, strain, stress/strain relationships, and rock mechanical properties significantly impact the TIF initiation and/or propagation. The following discusses these concepts and relates them to the TIF.

2.1.2.1 *Concepts of Stress and strain*

Both stress and pressure are defined as force per unit area. The pressure is often used with fluids whereas the stress concept is applied to solids. Pressure only acts perpendicular to a surface and is uniform in all directions whereas the stress can be different in different directions. If a solid body is considered, then the combination of all stresses acting on that body in different directions will be referred as the stress field Figure 2-4. Therefore, the main differences between the stress and the pressure is the considered medium and the direction component. Stress is a second order tensor with nine components of which six are independent (Figure 2-4).

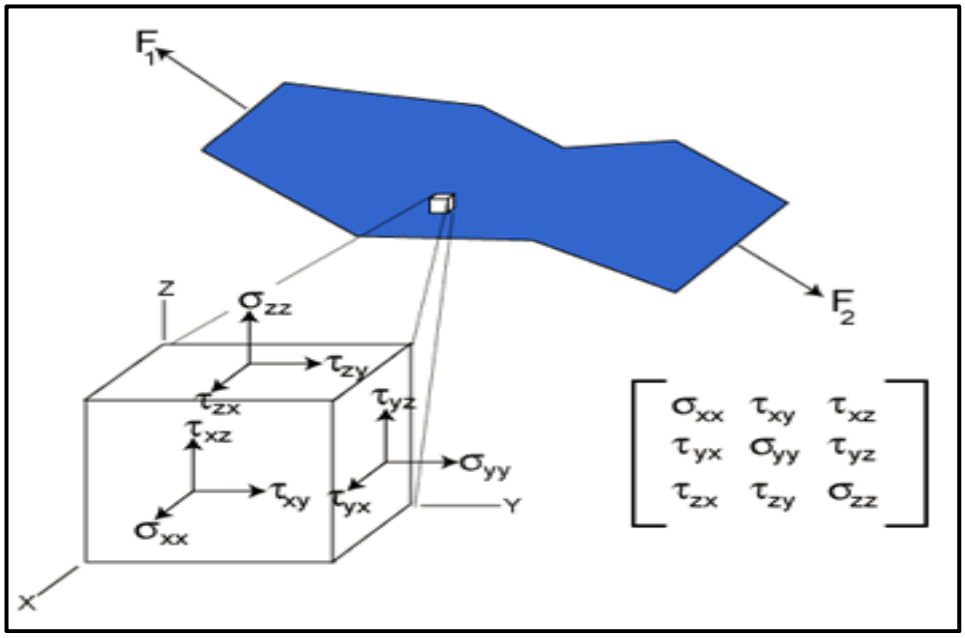

Figure 2-4: Components of stress in three dimensions [14]

Strain, by contrast, is the amount of deformation caused by the action of the stress divided by the initial length of the material. Deformation types can be translation (position change), rotation (orientation change), dilation (size change), and distortion (shape change). Translation and rotation are grouped as rigid body deformation, whereas dilation and distortion constitute strain. Since it is very difficult to measure dilation in most rocks in practice, the distortion (shape change) strain is only considered for analysis. Extension, shortening, and shear strains are shown in Figure 2-5.

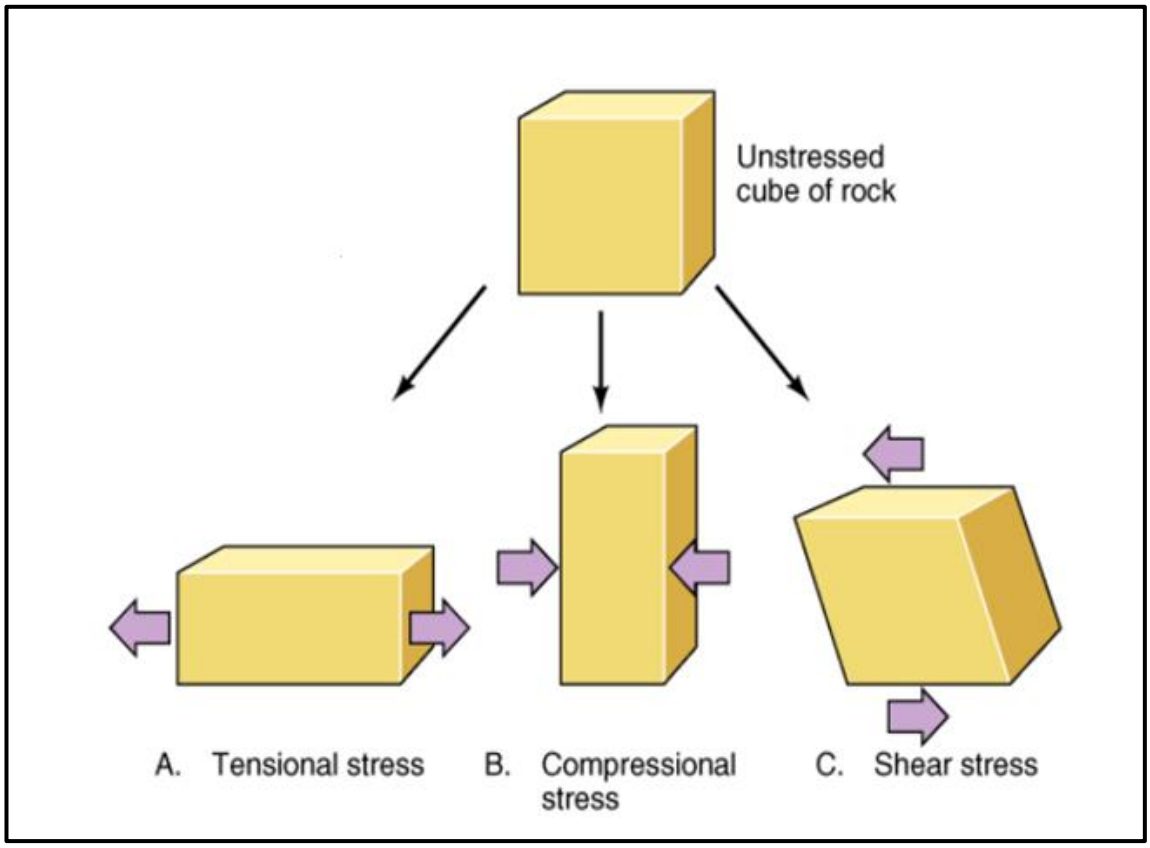

Figure 2-5: Extentional strain (tesnional stress), shortening (comperssion stress) and shear strain (shaer stress)[15]

2.1.2.2 ***Stress / Strain relationships***

The relationship between the stress and the strain depends on the composition and the mechanical properties of the rocks considered. There are two ideal types of response; elastic strain and plastic strain.

I. Elastic strain

In the ideal elastic strain behaviour, the distorted body returns to its original unstrained shape and size when the deforming stress is removed. The stress and strain are proportional to each other and governed by Hooke's law:

$$\sigma = E/e \qquad \text{Equation 2-1}$$

Where e is the extensional strain, σ is the stress applied, and E is constant known as Young's Modulus. Young's Modulus, characteristic of the rock, is the slope of the straight line in the ideal elastic stress /strain relationship represented in Figure 2-6.

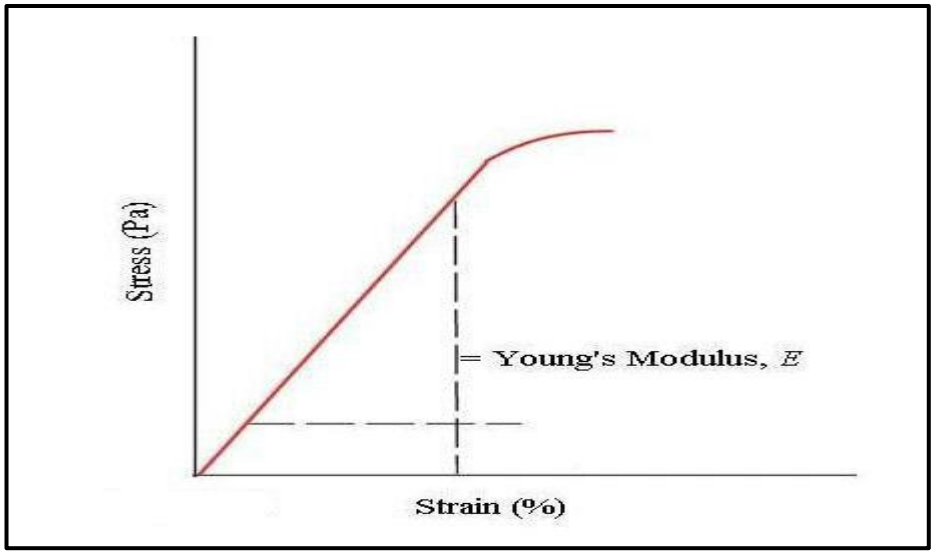

Figure 2-6: Ideal elastic stress/strain curve

II. Plastic Strain

In the ideal plastic strain behaviour, the rock deformation is non-reversible after removing the deforming stress. Stress-strain relationship in plastic region is given by the following equation:

$$\sigma = ke^n \qquad \text{Equation 2-2}$$

Where K is strength coefficient and n is the strain hardening coefficient. In reality, rocks normally combine the ideal elastic and plastic behaviours. The total stress then can be combined by the following Equation:

$$\sigma = E/e + ke^n \qquad \text{Equation 2-3}$$

Rocks usually respond to applied stress in two ways. They either break (brittle rocks) or they bend (ductile rocks). When a sufficient stress is applied, brittle materials lose cohesion by development of a fracture or set of fractures whereas ductile materials can have a large plastic deformation before fracturing (Figure 2-7).

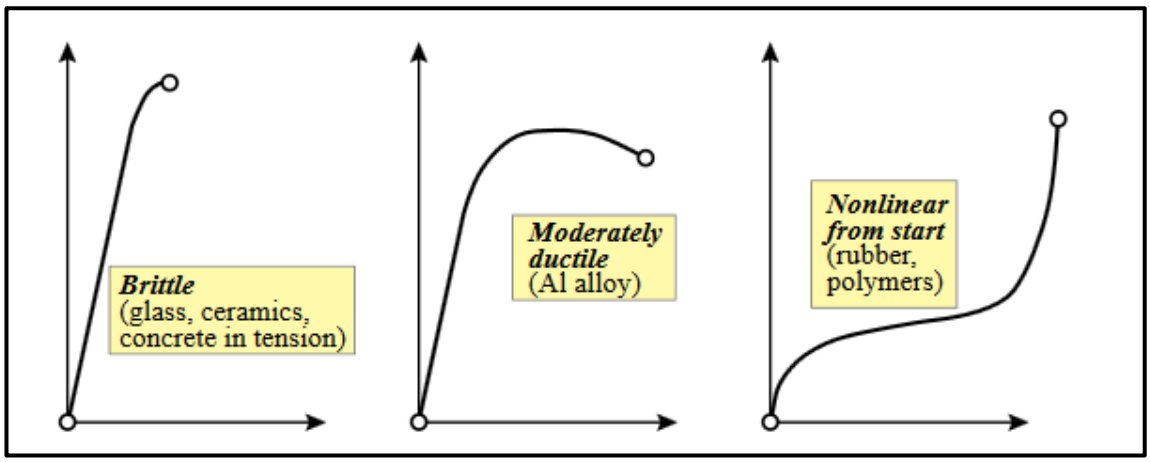

Figure 2-7: Three material responses as displayed in a tension test [16]

The consideration, in this thesis, is restricted to very specific rocks and response regime by making the following behavioural assumptions [16]:

1. Macroscopic model: the rock is mathematically modelled as a continuum body
2. Elasticity: stress/strain response is reversible.
3. Linearity: the relationship between strain and stress is linear i.e. doubling stresses doubles strain and vice versa.
4. Isotropy: the rock mechanical properties are independent of direction.
5. Small strains: deformations are considered so small that changes of geometry are ignored as the stress is applied.

These assumptions may not always hold true in reality e.g. for rocks containing microcracks, weak and soft clay-bearing rocks, porous rocks and evaporitic rocks [17]. Violation of these assumptions while modelling requires inclusion of nonlinear behaviour of the rocks into the model. This can further complicate the problem of TIF as the resulting complex relationship between the stress and strain needs to be included (i.e. nonlinear constitutive equations of rocks). The above assumptions, however, have been used successfully especially at depth with high stresses and with homogenous and isotropic rock mass [18].

2.1.3 Simplified Physical Description

A mathematical description is presented below to describe how rock stresses are affected when injecting cold water and how TIF becomes more probable. The effective stress (σ_e) concept is employed here to provide an understanding of how TIF occurs as a result of temperature/stress -induced changes. The maximum principal in-situ stress component at deep reservoirs is usually vertical, thus the minimum principal in-situ stress component acts horizontally (Figure 2-8). The minimum principal stress is in a

compressive state. Injecting cold water with time change the compressive state into tensile state. Since the change from compressive to tensile stress first occurs in the minimum principal stress direction, a vertical fracture perpendicular to the plane of minimum horizontal stress will form. Thus, the horizontal minimum principal stress is only considered in the effective stress equation below.

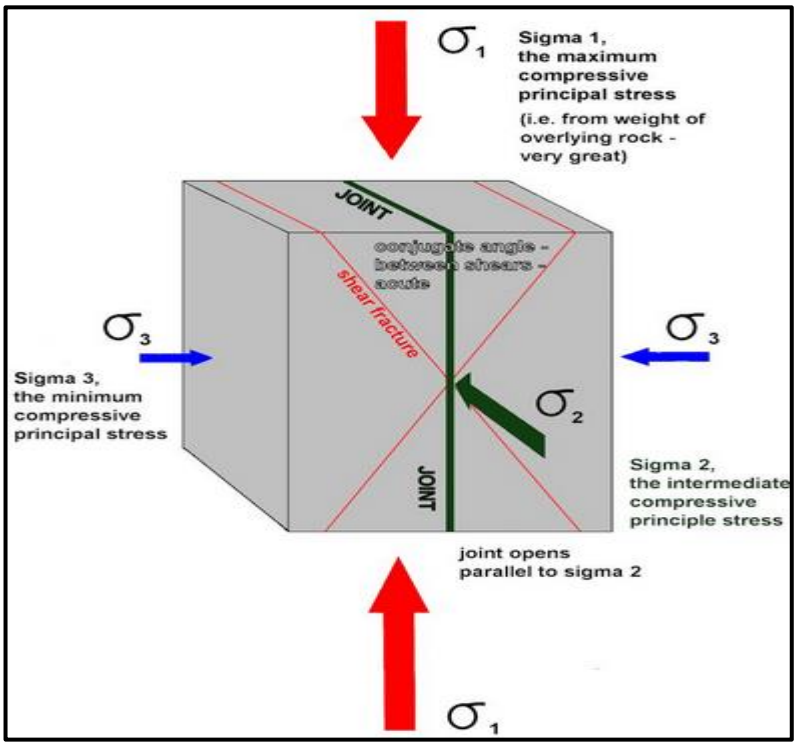

Figure 2-8: Three principal stresses at deep reservoirs where the maximum principal stress is vertical [19]

The far field effective stress state (σ_e) is given by [20, 21]:

$$\sigma_e = \sigma_{T,min} - \alpha P_p \qquad \text{Equation 2-4}$$

Where

$\sigma_{T,min}$=The total minimum horizontal stress

α = The Biot's constant

P_p = The pore fluid pressure

Consider stress state under initial conditions before injecting cold water. The total horizontal stress components i.e. a force that is likely to keep the fracture closed in deep reservoirs are usually much greater than the pore fluid pressure i.e. a force that is likely to keep the fracture open [20]. Therefore, the resulting effective stress is positive and the system is said to be in compressive state. Fractures cannot initiate and/or propagate when

the rocks are in compressive state. The stress state, however, will change after injecting cold fluid into hot reservoirs. This can be explained further by considering different components of the total minimum horizontal stress ($\sigma_{T,min}$). One of the components of this total minimum horizontal stress is related to temperature difference between the formation and the injected fluid. Injecting cold water into the formation causes the total minimum horizontal stress to reduce and hence the resulting effective stress reduces in Equation 2-4. When the effective stress becomes negative, the system is said to be in a tensile state. Fractures can initiate and/or propagate when the rocks are in tensile state

2.1.4 The effect of temperature and pressure changes on Poro-elastic and thermo-elastic stresses

The effect of temperature and pressure on the total minimum horizontal stress can be described by the following relationship [22]:

$$\sigma_{T,min} = \sigma_{hmin,i} + \sigma_{\Delta T} + \sigma_{\Delta P} \qquad \text{Equation 2-5}$$

Where

$\boldsymbol{\sigma_{hmin,i}}$ = The initial minimum horizontal stress,

$\boldsymbol{\sigma_{\Delta T}}$ = The thermo-elastic stress,

$\boldsymbol{\sigma_{\Delta P}}$ = the poro-elastic stress.

The thermo-elastic stress term is related to the effect of the temperature on the reservoir stress field whereas the poro-elastic stress is related to the effect of the pore pressure on the reservoir stress field. The thermo-elastic stress that results from injection of fluid colder than the formation is given by [20, 21]:

$$\sigma_{\Delta T} = \frac{\alpha E \Delta T \beta}{(1-\nu)} \qquad \text{Equation 2-6}$$

Where

$\boldsymbol{\alpha}$ = coefficient of thermal expansion for reservoir rocks

$\boldsymbol{E}$ = Young's modulus

$\boldsymbol{\beta}$ = Shape factor for the cooled region i.e. 0< β<1,

$\boldsymbol{\nu}$ = Poisson's ratio of reservoir rocks

$\boldsymbol{\Delta T}$= The new temperature caused by the cooling fluid minus the reservoir temperature

It can be noted from Equation 2-6 that the amount of change in thermo-elastic stress depends on rock mechanical properties of reservoir rocks i.e. Young's modulus and Poisson's ratio, thermal properties of reservoir rocks i.e. coefficient of thermal expansion, temperature difference caused by injecting cold fluid, and reservoir properties i.e. flood front shape factor. The poro-elastic stress that results from injection of fluid colder than the formation is given by [20, 21]:

$$\sigma_{\Delta P} = \frac{\mathrm{EJ\Delta P\beta}}{(1-\nu)} \qquad \text{Equation 2-7}$$

Where

$$J = \frac{(1-2\nu)}{E} - \frac{C_{gr}}{3} \qquad \text{Equation 2-8}$$

ΔP = The new pore pressure caused by injecting the cooling fluid minus the reservoir pressure of the reservoir

$\boldsymbol{C_{gr}}$ = grain compressibility.

It can be noted from Equation 2-7 and Equation 2-8 that the amount of change in poro-elastic stress depends on rock mechanical properties of reservoir rocks i.e. Young's modulus and Poisson's ratio, pressure difference caused by injecting cold fluid, and reservoir properties i.e. grain compressibility and flood front shape factor.

It can be noted from Equation 2-4 to Equation 2-6 that when the reservoir rocks are cooled, they can transform from a compressive state to a tensile state due to reduction of horizontal total stress and hence the effective stress. When this occurs, fractures may initiate and/or existing fractures may propagate. Cooling reservoir rocks mainly occurs by convection. It is documented that the thermal front will move at roughly one third of the speed of the saturation front since rocks heat capacity is approximately twice that of water [20, 21]. It can be noted from Equation 2-4, that injecting cold fluid increases the pore pressure and therefore decreases the effective stress. However, poro-elastic stress in Equation 2-7 is likely to yield an opposing but smaller increase in total stress. A numerical example computed with a reservoir simulation model of how temperature and pressure can affect the total stress is shown in Figure 2-9 [23]. In this figure, the total stress is illustrated while the pore fluid pressure effect is excluded. It can be noted from Figure 2-9 that injecting cold water will reduce the reservoir temperature while increase the pore fluid pressure. Lower temperature in the reservoir tends to decrease the total stress whereas higher reservoir pressure tends to increase the total stress[23]. The decrease in

total stress because of reservoir temperature decrease will generally be more significant than the increase of total stress because of reservoir pressure increase as illustrated in Figure 2-9 [23, 21]. When the net effective stress decreases around the wellbore to a negative value, the possibility of fracture initiation and/or propagation is increased. The Figure 2-9 thermal front is approximately one third distance to flood front, therefore thermally induced Fractures (TIFs) length are always shorter than the saturation front.

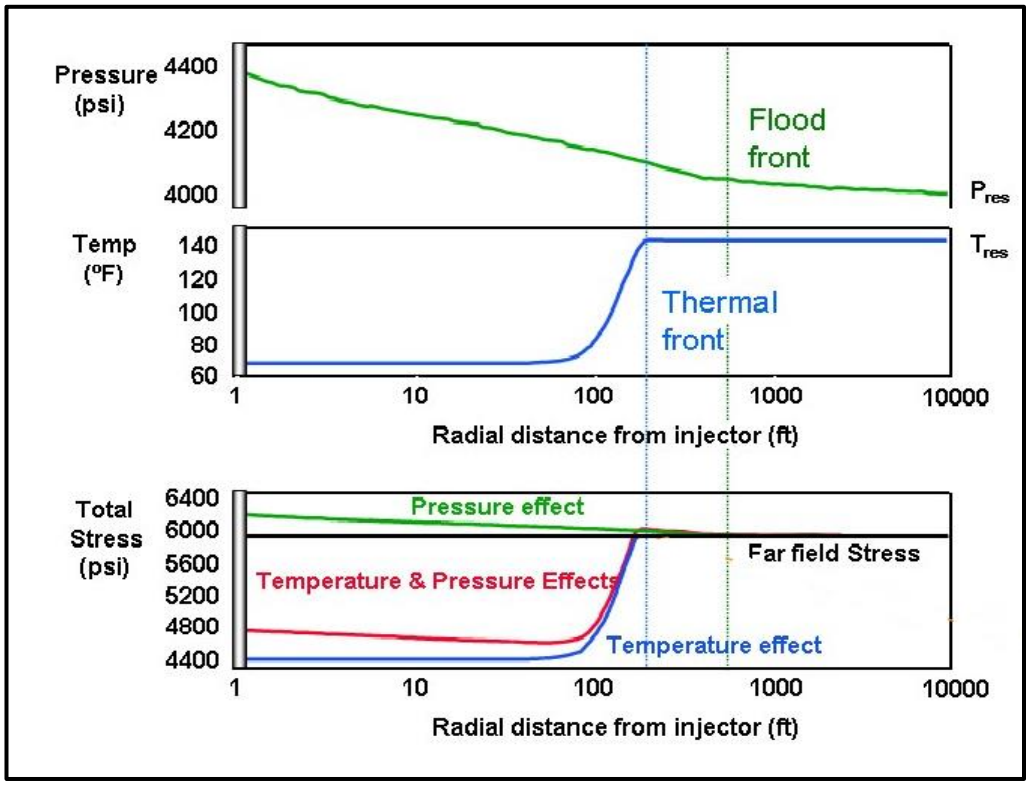

Figure 2-9:Predicted total stress resulting from temperature and pressure changes computed from a reservoir simulation model [8, 23].

2.1.5 TIFs initiation and growth

Knowledge of stresses magnitudes and orientation in the reservoir is critical in addressing extensive problems in oil industry including wellbore stability, hydraulic fracturing, sand production, long term reservoir response to cold water injection etc. Despite stress being a tensor with six independent components, it will be assumed in this thesis that there are three principal stresses i.e. the vertical stress,σ_v, and two horizontal principal stresses, σ_{Hmax} and σ_{hmin} as shown in Figure 2-10. Even though this simplification can be shown to be the case in many places around the world, it can be incorrect in other cases [24]. For example, the orientation of principal stress would be expected to be different in the shallow reservoirs and in salt bodies or the effect of temperature changes combined with pore pressure changes can initiate a new TIF or

propagate an existing fracture. It is imperative to discuss the type of fractures before going into details of TIFs initiation and/or propagation magnitude and orientation. There are three ideal types of fractures based on the angle with respect to σ_v i.e.1) tensile mode (mode I), 2) sliding mode (mode II), and 3) tearing mode (mode III), as shown in Figure 2-11. The type of fracture that will advance depends on [25, 24]:

I. The orientation and magnitude of in-situ stress in the formation
II. The orientation of pre-existing fractures
III. Tensile strength of the rock
IV. The orientation and magnitude of thermo-elastic stress and poro-elastic stress e.g. after water injection

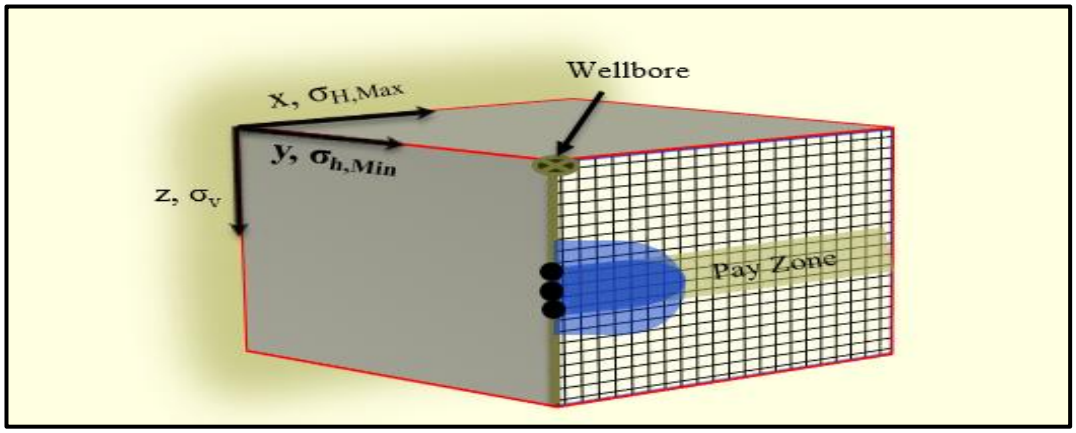

Figure 2-10: Schematic showing the direction of the three Principal stresses

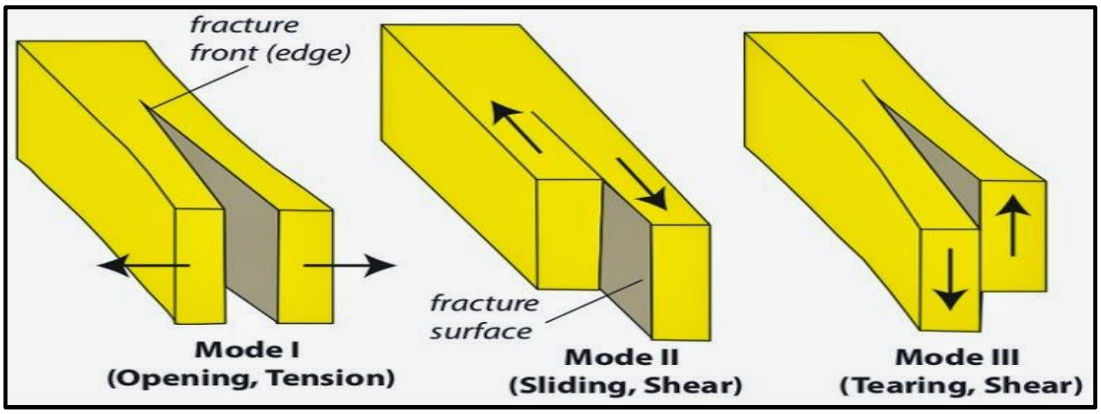

Figure 2-11: The three modes of fracture [25].

In this thesis, the initiation and propagation of tensile fractures i.e. mode I will be considered for primarily two reasons:

I. Tensile fractures initiate around the injection wells where temperature and pressure effects are the largest
II. Newly initiated TIFs are investigated in this thesis. Existing (natural) fractures are not considered i.e. where shear mode (mode II) may occur.

Tensile mode i.e. also known as Normal Faulting occurs when the largest (most compressive) stress is vertical stress and the smallest and intermediate stresses are horizontal ($\sigma_v > \sigma_{Hmax} \geq \sigma_{hmin}$).

Several criteria can be adopted to model the initiation and propagation of TIFs. The criteria and modelling of TIFs initiation and propagation are further in Chapter 3. When the criterion for TIFs opening is met due to thermo-elastic and poro-elastic changes in the reservoir, TIFs will propagate parallel to the direction of maximum horizontal stress and perpendicular to minimum horizontal stress because this requires the smallest amount of energy as shown in Figure 2-12 [7]. The propagation of TIFs depends on the following [25, 7, 24]:

I. The in-situ stress
II. Thermo-elastic and poro-elastic changes
III. Injection pressure
IV. Rock mechanical properties of the reservoir
V. Length of the TIF.

The above discussion showed the importance of quantification of the in-situ stress prior to injection to asses TIFs onset, direction, and impact. The methods of measuring in-situ stresses include direct methods e.g. injection tests and indirect methods e.g. calculation using published correlations based on sonic log data [26].

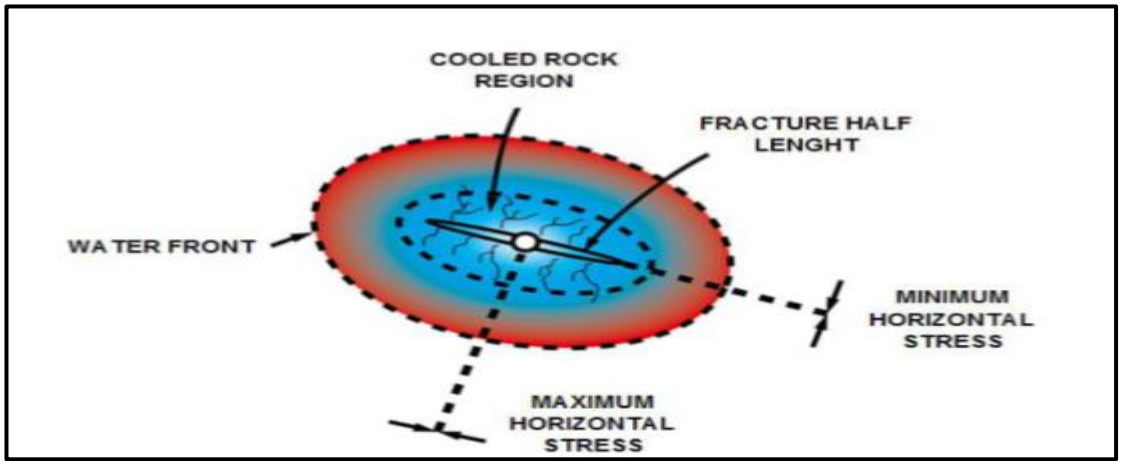

Figure 2-12:Direction of TIF in a horizontal plane [27]

2.2 Real fields experience with TIF

TIF has been documented in different fields around the world. TIFs may or may not have a negative impact depending on the type of injection wells and their applications. Generally, TIFs should be predicted and controlled even when a positive impact is expected e.g. in disposal wells to avoid further problems. The following explains real fields experience with TIF under various conditions and applications.

2.2.1 TIF in Waterflooding applications

2.2.1.1 *Prudhoe Bay Field (Alaska)*

This oil field is located on the north of Alaska (Figure 2-13), on the arctic coast. The permeability varies between 0.1 and 5 Darcy (D) [28] . Waterflooding in this field started in 1984 with peripheral pattern floods (Figure 2-14). The injected water source initially during early years was Sea Water (SW) with a temperature value of 80^0 F. However, reinjected Produced Water (PW) became the primary source of injection water later in the field life.

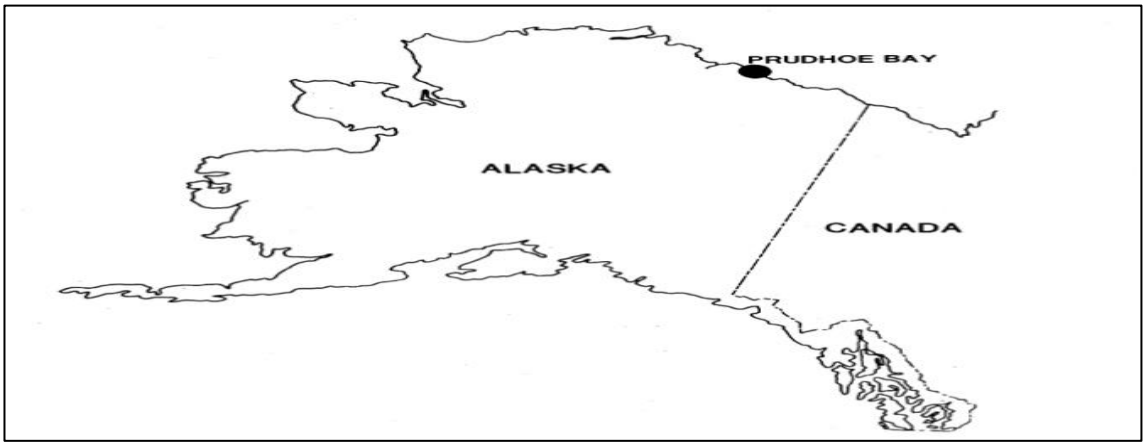

Figure 2-13: Location of the Prudhoe Bay oil field on the north slope of Alaska [11].

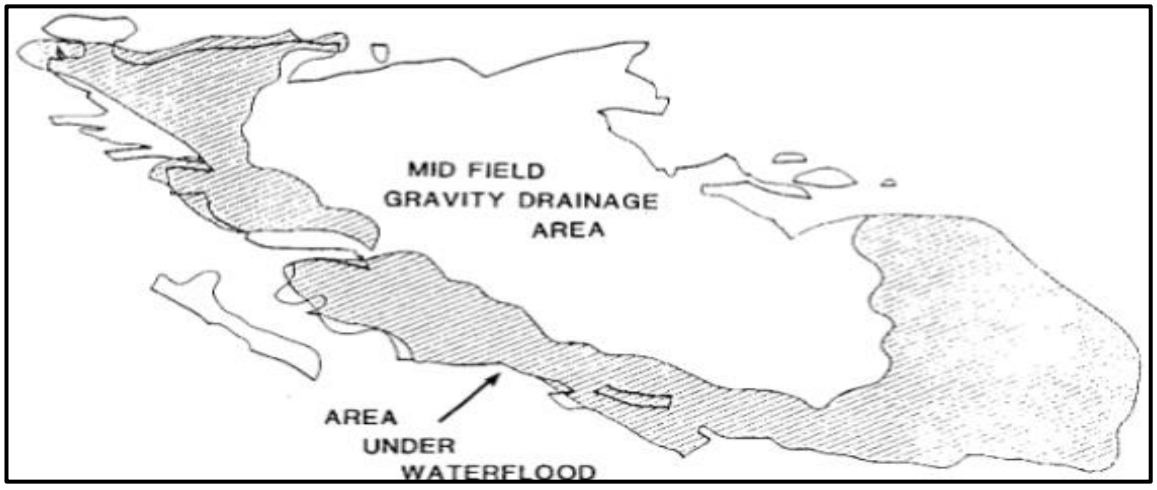

Figure 2-14: Prudhoe Bay oil field waterflood area [28]

Two studies were performed on this field at two different times to investigate TIF process impact on the vertical and areal sweep efficiency. The first study was conducted in 1989 to understand TIF in depth using Step-Rate Tests (SRTs), specially designed injection tests, and simulation studies for injection wells subjected to SW injection only [28]. The second study was conducted six years later in 1995 to investigate long term effects on water injectors' performance of water quality, TIF growth, fluid temperature,

and other factors [29]. Interestingly, both studies gave conflicting conclusions because of the long term impact of TIF. The first study compared static temperature surveys run in one of the injectors before fracturing i.e. 11/1985 and after fracturing to quantify TIF and its impact on waterflood performance (Figure 2-15). It was noted from this analysis as well as SRTs that TIF stayed confined vertically to the injected interval. It was found from numerical and analytical methods that TIFs were short and relatively stable. Another finding from multirate-injection surveys that although TIFs caused less control over injection profiles, oil production was accelerated as a result of TIF. It was decided by the operator that water injection at injection gradients higher than TIF gradients was accepted as a reservoir management strategy in Prudhoe Bay [28]. However, it was found after several years that this strategy was not the best one after conducting another extensive study in 1995.

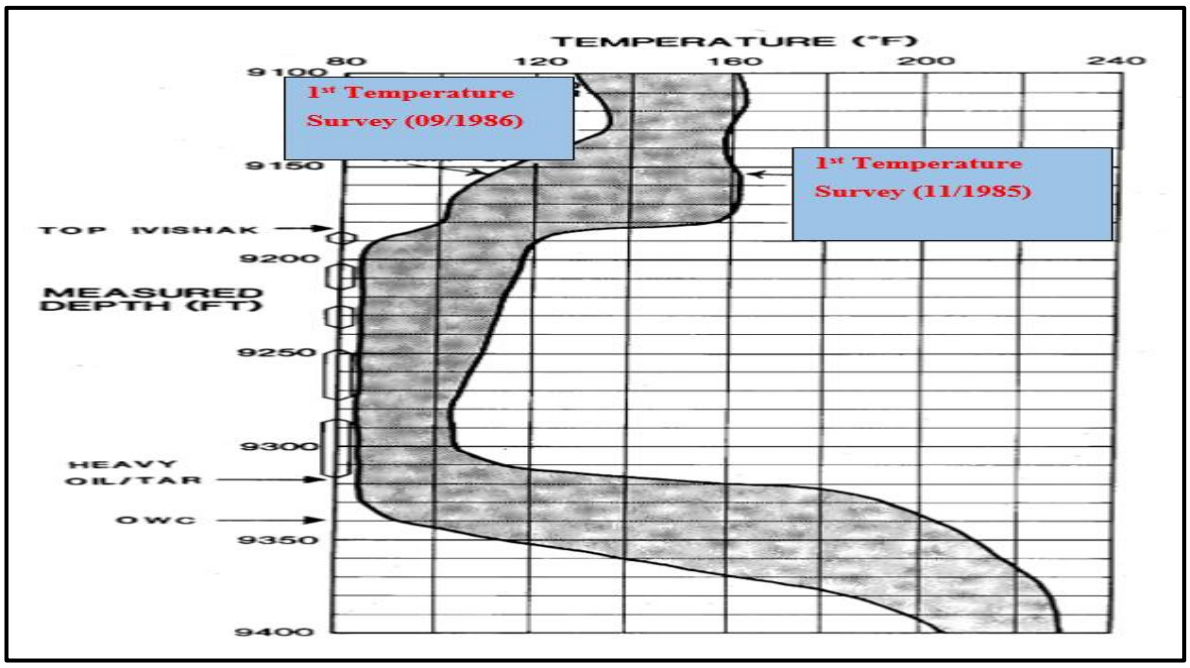

Figure 2-15:Comparison of one of the injector temperature profile before and after fracturing [28]

The second study, conducted in 1995, analysed 159 injectors from the same field that were subjected to periods of both SW and PW. It was found that the injectivity for almost all of the injectors to be poorer for PW than for SW due to higher temperature difference in SW injectors as shown in Figure 2-16 for one of the injectors. This injector had switched six times between SW and PW over a 7 years period. It can be shown from Figure 2-16 that the fracture opening pressure i.e the intersection of the straight line that intersects the pressure axis for SW (100 psi) is less than SW (500 psi). The poorer injectivity was one of the causes that voidage replacement ratio (VRR) fell to below 0.75 in some areas. It continued to decline for several years up to 06/1992 in the overall field

as shown in Figure 2-17. The increase in the VRR after 06/1992 increased the reservoir response pressure (due to the increased injection) and reduced the field's decline rate.

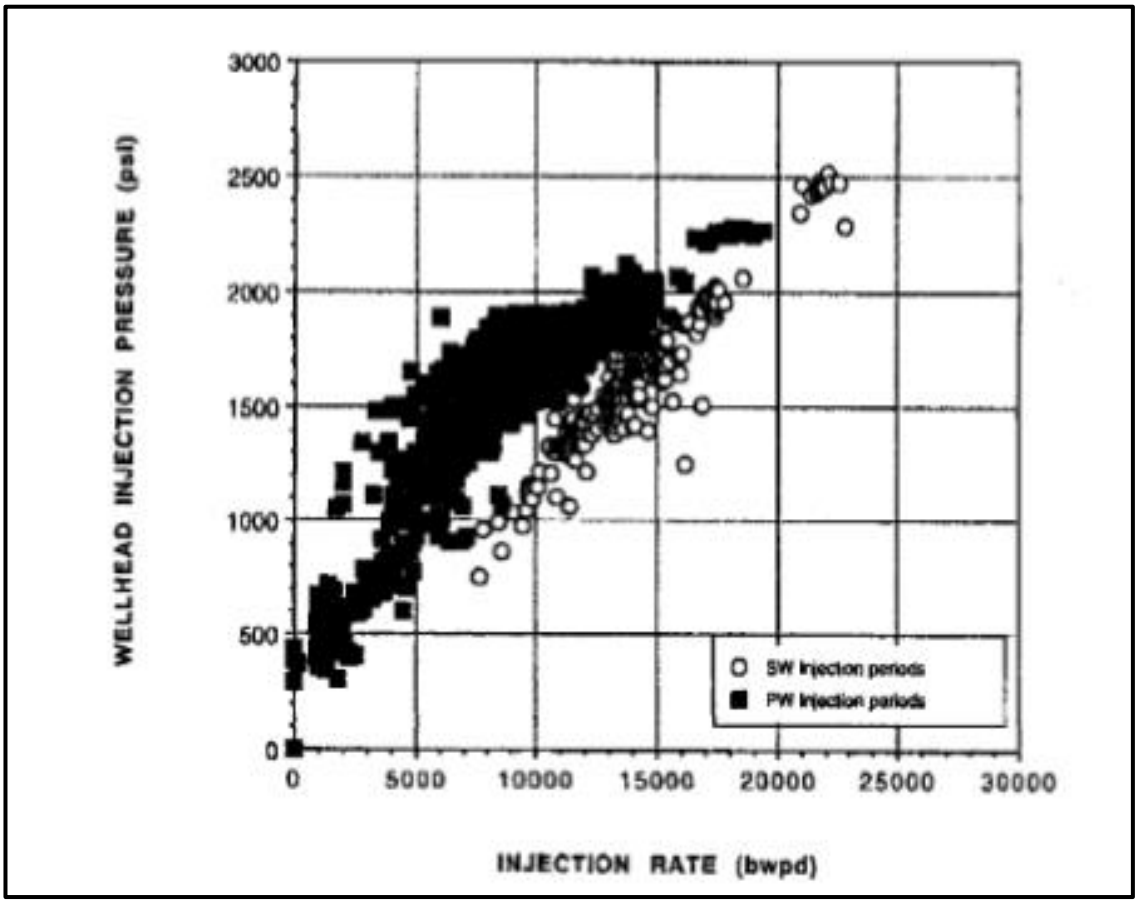

Figure 2-16: Performance plot for one of the injectors showing SW and PW injection periods [29]

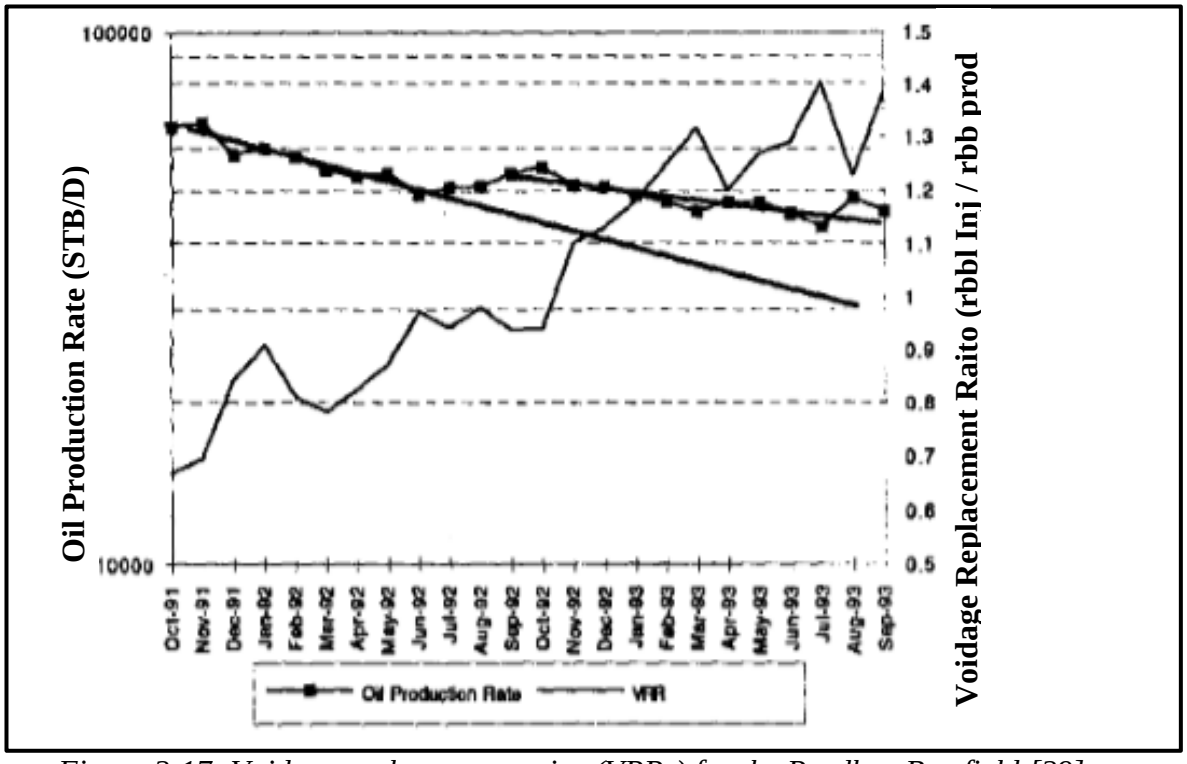

Figure 2-17: Voidage replacement ratios (VRRs) for the Prudhoe Bay field [29]

Another observation was that temperature surveys for one of the injectors indicated a considerable cooling occurred below the completion interval, Figure 2-18 especially when injecting SW. These observations led to the conclusion that TIFs could grow out-of-zone, causing injection water to be lost to the underlying high kh zone. This will also lead to a decreased oil recovery. It was also observed in this field that the well deviation and orientation with respect to the preferred TIF direction can significantly affect the injectors' performance (Figure 2-19). It can be note from this figure that the least favourably oriented wells require higher injection pressure. It was decided by the operator to impose injection limits for current injectors as well as consider the effect of well trajectory for planed future injectors. Another decision taken by the operator was to relax produced water quality specifications at the field because of TIF formation. These two studies on the same field confirmed that TIF can have unwanted effects that need to be taken into account when preparing the field development plan.

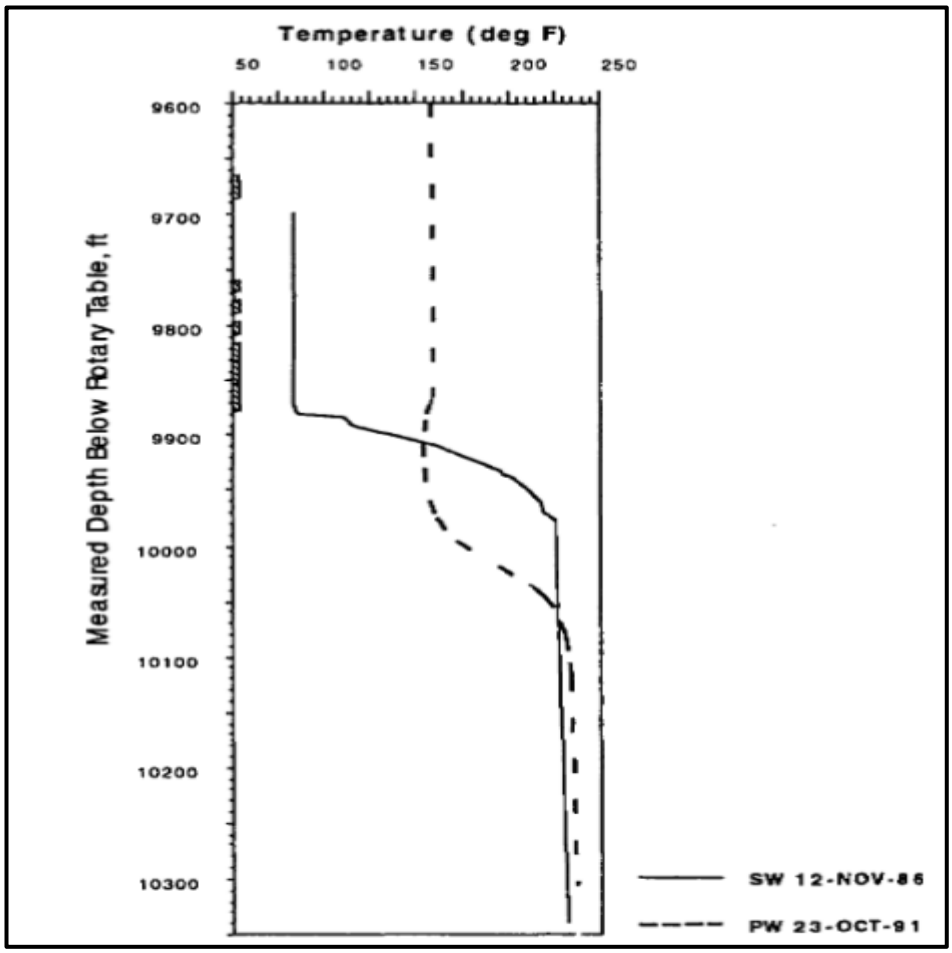

Figure 2-18: Temperature survey for one of the injector with SW and PW[29]

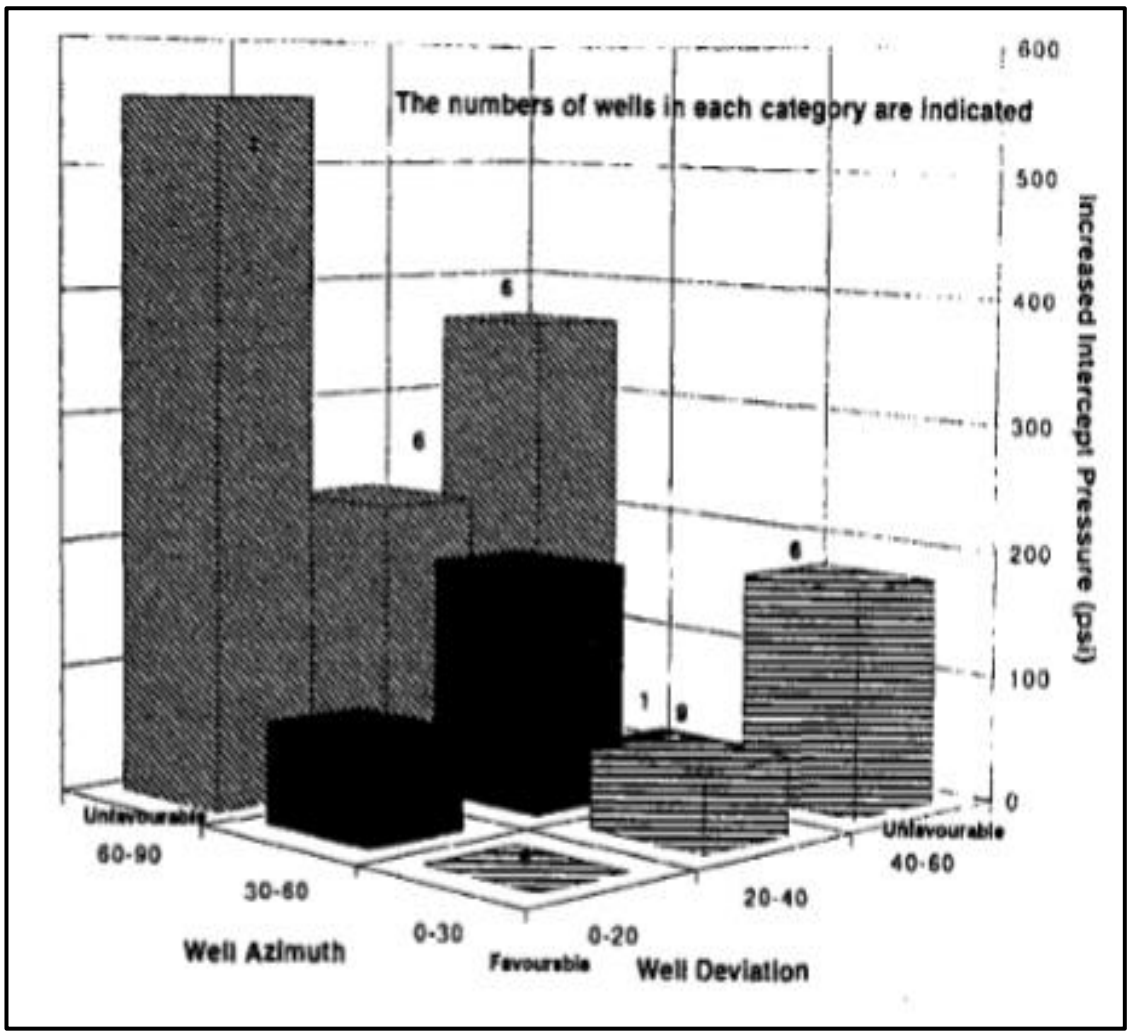

Figure 2-19: Effect of azimuth and deviation on intercept pressure [29]

2.2.1.2 ***Ula Field (North Sea)***

Ula field is located in North Sea approximately 180 miles southwest of Stavanger, Norway [7]. The field is a low permeability one with a permeability ranging between 1 and 75 mD. The field production start-up was in 1986. The reservoir crest is located about 10,825 ft below sea level. Water injectors were drilled to supplement the negligible aquifer support in this high temperature reservoir (average temperature of 295^0 F). Some of the injection water was used to cool the produced fluid in the production heat exchanger before being mixed with the reminder of the injection water. This heat exchanger, intended to improve the deoxygenation efficiency, caused the water temperature to increase to 104^0 F.

The injectors in this field could be divided into two categories namely low-rate injectors and higher rate injectors. It was noted by the operator toward the end of 1988 that there was a sudden increase in the injectivity in one of the high rate injectors as shown in Figure 2-20. This event coincided with the field‘s oil production being cut by about 50%. This cut caused less flow passing through the heat exchanger and resulted in a cooler

water injection i.e. injection water temperature dropped by 9^0 F (95^0 F from 104^0 F). The second increase in the injectivity was observed in February 1989 as shown in Figure 2-20. This increase corresponded to a complete production shutdown which caused water injection temperature to decrease further to 60^0 F. All these observations can be explained by the formation of TIFs. This was confirmed by a downhole flowmeter that showed the injection had associated with thin intervals affected by TIF [7]. It was observed that low-rate injectors were not affected by TIF in the same way as high-rate injectors because these completion zones had not been adequately cooled. A flowmeter survey indicated that the TIF had propagated in the highest permeability interval because they were being cooled at a faster rate (Figure 2-21). It can be noted from this figure that 28% of the flow leaving the injector over a 6 ft interval (zone 2A) which is several times more that would be expected without fracturing [29] .

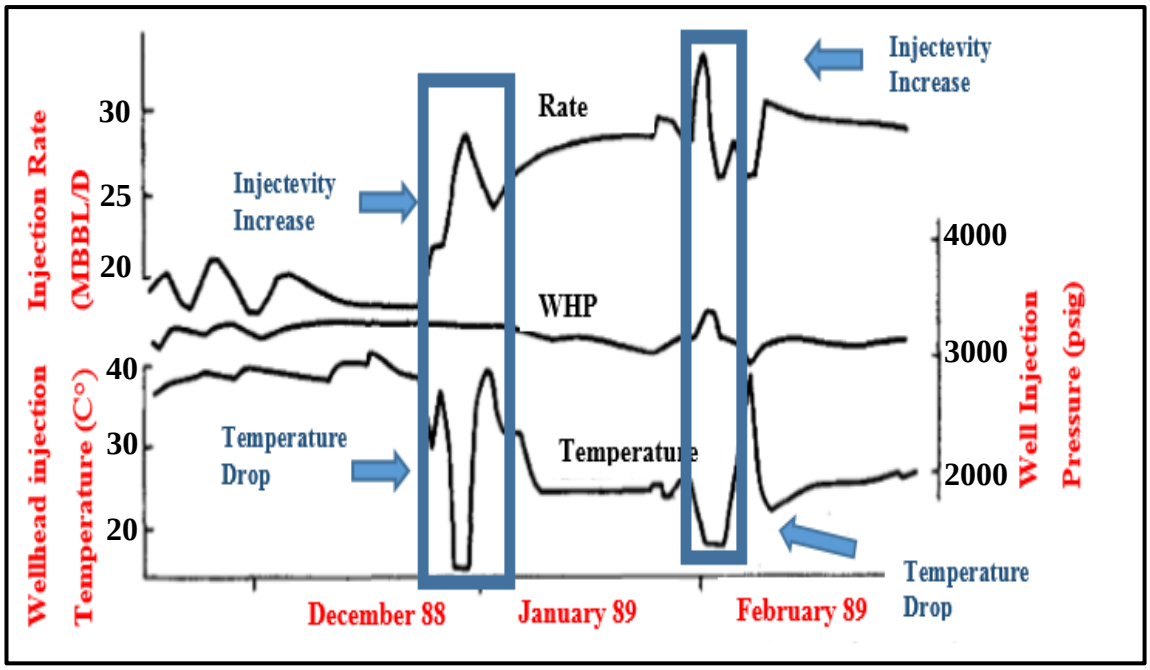

Figure 2-20: Injection data for a high-rate injector in the Ula field [7]

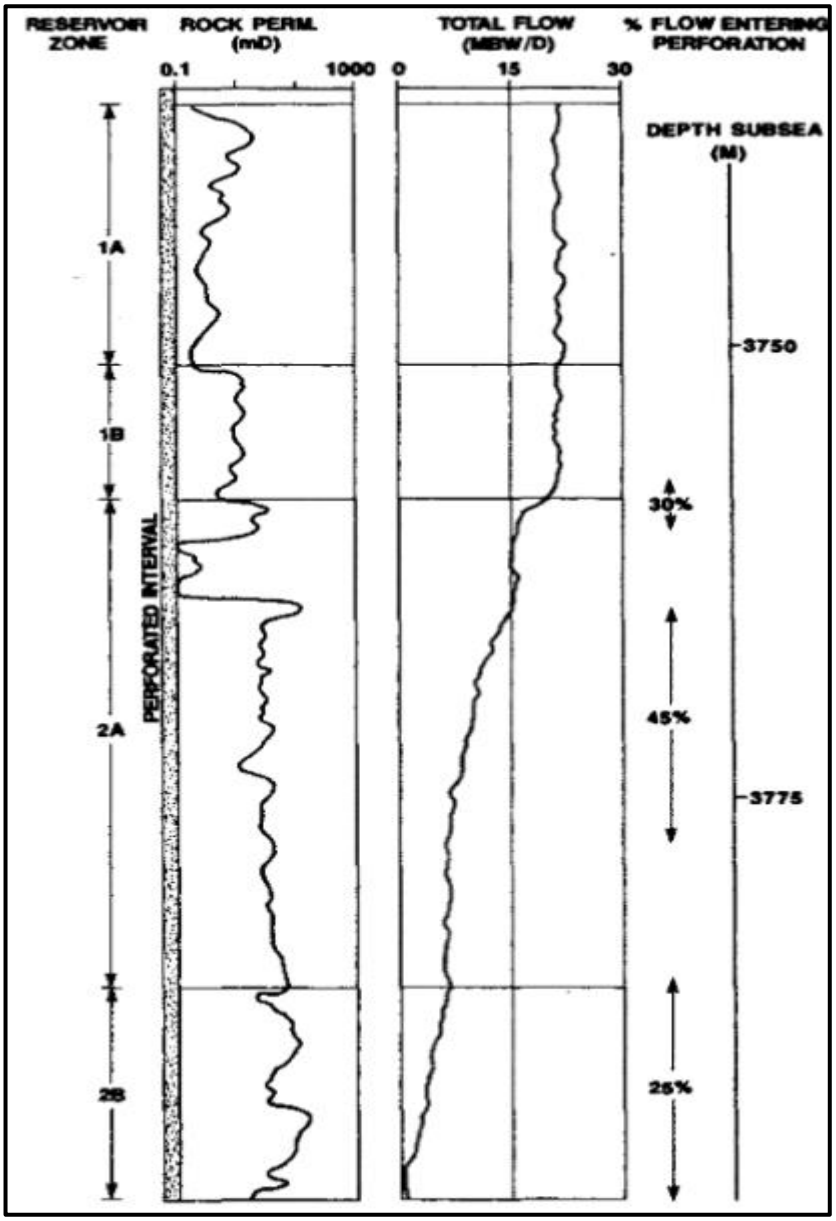

Figure 2-21: Flow profile and permeability for one of the injector [29]

TIF had a significant impact and improved the injectivity in this field. It was however decided by the operator to control the formation of TIF by modifying water temperature, injection pressure, and perforation policy to meet reservoir management requirements and avoid affecting the oil recovery. Water-quality specifications were relaxed by the operator because of the influence of TIF.

2.2.1.3 *Alwyn Field (North Sea)*

The Alwyn field is in the UK North Sea to the east of the Shetland Islands [5]. The reservoir is located below 3200 meters True Vertical Depth (TVD). The reservoir consists of two sandy formations i.e. Tarbet and Ness. The Tarbet itself is divided into

three sub-levels i.e. T1, T2, and T3. The formation average permeability is estimated at 43 mD from build-up tests. The reservoir temperature was 100^0 C (212^0 F).

A short term injection test was performed in one injector in the field to investigate the formation of TIF and validate a proposed numerical model. Both BHP and bottom hole temperature (BHT) were measured during the test. It was observed that the injectivity was constant up to 25 hours and then a sharp increase after that was noticed as shown in Figure 2-22. This sharp increase in injectivity corresponded to a decrease in BHP as shown in Figure 2-23. This sharp decrease in BHP was a sign of TIF opening in the formation since it will increase if it would have been hydraulic fractures This is further confirmed by the correlation between the injectivity and the BHT as shown in Figure 2-24. It can be noted for this figure that BHT decreased to 20^0 C (68^0 F).

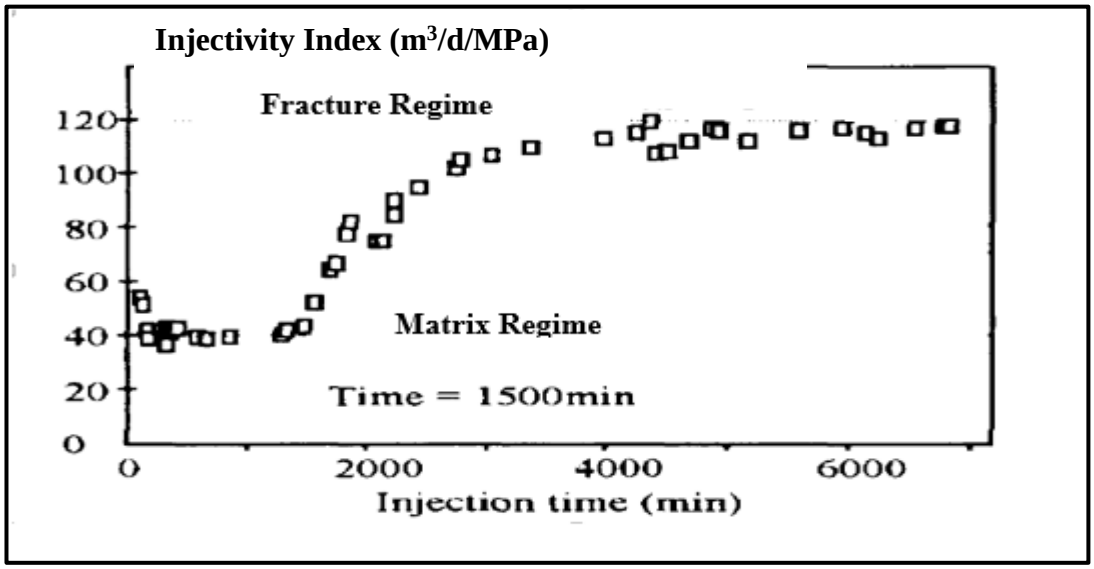

Figure 2-22: The injectivity index of one of the injector in the Alwyn field during short term injection test [5]

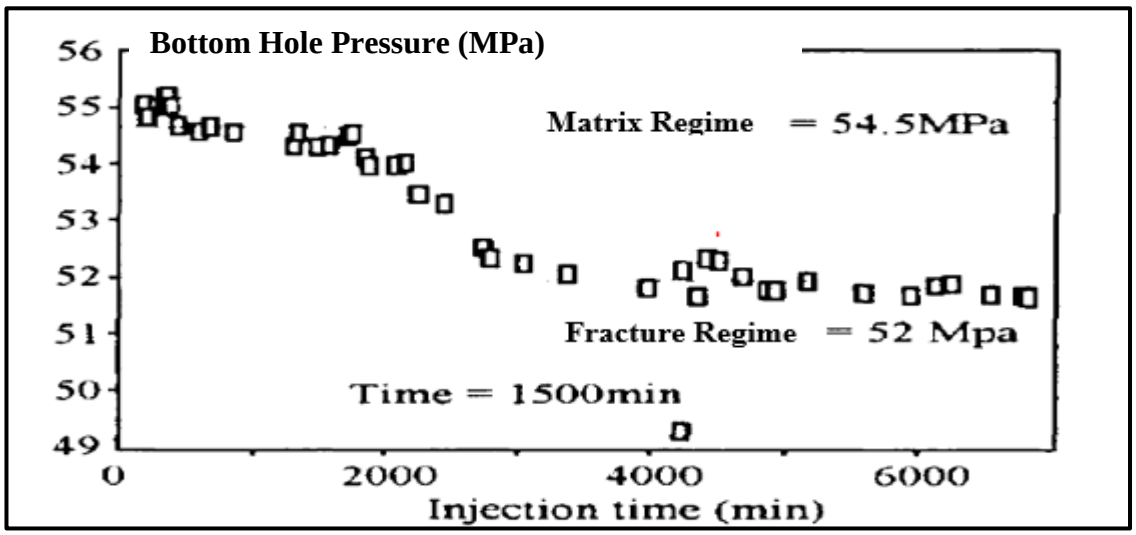

Figure 2-23: The measured BHP of one of the injector in the Alwyn field during short term injection test [5]

It was observed from the field data that 95% of the injected water was placed in Tarbet the T3 zone. This was expected to have a significant impact on the sweep efficiency. It was observed from modelling work that TIF height was different from the pay zone thickness and that the TIF may extend out-of-zone. These observations showed the impact of the presence of TIF on the injection performance of the Alwyn field [9]. This case study is discussed further in Chapter 5.

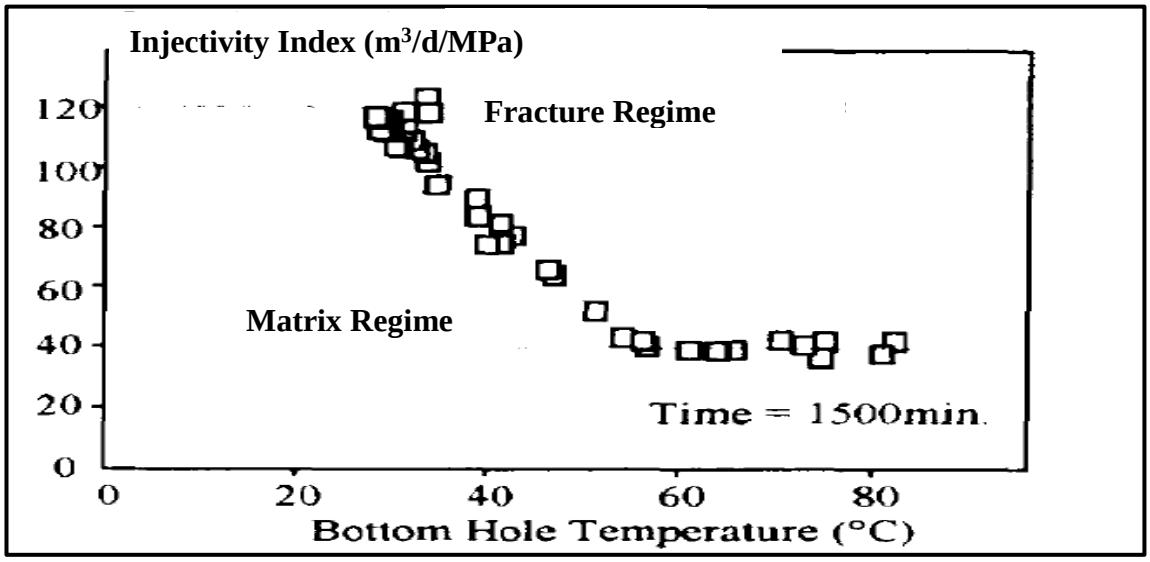

Figure 2-24: The measured BHT of one of the injector in the Alwyn field during short term injection test [5]

2.2.1.4 *A West African Field*

This reservoir is an offshore field located in West Africa [9] . The reservoir is approximately 4200 ft below the sea level with high reservoir temperature of 150 C^{o} (302 F^{o}). In this field, 10 injection wells had been injecting water for a period of 3 to 5 years prior to publishing this study.

It was observed for example in one of the injectors that there was a sudden increase in injection rate after 30 days at a constant Well Head Pressure (WHP) of 120 bar, as shown in Figure 2-25. The injection rate increased 10 fold from 200 m3/d to 2000 m3/d after 120 days as shown in the same figure. This significant increase was because of the propagation of TIF in the formation. The modelling work in this study showed that TIF propagated out-of-zone with a six fold increase in TIF height i.e.120 m form initial reservoir height 22 m.

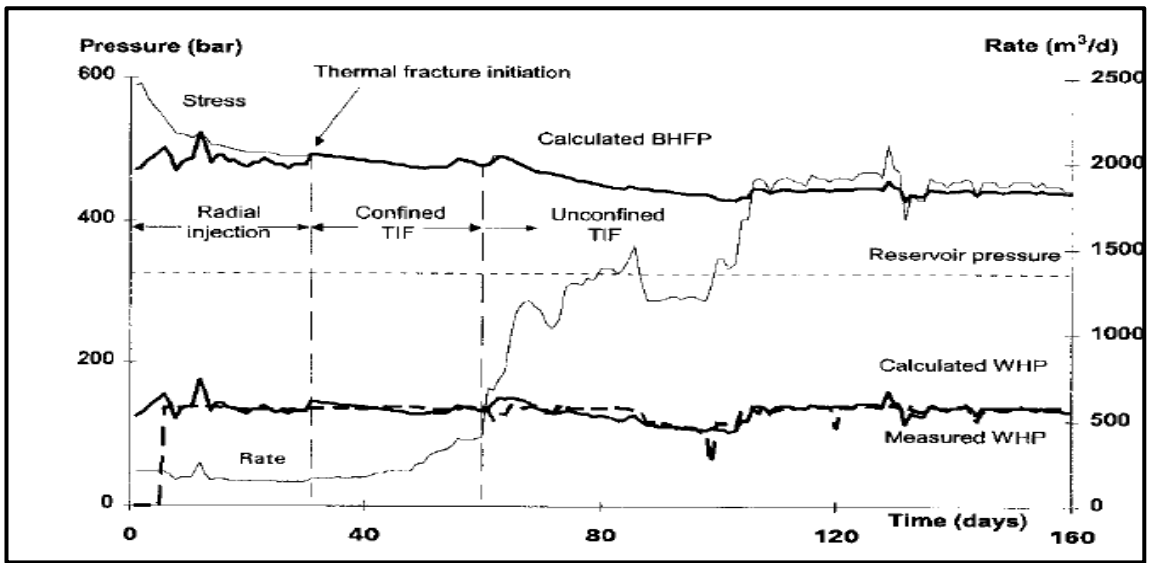

Figure 2-25: Historical BHP,WHP, and injection rate for one of the injection in the field [9]

This was further confirmed by temperature log of this injector as shown in Figure 2-26. It can be noted form this figure that the cooled zone had extended for a considerable distance above the perforated zone by 1989. This study did not discuss the impact of TIF on sweep efficiency and oil recovery, though, it is clear from the presented data that out-of-zone TIFs were observed which can be expected to affect the production and injection well's performance.

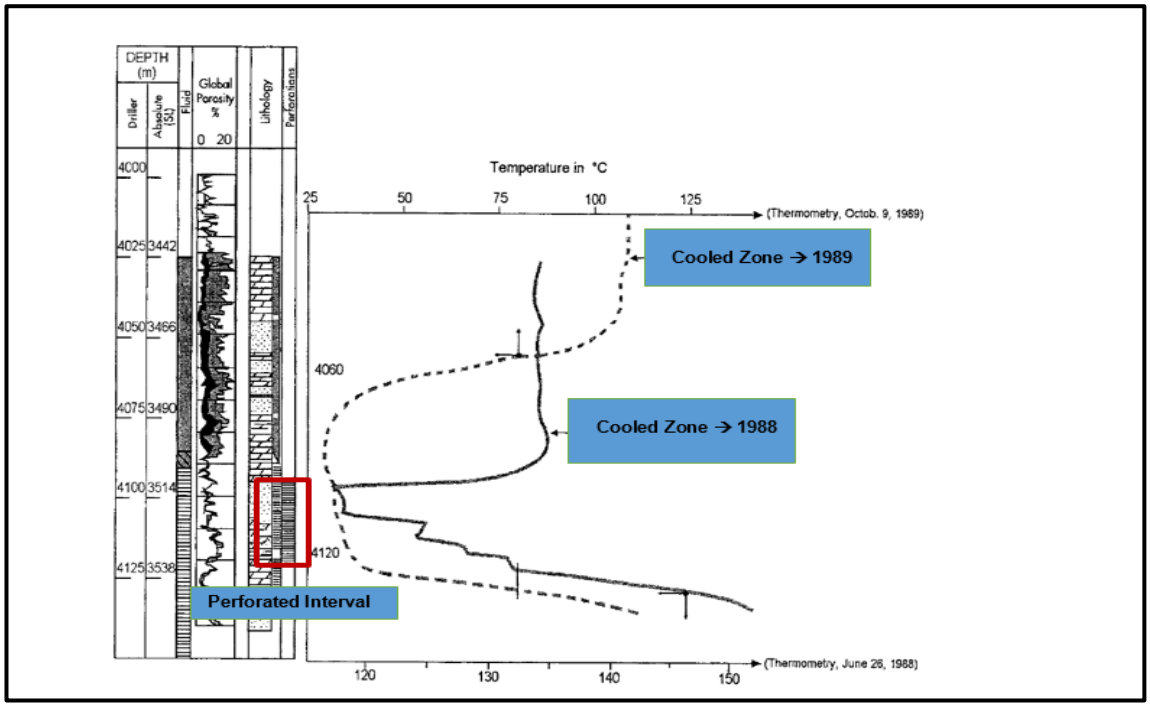

Figure 2-26: Temperature log in one of the injection well in the field ; at two different times [9]

2.2.2 TIF in non-Waterflooding applications

2.2.2.1 *Water disposal wells*

The purpose of disposal wells is to inject waste fluids in deep formations in an efficient and environmentally compliant manner. Disposal wells, similar to waterflooding injection wells used for pressure support and sweep efficiency, are subject to regulatory requirements to preserve the fresh water resources. The challenge in disposal wells is to maintain long-term high injectivity while avoiding fracturing above and/or below the target reservoir to avoid contamination of (potentially) usable aquifer. The following field studies review the impact of TIF on long term performance of disposal wells.

2.2.2.1.1 Mature Oilfields (Peru)

These fields are located in the Amazon rainforest in Peru. They were discovered between 1971 and 1980 with production starting in 1973 [30]. The formation consists of sandstone with a thickness between 10 m and 130 m thick and with a permeability between 0.5 to 5 D. The reservoir temperature is between 196^0 F and 238^0 F. The fields have a very high water cut, up to 96 %. The high volume of PW problem needs to be dealt with by the operator. It was decided to convert production wells with a 99% water cut into disposal wells for reinjection of PW. A study conducted [30] on these fields presented the field developments and experiences obtained during the first two years. The main concern was to maintain long term high injectivity despite the poor water quality.

During initial period, two injection tests were performed to evaluate the injectivity in water disposal wells. The first Step-Rate Test (SRT) was performed with water injection temperature varies between 190^0 F and 230^0 F whereas the second SRT was performed with water injection temperature varies between 150^0 F and 170^0 F (Figure 2-27). These tests showed that the same injection rates can be achieved at lower BHP with lower temperature water injection due to TIF formation. The SRTs indicated that all disposal wells were injecting under fracture gradient conditions. It was also observed within the two years that the injection rates increased while the Well Head Pressure (WHP) was almost constant (Figure 2-28).

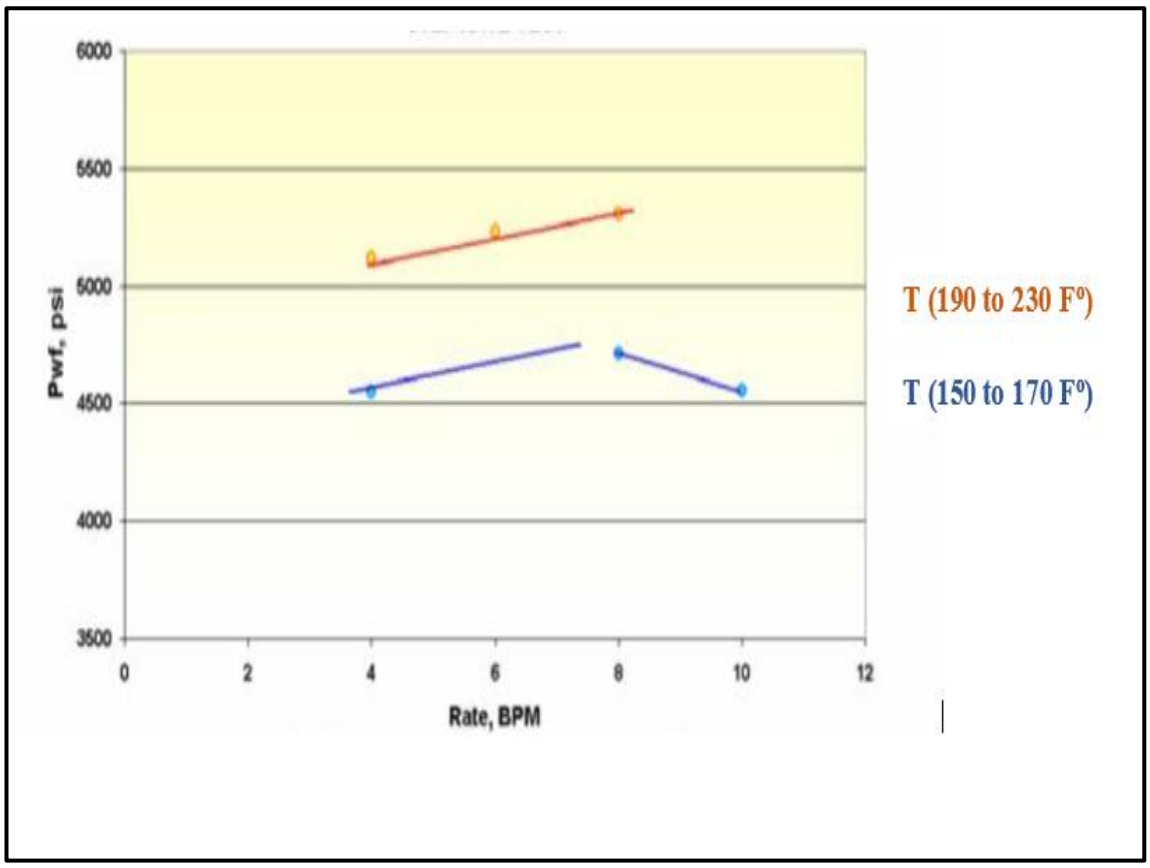

Figure 2-27: Interpretation of SRT for one injection well [30]

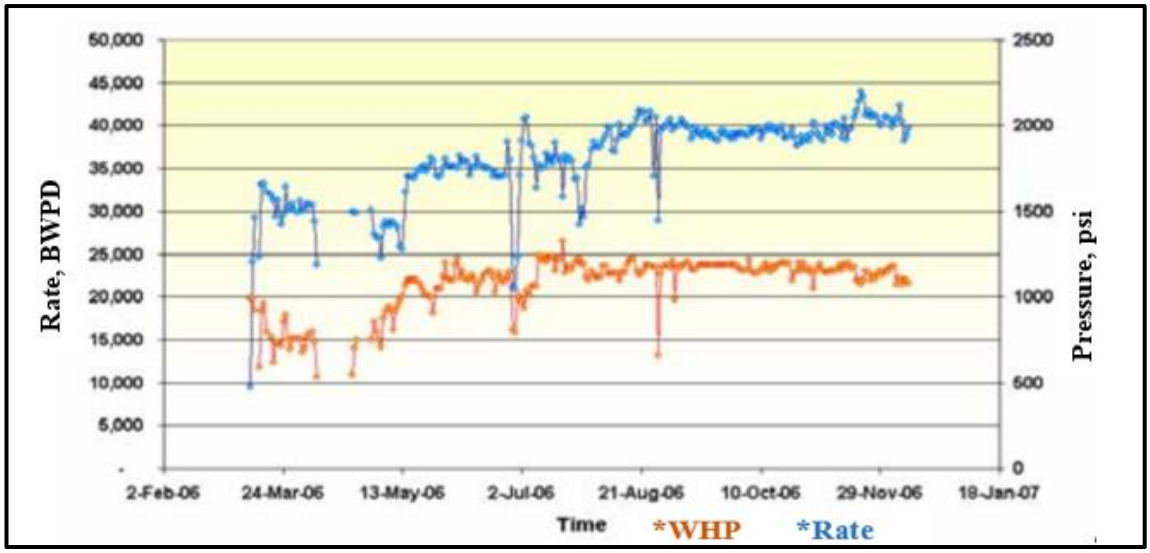

Figure 2-28: Injection history (WHP and injection rate) for one injection well [30]

Production logging showed that more than 80% of the injected water was being injected into the top interval confirming TIF formation (Figure 2-29). TIF enabled the operator to inject 100% of the PW into the subsurface at relatively low WHP under fracturing conditions. The reinjected PW entered deep reservoirs with good upper and lower shale layers that confined the TIFs, ensuring they did not extend out of zones and

affect any fresh water sources. The positive impact of TIF on disposal well performance was clearly demonstrated in this study. The TIF significantly improved the injectivity of the disposal wells, reducing the capital costs required for drilling new disposal wells.

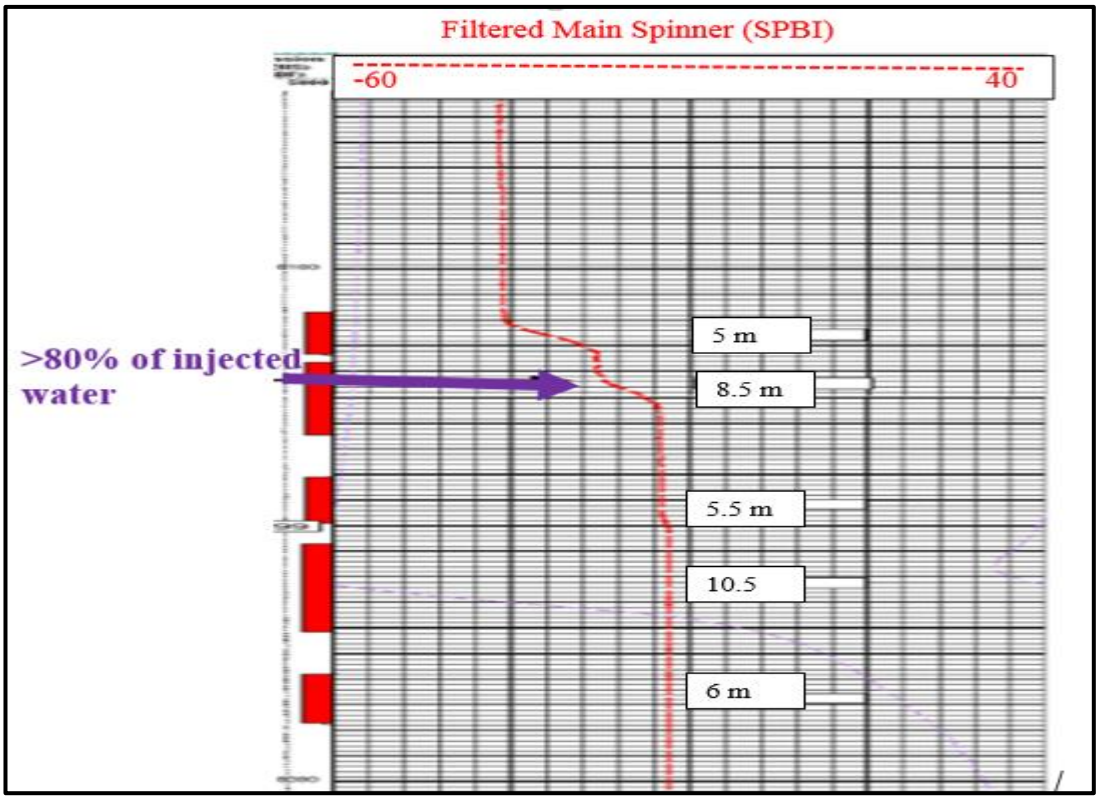

Figure 2-29: Production log shows > 80 % injection into the top intervals [30]

2.2.2.1.2 The Villano field (Ecuador)

This field is located in a rainforest in East of Ecuador [27]. The field was discovered in 1992 and the production started in 1999. The field has good formation characteristics with a permeability between 0.5 mD and 2 D. The field has a strong water aquifer, allowing pressure to be maintained all times by reinjecting the PW. The water management plan was required to dispose of the high amounts of PW i.e. Water-Oil Ratio (WOR) would be as high as 4:1. Three disposal wells were located in the Villano field to reinject the PW. The study [27] focused on the impact of TIF on the injectivity of the Villano field. The temperature of the Villano formation was 215^0 F.

TIF and its impact in injection well performance was initially a surprise, but was later utilised to further improve the well injectivity. In August 2012, the operator decided to install an Air-cooler to reduce the steam emission from the produced water tanks. The Air-cooler system reduced the PW temperature from 210 to 190^0 F (Figure 2-30). This 20% of temperature reduction was performed on three disposal wells on the field i.e. V-9, V-12, V-21. This triggered TIF and improved the injectivity in the three injection wells (V-9, V-12, and V-21) (Figure 2-31). The increase in injection rates correspond to the

reduction of the WHP and the temperature. This clear sign of TIF increased the injection rate by 25,0000 BWPD [27].

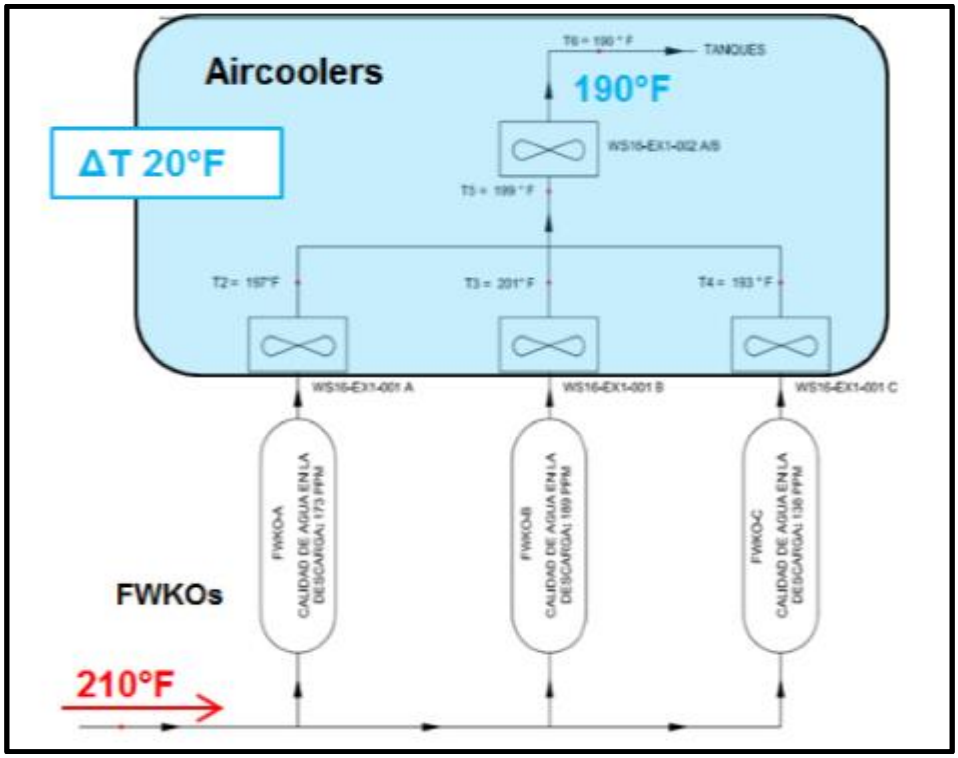

Figure 2-30: First Air-cooler system installed to reduce the PW temperature for steam emissions reduction [27]

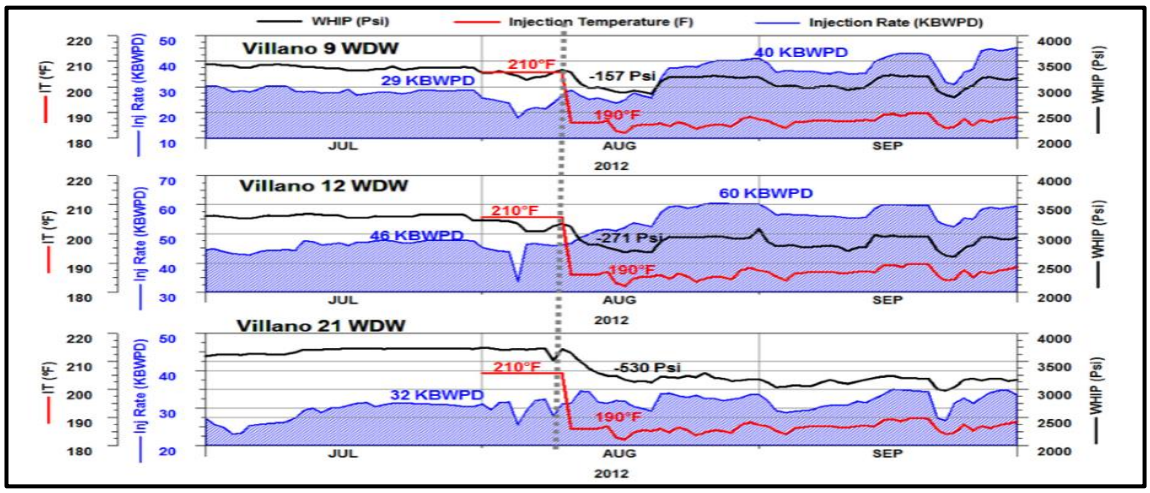

Figure 2-31: TIF impact on disposal wells in the Villano field in 2012 after installing Air-cooler system [27]

After achieving this good result, an extra Air-cooler system was added on December 2013. The objective here was to further improve the injectivty rather than reduce the steam emissions. The additional Air-cooler system reduced the temperature by further 10^0 F to 180^0 F (Figure 2-32) with an additional 9,000 BWPD being injected (Figure 2-33). TIF formation due to temperature reduction thus had a significant positive

impact on disposal wells performance in the Villano field. Figure 2-34 shows the significant increase in the injectivity index for both TIF events (August 2012 and December 2013).

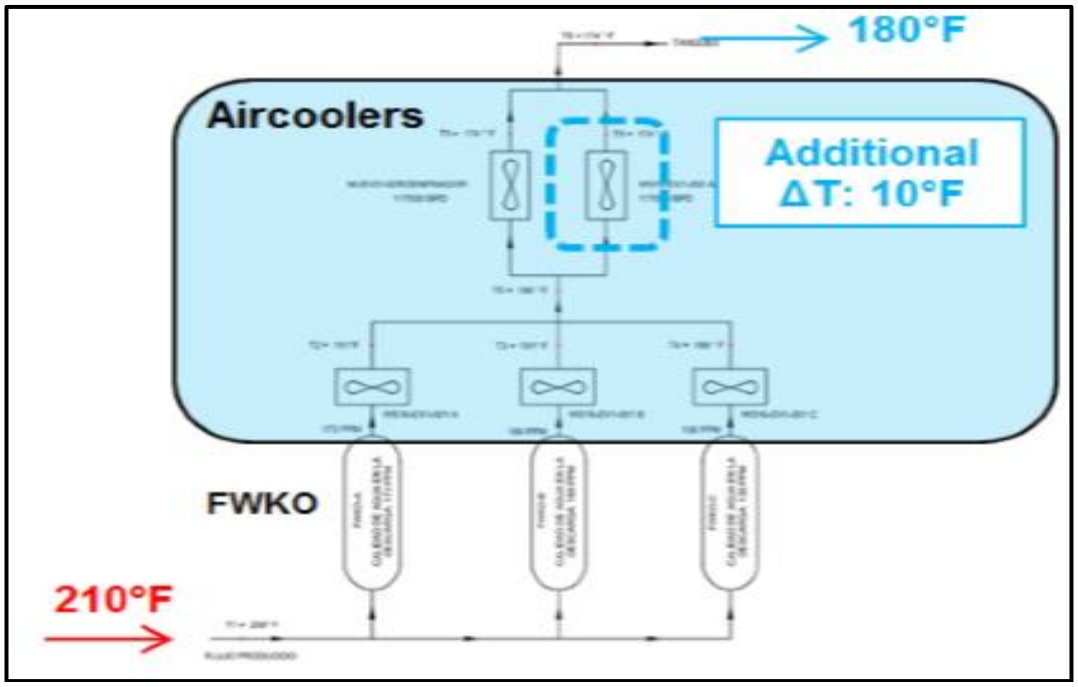

Figure 2-32: Additional Air-cooler system installed to reduce the PW temperature for injectivity improvment [27]

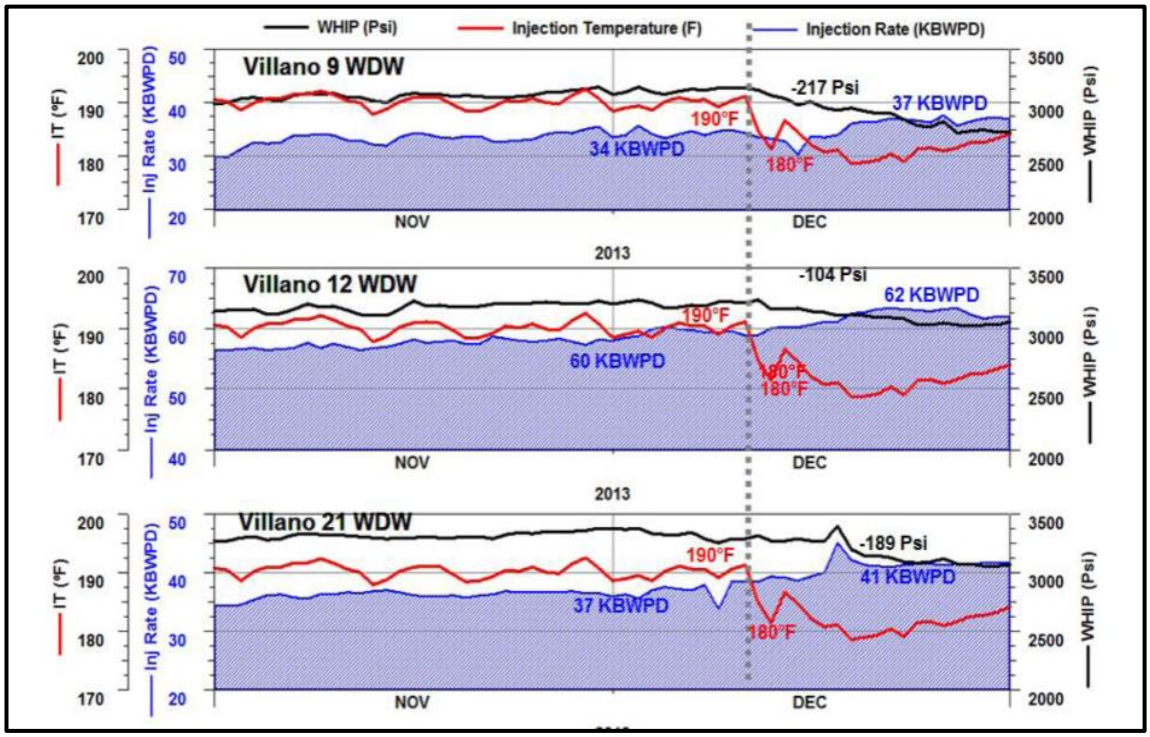

Figure 2-33: TIF impact on disposal wells in the Villano field in 2013 after installing additional Air-cooler system [27]

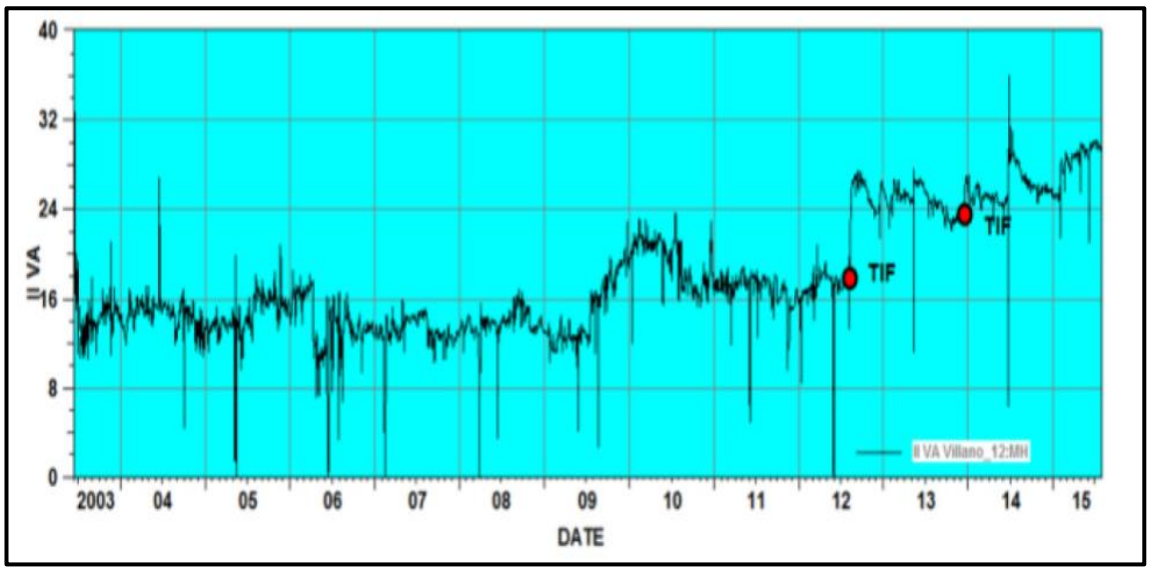

Figure 2-34: Historical plot of the injectivty index [27]

2.2.2.2 *Geologic CO_2 Sequestration*

Geologic CO2 Sequestration (GCS) is one of the technologies that inject greenhouse emission produced by various industries. GCS projects for CO2 storage can also be used in some [31] fields for enhanced oil recovery [31-33] (Figure 2-35). The successful implementation of such projects depends on the long term injectivity, carbon storage security, caprock integrity and low cost operations [34, 32, 33]. Literatures cover various studies that looked into the thermal aspect and TIF impact in GCS projects.

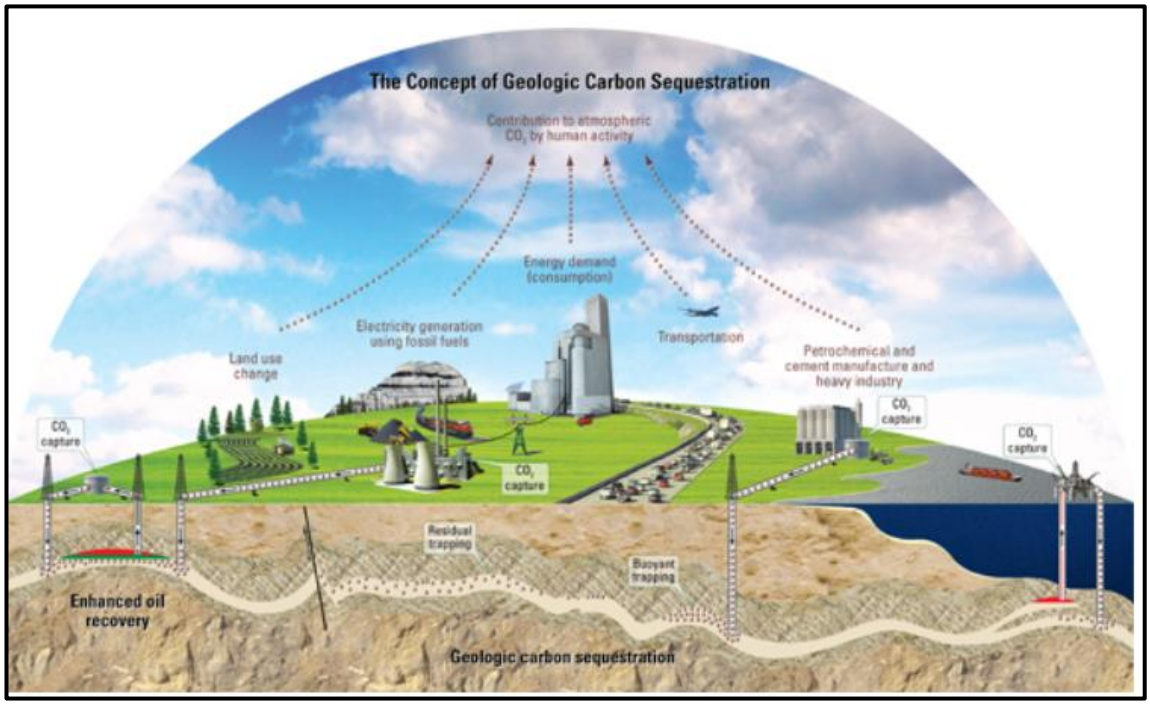

Figure 2-35: Illustration of the concept of GCS [31]

2.2.2.2.1 Cranfield (USA)

Cranfield is located in Mississippi, USA and was active between 1943 and 1966 [32]. CO_2 injection project started in 2008 for carbon storage as well as for enhanced oil recovery (EOR). The injection interval has an average permeability of 64 mD and an initial reservoir temperature of 122^0 C (252^0 F). The injection interval is in a deep-brine aquifer. Three wells, one injection well (31F-1) two observation wells (31F-2 and 31F-2) were drilled, as shown in Figure 2-36.

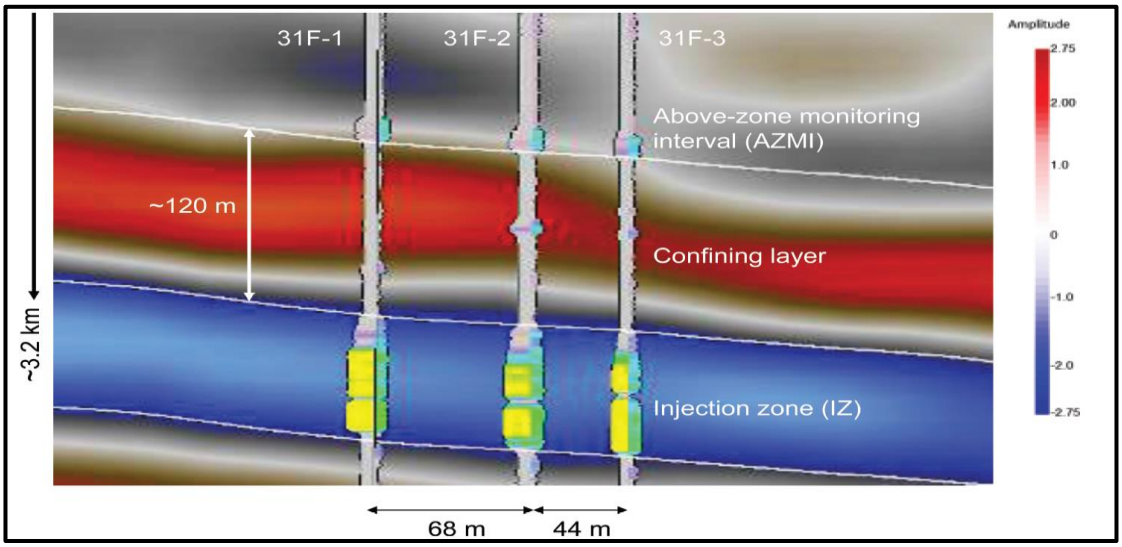

Figure 2-36: One injection well (31F-1) and two observation wells (31F-2 and 31F-3)[32]

The motivation of this study was to observe the increase in reservoir pressure of the above-zone (Figure 2-36). It was observed that the measured reservoir pressure of the above-zone monitoring interval increased (Figure 2-37), raising concern of undesirable migration of CO_2 from the injection zone. The initial injection rate was 175 kg/min (252 m^3/d), increasing to 350 kg/min (504 m^3/d) and later to 520 kg/min (750 m^3/d) after 150 days (Figure 2-38). This figure shows that these increases in injection rates are well correlated to the temperature reduction with only slight change in the BHP. The increase in injection rate was due to TIF formation. There was an uncertainty regarding the reason for reservoir pressure increase in the monitroring zone. The migration of brine water through the injection interval along the well could be the reason. Further geomechanical analysis was needed to identify whether TIF connected the injection zone with the above zone. More sophisticated gauges were recommended for monitoring the above-zone interval in any future tests.

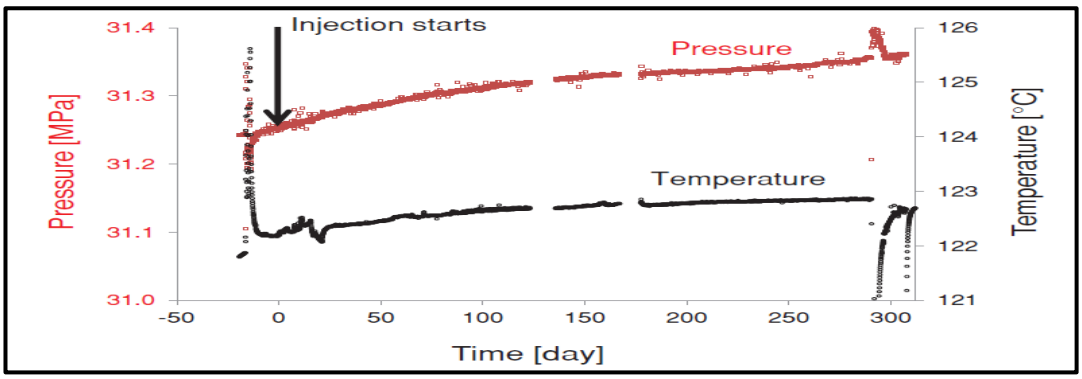

Figure 2-37: Measured BHP and BHT from observation well (32F-2)[32]

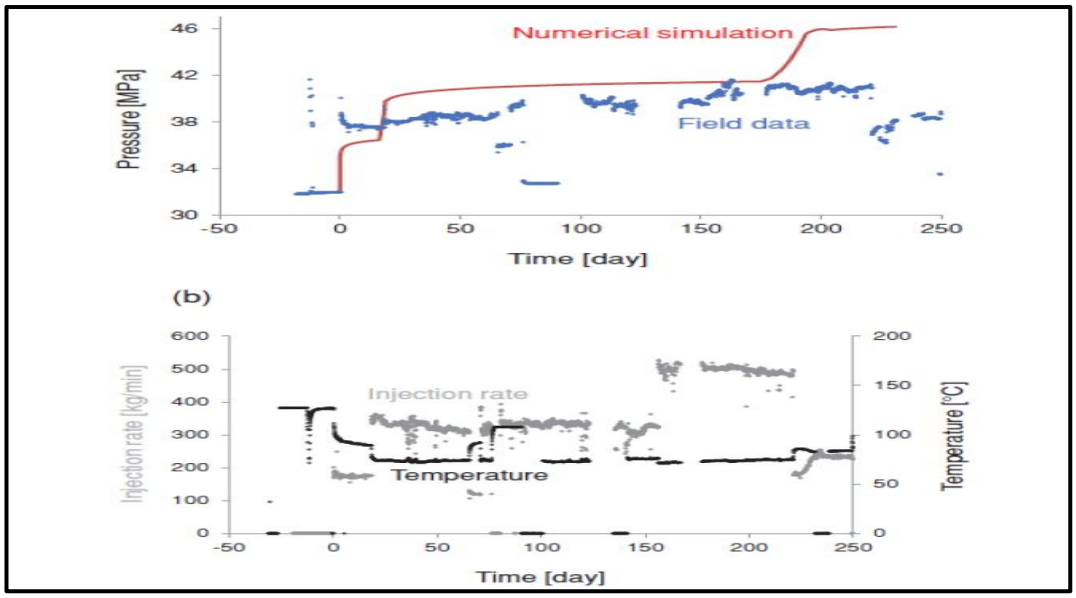

Figure 2-38: Measured injection BHP and BHT in the injection well (31F-1)[32, 33]

2.2.3 Sand Production

The sand production in production wells has been studied and reported extensively in the literature [35-39]. However, few discussions of sanding problems have been reported in water injection wells [40-42]. Injection wells can be the worst sand producers as it is not possible to transport or remove the produced sand [43] . Sand production is caused by rock failure as result of either hammer effect or back-production in injection wells.

Oyeneyin [44] indicated that TIF due to water injection cooling is one of the induced causes of sand production in injection wells especially in High pressure-High Temperate environments. Tovar et al [43] concluded that temperature decrease due to cold water injection has a significant impact on the strength of sandstone reservoirs. Sand production is hence expected to occur at lower pressures for hammer effect and at lower drawdowns for back flow because of the TIF and cooling effect in water injection wells.

Results of a study regarding the impact of sandstone strength's behaviour as a result of temperature changes in water injectors is discussed to emphasise how the cooling of the rock affects the formation mechanical properties. The Forestal Field is located in northern Peru [43]. The main reservoir found at ~ 9100 ft below sea level and composed of five high permeability (0.4-3 D) and high porosity sandstones. The net thickness of the reservoir is ~ 36 ft. In this study, the focus was not on the impact of TIF on the reservoir performance but on the effect of cooling on the strength of reservoir rocks [43]. The effect of temperature changes on the mechanical properties were investigated in this study to evaluate possible sand production during shut-in of the water injectors, but did not account for the water hammer effect. An extensive core testing program was developed to assess the effects of temperature changes on rock strength for various reservoir cores.

The modelling and core test data showed that the rock strength and the cooling were related. It was observed that temperature difference is inversely proportional to rock strength, as shown in Figure 2-39. The modelling work indicated that the sand production may take place earlier than predicted due to the cooling effect. It was recommended to initiate sand control methods earlier than originally planned. It was also observed that a lower drawdown pressure was needed to produce sand when the formation around the injector was cooler (Figure 2-40). It was recommended to apply a lower pressure drawdown if it was required to produce an injector so as to avoid sand production.

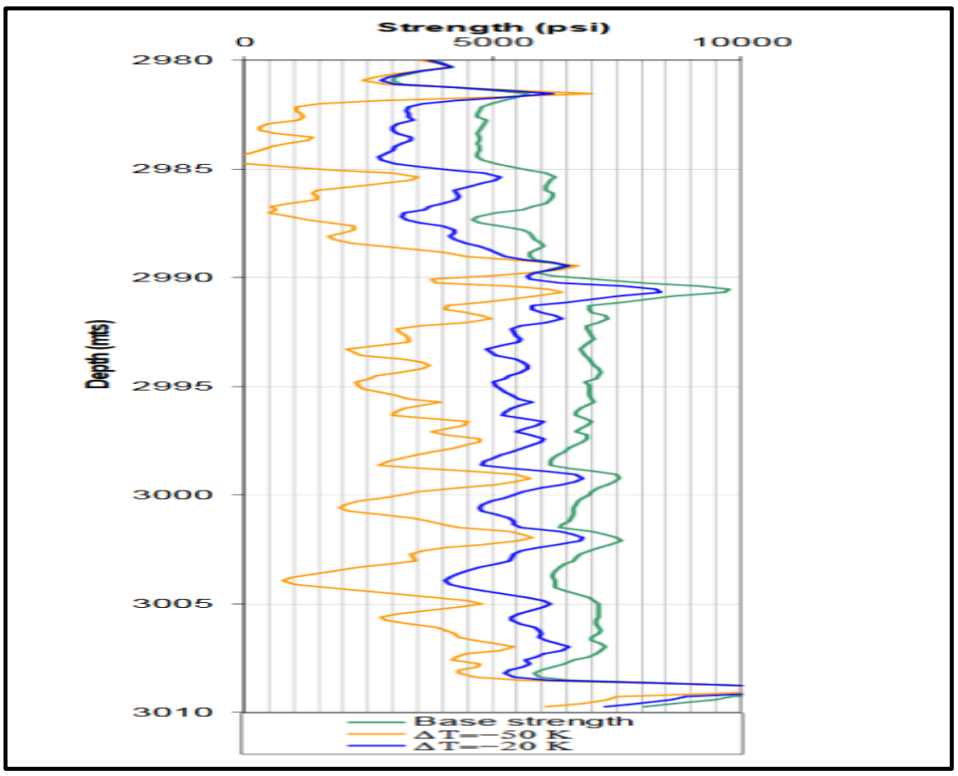

Figure 2-39: Change in formation strength as a function of temperature for the Forestal Field [43]

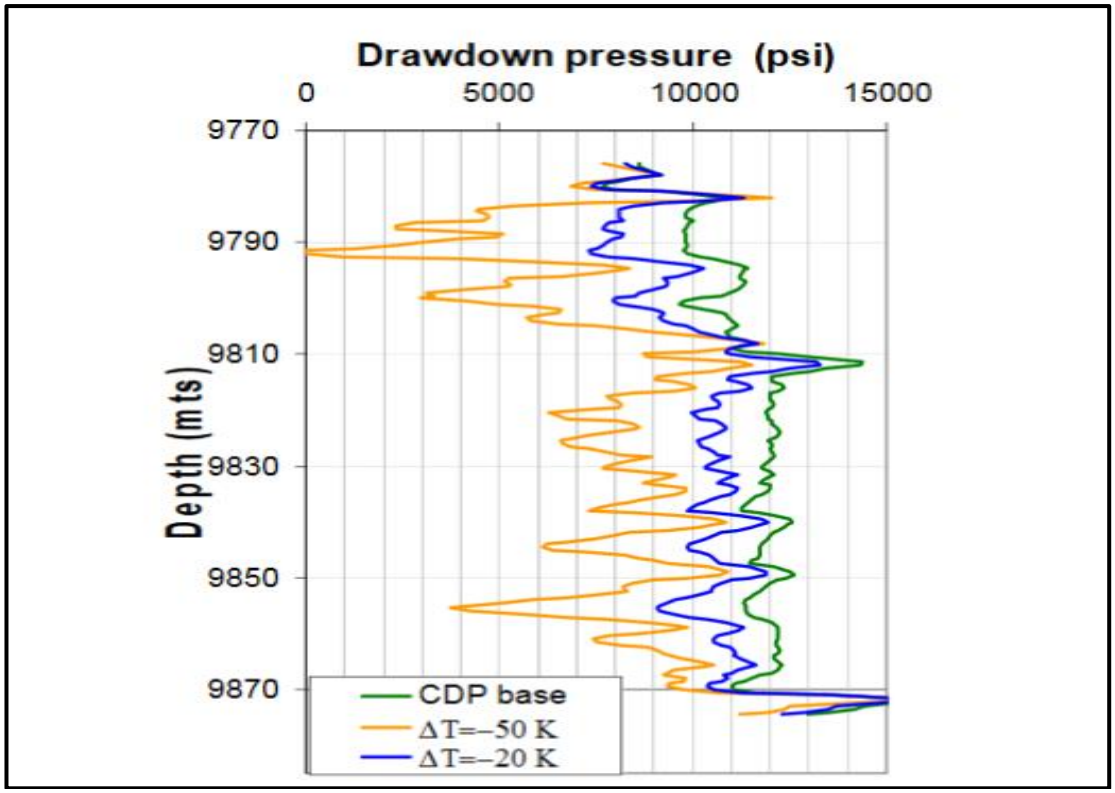

Figure 2-40: Critical Drawdown Pressure (CDP) during flow back as a function of temperature for the Forestal Field [43]

2.3 Advanced Well Completions

2.3.1 Introduction

Technology Developments in the drilling and completion in the oil industry enabled many operators to drill long horizontal and multilateral wells. The advantages of maximum reservoir contact (MRC) wells are well known. MRC wells increase the productivity index, reduce water and gas coning due to reduction in pressure drawdown, and give larger and more efficient drainage and hence more oil recovery [45-47]. However, these benefits come with challenges that need to be dealt with since maximising the reservoir contact does not ensure by itself a more uniform, thorough sweep of the reservoir. Reservoir heterogeneity with variable rock and fluid properties causes non-uniform inflow/outflow along horizontal and MRC wells which results in early breakthrough of unwanted fluid e.g. water and gas. Friction pressure loss along horizontal and MRC wells caused by fluid flow in the wellbore further results in a higher pressure drawdown in the heel of the well due to this Heel-to-Toe effect (HTE). HTE is the drive for water and/or gas coning in the heel section of a horizontal well in a homogeneous reservoir. Furthermore, horizontal and MRC wells have data gathering difficulties and

expensive logging tools and methods. These are only a few of the challenges faced by horizontal and MRC wells. These challenges need to be addressed from both the inflow control side as well as from the real-time monitoring side.

Advanced Well Completion (AWC) and Intelligent Well (IW) are the terms used to describe a completion system that combines permanent monitoring instrumentation, e.g. temperature and pressure gauges, and Flow Control e.g. Inflow Control Devices (ICDs) and Inflow Control Valves (ICVs). This system enables the operator not only to collect and transmit gathered data from downhole monitoring gauges, but also to control the well inflow and enhance reservoir performance. Figure 2-41 is an illustration of AWC, multi-zone well with ICD, ICV, packers, and a permanent downhole monitoring systems.

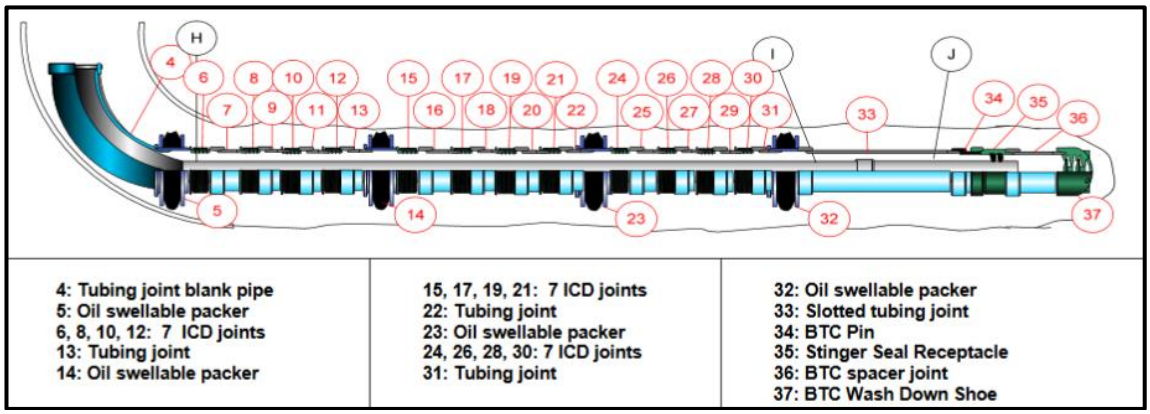

Figure 2-41: An example of a multi-zone, AWC [48]

AWCs include components such as ICDs, ICVs, Autonomous Flow Control Devices (AFCDs), and Annular Flow Isolation (AFI). AFI is a crucial component of AWC to minimise, or prevent annular flow (Figure 2-42). AFI installation segments the wellbore into compartments. This is often a necessity for ensuring the success of an AWC. The components of AWCs will be discussed in detail later.

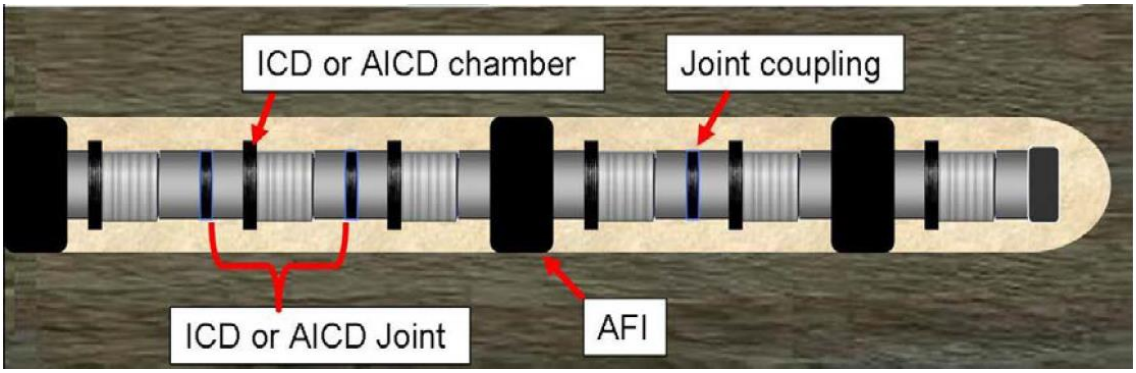

Figure 2-42 :(A) ICD and AFI wellbore placement [49]

AWCs applications in the oil industry are mainly driven by [50]:

I. Increasing ultimate recovery
II. Reducing the surface facilities

III. Reducing well cost

IV. Accelerating oil production

V. Reducing the well intervention cost

Figure 2-43 indicates AWCs business drivers and value contribution for an IW evaluated in the Norwegian oil industry.

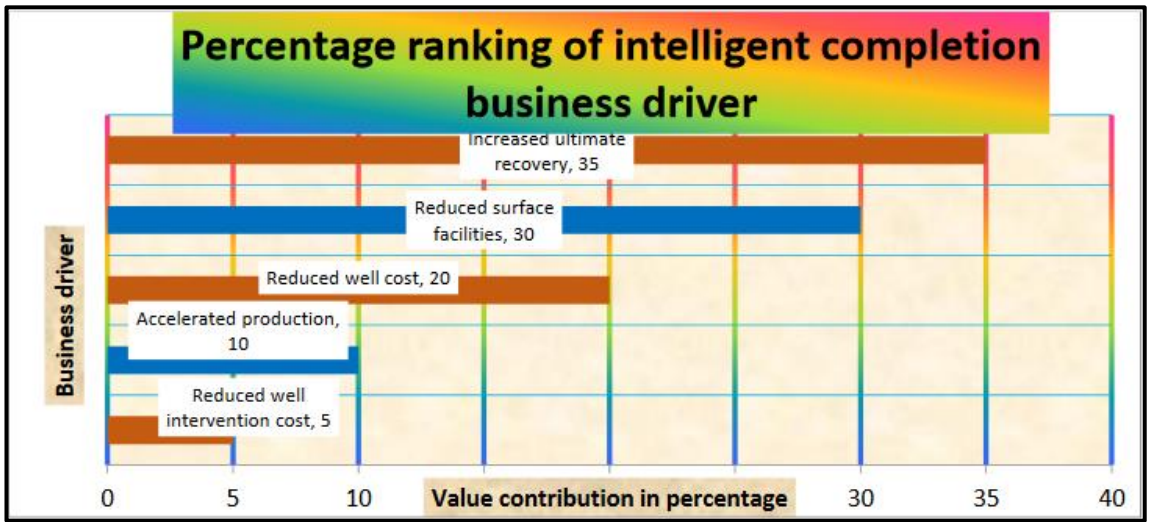

Figure 2-43: Advanced well completion business drivers to the Norwegian oil industry [50]

Downhole monitoring, an important aspect of AWCs, provides a real time evaluation of the wellbore and/or reservoir, reducing the need for expensive logging and related production shutdowns. An integrated framework of control and monitoring offers the advantage of faster decision making and respond to dynamic changing reservoir in real time [51, 52]. Downhole monitoring systems and their application will not be discussed further as they are out of the scope of this thesis.

2.3.2 Advanced Well Completion Components

AWCs have been installed since mid-1990's when the technology was first introduced. Downhole Flow Control (DFCs) ranging from passive (fixed) to active were applied in many oil fields for tackling different challenges. Their applications were proven to be beneficial with many reports of their successful applications to the development and optimisation of many fields around the world [53-56]. The key components of AWC are the following:

I. Inflow Control Device (ICD)

II. Interval Control Valve (ICV)

III. Autonomous Flow Control Device (AFCD)

IV. Annular Flow Isolation (AFI)

To-date FCDs are available in many different types, designs, and configurations (Figure 2-44). ICDs and their application will be emphasised in this thesis since they are the focus of this study.

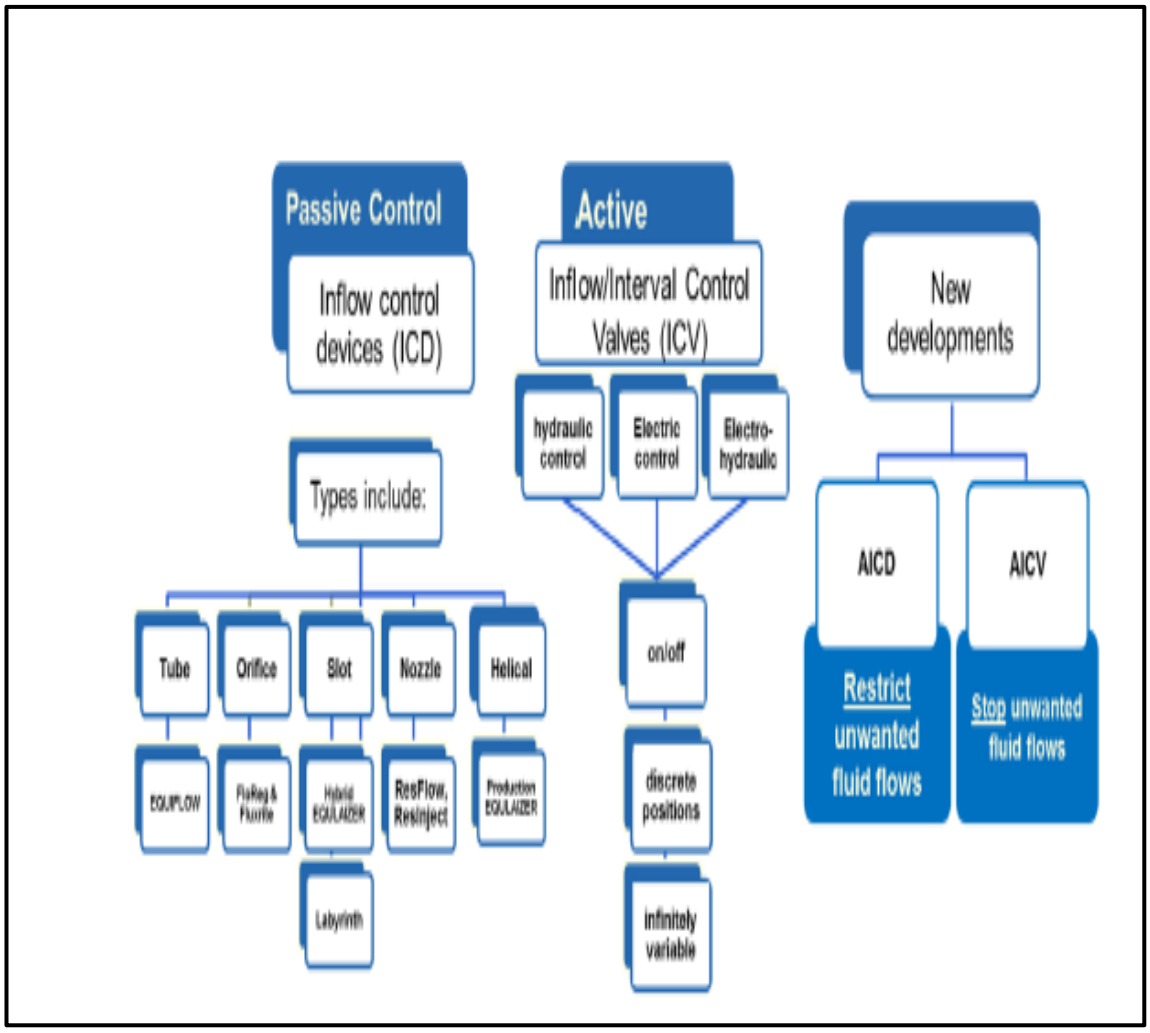

Figure 2-44: Types of FCDs including new developments [2]

2.3.3 Inflow Control Devises (ICDs)

2.3.3.1 *Background and Overview*

ICD technology was introduced initially by Norsk Hydro in mid-1990's in Troll oil field [57]. Troll field is located offshore Norway. The oil province of the Troll field contains a thin oil column of 4 m to 26 m sandwiched between a large gas cap and an active aquifer. This oil rim is located in high-quality sands with permeabilities between 3 D to 10 D. The first application of AWC was in a 500 m long horizontal well drilled in 1989. This well (partially) overcame the gas coning limitations associated with conventional vertical wells. Well tests showed a productivity of 5 to 10 times greater than that of an equivalent vertical well in the same field [58]. However, it was observed that 75 % of the inflow arrived at the first half of the completed interval i.e. near the heel

of the well. The pressure loss along the horizontal well caused the BHP to decrease in the heel of the well which results in a higher drawdown and flow rate. This is known as the Heel-Toe effect (HTE) (Figure 2-45). HTE is significant in long horizontal wells since it will cause an early breakthrough of water and/or gas at the heel and reduce the oil recovery (Figure 2-46).

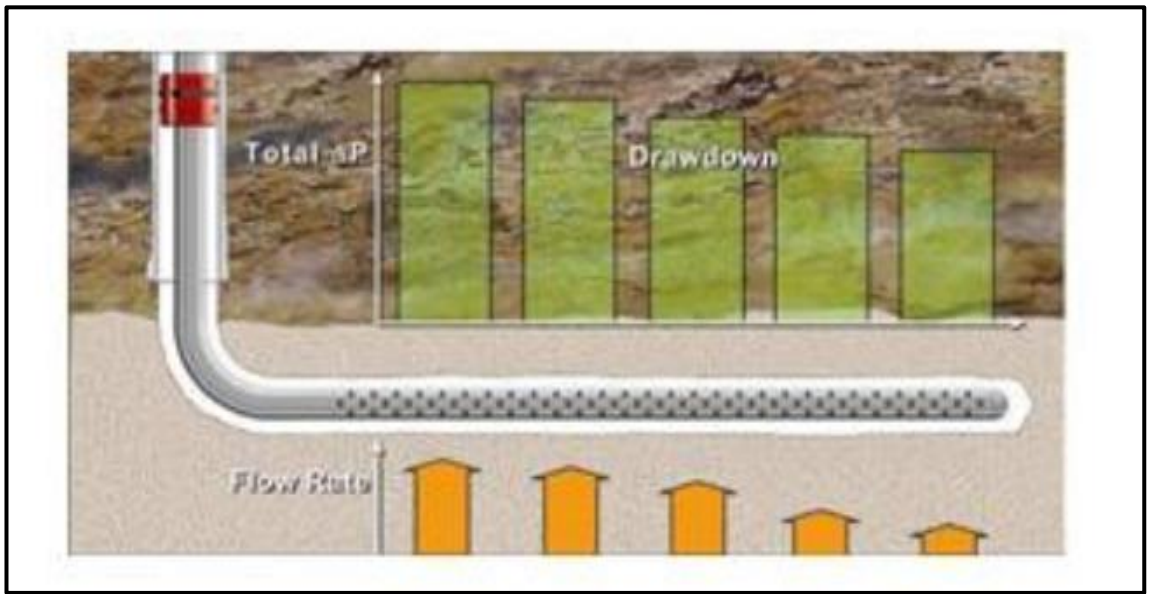

Figure 2-45: Higher drawdown and flow rate the heel of the well due to HTE (Courtesy of Halliburton)

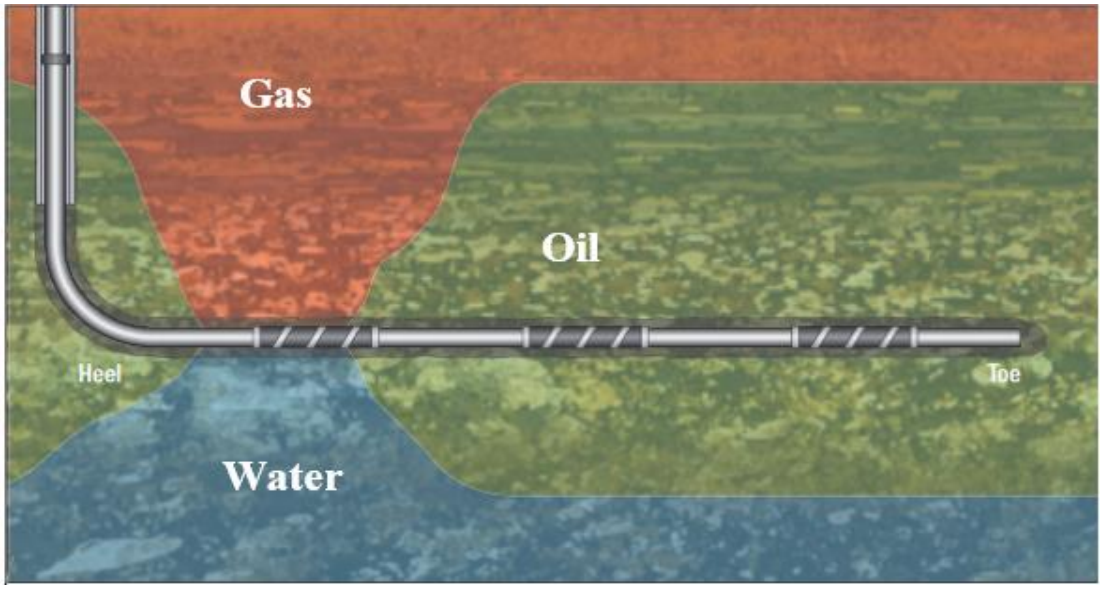

Figure 2-46:Water breakthrough at the heel of the well (Courtesy of Schlumberger)

Optimising the well completion design was necessary to maintain higher production rates for proposed horizontal wells as part of a new development plan. Three options were proposed to overcome the problem of HTE based on three principals [57]:

I. Reducing the specific productivity index (bopd/m of completion) towards the heel of the well by reducing the perforation density

- A variable perforation density design (Figure 2-47)

II. Redistribution of the pressure loss along the horizontal section of the well through changing the direction of the inflow

- A Stringer completion design (Figure 2-48)

III. Creating an optimal pressure profile along the horizontal section of the well by introducing inflow control along the wellbore

- A passive Inflow Control Device (Figure 2-49)

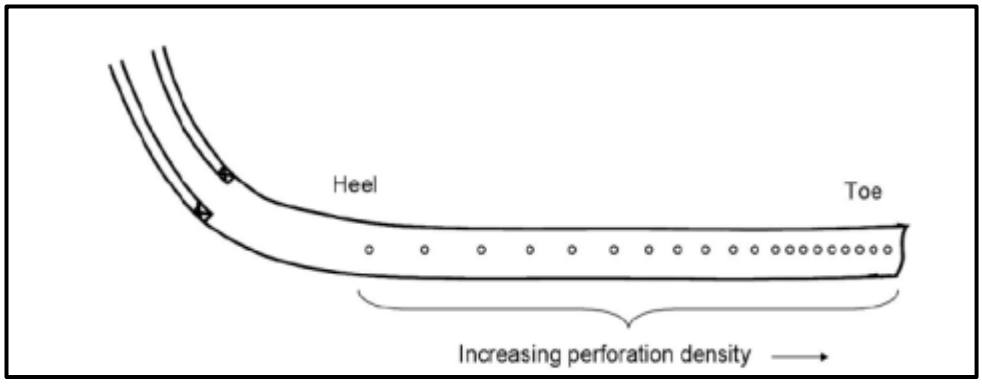

Figure 2-47: Variable perforation density design [49]

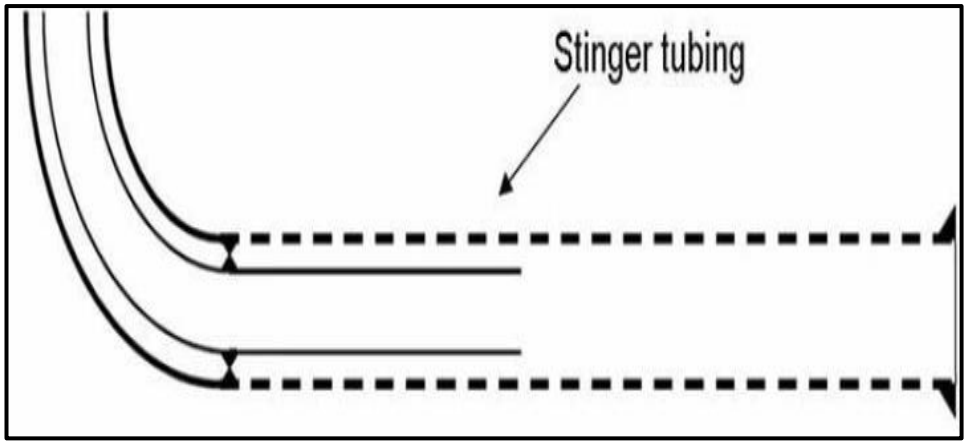

Figure 2-48: A passive stinger completion [49]

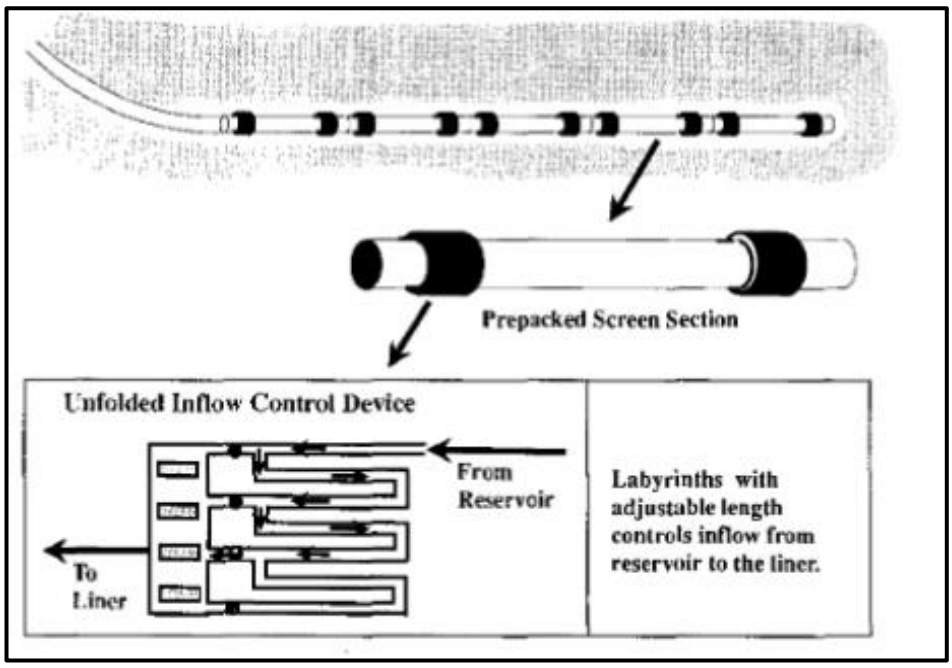

Figure 2-49: Schematic of proposed Inflow Control Device

The original Inflow Control Device (ICD) design had labyrinth channels with adjustable length and diameter installed in a prepacked liner mounted in a solid base pipe (Figure 2-49). The fluids passes from the reservoir to the liner through the screen and the channels of the ICDs. The flexibility of adjusting the labyrinth channels allows an effective and stable control of the inflow to the liner.

Simulation results showed that the use of a variable perforation density design and a stinger completion design provided up to 25% increase in the productivity index of the well during early time of the production. By contrast, the ICD design provides up to 66% increase in the well productivity [57]. It was concluded that the ICD gave the best performance, and most importantly, was a practical solution.

2.3.3.2 *ICDs Types*

ICD technology suppliers (Tejas, Baker Oil Tools, Easywell Solutions-Halliburton, Reslink-Schlumberger, Flotech and Weatherford) have developed different ICD designs using various mechanisms to create a pressure drop across the device. ICDs can either be mounted in a Stand Alone Screen (SAS) in unconsolidated reservoirs (to reduce the risk of erosion and plugging) or they can be combined with debris filter in consolidated reservoirs (to prevent blockage of the flow restriction) [49]. All ICD types use the same principle of creating a pressure drop that restricts the flow. The fluid inflow comes from the formation and passes through the screen. The fluid then passes through the flow conduit between the screen and the base pipe. Finally, the fluid flows through

the ICD restriction into the base pipe (Figure 2-50). Similar flow paths are found in most of the ICD types. It is reversed for injection wells. The following provides details of the current ICD types.

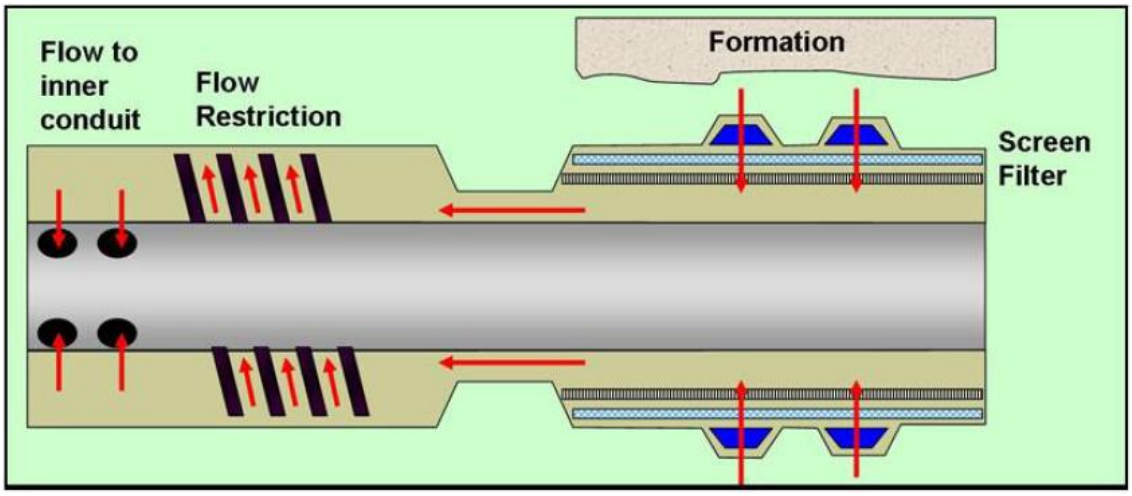

Figure 2-50: Fluid flow path from the reservoir to the base pipe [49]

2.3.3.2.1 Labyrinth Channel-type ICD

This type formed the original ICD concept as explained above. The labyrinth channel type has a number of channels installed on a pre-packed screen mounted on a base pipe (Figure 2-51). The length and diameter of channels can be adjusted to create a required pressure drop so as to achieve a balanced inflow along the length of the horizontal well. This mechanism makes the device's performance highly dependent on the fluid viscosity and velocity, but less dependent on the fluid density [59]. The dependence on frictional pressure losses rather than acceleration losses makes this type less susceptible to erosion. However, the device may form an emulsion if the oil-water mixture flow occurs.

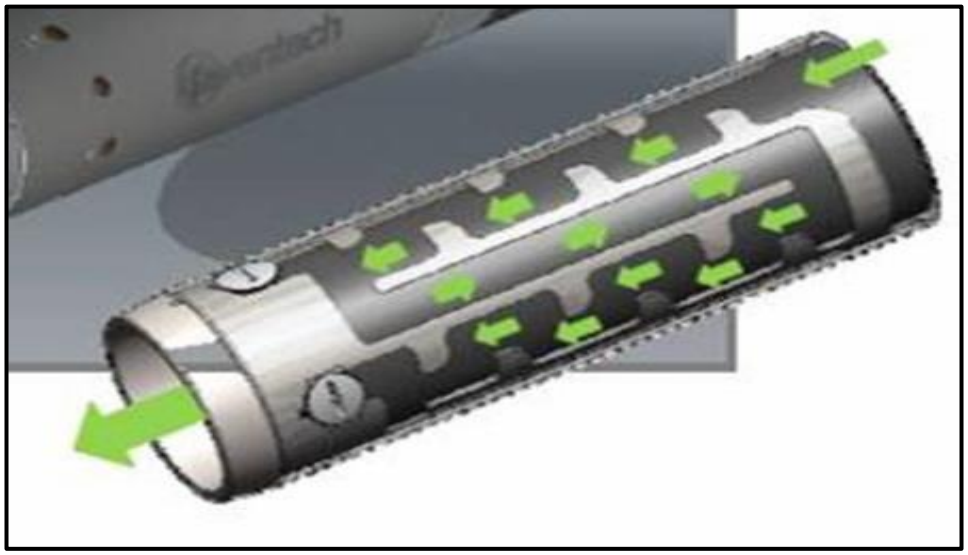

Figure 2-51: Labyrinth Channel-type ICD [49]

2.3.3.2.2 A helical channel-type ICD

The labyrinth was the original Norsk Hydro design. The helical channel is a lower cost and easier to manufacture version of the labyrinth. The flow resistance is created by channelling the produced or injected fluid through pre-set diameter and length helical channels (Figure 2-52). The device is available in various sizes with a choice of flow resistance of 0.2, 0.4, 0.8, 1.6,3.2 and 6.4 bar. The flow resistance is measured at a water flow rate of 26 sm^3/d/ICD [60, 61].

Figure 2-52: A helical channel-type ICD [53]

These various flow resistance ratings are obtained by changing the diameter, number of channels, length of the channels. The helical channel as labyrinth channel is less vulnerable to erosion and plugging but its performance will be influenced if emulsion forms due to occurrence of pressure drop over a greater distance compared to other ICD types.

2.3.3.2.3 Slot-type ICD

The slot type ICD was developed by Baker Oil Tools to provide a design that is insensitive to viscosity while maintaining the low erosion potential over the above other ICD types. There are two designs for this type of ICD:

I. A design which incorporates a series of flow slots with pre-set size (Figure 2-53) [62]
II. A design which is adjustable at the wellsite (Figure 2-54). This device has 4 quadrants in each restriction chamber. Different pressure drops can be achieved by changing the number of stages in each quadrant [59].

Figure 2-53: Fixed Slot-type ICD

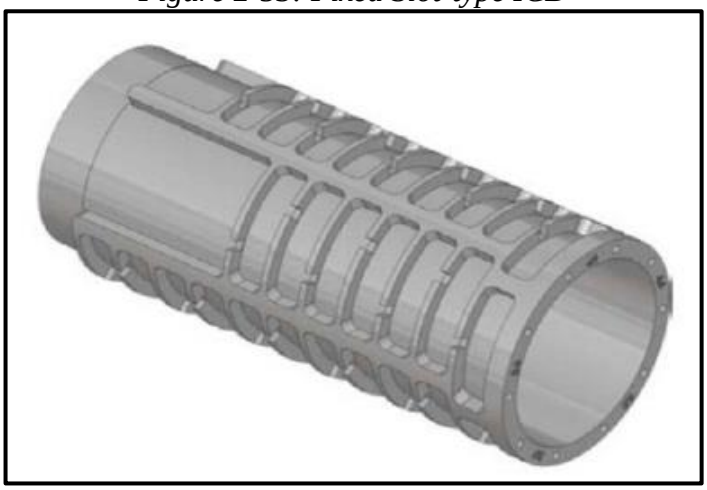

Figure 2-54: Adjustable slot-type

The device as helical channel-type ICD is available in various sizes with a choice of flow resistance of 0.2, 0.4, 0.8, 1.6, 3.2 and 6.4 bar for a water flow rate of 26 sm^3/d/ICD.

2.3.3.2.4 Tube-type ICD

This type is developed by Halliburton and uses various number of tubes. Each tube has a pre-set diameter and length to force a specific pressure drop for a specific flow rate (Figure 2-55). This type combines the effect of pressure drop created by fluid flow across a restriction and that of straight tubes. The number and length of the tubes are altered to achieve a required pressure drop which gives the tube-type ICD a greater flexibility to suit the produced or injected fluid properties [49].

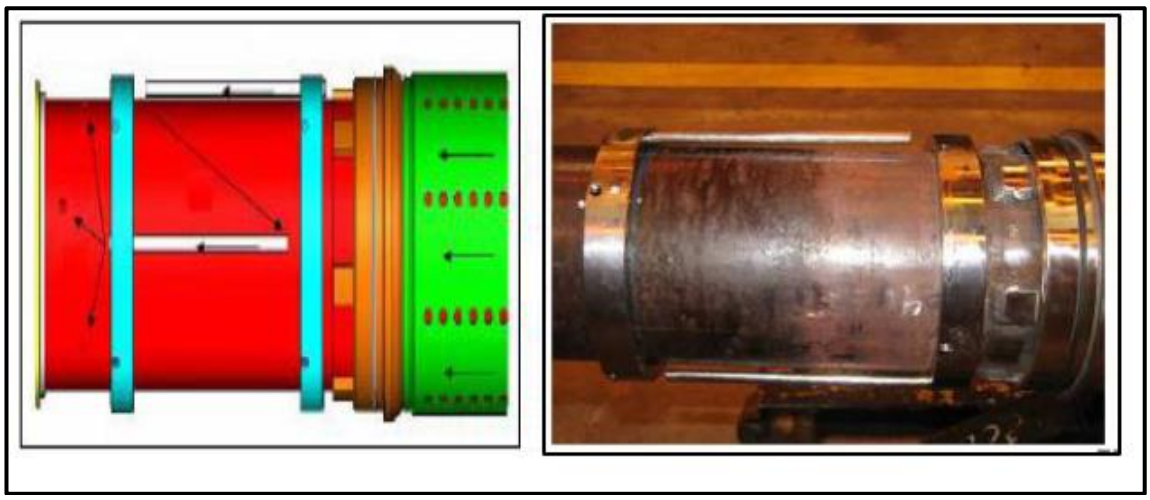

Figure 2-55: A diagram and actual Tube-type ICD [49]

2.3.3.2.5 Nozzle-type ICD

There are a number of providers for nozzle-type ICDs e.g. Schlumberger and Tendeka. The nozzle typed design uses nozzles as a restriction to create the pressure drop across the device (Figure 2-56). The number and diameter of nozzles can be altered to impose the required pressure drop for a specific flow rate.

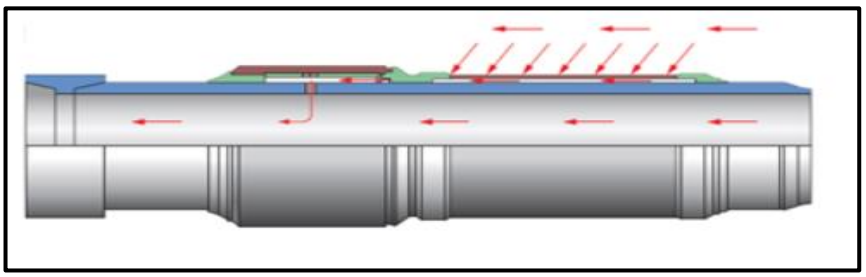

Figure 2-56: A nozzle Type ICD (Courtesy of Schlumberger)

The fluid passes through the screen and enters a pre-set number of nozzles of a pre-set diameter mounted in the inner section of the base pipe. The pressure drop across this nozzle-type ICD is more highly dependent on density rather than viscosity when compared to other devices. This dependence on the acceleration loss and velocity makes this device more susceptible to erosion and plugging.

Schlumberger developed a nozzle ICD type for injection wells. The nozzles for injectors are mounted on a jacket welded in the base pipe rather than grooved into the base pipe for producers (Figure 2-57) [49].

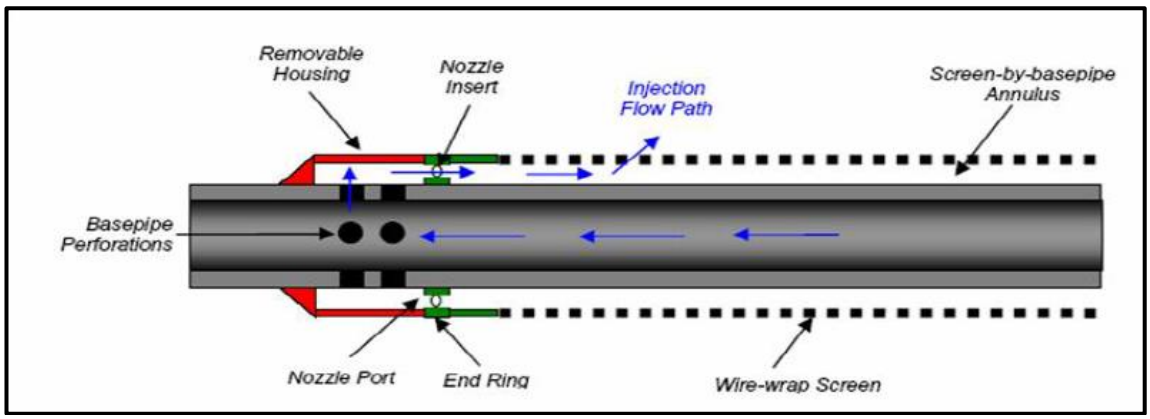

Figure 2-57: Nozzle-type ICD for injectors [63]

2.3.3.2.6 Orifice-type ICD

The Orifice-type ICD has a number of orifices of known diameter and flow characteristics e.g. discharge coefficient (Figure 2-58). Adjusting the number of orifices on the ICD creates the required flow resistance to balance the fluid inflow or outflow.

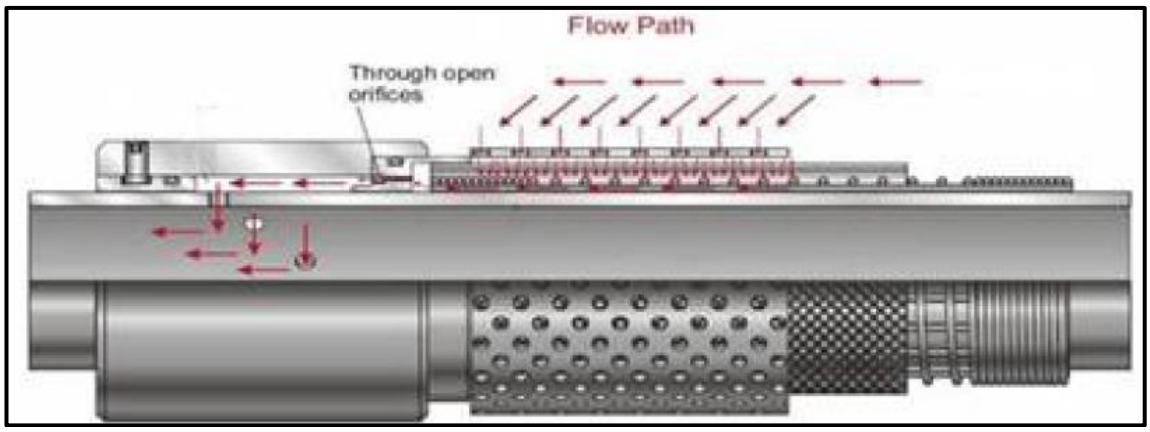

Figure 2-58: Orifice-type ICD

Orifice and nozzle-type ICDs have similar flow characteristics, but differ in design of the orifices/nozzles and their location within the ICD. The orifices in orifice-type ICD are located in a jacket installed around the base pipe i.e. similar to Nozzle-type ICD for injectors while nozzles in nozzle-type ICD are grooved in the wall of the base pipe [53]

2.3.3.3 *Objectives and principle s of ICD*

Various types of ICDs use different mechanisms to create the differential pressure. This changes the objectives of each ICD type. ICDs are applied in the oil industry to achieve mainly two objectives based on the type of ICD:

I. Reduce the inflow or outflow imbalance along the horizontal section of the wellbore. This imbalance can be caused by either the HTE due to frictional

pressure drop or by productivity differences along the wellbore due to reservoir properties. All ICDs types can accomplish this objective.

II. Reduce a specific flow of unfavourable fluid e.g. gas and water. Oil–associated, or free, gas flow will be promoted by all types of ICDs. By contrast, nozzle, orifice, and slot types ICDs reduce the flow of oil–associated, or free, water due to their dependence on the density. However, other ICDs types will encourage the water inflow due to their dependence on viscosity.

Table 2-1 provides details on various ICD types, their providers and applications [49].

Table 2-1: Current types of ICDs; differences and similarity [49]

ICD Pressure Drop Element	Channel		Slot	Tube		Nozzle		Orifice	
	Tejas	*Baker*	*Baker*	*Halliburton*		*Reslink*	*Flotech*	*Weath-erford*	*Schlum berger*
				LT	*ST*				
Source of Pressure drop:									
Friction	H	H	L	H	L	N	N	N	N
Acceleration	L	L	H	L	H	H	H	H	H
Oil associated fluid phase restriction:									
Gas	H	H	H	H	H	H	H	H	H
Water	L	L	H	L	H	H	H	H	H
Importance of Emulsion	H	H	N	H	L	N	N	N	N
Risk of Erosion	L	L	M	L	L	M	M	M	M
Risk of Plugging	L	L	M	M	M	M	M	M	M
Flexibility at Wellsite	L	L	L	L	L	H	H	H	H
LT = Long Tube, ST = Short Tube, Dependence: H= High, M= Moderate, L= Low, N = No dependence									

The principle of the nozzle or orifice ICD types is based on Bernoulli. The generated pressure drop (ΔP_{ICD}) added by installing ICDs is directly proportional to the square of the flow rate (q^2) and a calibration factor (a) i.e. known as "ICD strength". This is explained by the following Equation [64] :

$$\Delta P_{ICD} = a\, q^2 \qquad \text{Equation 2-9}$$

A similar equation also applies to the friction-based ICDs (e.g. tube or channel ones) due to the frictional pressure losses being quadratically dependent on flow rate in turbulent mode in ICDs.

The term (a) is a measure of the degree of restriction and is different for different ICD types depending on the ICD configurations. The differential pressure may be generated by the following mechanisms:

I. Flow through small channels to create the pressure drop i.e. pressure drop due to friction. This mechanism depends on the viscosity of the fluid flow. The viscosity term is included in Equation 2-10 for channels ICDs. Labyrinth and helical channels ICDs are examples of ICDs using this mechanism.

II. Flow through local restrictions to create the pressure drop i.e. pressure drop due to acceleration. The flow across the ICD is in the turbulent regime because of the high velocity. The viscosity term is neglected in Equation 2-10for nozzle and orifice ICDs. Nozzle and orifice ICDs are examples of ICDs using this mechanism.

ICD strength (a) based on these mechanisms is defined for different ICD types in the following Equation:

$$a = \begin{cases} \left(\frac{\rho_{cal}\mu}{\rho_{cal}\mu_{cal}}\right)^{\frac{1}{4}} \frac{\rho}{\rho_{cal}}\, l_{ICD}^2 B^2 a_{ICD} & for\ Channel\ ICD \\ \frac{C_u \rho l_{ICD}^2 B^2}{C_d^2 d^4} & for\ nozzle\ and\ orifice\ ICD \end{cases}$$

Equation 2-10

Where:

ρ_{cal} = Density of calibration fluid (water)

μ_{cal} = Viscosity of calibration fluid (water)

ρ = Density of produced or injected fluid

μ = Viscosity of produced or injected fluid

l_{ICD} = Length of the ICD joint

C_u = Conversion factor

C_d = Discharge coefficient for nozzle or orifice

C_u = Conversion factor

d = Nozzle or orifice diameter

Details of the different ICDs performance under single phase and multi-phase flow conditions can be found in [65-67].

2.3.4 Inflow Control Valve (ICVs)

An ICV, unlike a passive ICD is an active downhole control device that is operated remotely from the surface by an electric or hydraulic system (Figure 2-59). Hydraulic ICVs to manage complex reservoirs and well completions were initially developed from the traditional sliding sleeve device. The ICV system contains five main components; (1) control lines, (2) connectors, 3) control equipment at the surface, (4) gauges for monitoring the flow and (5) the valve itself [49].

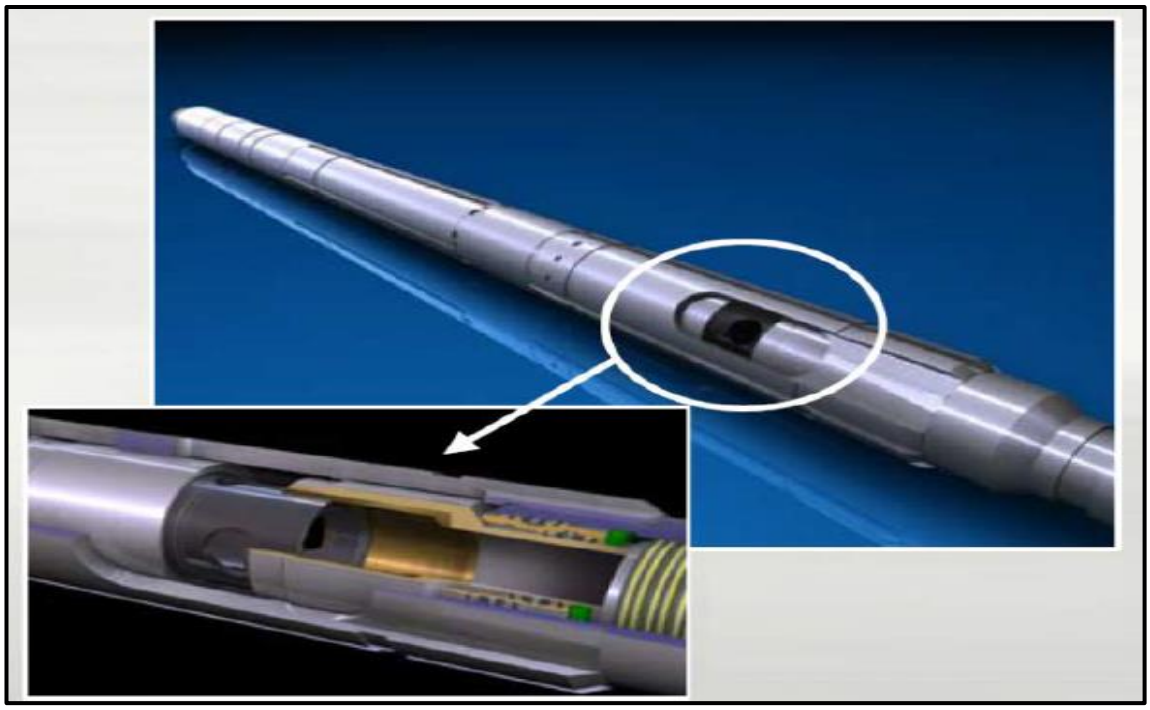

Figure 2-59: Inflow Control Valve (ICV)

ICVs were developed to achieve the following objectives [49, 68] :

I. Zonal control of multiple zones or reservoirs in a field.
II. Actively manage the water and/or gas flood front and sweep efficiency.
III. Actively manage "Water dump-flooding" between reservoir for pressure maintenance and sweep efficiency in injection wells.
IV. Control and shut-in excessive sand, water and/or gas producing formations
V. Optimise the field production or injection in real time.
VI. Isolate and protect the hydrocarbon bearing formation from workover and intervention fluids.
VII. Divert stimulation fluids.

There are different designs and types of ICVs based on their intended applications and the suppliers. They can be divided into two types:

I. On/Off ICV: This type allows (fully open) or prevents (completely shut) the inflow or outflow of a specific zone. This type does not have the possibility of partially shutting a specific zone.

II. Variable ICV: This ICV type can be either discrete with a fixed number of positions, typically 10 or fewer, or it can be infinitely variable, allowing any position between fully open and fully closed.

A control strategy for ICVs is critical since they can be controlled from the surface at any time. The control polices to maximise oil production and/or NPV and delay the unwanted fluid breakthrough can be either a "Reactive" or a "Proactive" strategy. Proactive strategy requires controlling the ICV before unwanted fluid breakthrough into the well whereas the Reactive strategy requires controlling the ICV after unwanted fluid breakthrough into the well [69].

Applications of ICVs and ICDs overlap. Al-Khelaiwi et al.2010 [70] provided a comprehensive comparative study of ICV and ICD applications (Figure 2-60).

Table 2-2 can be used as a simplified screening tool when selecting between ICD and ICV.

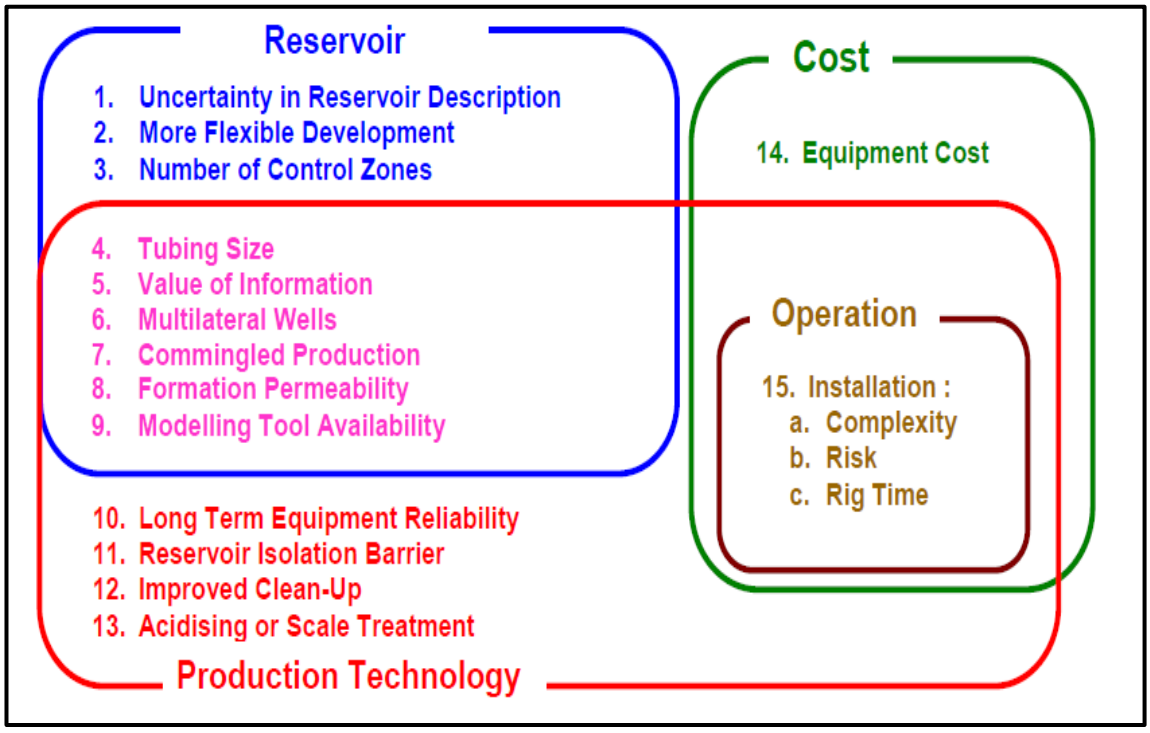

Figure 2-60: ICD and ICV comparsion framework [49]

Table 2-2 : Comparison of ICV and ICD applications [70, 71]

Aspect		ICD vs. ICV
1. Uncertainty in Reservoir Description		ICV
2. More Flexible Development		ICV
3. Number of Controllable Zones		ICD
4. Inner Flow Diameter		ICD
5. Value of Information		ICV
6. Multilateral Wells	Control **of** Lateral	ICV
	Control **within** Lateral	ICD
7. Multiple Reservoir Management		ICV
8. Formation Permeability	High	ICD
	Medium-to-Low	ICV
9. Modelling Tool Availability		ICV
10. Long Term Equipment Reliability		ICD
11. Reservoir Isolation Barrier		ICV
12. Improved Well Clean-Up		ICV
13. Acidizing / Scale Treatment		ICV
14. Equipment Cost		ICD
15. Installation (Risk, Cost and Complexity)		ICD
16. Gas Fields		ICV

2.3.5 Autonomous Flow control Devices (AFCDs)

AFCDs, evolved from the passive ICD, combine the passive control aspect with an active element. AFCDs have advantages over ICDs and ICVs in that they have the ability to reduce or stop inflow of an unwanted fluid without the need for well intervention. The differential pressure across the AFCD is dependent not only on the flow rate but also on the fluid compositions and properties. AFCDs react autonomously to different fluid properties by two mechanisms; (1) altering the geometry of the fluid's flow, (2) changing the flow path itself based on the controlling properties [72]. The AFCD currently has the following characteristics [73]:

- Functions autonomously.
- Contains no electronics, or connections to the surface.
- Needs no intervention.
- Will reverse the flow restriction if the unwanted fluid is no longer being produced.
- Designs are available to produce oil and restrict unwanted fluid e.g. gas, liquid or gaseous (steam) water.
- Operates as a standard ICD prior to water/gas breakthrough.
- Each of the many devices installed in the completion functions independently in response to the local reservoir conditions.

Currently, the AFCDs can be characterised based on their mechanisms as:

I. Autonomous Inflow Control Devices (AICDs): These devises use either the concept of lift-off pressure or flow inertia principle to restrict the unwanted fluid after breakthrough.

II. Autonomous Inflow Control Valves (AICVs): these devices contain a moving piston that responds to the reservoir fluids to stop the unwanted fluid productions after breakthrough.

These devices with current designs can be installed only in production wells, hence they will not be analysed in detail in this thesis. Detailed analysis on their performance, modelling, and applications can be found in [2].

2.3.6 Annular Flow Isolation (AFI)

The annulus space between the production tubular and the sandface or the cemented and perforated casing provides the least resistive flow pathway (Figure 2-61). The annular flow within this annulus can cause many potential problems in both production and injection wells. These problems include screen erosion, plugging as well as sand production related problems. Therefore, AFIs constitute essential components of AWCs to ensure elimination of annular flow and AWCs added value.

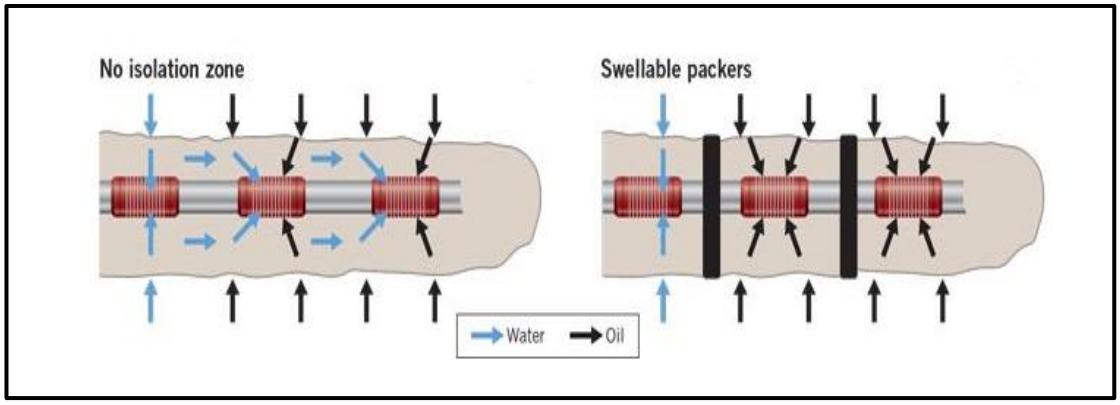

Figure 2-61: Packers (AFIs) installed between joints for annular flow elimination [74]

AWCs integration with AFIs requires optimisation of AFI distribution to ensure AWC's added value. The AFI distribution require optimisation considering (but not limited to):

1. The reservoir heterogeneity and pressure variations.
2. Number of zones to control.
3. Number of wells (laterals for example).

Further details about AFI optimisation can be found in [75].

2.3.6.1 *Causes and Impact of Annular Flow*

Annular flow takes place in the fully or partially open annulus space due to several factors [49, 2]:

1. The relatively large annular flow area compared to the area of the inner flow conduit.
2. Variations of permeability along the wellbore.
3. Commingled production or injection in various zones with different pressures.
4. Poor gravel packing of the annular space especially in horizontal wellbores.

Annular flow existence has an adverse impact not only on the well productivity but also on the completion integrity. Table 2-3 provides expected problems and their impact due to annular flow.

Table 2-3: Annular Flow Impact [2]

Problem	Consequence/ Impact
Sand grain "dislodging", sorting and transportation along the length of the well.	1. Plugging at parts of the annulus. 2. Plugging of the screen mesh caused by fine (often shaly) particles. 3. Erosion of the sandface due to the potential high velocity flow. 4. Formation of "hot-spots due to divergence of the fluid flow direction toward the screen or pre-perforated liner.
Loss of well productivity	1. Formation plugging. 2. Uneven influx of fluid along the length of the wellbore. 3. Loss of AWC's added value. 4. Uneven clean-up of the sandface and damaged zone around the wellbore.

Annular flow isolation can be accomplished by using packers or gravel packs. Furthermore, the sandface collapse around the completion provides an isolation of annular flow as well. Since gravel packs are applied to reduce sand production and cause a high well impairment, packers are the most common used AFI.

There are six categories of openhole packers as follows:

1. Mechanically set packers.
2. Hydraulically set packers.
3. Inflatable packers.

4. Expandable packers.
5. Chemical packers.
6. Swell (elastomers) packers (SP).

Further details of these types can be found in [49].

Table 2-4 provides a comparison of the available AFIs.

Table 2-4: Comparison of available AFIs [49]

Packer Type	Mech./ Hydr.	Inflatable	Expandable	Chemical	Swell
Applicability in (A)ICD and ICV completions	Y	N	N	N	Y
Operational Flexibility	H	H	M	M	H
Control line feed-through	Y	N	N	Y	Y
Risk of: Premature setting Damage/loss of isolation	 M L	 L M	 L L	 M M	 M L
Pressure difference	H	M	M	M	M
Y = Yes, N = No, Dependency: H = High, M = Moderate, L = Low					

2.4 ICDs Applications in Injection Wells

ICDs are a proven technology to enhance the performance of production wells. In addition to ICDs application in production wells, ICDs have been applied in injection wells with various configurations in different fields around the world [60, 76-80]. The focus on the applications of ICDs in water injection wells in this thesis is to ensure their effectiveness in mitigating different reservoir challenges and relate these findings to the problem of TIF.

In the following subsections, ICDs applications in injection wells in different fields around the world are detailed based on the outflow problems associated with complex reservoirs.

2.4.1 Heel-to-Toe Effect (HTE) and Reservoir heterogeneity (RH)

The first application of ICDs installation was on Urd field located in the Norwegian Sea [81]. ICDs implementation for injection wells was considered since the reservoir consists of a heterogeneous pay zone. Therefore, ICDs were expected to optimise the pressure support and sweep efficiency for different zones. The ICDs were

installed in a 250 m long vertical well to provide an efficient injection performance. The objectives of the project were achieved. The data indicated that the ICD injector resulted in more efficient sweep efficiency and pressure support in different zones (Table 2-5)

Table 2-5: Injector design evaluation for an ICD injection Urd field [81]

	Standard Screen	*ICD, with same nozzle size 1.2 cm/joint in all zones*	*ICD, with different configuration*	*Target rate Sm^3/d*
Zone 1 (121 m) 1800-800 mD Nozzle: 9 mm/joint	*5800*	*4604*	*3570*	*3500*
Zone 2 (51 m) 200-500 mD Nozzle: 7 mm/joint	*748*	*1233*	*820*	*800*
Zone 3 (77 m) 2000-100 mD Nozzle: 22 mm/joint	*961*	*1677*	*3128*	*3200*
Total Injection Rate	*7509*	*7514*	*7518*	*7500*

Another example of a successful ICD injector installation was in the Marlim field, an oil field located 110 km off-shore from the state of Rio de Janeiro, Brazil [82]. The horizontal injector was intended to provide both pressure support and sweep efficiency. An injection profile log confirmed that the ICD completion successfully achieved an equalising injection profile along the horizontal completion (Figure 2-62).

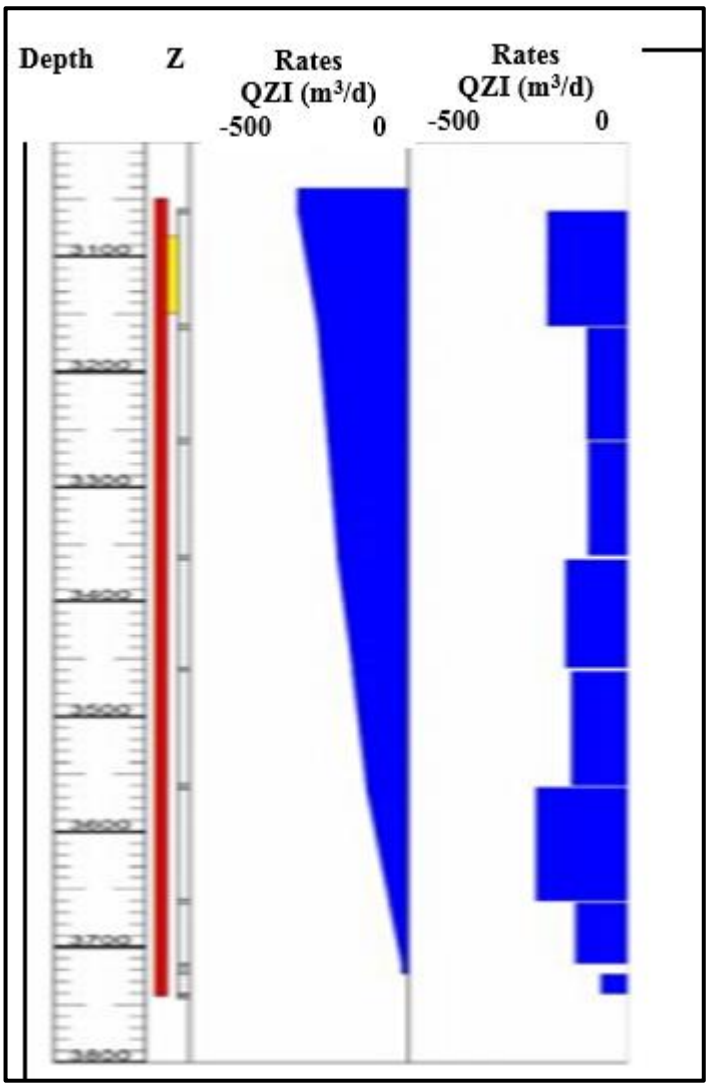

Figure 2-62: Injection log run at 5 bpm injection rate in the ICD completed injector

Further published applications of ICDs in injection wells prior to October 2017 along with ICD challenges in injection wells are summarised in (Table 2-6).

2.4.2 Wormhole Channels and Natural Fractures

Wormhole channels that develop when heavy oil is produced simultaneously with sand adversely impacts the sweep efficiency as the water pass through these wormholes channels to the producer leaving the rest of the reservoir unwept. Natural fractures and faults are another challenge in injection well. They distort the water flood front and reduce the oil recovery and/or cause uneven pressure support. ICD technology proven to be mitigating these problems.

Stag field in offshore Australia contains heavy and viscous oil [83]. This caused a sand production as well as wormhole development that affected the sweep efficiency of the reservoir. One horizontal injector was completed with various nozzle-based ICD type after observing a poor performance in conventional injection wells in the field. Modelling

work and later an injection test showed that ICD completion improved the water outflow into lower permeable zone while restricting water outflow into high permeable zone (Figure 2-63).

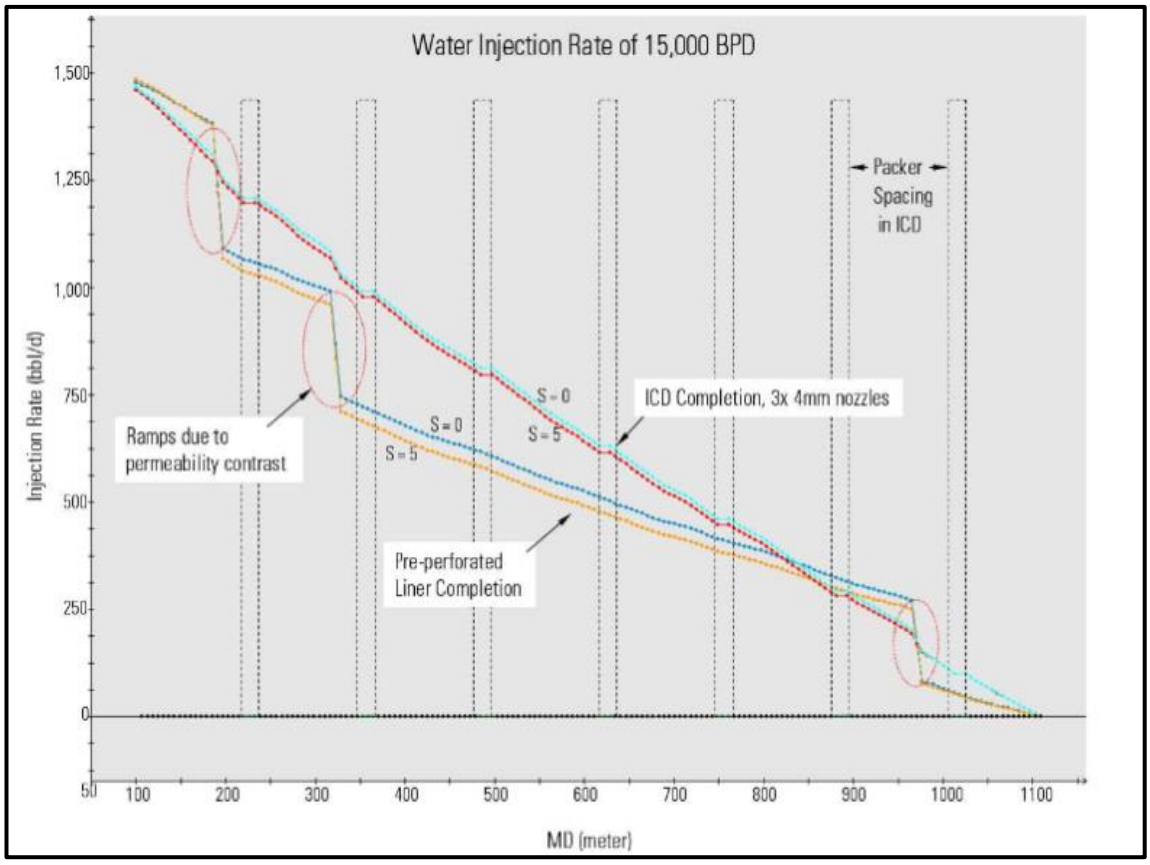

Figure 2-63: Modelled injection profile for a liner completion and an ICD completion in one of the injectos in the field

.

Another example for successful ICD story was in the largest oil field in the world i.e. the Ghawar field located in the east of Saudi Arabia [13]. The subject injector well was located in a highly fractured reservoirs with non-uniform injection profile and poor sweep efficiency. The study [13] concluded that the ICD completion provided an optimal pressure support and water flooding of the reservoir (Figure 2-64).

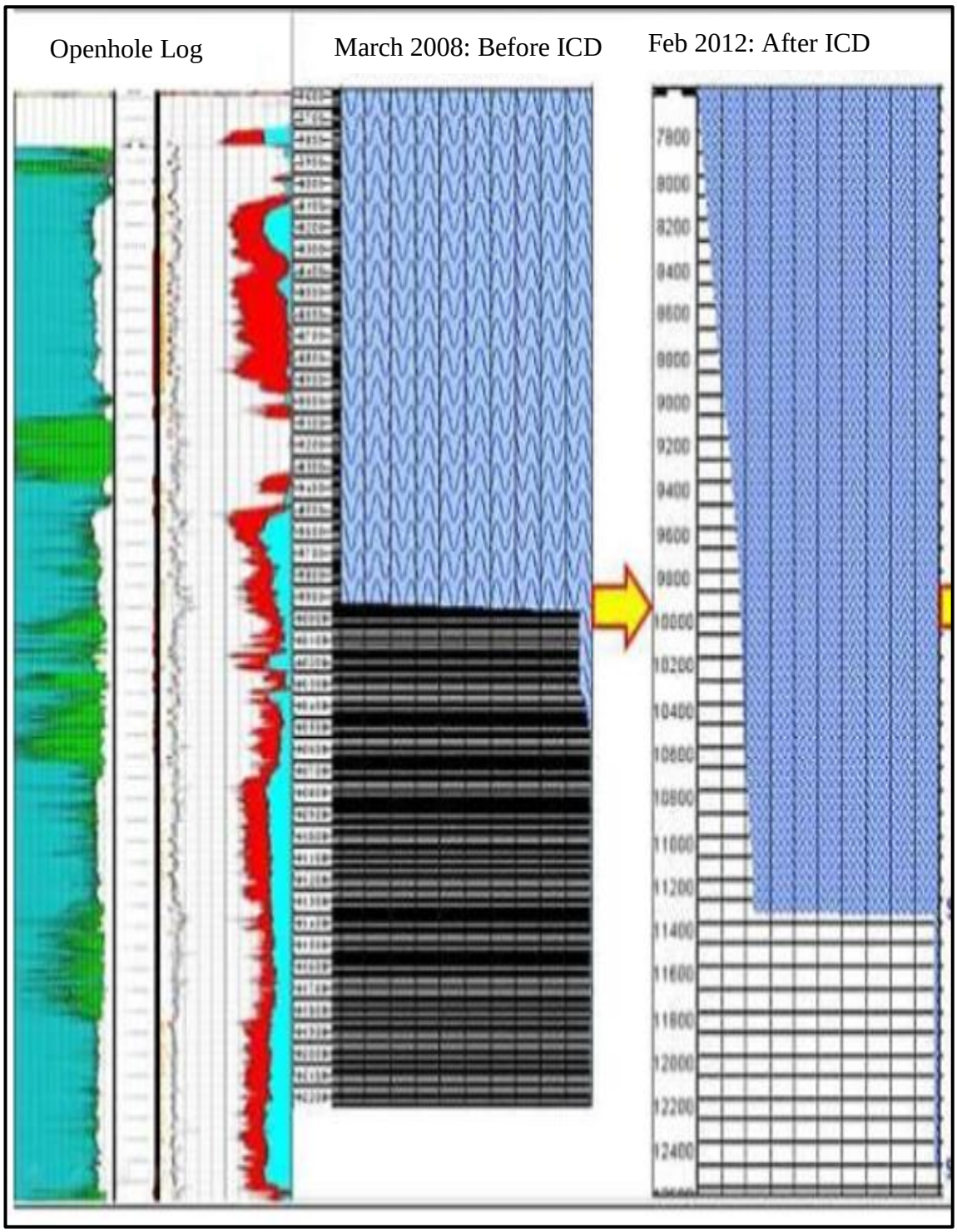

Figure 2-64: Injection Pofile for the considered injection well before and after ICD installation

Table 2-6: Summary of Published ICD Applications in injection wells

Field	Well Configuration	ICD Type	Permeability	Challenges
Nikaitchuq [84]	H	TT & SL	100- 1000 mD	WD
Urd [81]	v	NZ	0.1-2.0 D	RH, NF & HTE
Erha [85]	v	NZ	Multi-D	RH
Marlim [82]	H	HC	~ 2,000 md	RH
Stag [86]	H	NZ	~	WD & RH
Enfield [87]	D	NZ	300-500 md	FC
Offshore Abu Dhabi [88]	H	HC	~	RH, NF & HTE
Ecuador [48]	D	NZ	~	RH & HTE
Ghawar [13]	H	TT & SL	237 md	NF
Offshore Abu Dhabi [89]	D & H	ICD& SL	~	RH

H: Horizontal, D: Deviated, HC: Helical Channel-type ICD, NZ: Nozzle-type ICD, TT: Tubing-type ICD, SL: Sliding Sleeve, HTE: Heel-Toe Effect, WD: wormhole development, RH: Reservoir Heterogeneity, NF: Natural Fractures

2.4.3 SAGD injection wells

It has been shown successful applications of ICD in waterflood operations and their effectiveness to mitigate many reservoir/well related problems. Similar benefits can be expected in the Steam Assisted Gravity Drainage (SAGD) applications. SAGD process involves a horizontal injector injecting a hot steam above a secondary horizontal producer to extract extra heavy-oil resources (Figure 2-65).

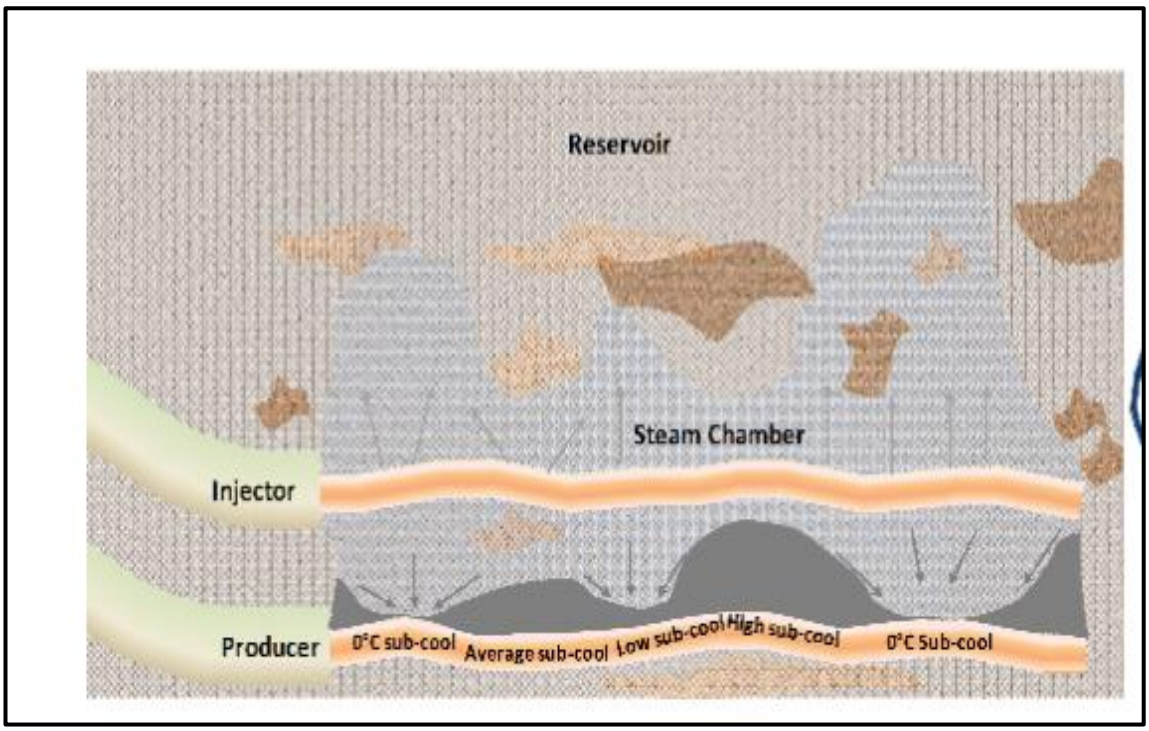

Figure 2-65: Horzoitnal well pair in SAGD application[90]

Imbalance injection profile of steam due to various reasons e.g. Heel-to-Toe Effect (HTE) and Reservoir heterogeneity (RH) causes an inefficient bitumen recovery [90]. Several studies has designed, tested, and evaluated field performance of ICDs in SAGD wells [90-92]. It was concluded from these studies that ICD technology is a potential solution for SAGD wells challenges. Their installation in SAGD wells will enhance the bitumen recovery and improve the thermal efficiency.

2.5 Potential ICD application with TIF

The application of an ICD completion in injection wells with possible TIF occurrence has not been reported prior to this work. ICD completions are expected to mitigate the impact of TIF. ICDs are capable of equalising cold water injection as efficiently as their performance in the production wells. Therefore, delayed TIF initiation and more distributed TIFs can be expected. This will enhance the sweep efficiency and pressure support. This thesis will investigate such applications and provide real field case studies as well as synthetic cases to show the added value of the ICD completions in TIF prone environment.

Chapter 3 Modelling of Thermally Induced Fractures

3.1 Introduction

Over the past 50 years, many analytical and numerical models have been developed to simulate conventional fracturing characteristics i.e. Hydraulic Fracturing (HF). The two famous 2D analytical models are PKN, developed by Perkins, Kern and Nordgren in 1961, and KGD, developed by Khristianovitch, Zheltov, Geertsma and de Klerk in 1955. These were the first proposed to model HF in the oil and gas industry. More numerical models were developed to overcome simplifications in these models. On the other hand, these models are not adequate for unconventional fracturing method e.g. TIF, CO_2 Sequestration (GCS), produced water reinjection, solids injection, and coalbed methane stimulation. TIF modelling differs significantly from HF modelling. The following factors, important in TIF, are usually neglected in the conventional HF models [93, 10]:

I. The time scale of HF is in the order of a day or less while TIF propagates and forms in the reservoir for years.
II. TIFs are leak-off dominated while HF are leak-off controlled .The leak-off rates are very high in TIF dominated injection wells.
III. Long-term cold water injection creates a thermally different zone with altered fluid properties and stresses.
IV. Local reservoir pressure and stresses change during the time of propagation in TIF. Therefore, it is not reasonable to assume that the fracture will propagate through a reservoir with constant properties.
V. TIF growth is normally determined through an equilibrium with fluid flow pressure and stress field. Stress fields are normally affected by changes in the formation's temperature, a factor that is normally overlooked in conventional HF models.

The factors above were the drivers for developing the first analytical models for analysing TIF. The first analytical model considering poro-elastic and thermos-elastic changes include Hagoort (1980), Perkins (1985), and later by Koning (1988) [94, 95, 23]. However, the complexity of interaction between fluid flow in the fracture, geomechanical changes, and reservoir matrix in "real world" situations requires more advanced, numerical models. Coupling fracture mechanics to

geomechanical models and reservoir simulation simultaneously is the only means of modelling these complex phenomena in an accurate manner.

3.2 Historical Background and modelling development

TIF has been documented in many different fields around the world not only in waterflooding applications but also in reinjection i.e. disposal and GCS applications. In the past 37 years, various analytical models and numerical simulation approaches of varying degrees of complexity have been developed in order to simulate TIF. Models have evolved from simple 2 dimensional (2D) to Pseudo 3-dimensional (P3D) to fully 3D models (Figure 3-1).

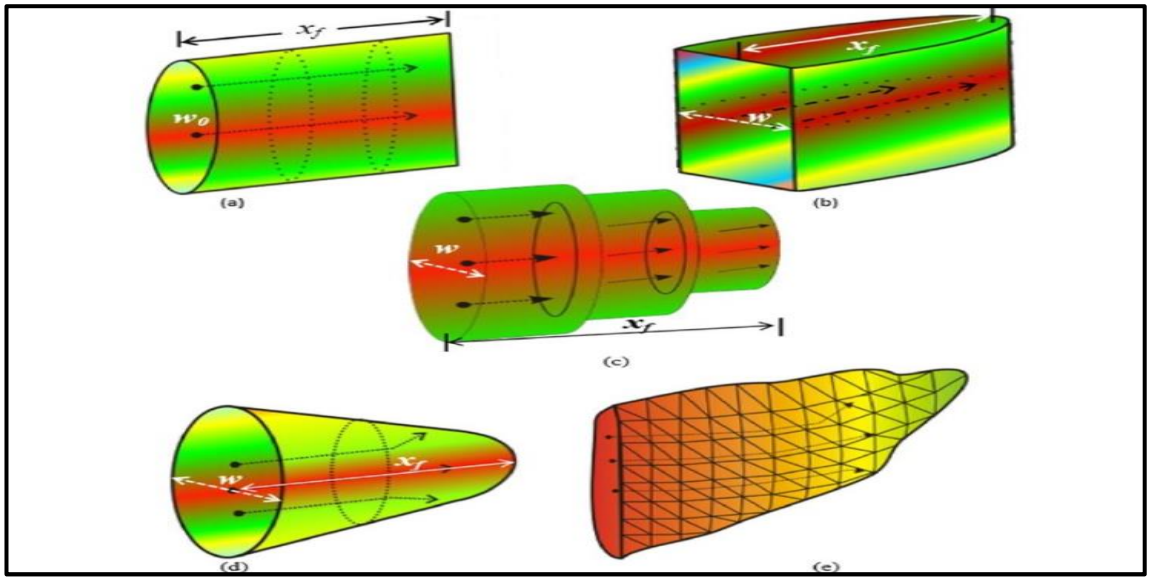

Figure 3-1: Fracture geometry models: (a) and (b) 2D models, (c) P3D model, (d) and (e) 3D models [96]

In the early eighties, Hagoort [94], developed a semi-analytical model for simulating the propagation of injection induced fractures during waterflood. The model was a function of (1) injection rate, (2) injection pressures, (3) reservoir and fluid properties, and (4) formation-fracturing pressures. However, the model neglected the thermo-elastic stress as well as heat transfer between the formation and injected water. Then, in the mid-eighties, the first attempt at modelling TIF was initiated by Perkins and Gonzales [97]. They constructed an analytic model of 2D TIF based on the assumption of elliptical flow around the fracture. The model included a thermo-elastic analysis to determine the effects of reservoir temperature variations and pore pressure on the in-situ stresses. Koning [22], presented an analytical model of TIF from a single well in an infinite reservoir. The geometry of the fracture was assumed to be based on the traditional

2D Perkins-Kern-Nordgren (PKN) model. The calculation of 3D poro-elastic stress changes was performed analytically.

The numerical simulation development followed quickly and P3D model for TIF was soon proposed by Dikken and Niko [98]. The poro and thermo-elastic stress changes and fracture growth were calculated numerically. Dikken and Niko work was an extension to the methods developed by Koning [22]. The need for more advanced modelling tools to consider the complexity of both the reservoir and fracture mechanics introduced 3D models. Clifford [99] and Settari [10] presented a full 3D numerical model of the TIF. In their work, finite-element and boundary-element formulations were applied to accurately simulate the fracture geometry. Hustedt [100], Ji [101], and Chin [102] have also proposed computationally complex and time consuming numerical approaches.

In this thesis, 3D Finite Difference (FD) thermal reservoir model coupled to 3D Finite Element TIF and FD geomechanical models is considered. This is discussed further in section 3.6.

3.3 Analytical TIF Modelling

One of the earliest fracturing models that consider the change of the stress due to temperature and pressure changes during the injection is Perkins and Gonzalez Model [23]. They constructed a simplified 2D TIF model for a single well in an infinite reservoir. The thermo-elastic stresses in this model are determined from cooled regions of finite thickness with an elliptical cross section (Figure 3-2). Three zones were defined. The zones are:

I. Cooled elliptical zone next to the wellbore.
II. Flooded elliptical zone after the cooled zone that is at the initial temperature as the reservoir but has a different pore pressure.
III. Undisturbed reservoir after the flooded ellipse zone.

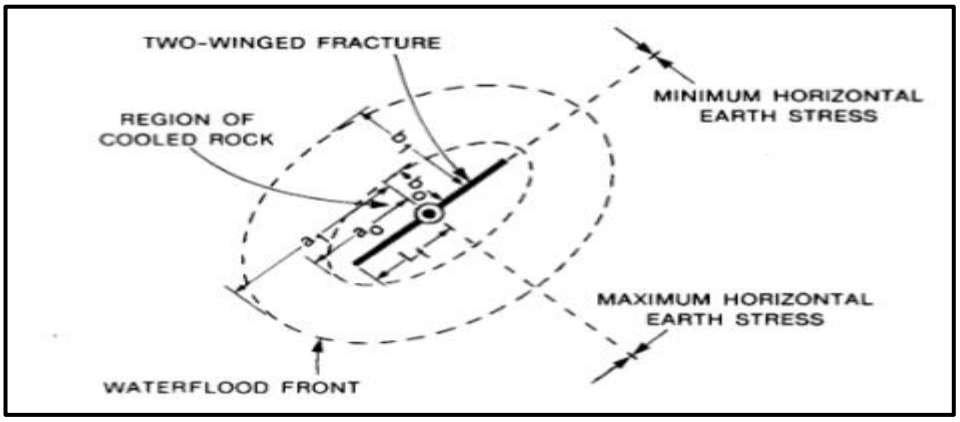

Figure 3-2: A two-winged vertical fracture oriented perpendicular to the plane of the minimum horizontal in-situ stress [23]

Empirical equations were developed to approximately calculate the thermo-elastic stresses for an elliptical cross section and a fixed height. Poro-elastic stresses that resulted from pore pressure changes are calculated using the same equations derived for thermo-elastic stresses. The TIF dimensions i.e. TIF length and width are determined as a function of injection rate or time by coupling the calculated thermo-elastic stresses and poro-elastic stresses to the PKN hydraulic fracturing model. In this model, the temperature was assumed to be constant in the elliptical region. The pore pressure, by contrast, is not uniform and is determined from the reservoir model.

Perkins [23] provided examples using this model and showed that the stress reduction due to temperature contrast is significant and cannot be neglected i.e. thermal aspect must be taken into consideration when modelling waterflooding projects. These findings led to further research in modelling methodologies in the area of cold water injection simulation. The advantage of the Perkins model is that it is simple and computationally inexpensive. However, it has the following drawbacks [103, 93]:

I. Geomechanical properties cannot be updated simultaneously with the injection.
II. Complex injection schemes i.e. two-phase flow, evaluation of the reservoir pressure are not allowed in this model.
III. The temperature was assumed to be a uniform elliptical temperature profile in the reservoir.
IV. The height of TIF in this model is assumed to be constant. Out-of-zone TIFs therefore cannot be investigated with this model.
V. The reservoir is homogenous with a piston –like displacement.
VI. This model can be applied only to one well with infinite conductivity fracture i.e. the fluid pressure drop along the fracture is neglected.

3.4 Pseudo Three-Dimensional TIF Modelling

P3D formulation involves a 2D TIF fracture model i.e. TIF length and width extended to allow variable TIF height as opposed to fixed height in analytical models. The geometry of TIFs in P3D is approximated either by ellipses i.e. lumped P3D or fracture's lateral dimension divided into elements where each element has its own height i.e. cell-based P3D [104]. The P3D model was originally developed to describe reasonably the geometry evolution of the fracture. In P3D models, the fluid flow and fracture opening equations are coupled to an efficient scheme for describing the vertical

fracture growth i.e. the height change [105] . There were several P3D models developed to overcome some of the limitations of the analytical 2D models. Settari [105] developed and tested a P3D model designed for a range of conditions for modelling hydraulic fracturing. P3D model coupled a one dimensional (1D) description for the lateral direction (the fracture length) to a 2D model vertical fracture propagation (the height of the fracture in a plane of constant height at any cross section) see Figure 3-3. However, this model was designed for Hydraulic fracturing simulation purposes and did not consider the effect of the temperature variations on the in-situ stress.

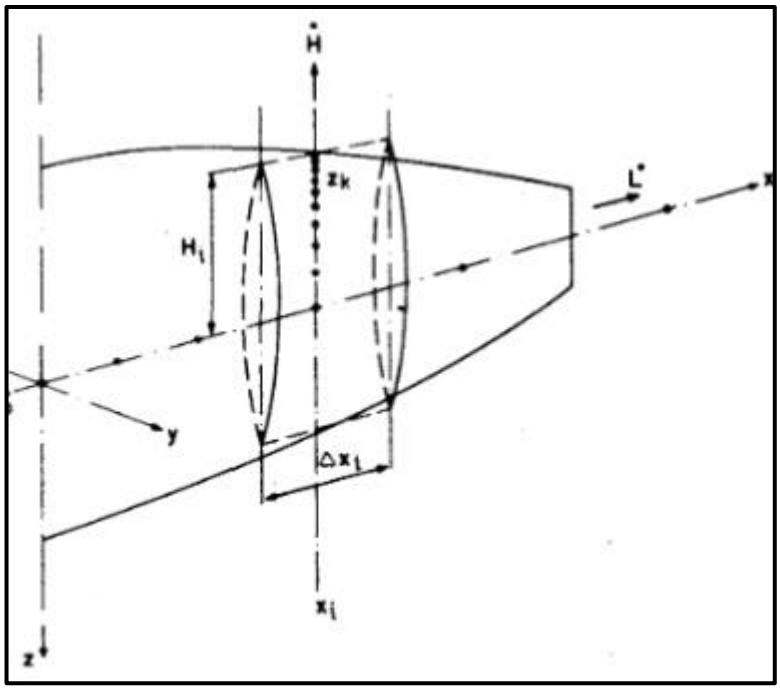

Figure 3-3: The concept of P3D model formulation [105]

The work of Dikken [98] and van den Hoek [106] are examples of P3D models developed for TIF modelling. Dikken, for example, extended Settari [105] P3D model. Dikken [98] used an uncoupled approach in his modelling work. Thermal reservoir simulation was used to calculate the temperature and pressure. A finite-element stress analysis model was used to determine the thermo-elastic and poro-elastic stress due to changes in temperature and pressure. Settari's [105] P3D model was then used to predict the characteristics of TIF. These models gave more accurate TIF prediction than these generated by analytical models, while being less computationally complex and faster than the fully 3D models. However most of the P3D models have the following drawbacks.

I. Areal reservoir heterogeneity is not accounted for.
II. Thermo-elastic and poro-elastic stresses are constant along the fracture.
III. Constant pressure along the fracture.

IV. Homogenous mechanical properties for each layer.

3.5 Fully 3 Dimensional TIF Modelling

The use of fully 3D models provide a more accurate way to simulate complex fracture geometries than conventional models e.g. 2D and P3D models cannot investigate out of plane or uncontained fractures. 3D models that include the temperature changes in their analysis are considered. Clifford [99] and Settari [10] have both presented a full 3D numerical model of TIF propagation. More recent numerical approaches that are computationally complex and time consuming have been proposed by Hustedt [100], Ji [101], and Chin [102].

The Clifford [99] 3D model will be discussed in detail since it was one of the first introduced TIF 3D models. This 3D model has been used later in this thesis for further analysis. This model couples a finite–volume reservoir model to a finite-element TIF propagation model. Clifford [99] modelled TIFs as planar fractures of arbitrary shape using a 3D finite element method (Figure 3-4). Linear Elastic Fracture Mechanics (LEFM) is governing the growth of TIF. The TIF propagation criterion is based on comparing a stress intensity factor (K_I) and a user input of fracture toughness of the rock.

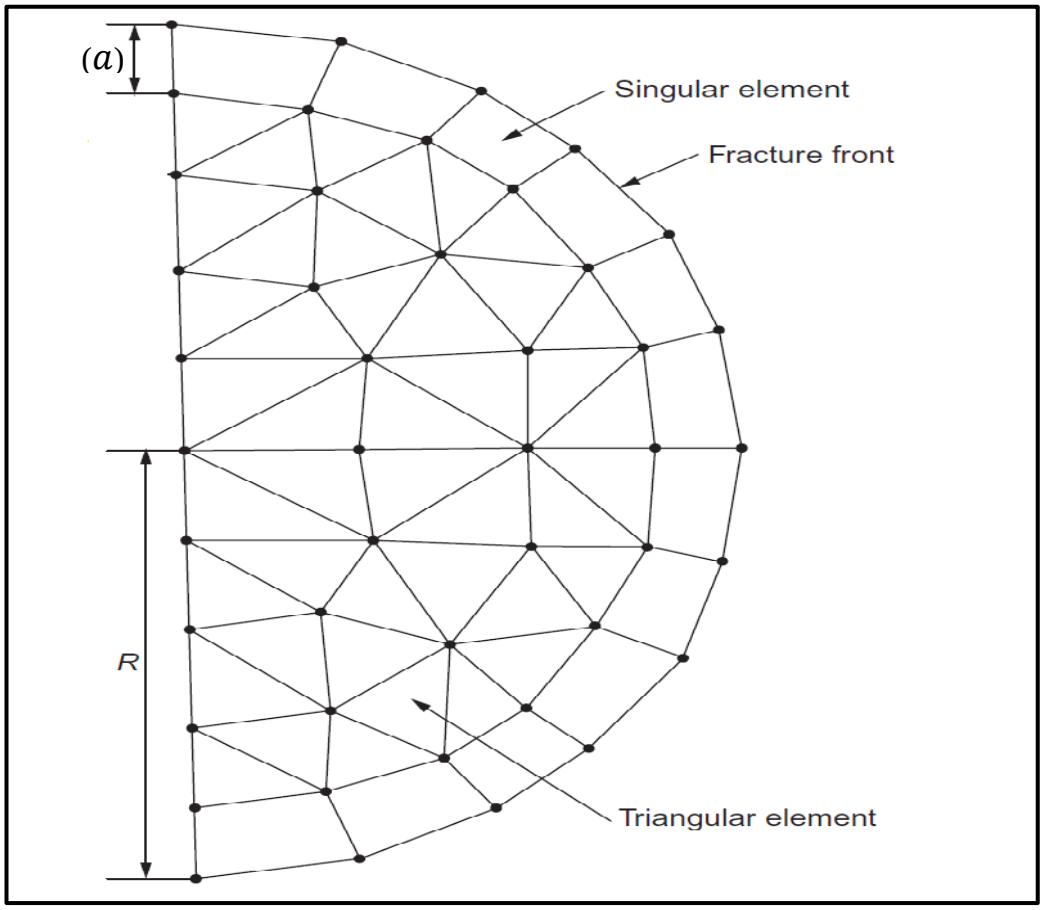

Figure 3-4: Example of 3D finite element fracture [99]

The 3D TIF model is coupled with the reservoir flow model to determine the temperature and pore pressure changes. The reservoir model is based on a 3D finite difference method. At each time step during the injection, the pressure, saturation, and temperature are computed in the grid cells of the reservoir model. The stress changes due to temperature changes (the thermo-elastic stress) and pressure change (the poro-elastic stress) are calculated numerically by integrating a 3D integral. The stress state of the fracture is calculated at stress intervals defined by the user. The fracture geometry is then updated so that it is in equilibrium with the new stress state.

This model overcomes some of the challenges that cannot be handled by either 2D or P3D models, but still it has the following drawbacks [100]:

I. The model is not a purpose built model i.e. the reservoir model is an in-house model that is not universally applicable.
II. The TIF propagation model is oversimplified.
III. Numerical stability is questionable.

3.6 Thermally Induced Fracture Modelling Methodology used

3.6.1 Introduction and Underlying Assumptions

The common method to model hydraulic fractures within a reservoir simulator is to modify the flow in a Finite Difference (FD) reservoir by changing the grid properties to thin blocks with high porosity and permeability in order to simulate the fracture flow. The alternative methods that have been adopted for hydraulic fracture modelling are the Local grid refinement (LGR) and equivalent effective wellbore radius method. They are not suitable for TIF modelling for the following reasons[99]:

I. The importance of flow in the reservoir for TIF long-term growth modelling is not appreciated.
II. Large time steps are required for TIF modelling.
III. TIFs have much higher leak-off rates.
IV. Thermal aspects are normally neglected in hydraulic fracture models i.e. the thermo-elastic stress is not considered.

Therefore, modelling of TIF requires coupling of dynamic, Finite Difference (FD) thermal reservoir model with a Finite Element (FE) fracture mechanics and detailed wellbore system. TIF propagation changes are dynamically dependent on the following parameters:

1. Flow rate, pressure, and temperature of the injected fluid.

2. Rocks mechanical properties.
3. Reservoir properties.

The TIF modelling results reported in this thesis use a 3D Finite Element (FE) fracture model coupled to a reservoir flow simulator and a detailed wellbore model developed by Petroleum Experts (Figure 3-5) [8]. The shape of the TIF in the x-direction is shown in Figure 3-6.

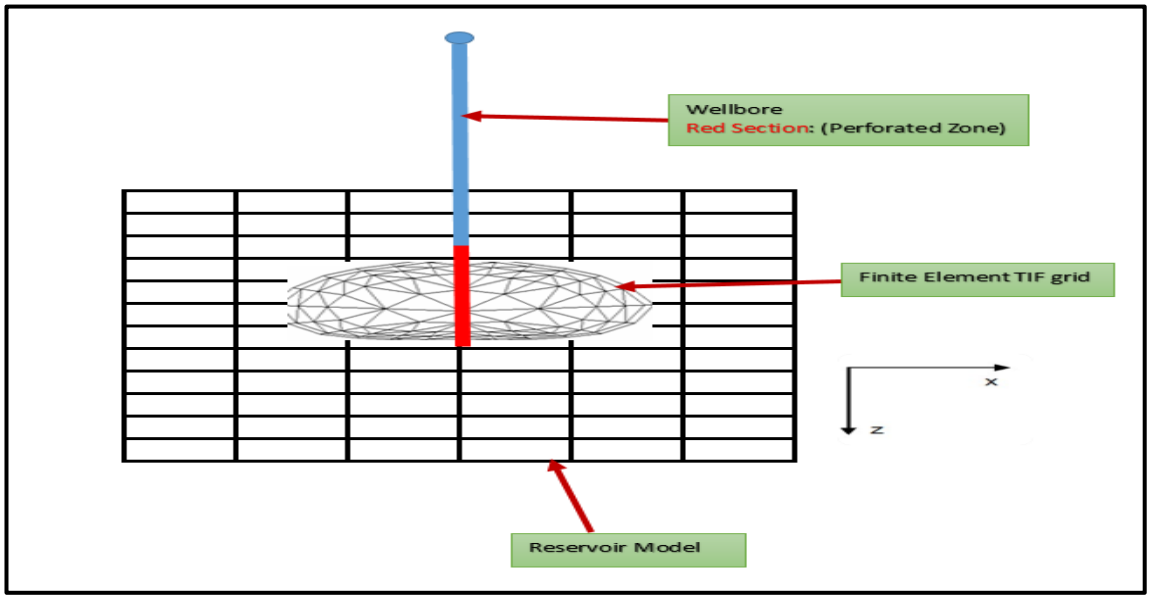

Figure 3-5: A vertical FE TIF model coupled to FD reservoir model and a detailed model of an injection well

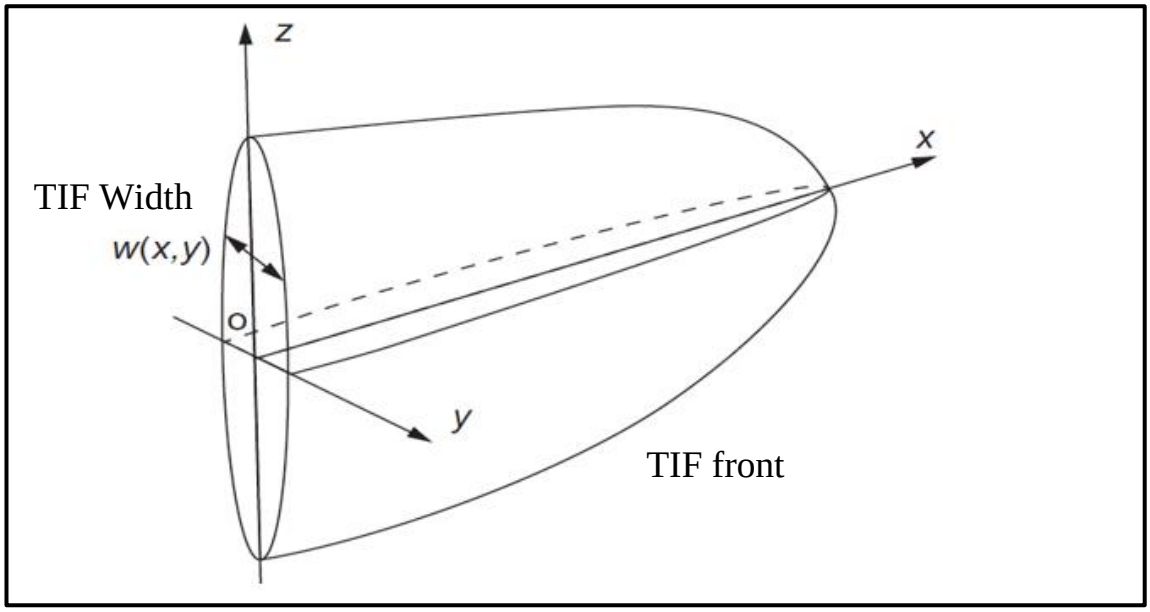

Figure 3-6: Shape of the TIF in x-direction [107]

The first step when modelling the development of a TIF requires estimation of the stress field in the reservoir. The subsequent changes in the stress field due to the water injection are a function of the (1) in-situ stress (2) reservoir pressure (3) reservoir

temperature (5) Poisson's Ratio (6) Young's Modulus (7) and thermal properties of the rocks and fluids. Once the stress field calculations is performed, the flow within TIFs is computed based on different TIF conductivity models. These conductivity models can be either dependant or independent on the TIF width. The leak-off flow can be determined from the difference between the pressure in the TIF and in the reservoir. TIF initiation and/or propagation is determined by a rock mechanical equation that is based on the stress-strain relationship. This relationship tests whether the TIF initiates and/or propagates based on the flowing parameters [8]:

I. Difference between BHP and the minimum horizontal stress.
II. Rock mechanical properties e.g. Poisson's Ratio and the Young's Modulus.
III. The critical stress intensity (K_{IC}) i.e. rock toughness.

Based on the flow and rock mechanics equations, iterations are performed on TIF geometry to calculate the stress intensity (K_I) at the tip of the TIF. TIF will propagate only if the calculated stress intensity is higher than the input critical stress intensity factor K_{IC} i.e. fracture toughness of the rock. Figure 3-7 summarises different relationships used in the TIF model to examine TIF initiation and growth geometry within a dynamically coupled reservoir and well bore system.

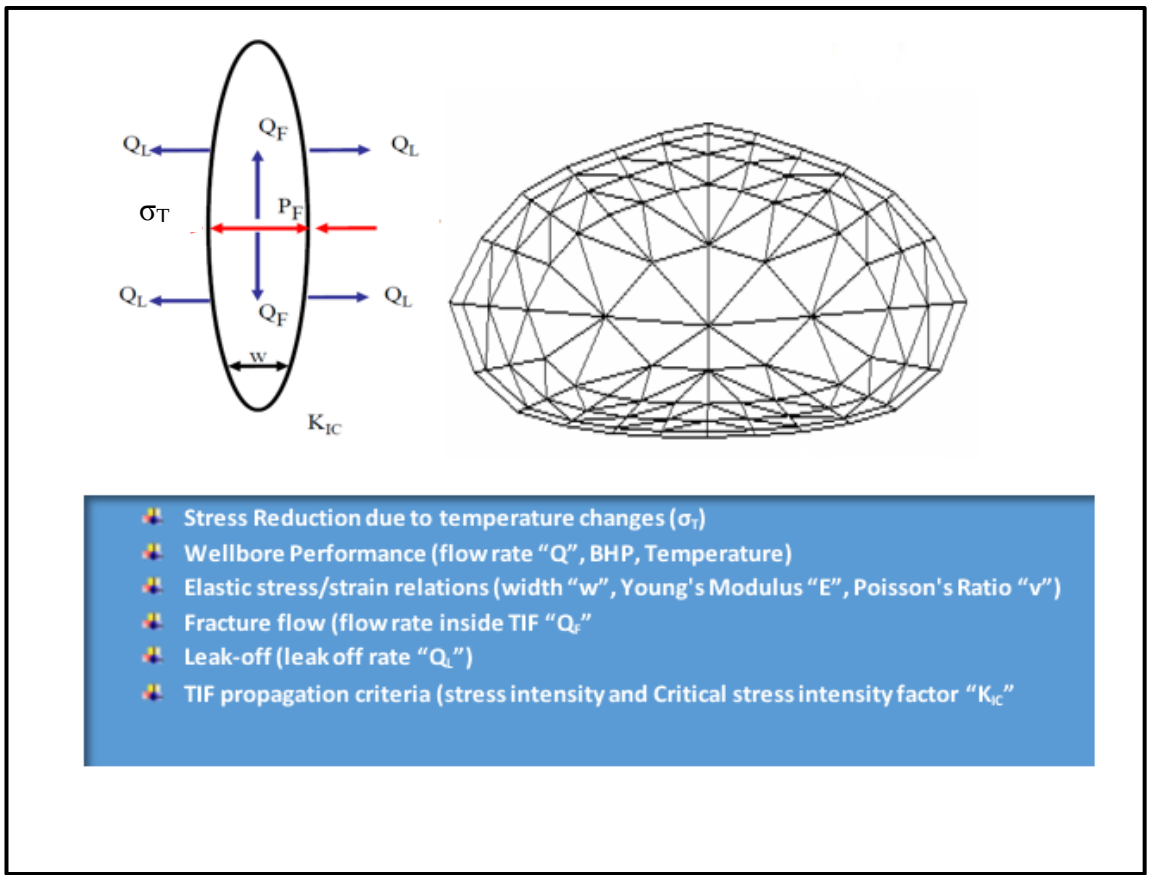

Figure 3-7: Various relationships invloved in the TIF model [8]

The TIF model being used in this thesis will incorporate all essential elements of coupling between the fluid, heat flow, and the rock mechanics. The TIF model being used in this thesis has the following assumptions:

I. Formation rocks are continuous and linear elastic.
II. Rock mechanical properties of the formation are homogenous and isotropic.
III. TIF develops as a plane i.e. vertical TIF oriented orthogonal to the direction of the minimum horizontal stress.
IV. Reservoir porosity and permeability are independent of the fluid pressure and the formation stresses.
V. TIF propagation is controlled by Linear Elastic Fracture Mechanics (LEFM) i.e. K_{IC} is a measure of the intensity of the stress near the tip of TIF that is required for TIF propagation to occur.
VI. Stress regime is normal faulting: $\sigma_v > \sigma_{Hmax} > \sigma_{hmin.}$
VII. The magnitude of the in-situ stresses varies with depth.

The overall approach in this model is to subdivide the TIF into discrete elements (Figure 3-4). The width, temperature, pressure and internal stress of the TIF are defined at the FE nodes. The detailed governing equations on the TIF model used in this thesis comprise the:

I. Elasticity equations that relate the pressure on the TIF tip to the TIF width.
II. Fluid flow equations that relate the fluid flow and the pressure in the TIF.
III. Geomechanical equations that calculate the in situ stresses accounting for the effect of temperature and pressure changes on the reservoir stress field.
IV. TIF propagation criterion that relates the stress intensity at the TIF tip to the critical stress intensity factor for the rock (K_{IC}).

The elasticity, fluid flow, geomechanical and TIF equations are reviewed in the following sections.

3.6.2 Elasticity Equation

The growth of TIF is a 3D computational problem evaluated using the FE technique. The elasticity equation solves the stress intensity (K_I) values at points around the TIF boundary. This requires defined nodes with an identified pressure distribution within the TIF and stress over the TIF surface [99]. The TIF surface is defined with FE grid shape (Figure 3-4) with the stress intensity values computed at discrete nodes on the TIF boundary. Stress intensity values at each node are obtained by computing the TIF's

width at all nodes of the (x, z) plane of the FE grid (Figure 3-4). The TIF width at different nodes and the pressure are related by the following equation [99, 108]:

$$(P_F - \sigma_{T,min})(x,z) = \frac{\mathrm{G}}{4\pi(1-\upsilon)} \int \left[\frac{\partial}{\partial x}\left(\frac{1}{R}\right)\frac{\partial w_f}{\partial x'} + \frac{\partial}{\partial z}\left(\frac{1}{R}\right)\frac{\partial w_f}{\partial z'} \right] dx'z' \quad \text{Equation 3-1}$$

Where:

$\sigma_{T,min}$ = Total minimum horizontal stress normal to the TIF plane (y-direction in Figure 3-6) (psi)

P_F = Fluid pressure along the TIF

$\mathrm{w_f}$ = TIF width (ft)

G = the shear modulus (psi) and defined by Young's modulus (E) and Poisson's ratio (υ). G is defined as:

$$G = \frac{E}{2(1+\upsilon)} \quad \text{Equation 3-2}$$

υ= Poisson's ratio

E= Young's Modulus (psi)

R = the distance between the source point (x', z') at which the integrand is evaluated and the field point at which the pressure is evaluated (x, z) (Figure 3-4). R is defined as

$$R = [(x-x')^2 + (z-z')^2] \quad \text{Equation 3-3}$$

Details of FE mesh and node generation as TIF propagates as well as the numerical method for finding an approximate solution of TIF width i.e. $w_f(x,z)$ can be found in [108, 107].

3.6.3 Fluid Flow Equation

The fluid flow in the TIF is idealised as that of the laminar flow of an incompressible fluid. Furthermore, the fluid flow in the TIF is assumed to flow between parallel porous walls. Leak off through the TIF surface is determined by the difference between the pressure in the TIF and in the reservoir [109, 110]. A 2D flow is obtained by integrating the governing equations through the width of the TIF. The flow and pressure within the TIF are related to TIF leak-off rate by:

$$-\int \frac{{w_f}^2}{12\mu}\nabla^2\left(P_F-\frac{\rho h}{144}\right)\mathrm{dV}+\int M\left(P_F-P_p\right)\mathrm{dA} + \frac{\int w_f dA - V_0}{\Delta t_f} - Q_f = 0 \qquad \text{Equation 3-4}$$

Where:

P_p= Pore pressure at far field (psi)

Δt_f= Time increment (sec)

M= Mobility connection factor defined as:

$$M = 8\,\frac{k_y}{\Delta Y}\sum\frac{Kr_w}{\mu_w} \qquad \text{Equation 3-5}$$

k_y= Reservoir permeability in y-direction (Figure 3-6)

Kr_w= Water relative permeability (md)

μ_w= Water viscosity (cp)

The first term in Equation 3-5 ($-\int \frac{{w_f}^2}{12\mu}\nabla^2\left(P_F-\frac{\rho h}{144}\right)$) is the flow rate within the TIF, the second term ($\int M\left(P_F-P_p\right)\mathrm{dA}$) is the leak-off rate, the third term ($\frac{\int w_f dA - V_0}{\Delta t_f}$) is the volumetric storage rate within the TIF and the forth term (Q_f) is the total TIF injection rate added to the central node of the FE grid. The leak off rate is assumed to be linear in the normal (y) direction (Figure 3-5) from both vertical sides of the TIF. The mobility connection factor (M) in the leak-off term (Equation 3-4) is the mobility factor associated with the grid block intersecting the TIF with an area (A) and pressure difference between the TIF and the pore pressure ($P_F - P_p$).

3.6.4 Geomechanical Equations

The stress calculation constitutes an important part of the coupling between the fluid flow and elasticity equations within the FE grids of the TIF. The stresses that result from temperature and pressure changes in the reservoir are computed using the Goodier displacement method in the absence of TIF i.e. over the FD grids, then the computed stresses are interpolated into the 2D TIF surface using a simple model [99]. A single stress component normal to the TIF surface i.e. y-direction in Figure 3-6 is only considered in the calculation of the total stress since it is necessary to calculate only the stress at the expected TIF surface.

3.6.4.1 *Stress Calculation in the 3D FD main reservoir grid*

The stress field in the FD reservoir is calculated from the in-situ stress and rock mechanical properties. The in-situ stress is defined as a function of the reservoir depth. In this thesis, the Goodier displacement potential is used in the stress calculation [22]. The Goodier displacement method assumes zero displacement at the boundary of the reservoir model. In other hand, Oedometric Displacement potential allows vertical starin to be included. The Goodier displacement method is selected since vertical strain displacement and compaction are not considered in this thesis. Thermo-elastic and poro-elastic stresses are calculated from Goodier displacement potential by using methods developed by Koning [22]. The stress resulted from temperature and pressure changes can be described by the following equation:

$$\sigma_{T,min} = \sigma_{hmin,i} + \Delta\sigma_T + \Delta\sigma_P = \sigma_{hmin,i} + \Delta\sigma_y \qquad \text{Equation 3-6}$$

Where:

$\sigma_{hmin,i}$ =Initial minimum horizontal stress (psi)

$\Delta\sigma_T$ = Thermo-elastic stress due to temperature change (psi)

$\Delta\sigma_P$ = Poro-elastic stress due to pressure change (psi)

$\Delta\sigma_y$ = Total stress reduction due to temperature and pressure change (sum of thermo-elastic and poro-elastic stresses) (psi):

The total stress reduction due to temperature and pressure change is calculated by:

$$\Delta\sigma_y = \frac{(1+\nu)}{E}\nabla^2 X + (A_P \Delta P + A_T \Delta T) \quad \text{Equation 3-7}$$

ΔP = Pressure Difference between the flooded zone and the reservoir pore pressure (psi)

ΔT = Temperature difference between the injected fluid and reservoir (F^0)

A_P = Poro-elastic Constant (psi/psi):

$$A_P = \frac{\left(1 - \frac{C_g}{C_b}\right)(1-2\nu)}{(1-\nu)} \quad \text{Equation 3-8}$$

C_g = Grain Compressibility (psi^{-1})

C_b = Bulk Compressibility (psi^{-1})

A_P = Poro- elastic constant (psi/ F^0):

$$A_T = \alpha_T \frac{E}{(1-\nu)} \quad \text{Equation 3-9}$$

α_T = Thermal expansion coefficient (1/ F^0)

$\nabla^2 X$ = Goodier displacement potential

Goodier displacement potential is computed first over the entire FD grid [8]. The Goodier displacement potential ($\nabla^2 X$) is given by the following equation:

$$\nabla^2 X = \frac{(1+\nu)}{E}(A_P \Delta P + A_T \Delta T) \quad \text{Equation 3-10}$$

3.6.4.2 ***Stress Calculation on the 2D TIF surface***

The resultant change in the minimum horizontal stress ($\Delta\sigma_y$) due to temperature and pressure changes computed using the Goodier displacement potentials are interpolated onto the 2D FE TIF surface [8] once the TIF has extended beyond its initial grid block. Analytical model developed by Gonzales and Perkins [97] (Equation 3-11) with a circular shape function of 0.5 is used for the interpolation [8]:

$$\Delta\sigma_y = 0.5\left[A_P(T_i - T_R) + A_T\left(P_F - P_p\right)\right] \quad \text{Equation 3-11}$$

Where:

T_R = Reservoir temperature (F^0)

T_i = TIF surface temperature (F^0)

3.6.5 TIF propagation criterion

Propagation of the TIF is controlled by the fracture criterion of LEFM. The TIF propagation happens in such a way that the stress intensity factor (K_I) at each node is greater than the critical stress intensity factor (K_{IC}). Because the TIF width (w_f) near the TIF tip region is proportional to the stress intensity factor at the boundary, the condition for TIF propagation can be given in terms of (w_f) as [8, 108] :

$$w_f < w_c \quad \text{No TIF propagation} \qquad \text{Equation 3-12}$$

$$w_f > w_c \quad \text{TIF propagation} \qquad \text{Equation 3-13}$$

Where

$$w_c = \frac{4K_{IC}(1-\upsilon)}{G}\sqrt{\frac{a}{2\pi}} \qquad \text{Equation 3-14}$$

Where:

w_c = Critical Width at a fixed distance (a) from the tip of the TIF (ft.)

a = Defined at a small distance from the tip of the TIF ($ft^{1/2}$) (see Figure 3-4)

K_{IC} = The critical stress intensity factor ((Rock fracture toughness)) (psi. $ft^{1/2}$.)

υ = Poisson's ratio

G = The shear modulus (psi)

The critical stress intensity factor (K_{IC}) relates the additional pressure above the minimum horizontal stress required to open a TIF sufficiently to propagate. The critical stress intensity factor (K_{IC}) i.e. fracture toughness can be obtained for a brittle elastic solid from laboratory testing. Fracture toughness experiments performed on various rocks indicated that (K_{IC}) is of the order of 10^3 psi-$in^{1/2}$ [108, 111, 112].

After computing w_f from Equation 3-1, it is then compared to w_c that is computed from Equation 3-14. Following the propagation criterion above, TIF propagation is determined.

3.6.6 Solution method

The finite element (FE) elasticity and fluid flow equations within the TIF i.e. (Equation 3-1 and Equation 3-4) are combined and solved iteratively for the TIF widths (w_f) using the Newton Raphson method. The iteration is performed in the following manner [8]:

I. The combined FE equations solver is supplied with a total rate (Q_f).
II. The geometry of the TIF is iterated until a constant TIF geometry is found i.e. $w_f = w_c$. The pressure at the centre of the TIF (P_F) is returned and another level of iteration is performed.
III. The iteration continues until the (P_F) and (Q_f) are consistent with the total well injection rate and the BHP.

3.6.7 Implementation Workflow

The 3D FE TIF solution is coupled to FD multiphase 3D flow in the reservoir as shown in Figure 3-5. The reservoir flow module and the TIF module are connected by a set of connection factors. The coupled elements include:

I. Reservoir model: A multiphase 3D fluid flow (pressure and saturations) modelled with FD method using black-oil pressure, volume, and temperature variables.
II. Geomechanical solution: The geomechanical solution uses a FD method to solve 3D stresses in the rock within the reservoir. The solution uses Goodier Displacement potential method which assumes zero displacement around the reservoir model i.e. at the reservoir boundary. Once the stress is calculated over 3D reservoir model, it is then interpolated in the 3D TIF model.
III. TIF model: the TIF model is a FE grid with triangular internal elements and quadrilateral boundary elements (Figure 3-4). The FE fluid flow and the elasticity equations within the TIF are solved iteratively to obtain the TIF

widths. The TIF propagation criterion is then applied to define the TIF shape and dimensions.

The coupling process and solution methods among all these elements is shown in Figure 3-8 and Figure 3-9.

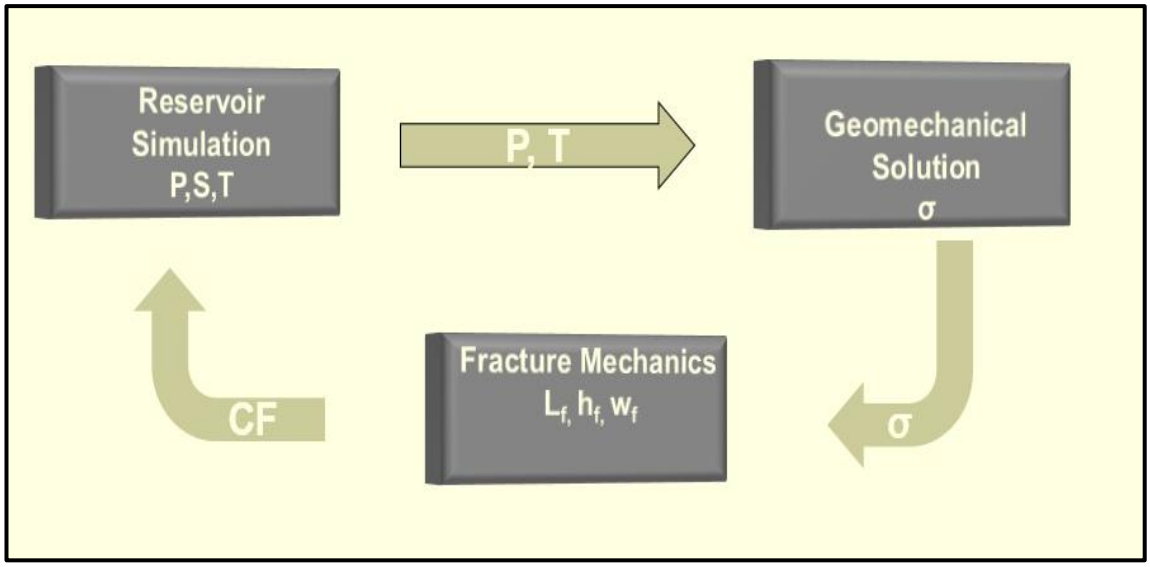

Figure 3-8: Workflow coupling among the reservoir model, the geomechanical solution and the TIF model.

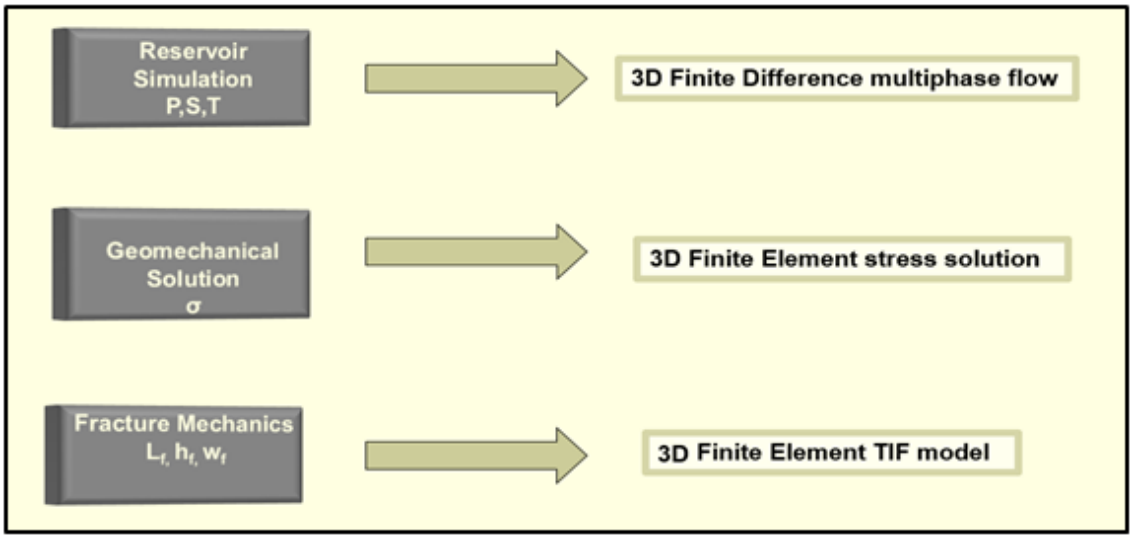

Figure 3-9: Solution methods used for each element of the coupled models

3.6.8 General Thermally Induced Fractures Modelling Notes

The TIF model used in this thesis has the following general notes:

I. The potential TIFs are "seeded" in the most promising locations along the well. These TIFs are tested each timestep for initiation. Once TIF is initiated, it will be included in the propagation analysis.

II. The TIF dimensions i.e. the half-height above and below the TIF origin, the half-length, and the initial width are required as an input. Prior to initiation, no flow from the TIF is assumed.

III. The dimensionless fracture conductivity (F_{CD}) values of 500 for modelling permeability within the TIF is assumed. This value represents the infinite conductivity approximation i.e. pressure drop within the TIF is neglected.

IV. In this model, the injection well has to be controlled by a fixed THP with a well injection curve with BHP and temperature defined for a range of injection rates. This is realistic, but is also because of the iterative nature of the elasticity and fluid flow equations within the TIF. Controlling the TIF with a fixed rate will produce an unrealistic TIF shape.

V. The stress behaviour for the reservoir rock is defined as a single stress layer. The in-situ stress varies with depth through defined stress gradient.

VI. The rock mechanical properties e.g. Young's Modulus, Poisson's Ratio, Biot's coefficient, and critical stress intensity are assumed to be homogenous and isotropic through the reservoir.

Chapter 4 Identification and Characterization of Thermally Induced Fractures by Integrating Analytical and Semi-analytical Techniques

4.1 Introduction

It has been shown that that TIFs do improve injectivity but may also reduce the oil sweep efficiency, pressure support and oil recovery [5, 113, 29, 7, 28].

Identifying and characterising dynamic TIF growth is thus a critical step when defining field development strategies and making day-to-day reservoir management decisions. A practical workflow is thus required to detect TIFs as well as monitor and evaluate the waterflood's performance in a timely, cost-effective manner. Reservoir simulation is frequently the preferred tool for reservoir management. However, dynamic and fine scale events, such as TIF, formation damage and plugging [114], are often neglected. Simpler, data-driven injection performance techniques (Hall plot, rate vs. pressure plot, injectivity index vs. time plot, pressure fall off tests, etc.) can be used for TIF identification. However, these history analysis methods often lack:

I. High resolution detection of TIF.
II. Identification of subtle, short-term changes.
III. Evaluation of the impact of TIF at different levels i.e. field-level and producer/injector pair-level.
IV. Identification of the likely TIF propagation direction.

A workflow is developed in this thesis to integrate a recently developed analytical model, the Modified Hall Integral (MHI), with a semi-analytical model, the Capacitance–Resistance Model (CRM), to identify the onset of TIF, its propagation properties, direction and impact during reservoir dynamic events occurring at different levels. The value of integrating MHI and CRM models comes due to their ability to:

I. Manage waterfloods remedial measures.
II. Provide a real time surveillance workflow.
III. Condition the reservoir simulation models.
IV. Guide history matching efforts.
V. Obtain valuable information in a timely, cost-effective manner.
VI. Apply new strategies in future field development plans.

4.2 Methodology

This chapter presents an integration of MHI and CRM models in order to monitor, detect and characterise TIF as well as evaluate its impact at both the well and the reservoir level. This can be performed using readily available data without the need to run expensive, time consuming tests. The Figure 4-1 workflow shows the transformation of dynamic field data into reservoir management decisions. The first step is to obtain production/ injection and pressure history. The second step analyses the data by using analytical and semi-analytical models. The analytical models provide information at the well level while the semi-analytical models evaluate the impact of TIF on the flow performance of well pairs and the inter-well communication. This workflow focusses on the combination of MHI and CRM, but other analytical models and injection monitoring techniques will be also used to support the findings and show the added value of combining models and techniques. The final step in the workflow is to transform these findings into reservoir management decisions.

Synthetic cases showing TIF behaviour during cold water injection were prepared using a numerical reservoir simulator coupled to a 3D geomechanical solution and a finite element TIF model that allowed modelling of TIF initiation and propagation. The two cases discussed have a different TIF direction while all other geomechanical and reservoir properties are the same. The generated well performance data was analysed with the proposed workflow and the results used to show the value derived from the analysis. Finally, a real field example is presented to illustrate and corroborate the workflow.

The novelty of the presented approach is in efficiently integrating the recent, analytical and semi-analytical models to identify the onset, propagation, characteristics, and impact of TIF from the generally available well injection production history data. The practical workflow employed here will help engineers detect and monitor TIFs; as well as evaluate the metrics describing waterflood performance, namely flood efficiency, inter-well communication and pressure maintenance.

The only input required by this workflow is the standard well injection/production history data.

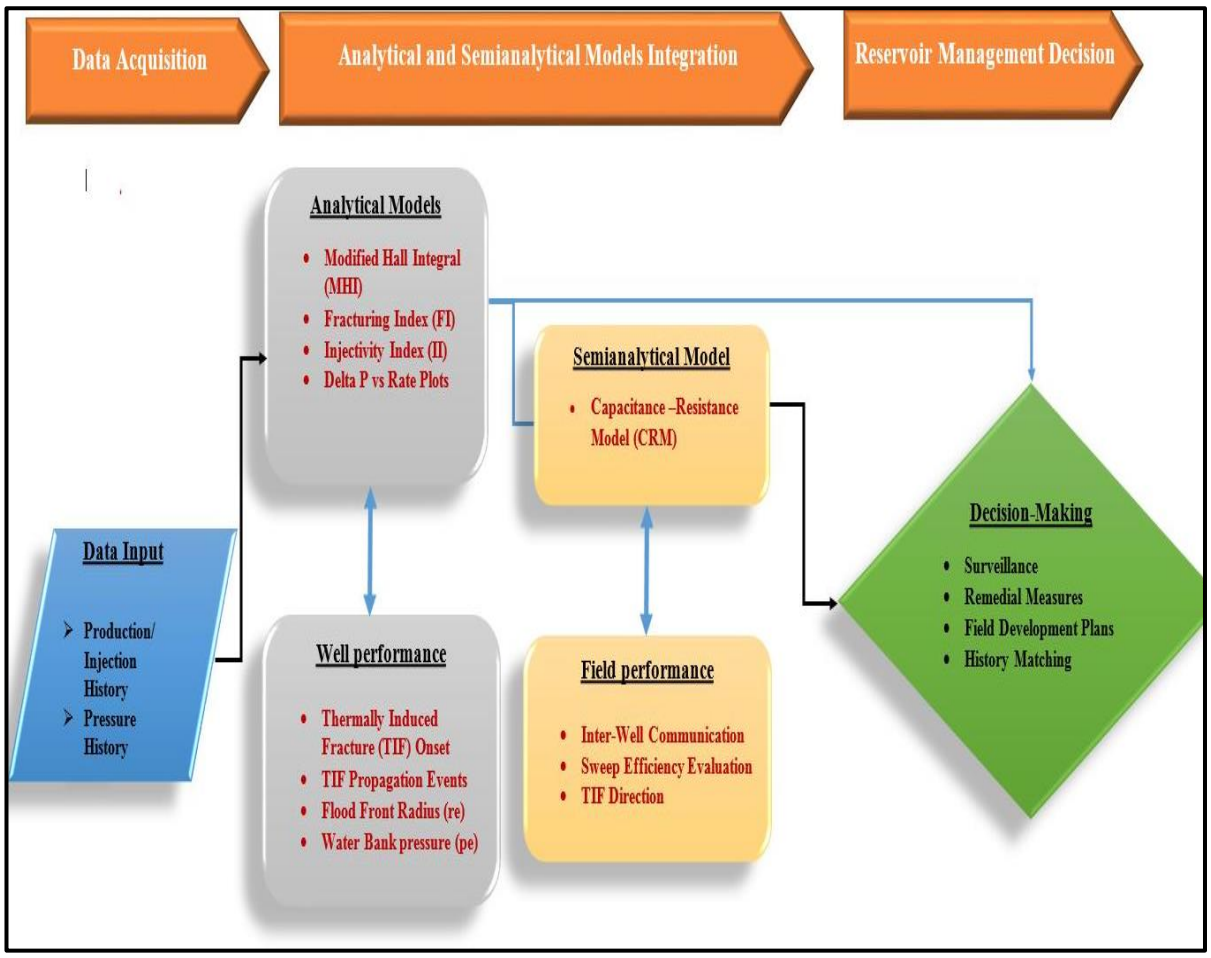

Figure 4-1: Integrating analytical and semi-analytical models workflow

4.3 Conventional TIF Diagnostics Techniques

Monitoring injection wells performance is essential to understand the reservoir performance. The changes in injectivity can have a significant impact on the reservoir pressure and the sweep efficiency and therefore the ultimate oil recovery. Effective monitoring of injection wells and early detection of TIF or even any loss in the injectivity can provide the opportunity to prescribe quick and effective remediation measures throughout the life of the injection well. The conventional methods as well as the recently developed analytical and semi-analytical methods are discussed in the following sections.

4.3.1 Hall Integral

The Hall Integral (HI) was developed by Hall (in 1963) to account for different effects at an injection well. The plot is a straight line during normal conditions, with any deviation from the straight line indicating change of injection conditions. Analysing the plot can help to draw conclusions regarding the damage or fracturing near the injection well. The following data are required for HI analysis [115] :

I. Monthly BHIPs.

II. Average reservoir pressure.

III. Monthly water injection volumes.

IV. Number of injection days of the month.

The HI is based on the ideal Darcy radial flow equation for steady state flow. The injection rate expressed in oilfield units is:

$$i_w = \frac{0.00707\ Kh\ (P_{wf} - P_{ave})}{\mu\ \left[In\frac{r_e}{r_w} + S\right]} \qquad \text{Equation 4-1}$$

Where

i_w = Water injection rate,

P_{wf} = The bottomhole pressure

P_{ave} = The average reservoir pressure

h = The reservoir thickness,

K = The reservoir permeability

S = The skin factor

r_e = The reservoir effective radius

r_w = The wellbore radius,

μ = The fluid viscosity.

Equation 4-1 is based on the following assumptions:

I. The fluid is homogenous and incompressible

II. The reservoir is vertically confined and uniform i.e. with relation to permeability and thickness

III. The reservoir is horizontal and gravity effect is neglected

IV. The flow is steady state

V. The oil/water mobility ratio is 1

VI. The pressure at distance = r_e is constant.

Based on the above assumptions k_w, h,μ_w,r_e, r_w are constant and Equation 4-1 is expressed as:

$$i_w = \text{II}\ (P_{wf} - P_{ave})$$ Equation 4-2

Where:

$$II = \frac{K_W h}{141.2\ B_w \mu_w\ \left[In\frac{r_e}{r_w} + S\right]}$$ Equation 4-3

Rearranging Equation 4-2 yields the following:

$$(P_{wf} - P_{ave}) = \frac{i_w}{\text{II}}$$ Equation 4-4

Integrate both sides of Equation 4-4:

$$\int_0^t (P_{wf} - P_{ava})dt = \frac{1}{\text{II}}\int_0^t i_w\,\text{dt}$$ Equation 4-5

The integral in the right side of Equation 4-5 is the cumulative water injection. Therefore Equation 4-5 can be expressed as:

$$\int_0^t (P_{wf} - P_{ava})dt = \frac{W_i}{\text{II}}$$ Equation 4-6

Where W_i = Cumulative volume of water at injected time t. A plot of the left side versus the right side of Equation 4-6 is, a straight line with a slope of 1/II. This plot is called the Hall plot (HI). The slope II is a constant providing all the parameters k, h, μ, r_e, r_w from Equation 4-3 are constant. The slope of II will also change if any one of these parameters change. This is where the diagnostic value of HI lies. Figure 4-2 is an example of HI signatures for different injection well conditions. This method is a real time monitoring tool that provides a qualitative indication of the injection well's performance. This method has the following drawbacks [116]:

I. HI does not capture the short term changes and therefore can result in delayed remedial measures.

II. It is necessary to conduct regular pressure falloff tests (PFO) as well as monitor monthly Voidage Replacement Ratio (VRR) plots to determine whether the average reservoir pressure is changing.

III. A change in the value of the parameters that are assumed to be constant are not immediately apparent on a daily/weekly basis due to the long-term scale and the level of "noise" present in the measured data.

IV. HI method assumes water breakthrough at the time of application. Hence it is unreliable for water pre-breakthrough situations.

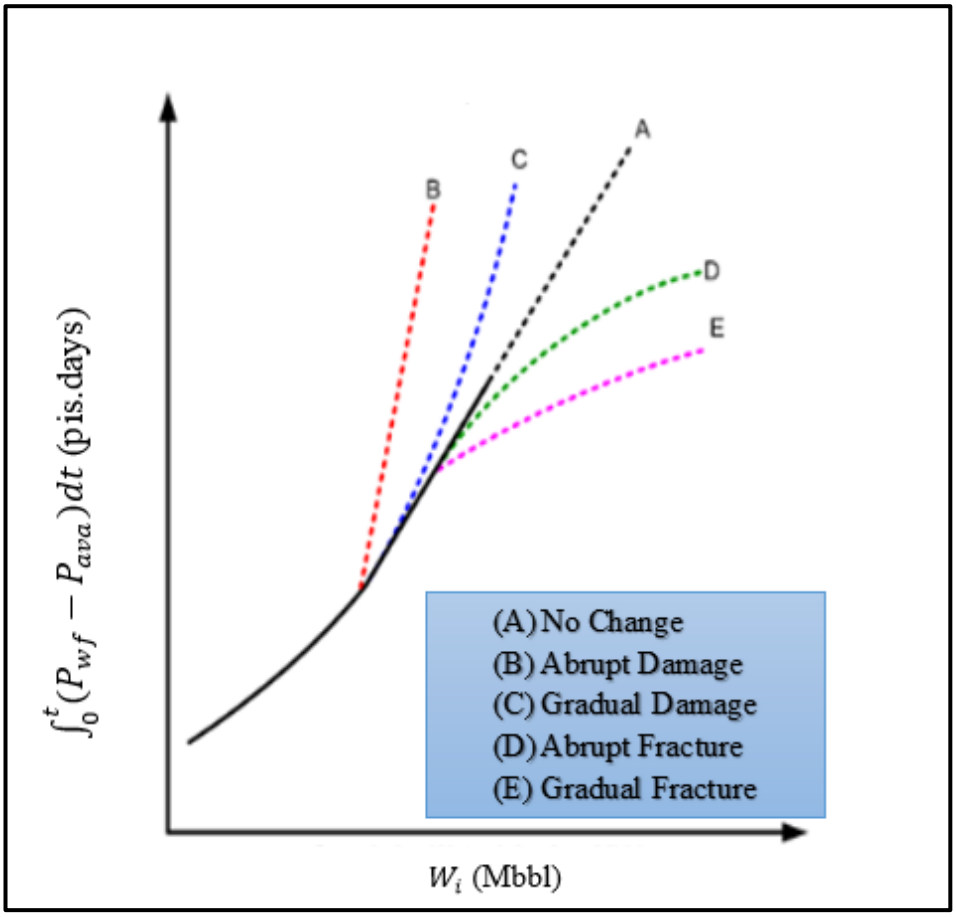

Figure 4-2: Overview of HI showing trends of various well injection conditions

4.3.2 The Injectivity index (II) and Reflectivity of Injectivity Index (RII)

The Injectivity index (II) combines all factors affecting the injection well performance e.g. permeability to water (K_W), injection zone height (h), water viscosity (μ_w), and skin (S). The tool is simple using the measured injection rate and injection pressure, once they have been corrected for bottomhole condition and the reservoir pressure. II is simply the ratio of the injection rate and the pressure differential across the sandface expressed in Equation 4-6 .

This tool is a valuable one for tracking the injection well performance over time. It has also been used to evaluate the effectiveness of injection well stimulation treatments [116]. This method, however, has the following disadvantages:

I. Fluctuations in the measured rates and pressures result in fluctuations in the II. These fluctuations can be extreme and real trends are difficult to be identified.

II. The difficulty in estimating effective reservoir pressure P_e in vicinity of the injection well. PFO tests are needed to obtain an accurate value of P_e. This requires shutting-in the injection well on a regular basis.

The Reflectivity of the Injectivity Index (RII) is simply the reciprocal of the II. RII when plotted against time is normally less sensitive to operational fluctuations.

4.3.3 Other methods

There are other methods commonly used to monitor injection well performance. These include:

I. **Rate and Pressure Plots**: Continuous monitoring of rate and and bottom hole pressure plots is the simplest method of monitoring. Generally, an increase in the injection pressure over time for a stable or declining rate can be an indication of impairment bulidup. In contrast, a decrease or stable injection pressure over time for an increasing injection rate is taken as indication of fracturing. Analysis of such plots can be difficult due to the variation of pressure and rate [117].

II. **Voidage Replacement Ratio (VRR)**: VRR is the ratio of injected reservoir volumes to the produced reservoir volumes. VRR can be expressed mathematically as follows:

$$VRR = \frac{B_W i_w + B_g i_g}{B_O Q_O + B_W Q_W + B_O (GOR - R_S) Q_O} \qquad \text{Equation 4-7}$$

Where is $B_W \; and \; B_g$ are the water and gas FVF and $Q_O \; and \; Q_w$ are the oil and water production rate. The third term in the denominator represent the free gas produced in addition to the dissolved gas in the oil. The second term in the numerator can be omitted if only water is injected. VRR can be calculated instantaneously by considering the injected and produced volumes. If the calculated VRR is equal or greater than 1, then the reservoir pressure is being

maintained or increased for that period. In contrast, the reservoir pressure decreases if VRR is less than 1. This simple method is a good tool to monitor reservoir pressure in the vicinity of the injection well but no information can be obtained about the potential causes of a variable reservoir pressure.

III. **Injection Tests:** such as Pressue Fall-off (PFO) and Production Logging Tool (PLT). PFO testing can provide quantitative information about the effective reservoir pressure, effective permeability-thickness product (kh), skin and presence of fractures [117]. These tests are usually expensive and kept at minimum.

IV. **Step Rate Testing (SRT):** SRTs are conducted to estimate the transition from matrix flow to fracture-dominated injection. SRT involves increasing the injection rate in discrete increments and reading the corresponding pressure. The fracture pressure is determined as the point of intersection of a best fit lines for the two slopes [116]. The minimum injection BHP for fracture propagation can be obtained by this method. Reservoirs exhibiting TIF are expected to have a reduction in the fracture pressure with time due to the cool injection water reducing the reservoir's temperature and minimum horizontal stress (Figure 4-3). Both SRTs and PFO methods involve a production deferral associated with the shut-ins. This is not desirable since they often cause significant costs. These tests are thus conducted infrequently on an opportunity basis which results in a loss of data continuity and quality [116].

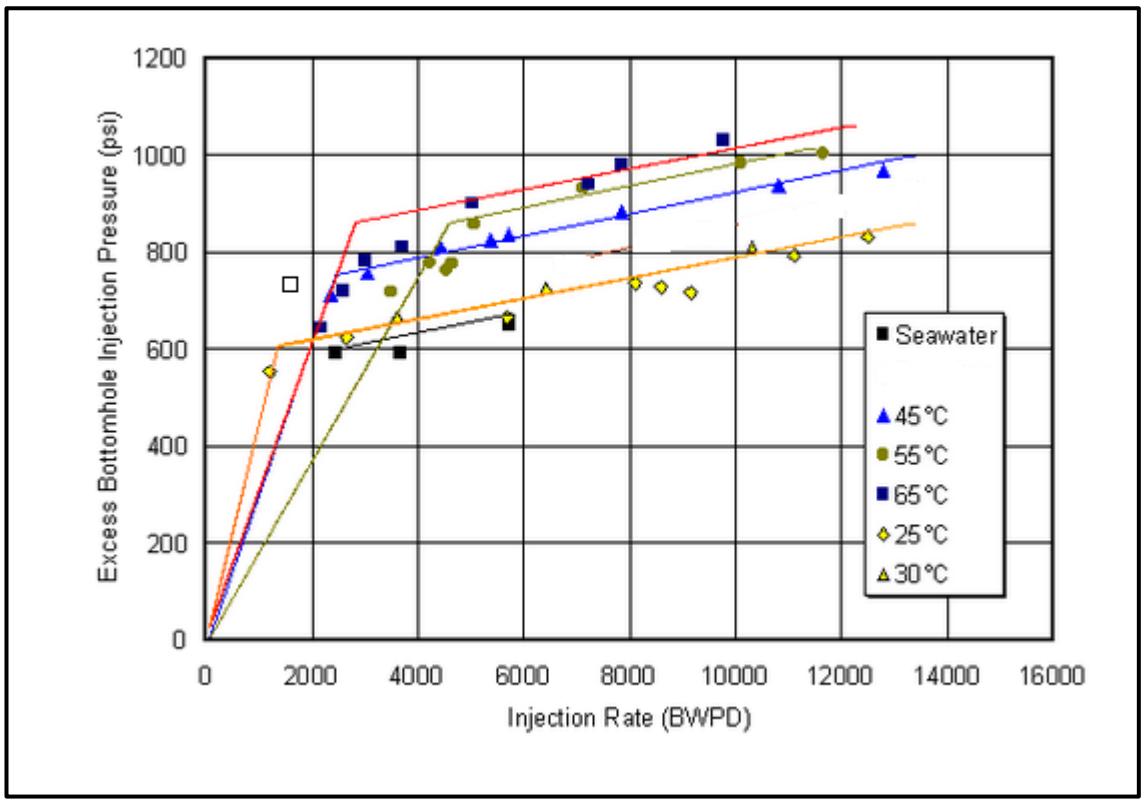

Figure 4-3: SRTs conducted in one of the injection wells in the Shell Eider field show the variation of fracture pressures with injection water temperature [117]

4.4 Recent Analytical Methods

The conventional injection monitoring methods mentioned above provide varying degrees of surveillance capabilities. However, these methods have the following limitations:

I. Longer time needed for identification of TIF initiation or formation damage.
II. Low resolution detection of changes from planned injection performance.
III. Some methods are expensive and cause deferred production.
IV. Some methods are not applicable to all situations e.g. the transient flow ones

Recent methods have been developed to overcome some of these limitations e.g. Fracturing Index (FI) model and Modified Hall Integral (MHI). The new methods, explained below, have the following advantages [118, 116, 119] :

I. More robust and suitable for pre-breakthrough situation i.e. transient and pseudo steady state situations
II. More discriminating for identifying deviations from planned performance.

4.4.1 Fracturing Index (FI) model

An analytical model developed by Slevinsky [119] couples the growth of a TIF with the fluid leak-off equations. The model is treated as if the injection is one big hydraulic fracture. Hydraulic fracture analytical model from Geertsma and deKlerk [120] was used as a basis for this model as follows :

$$L_f = \frac{1}{2\pi}\frac{i_w\sqrt{t}}{HC} \qquad \text{Equation 4-8}$$

Where

L_f = The TIF half length

H = The TIF height

t = Time of injection

C = Leak-off coefficient.

i_w = Injection rate

The leak-off coefficient C is replaced by an equation in terms of fluid and reservoir properties. Williams [121] developed the leak-off equation that accounts for permeability plugging at the tip of the TIF as well as in the formation. This equation can be expressed in oilfield units as:

$$C = 0.00148\sqrt{\frac{F_d K \varphi \Delta \mathrm{P}}{\mu_w}} \qquad \text{Equation 4-9}$$

Where

F_d = The damage factor due to plugging

ΔP = The pressure difference between the bottomhole flowing pressure and the average pressure of the drainage area

μ_w = Injection fluid viscosity

K = Permeability

φ = Porosity

Combining Equation 4-8 and Equation 4-9 and correcting them to metric units gives the following equation:

$$L_f = \frac{25.087\, i_w\sqrt{t}}{H\sqrt{\frac{F_d K \varphi \Delta \mathrm{P}}{\mu_w}}}$$ Equation 4-10

i_w and ΔP can be estimated or measured. Hence Equation 4-10 can be rearranged as the following in terms of the known parameters:

$$\frac{\Delta \mathrm{P}}{{i_w}^2} = FI = \frac{629.381\, t\mu_w}{L_f^2 H^2 F_d K \varphi}$$ Equation 4-11

The term $\frac{\Delta \mathrm{P}}{{i_w}^2}$ is called Fracturing Index (FI). FI reflects the interactions between formation/TIF plugging and TIF propagation. The II can be obtained from Equation 4-11 by (1) rearranging it in the form of a traditional II and (2) replacing $(i_w.t)$ by the cumulative water injection W_i as in the following equation:

$$\frac{i_w}{\Delta \mathrm{P}} = II = \frac{L_f^2 H^2 F_d K \varphi}{629.381\, W_i \mu_w}$$ Equation 4-12

Plotting both FI and II vs. cumulative injection on a log-log plot monitors the TIF growth in real time by use of a triangular overlay (Figure 4-4). the following implications can be denoted from combining Figure 4-4 with Equation 4-11 and Equation 4-12 [119]:

I. The FI should increase linearly with cumulative water injection for a constant TIF length i.e. no TIF propagation
II. FI should reduce during TIF propagation i.e. TIF growth increases the injectivity at a greater rate than an increasing formation damage factor decreases the injectivity.
III. The longer the TIF, the lower the slope of the FI plot versus cumulative water injection.
IV. The II should increase during TIF propagation, and decrease if damage occurs and the TIF length remains constant or grows slowly.

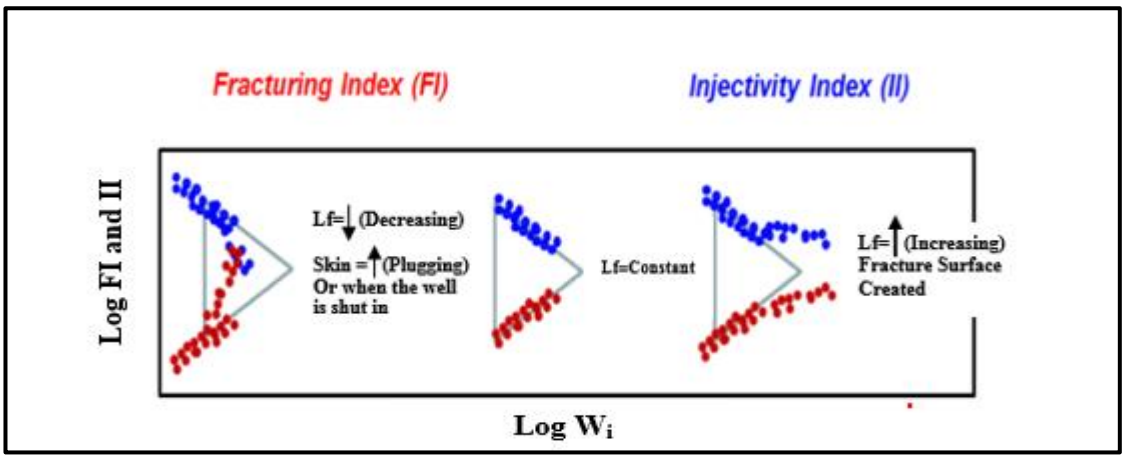

Figure 4-4: Interpretation of FI and II (vertical axis) w.r.t. Cumulative Water Injection Volume (horizontal axis) for TIF Evaluation [27]

FI is used to determine TIF onset, propagation, the extent of any fracture face plugging as well as support the findings of the MHI formulation (section 4.4.2).

4.4.2 Modified Hall Integral

Modified Hall Integral (MHI) method builds on the classical Hall plot with new diagnostic capabilities developed by Izgec and Kabir [118]. The fundamental idea for proper application of HI was to update the oil/water interface pressure (Pe) at every time step. Two approaches, transient and pseudo-steady state for updating (Pe) are used. The Pseudo-steady-State and transient equations for determining (P_e) are derived in Appendix A and Appendix B.

Starting with integrated pseudo-steady-state, radial flow as per Darcy's law, the Hall Integral in oilfields units is:

$$\int (P_{wf} - P_e)\,\mathrm{dt} = \frac{141.2\, W_i\, B\mu}{\mathrm{kh}}\left[In\left(\frac{r_e}{r_w}\right) - 0.5 + s^*\right] \qquad \text{Equation 4-13}$$

The derivative of the Hall Integral (HI) was solved both analytically and numerically in Equation 4-14 and Equation 4-15. Derivations of these equations can be found in Appendix C.

$$D_{HI} = \alpha_1\, W_i \left(In\,\frac{r_e}{r_w} + s^*\right) \qquad \text{Equation 4-14}$$

where $\mathrm{D_{HI}}$ is the analytical derivative, $\mathrm{W_i}$ is the cumulative water injection, and α_1 is defined as:

$$\alpha_1 = \frac{141.2B\mu}{kh}$$ Equation 4-15

Pseudo-skin S^* in Equation 4-14 provides diagnostics clues as well and has a merely qualitative purpose. The methodology developed by Zhu and Hill [122] (see Appendix B), allows the pseudo-skin to be continuously updated with the following equation:

$$S^* = \frac{1}{0.868}\left[\frac{b}{m} - \log\left(\frac{k}{\emptyset\mu c_t r_w^2}\right) + 3.23\right]$$ Equation 4-16

(b and m) parameters in Equation 4-16 are defined in Appendix B. The numerical derivative (D_{HIn}) of the Hall integral can be expressed as:

$$D_{HIn} = \left(\frac{I_H^{n+1} - I_H^n}{\ln (W_i)^{n+1} - \ln (W_i)^n} \right)$$ Equation 4-17

Plotting HI, D_{HI}, and D_{HIn} on the same graph provides an overview of the well's injection performance. The relationship between the integral and the derivatives provides a distinctive signature that identifies matrix injection, fracturing or plugging (Figure 4-5):

I. No separation of HI and its derivative indicates matrix injection.
II. Downward separation of the derivative from HI indicates formation fracturing due to a negative pseudo-skin.
III. Upward separation of the derivative from HI indicates formation plugging due to a positive pseudo-skin.

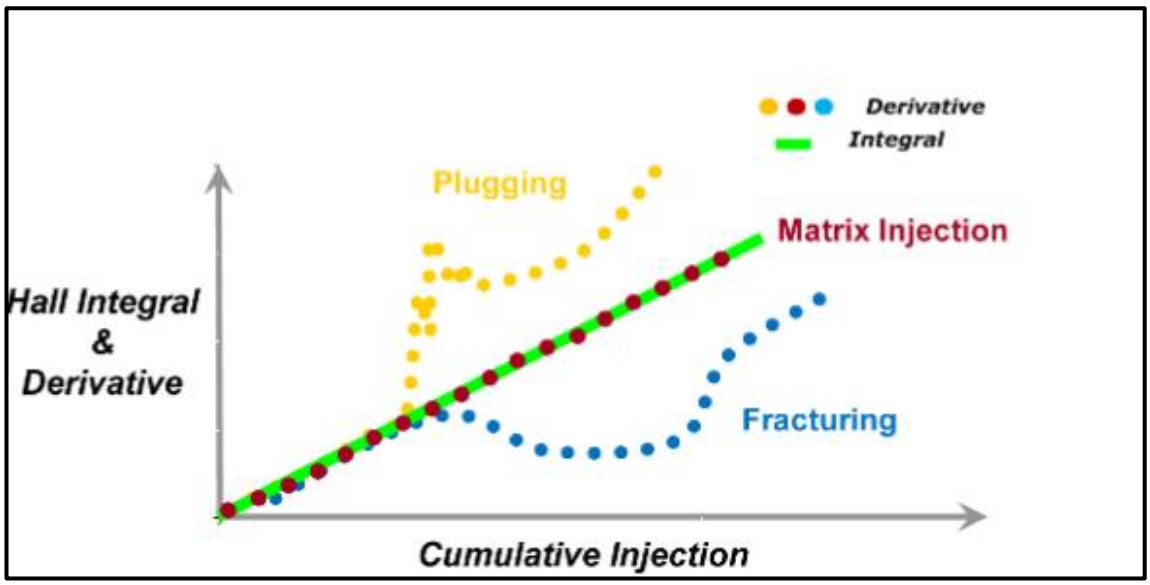

Figure 4-5: Modified Hall Integral analysis [123]

The advantage of MHI analysis is the employment of multiple curves instead of restricting the analysis to the single curve of HI analysis. MHI can clearly identify TIF initiation and propagation, as will be shown later.

The variable radial distance of the water injection front (r_e) can be updated at every time step using Equation C-5, Appendix C. Equation A-4, Appendix A is the pseudo-steady state (PSS) approximation for pressure (P_e). It is used to evaluate P_e at the flood front (r_e) makes MHI a robust tool for real time monitoring. The position of the injection bank (r_e) also gives guidance for the allowable length of a TIF. The piston-like, flood-front assumption makes this formulation accurate for flood advance and pressure evaluation, though it is not so well suited for diagnosing efficiency of the waterflood in terms of recovery efficiency [118].

4.5 Semi-Analytical Method

4.5.1 Capacitance Resistance Model (CRM)

CRM is a material balance, data-driven model that measures the communications between wells in a waterflooded reservoir. It captures the essential reservoir information despite not using any spatial geological details. CRM has been given much attention in the recent years since, unlike many other data-driven methods, it honours fundamental reservoir engineering concepts. It treats the basic production/injection history data (BHP and flow rate) as input and output signals while quantifying the inter-well connectivity (resistance) and drainage volume (capacitance) by a data-fitting process. The term "connectivity" (resistance) here is equivalent to the fraction of fluids flowing from an

injector to a specific producer. The drainage volume (or capacitance) is a measure of fluid storage between the wells. CRM analysis has been shown to provide information on the flood's well sweep-efficiency, the development of channelling along high permeability layers, etc., data that would otherwise require expensive tests and/or time consuming computationally extensive history matching [124, 125]. This thesis introduces a new application of CRM, identifying the likely direction of TIF propagation and its impact on the sweep efficiency.

This thesis uses CRMIP (CRM injector–producer control volume (Figure 4-6) for each injector-producer pair [126]). This formulation, being sensitive to high reservoir heterogeneity [127], is appropriate for a TIF study (see Appendix D):

$$q_j(t_n) = \sum_{i=1}^{N} q_{ij}(t_0) e^{\frac{-(t_n - t_0)}{\tau_{ij}}} + \sum_{i=1}^{n} \left\{ \sum_{k=1}^{n} \left[\left(f_{ij} I_i^k - J_{ij} \tau_{ij} \frac{\Delta P_{wf}}{\Delta t_k} \right) \left(1 - e^{\frac{-\Delta t_k}{\tau_{ij}}} \right) e^{\frac{-(t_n - t_k)}{\tau_{ij}}} \right] \right\} \quad \text{Equation 4-18}$$

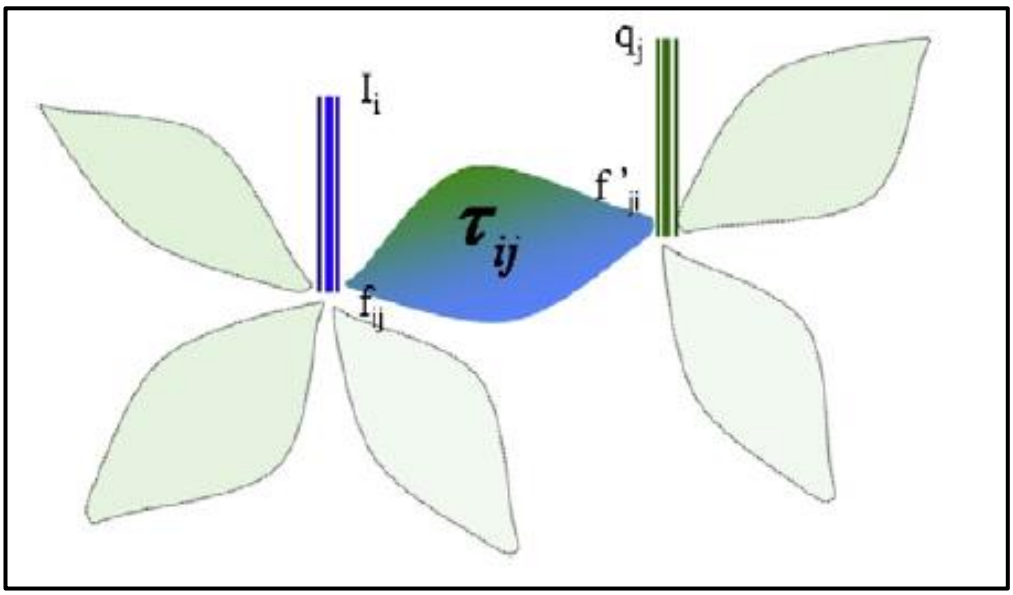

Figure 4-6: CRMIP Model of Flow between an Injection and a Production Well [126]

Where f_{ij} is fraction of injection from injector i flows to producer j (producer gain), τ_{ij} is the time constant and J_{ij} is the productivity index. Figure 4-6 explains the CRMIP parameters describing the flow between an injector, subscript i, and a producer, subscript j. f_{21} is thus the connectivity between Injector 2 and Producer 1. CRMIP requires sufficient well production/injection history data and a robust optimisation algorithm to match the parameters in a multi-well, multilayer waterflood case. Excel solver proved to

be sufficient for the scenario of a single layer and a few wells used in this study. (Thanks to my colleague Bona Prakasa for his contribution in the CRM analysis).

4.6 Synthetic Case Histories

Coupling a reservoir simulator with a 3D finite element TIF model and geomechanical model allows modelling the fluid flow as well as the dynamic propagation and the shape of a TIF. Such a model was used to generate data for two typical cases of cold water injection. Both cases employed the same (Table 4-1) reservoir and geomechanical properties, but with different growth directions for the TIF. The reservoir simulation model (Figure 4-7) has 1875 (25 x 25 x 3) cells of size 200 x 300 x 20 ft with 4 vertical wells, 2 producers (P1 and P2) and 2 injectors (I1 and I2). A system of two injector-producer pairs was selected to clearly indicate the effect of changing the TIF direction. The performance of the two producers (P1 and P2) will be sensitive to the direction as well as the location of the flood front and to the oil recovery.

Table 4-1: Reservoir and Geomechanical Parameters for Cases 1 and 2

Reservoir Parameters		Geomechanical and Thermal Parameters	
Initial Reservoir Pressure, psi	4500	Young's Modulus, psi	2×10^6
Permeability, md	200	Poisson's ratio	0.35
Porosity	0.2	Biot's coefficient	0.67
Initial Water Saturation	0.2	Fracture toughness psi.ft-1/2	400
Reservoir Temperature, ^{0}F	200	Vertical Stress Gradient, (psi/ft)	0.9
Water Viscosity, cp	0.34	Maximum Horizontal Stress, psi/ft	0.85
Oil Viscosity, cp	1.8	Minimum Horizontal Stress, psi/ft	0.8
Injected Water Temperature, ^{0}F	70	Rock thermal expansion coefficient ($1/^0$F)	0.00012

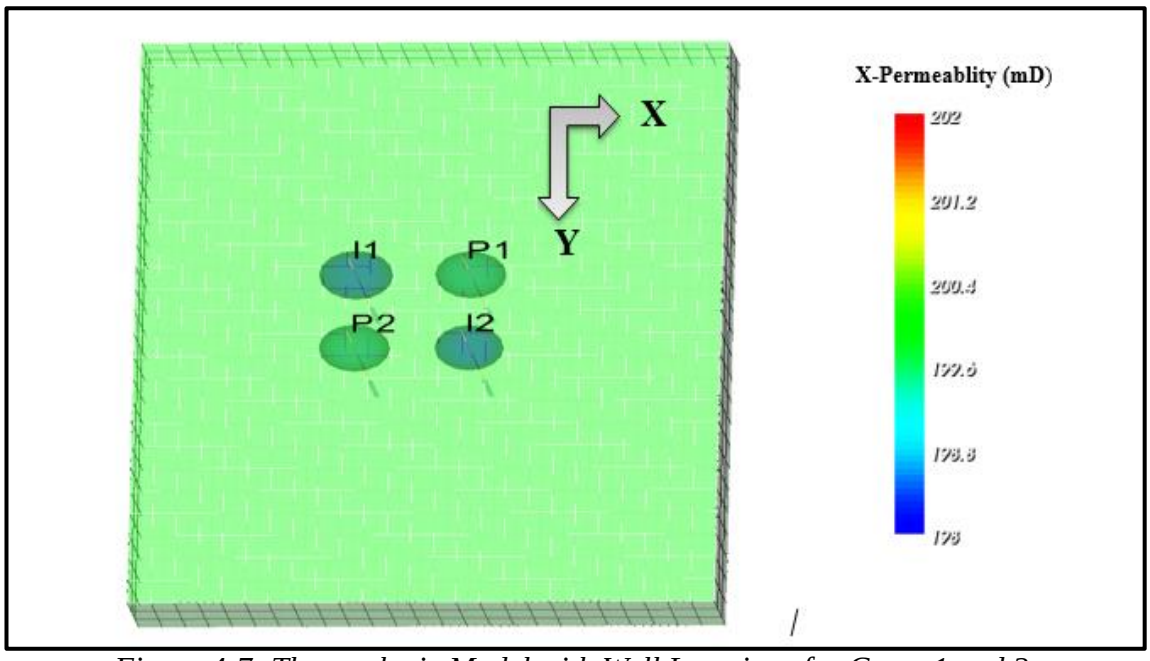

Figure 4-7: The synthetic Model with Well Locations for Cases 1 and 2

TIF is modelled in Well I1 which is being operated at a variable rate and a constant tubing head pressure while I2, P1 and P2 are operated under variable liquid rate between 4,000 and 4,500 STB/D (Figure 4-15). This mimics the rate variations observed in a real field. It has the additional benefit of improving the quality of data fitting process when carrying out CRM calculations. TIF direction in well (I1) is in the x-direction for case 1 (Figure 4-7) and in the y-direction for case 2 (Figure 4-7).

4.6.1 Synthetic Case 1 Histories

This case modelled a TIF growing from injector 1 (I1) in the x-direction towards producer 1 (P1) (Figure 4-8). Cold water injection reduces the reservoir temperature (Figure 4-9), causing a significant reduction in the in-situ stress. Figure 4-10 plots the dynamics of TIF initiation and growth after 155 days of injection. The I1 injection BHP is stable throughout the simulation. TIF occurred at a BHP considerably lower than the original, minimum horizontal stress (approximately 5288 psi from Table 4-1). The initial increase in injection rate is due to the higher production rates, hence higher drawdown from nearby production wells i.e. P1 and P2 (Figure 4-9). The sharp significant increase in injection rate at point 1 is due to the initiation of the TIF. The increase of BHP after TIF after point 2 in Figure 4-10 is due to the increase in reservoir pressure.

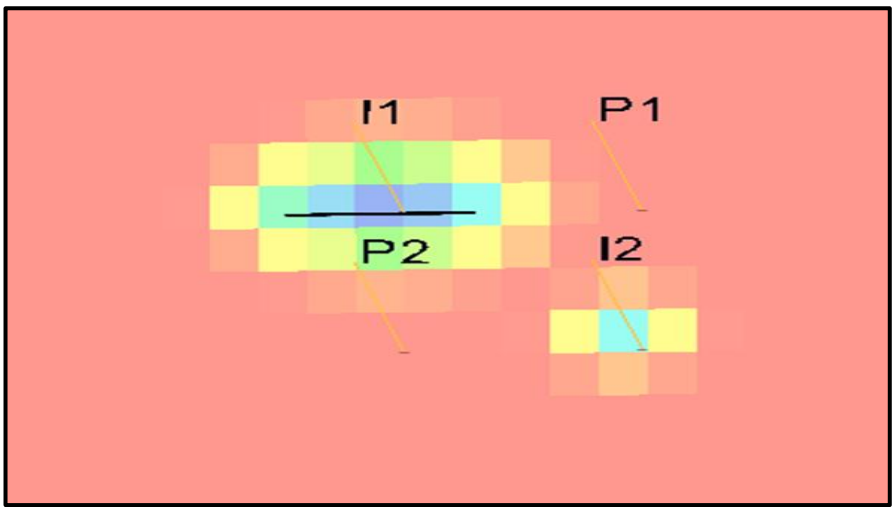

Figure 4-8: TIF growing from injector 1 (I1) in the x-direction towards producer 1 (P1)

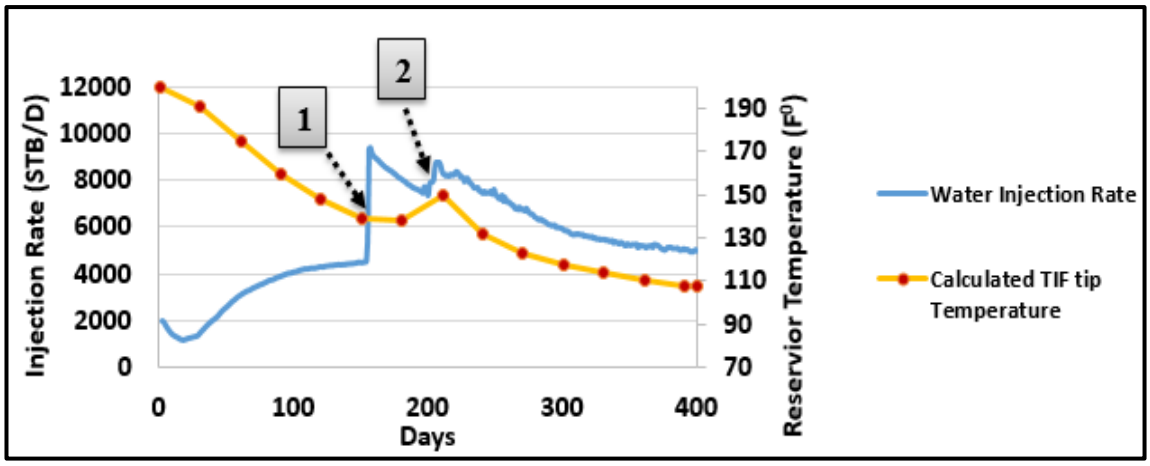

Figure 4-9: Case 1: Cold Water Injection reduces the Reservoir Temperature

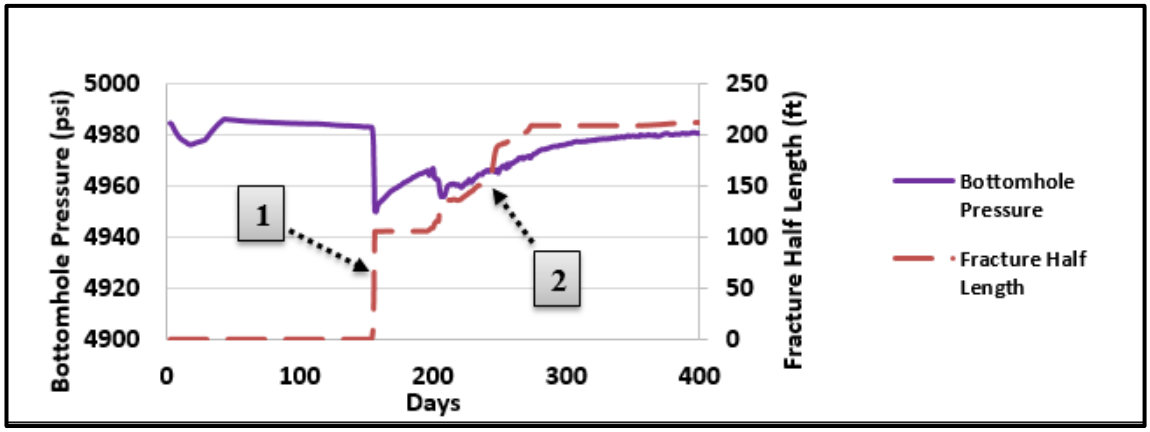

Figure 4-10: Case 1: BHP and Fracture Half Length vs. Time for I1

The performance of the analytical models developed previously has been compared to simulation results using the BHP and injection rate history data for Case 1. Case 1 was analysed with the **MHI** method. Figure 4-11 demonstrates downward separation of the two derivatives from HI for Injector I1. This indicates TIF initiation. Figure 4-11 indicates that TIF started after an injection volume of 0.5 MM bbls,

corresponding with a period of about 155 days (point 1). This is in agreement with the (Figure 4-10) simulation volume (point 1). TIF second propagation can be identified from Figure 4-11 as well after an injection volume of 0.85 MM bbls, corresponding to the period of about 200 days (point 2). Another way of showing the same data is by analysing the pseudo-skin evolution with time. There is a significant reduction in pseudo-skin (Figure 4-12) after 155 and 200 days (point 1 and 2) confirming the development and propagation of a TIF. The BHP increased after point 2 due to the increased reservoir pressure.

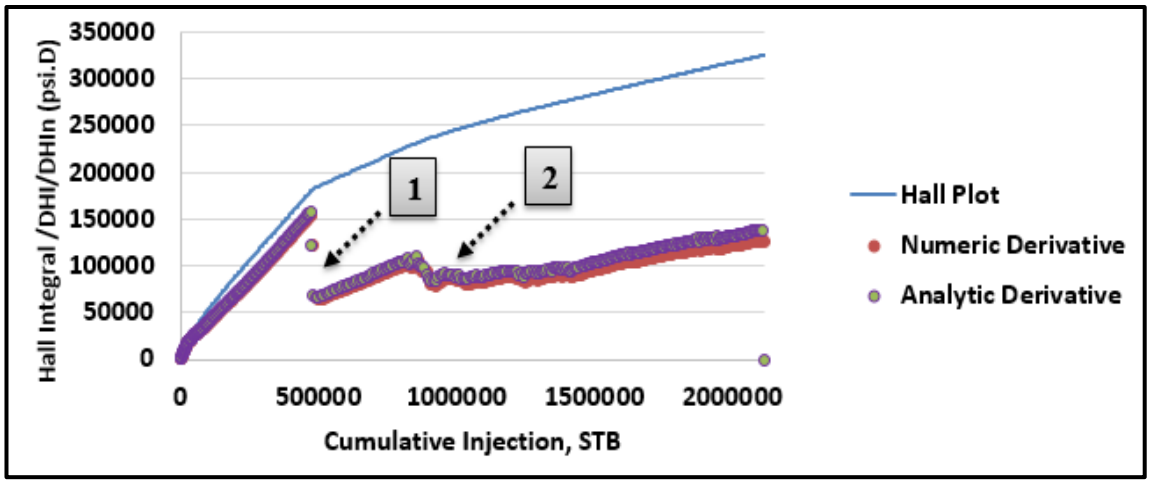

Figure 4-11: Case 1: MHI Plot for I1 with a Downward Separation of the Derivatives, indicating TIF

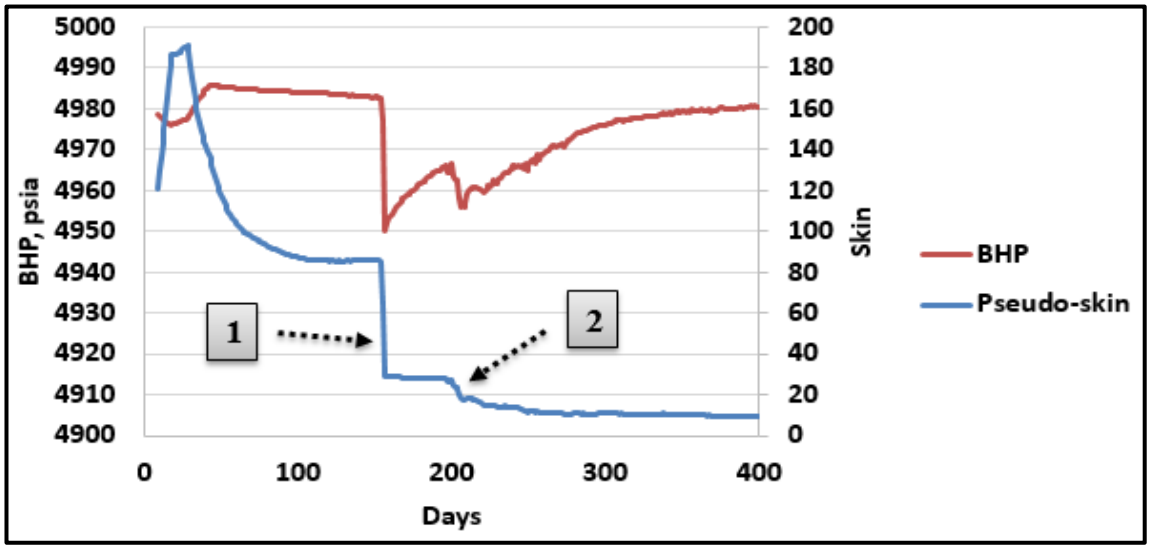

Figure 4-12: Case 1: Pseudo-Skin Evolution vs. Time for I1 shows a significant reduction after 155 and 200 Days

FI and **II:** Figure 4-13, a plot of FI and II as a function of injected volume for well I1, also provides real time monitoring of TIF onset and propagation. TIF initiation occurs after an injection volume of 0.5 MM bbls is reached, or after 155 days. Triangle 1 indicates the constant TIF length period between 0.5 and 0.85 MM bbls (155 and 200

days) of injection. The period between triangles 1 and 2, 0.85 MM bbls (200 days) and 1.2 MM bbls (280 days) shows an increasing TIF. Both FI and II again follow the diagnostic triangle (triangle 2) after 280 days, indicating a constant TIF length. Figure 4-13 supports the Figure 4-11 MHI analysis as well as corresponding to the TIF half-length simulation results shown in Figure 4-10.

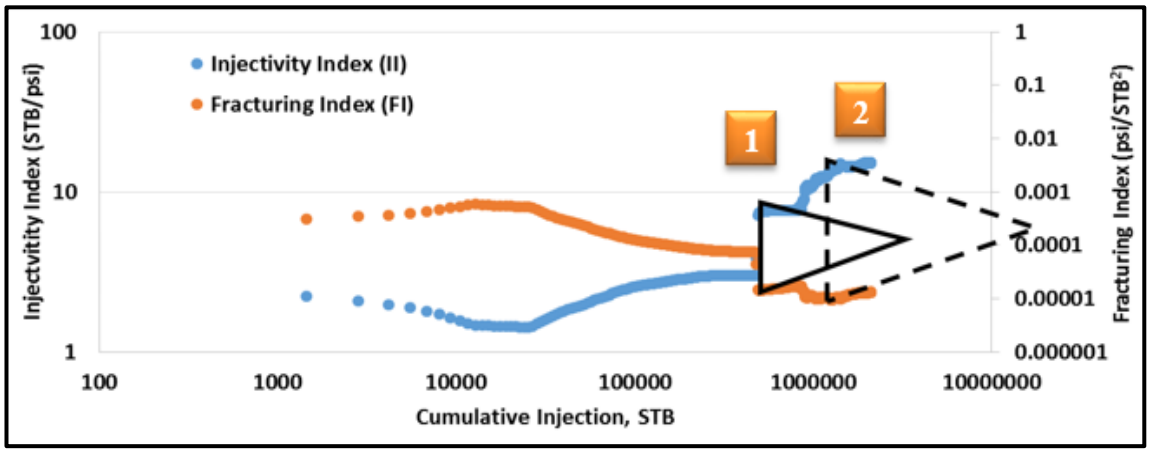

Figure 4-13: Case 1: Log-Log plot of FI and II vs Injected Volume for I1 Monitors TIF Initiation and Propagation

Equation A-4, Appendix A, evaluates the flood front radius (r_e) and the corresponding pressure (P_e). Figure 4-14 shows a decreasing P_e value for the first 155 days, indicating insufficient water injection to achieve voidage replacement. The recovery in P_e after 155 days coincides with a TIF initiation. There is also an increase in the rate of advance of the injected water front after this date (Figure 4-14).

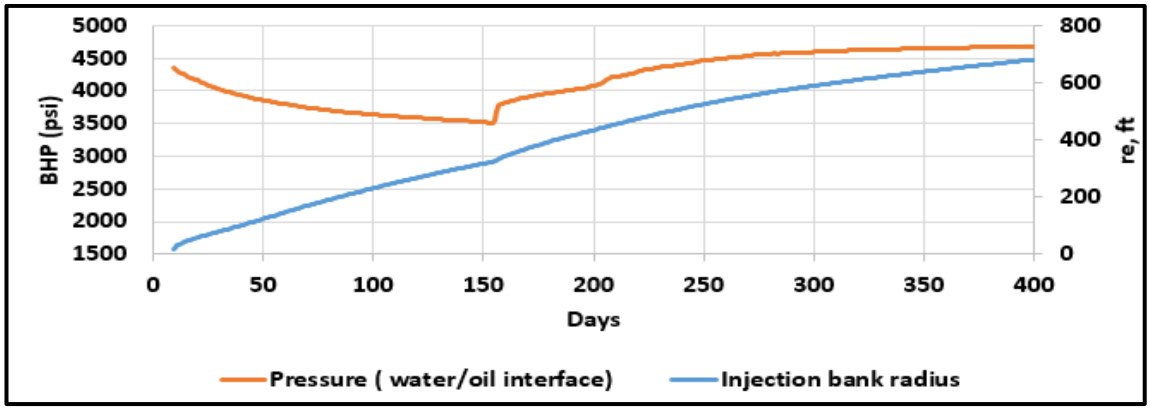

Figure 4-14: Case 1: Rapid Response of Reservoir Pressure after TIF initiation at 155 days observed in injector I1

CRMIP is used to identify inter-well communication and evaluate the sweep efficiency. The synthetic model production and injection history data feeds the CRMIP calculation. CRMIP results for time-interval prior to TIF onset is defined as the base case (Pre-TIF). Subsequently, it is compared to the CRMIP results for the production history data taken after the TIF stopped propagating (post-TIF).

The unknown CRMIP parameters were derived using Excel solver's fitting routine for non-linear regression. The fitting routine minimizes the mismatch between the estimated production results (from the CRMIP calculation) and observed production history data (from the reservoir simulation in the synthetic case being analysed here). The data-fitting process must also satisfy the constraints (Appendix D) that the volume fraction flowing towards each producer (the connectivity) from each injection well has to be a positive number or zero, while their sum should equal-or-less than unity.

The producer and injector wells in the synthetic case are perturbed, and data points (taken from the reservoir simulator) for each time step are used to calibrate the unknown CRMIP parameters. Figure 4-15 shows a good agreement between the CRMIP results and observed data. Figure 4-16 demonstrates that, pre-TIF, equal volumes of water flow towards P1 and P2 for Case 1. The post-TIF situation changes dramatically with 90% of the injected water supporting P1 (f_{11}) while that for P2 (f_{12}) decreases. Integrating this and the MHI and FI results leads to the conclusion that the TIF is propagating toward P1, as confirmed by the Case 1 reservoir simulation. Further, P2 is being supported by I2 with a minor contribution from I1 after TIF initiation and the I1-P2 sweep efficiency reduced.

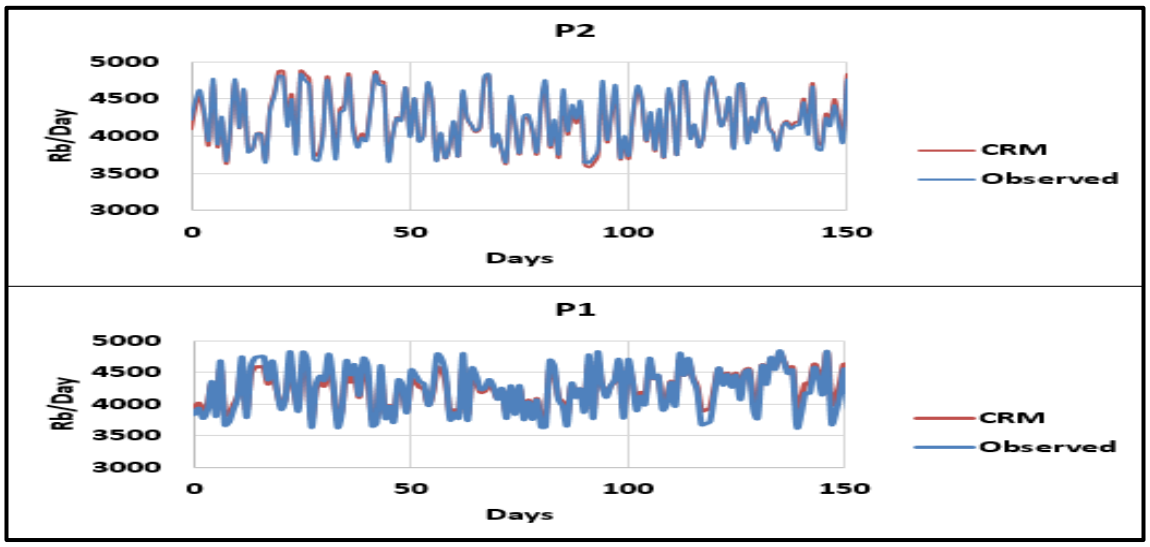

Figure 4-15: Case 1: Pre-TIF comparison of Production Rate and CRM Calculations for P1 and P2

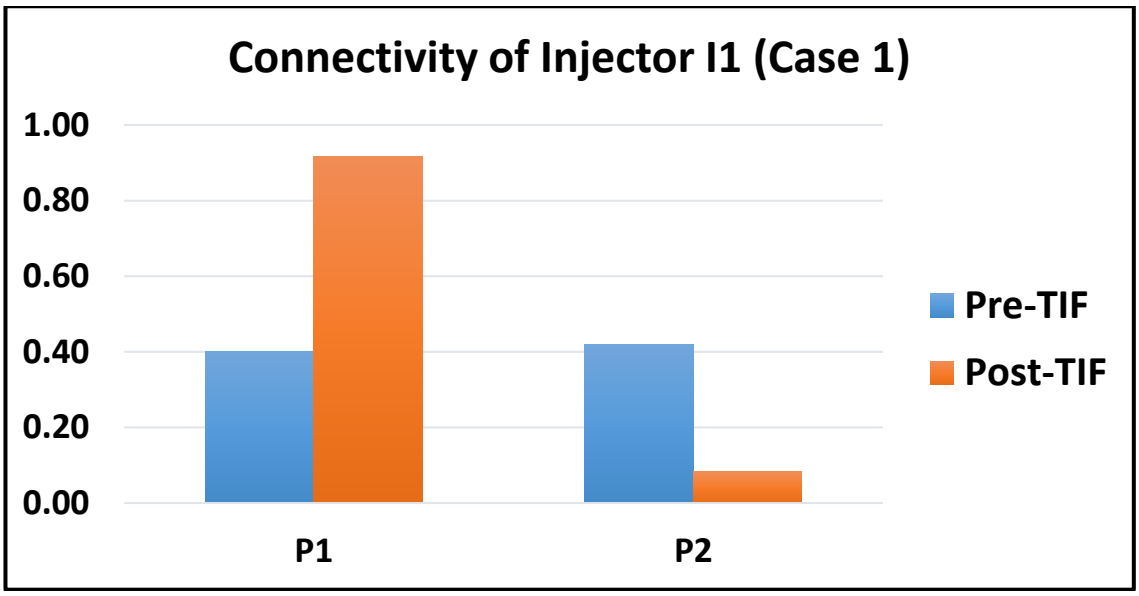

Figure 4-16: Connectivity of I1 and gain of P1 and P2 for Case 2 pre-TIF and Post-TIF

4.6.2 Synthetic Case 2 Histories

This case modelled a TIF growing from injector 1 (I1) in the y-direction towards producer 2 (P2) (Figure 4-17). Analysis of the case 2 data with the MHI and other analytical models gave similar results to those discussed above for case 1 (see Appendix E for all Case 2 figures) while the CRM analysis was different for the two cases. Equal, pre-TIF flow connectivity was observed between well I1 and wells P1 and P2 (f_{11} *and* f_{12} in Figure 4-18). These initially similar results to those of case 1 changed significantly after TIF onset with f_{11} decreasing and f_{12} increasing. The TIF propagates from I1 towards P2, a conclusion confirmed by the reduced sweep efficiency observed between I1 and P1 after TIF onset.

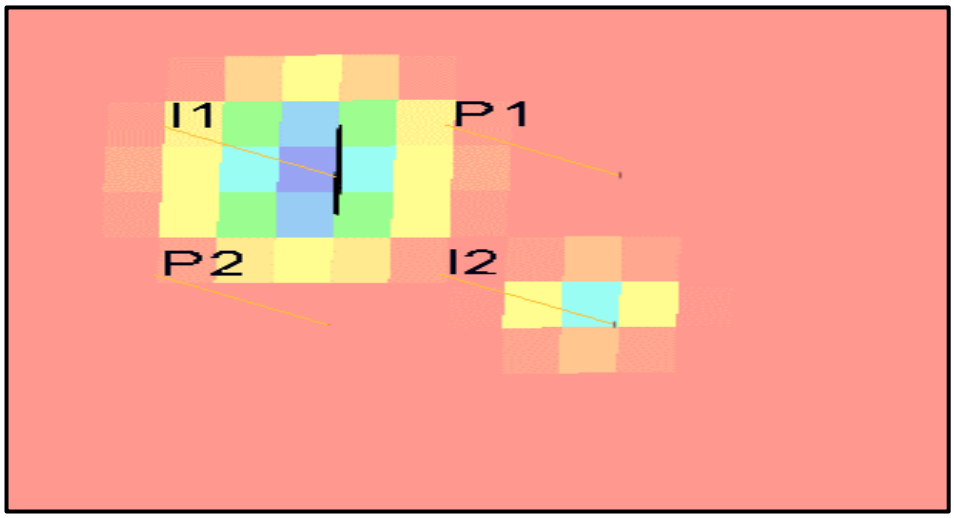

Figure 4-17: TIF growing from injector 1 (I1) in the y-direction towards producer 2 (P2)

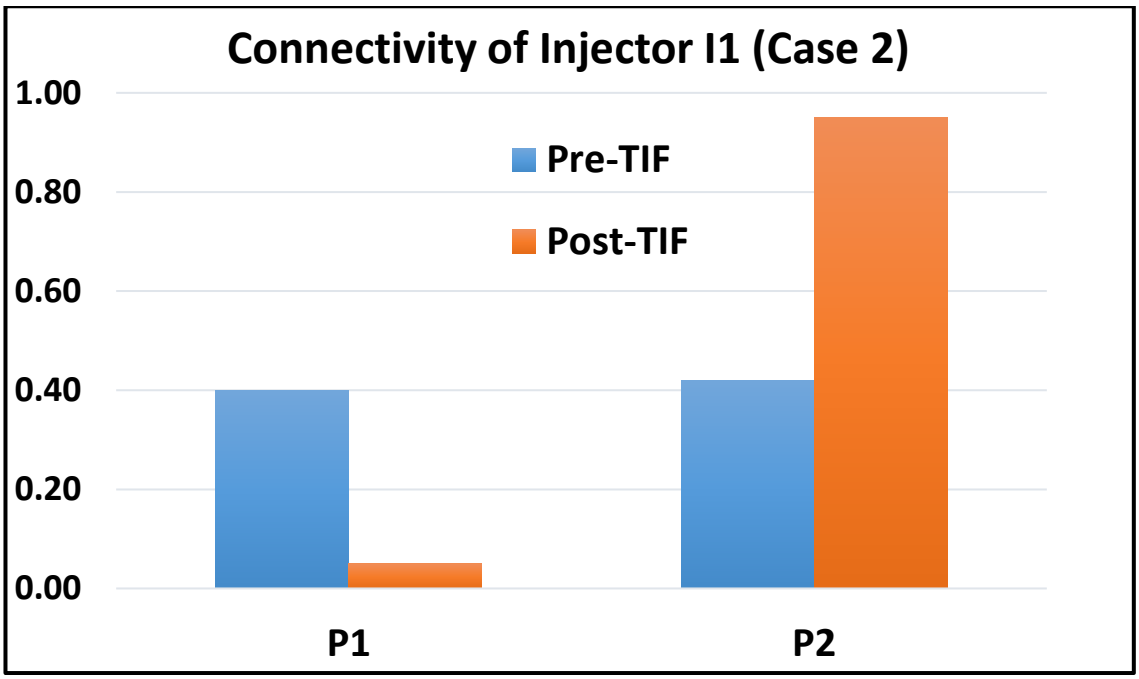

Figure 4-18: Connectivity of I1 and gain of P1 and P2 for Case 2, Pre- and Post-TIF

The reservoir simulation results also confirmed that the sweep efficiency for Case 1 and Case 2 was reduced compared to the No-TIF case (Figure 4-19). The different recovery factors of Case 1 and Case 2 are due to the unequal cell size in the x and y direction and the variable well control.

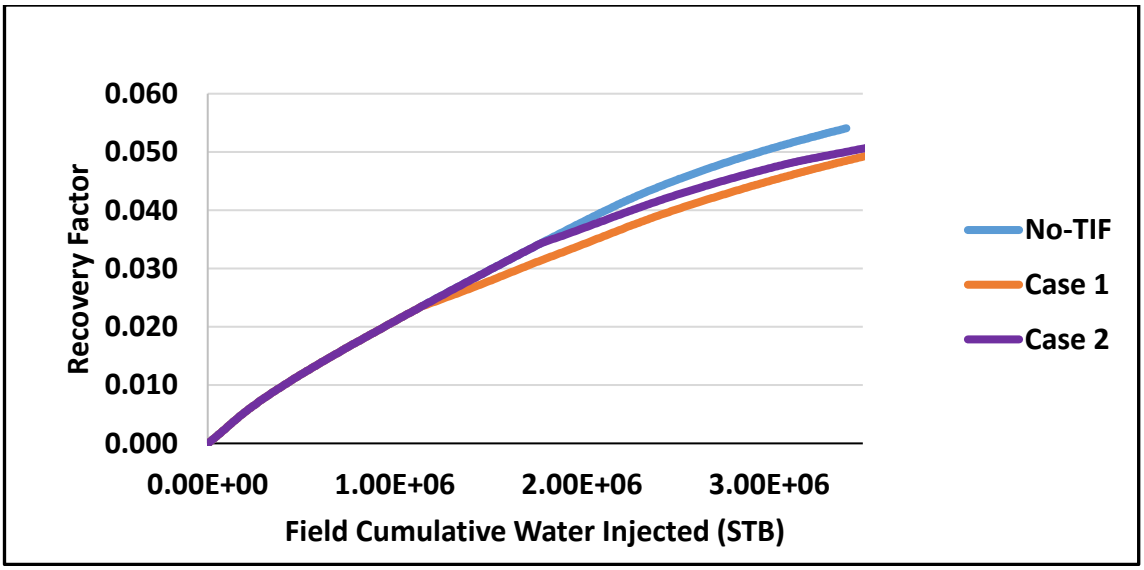

Figure 4-19: No-TIF case has the highest recovery factor indicating the impact of TIF on Cases 1 and 2

4.7 Real Field Case History

A sector of reservoir "N" has been developed by a total of four wells: three horizontal wells; Producer "NP4", injector "NI5_H", and injector "NI5_T and the vertical injection well "NI6" (Figure 4-20). The injection history of the three injection wells was analysed for evidence TIF. Injection well NI6 history data (Figure 4-21) indicated that

TIF had occurred at 690 days. The injection rate increases after this date while the BHP significantly decreased. A further sign of TIF is that the injection water's wellhead temperature appears to be inversely correlated with the injection rate after 690 days (points 1, 2 and 3 in Figure 4-22). This is not the case prior to 690 days.

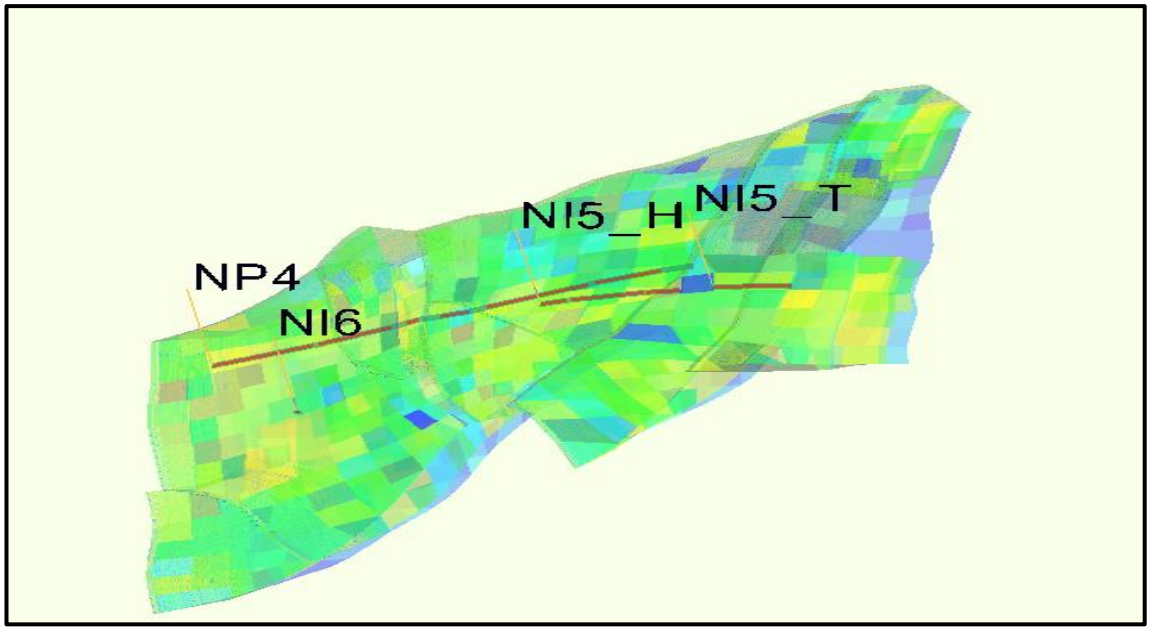

Figure 4-20: Locations of injectors NI4, NI6 with respect to producer NP4

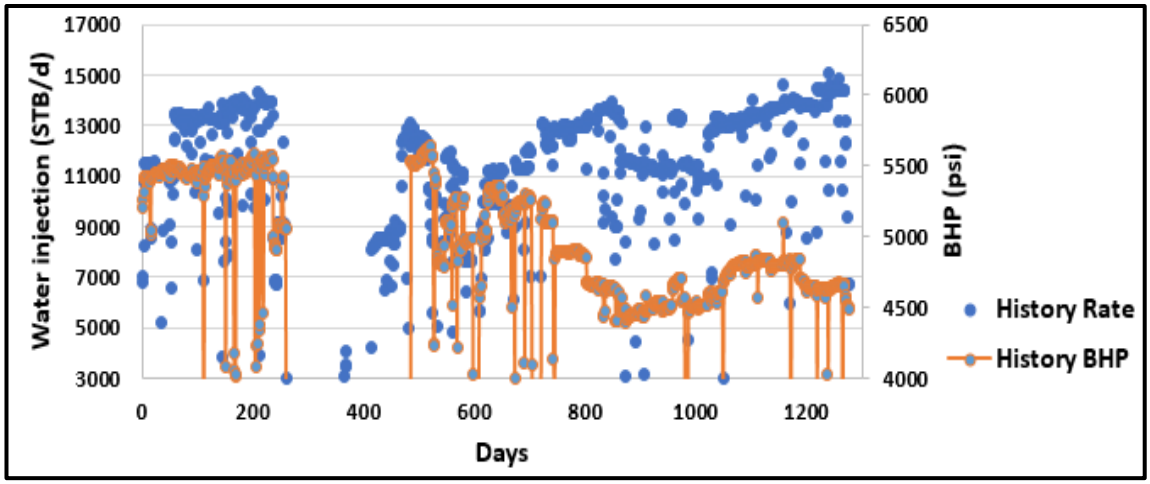

Figure 4-21: Injection Rate and BHP history for injector NI6

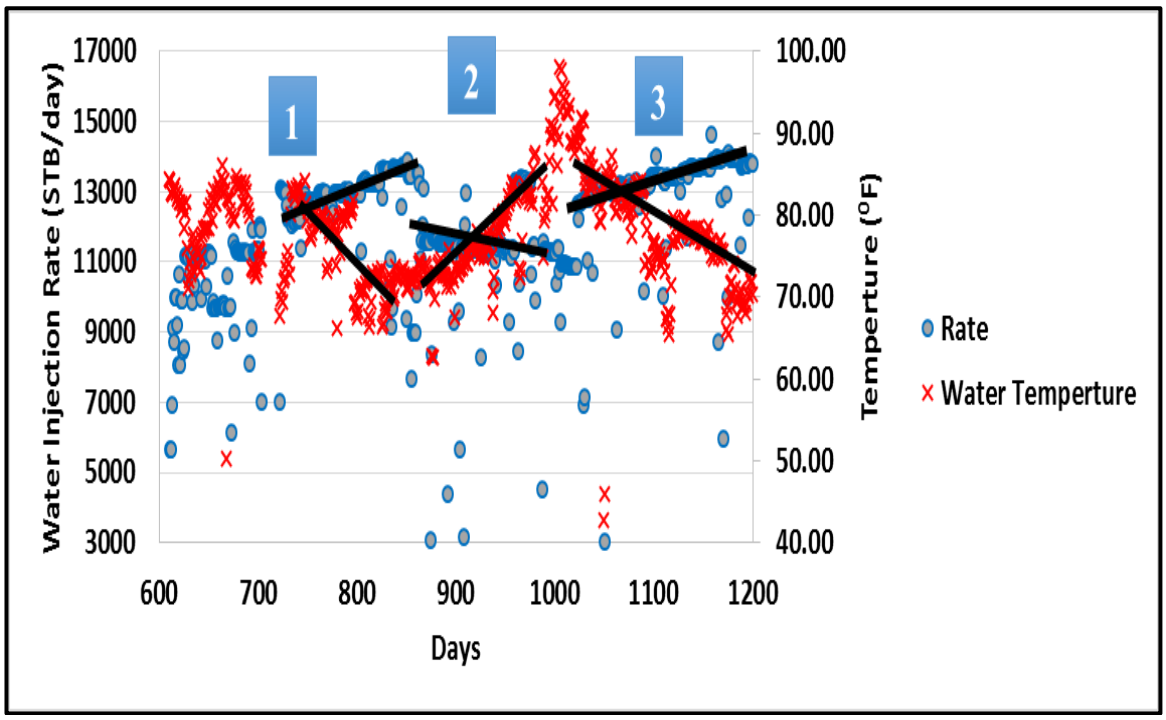

Figure 4-22: Wellhead Water Temperature and Injection Rate appear to be correlated for Injector NI6

Conventional methods, namely injectivity Index (II) and Reflectivity of injectivity Index (RII), and VRR are used here and compared to the proposed methods. II and RII showed an improvement of injectivity after 600 days (Figure 4-23). RII plot showed the injectivity signature more clearly than II. However, both methods needed longer time to capture the changes in the injectivity. Furthermore, subtle changes were difficult to be identified because of the fluctuations in the data. These methods also did not recognise the exact TIF onset or propagation periods clearly. Data was not available for the period between 360 days and 460 for the II and RII analysis due to the failure of the downhole pressure gauge.

VRR plot provides information about the voidage and the pressure support needed in the reservoir (Figure 4-24). The VRR is not correlated to II in Figure 4-23. The VRR also was greater than one for almost all time due to considering other producers in the same reservoir. This method is not informative when analysing the performance of one injector. VRR is also not helpful for identifying TIF onset, propagation or impact. More robust methods applicable to all situations, are needed for early, accurate and high resolution identification of changes in an injection well's performance.

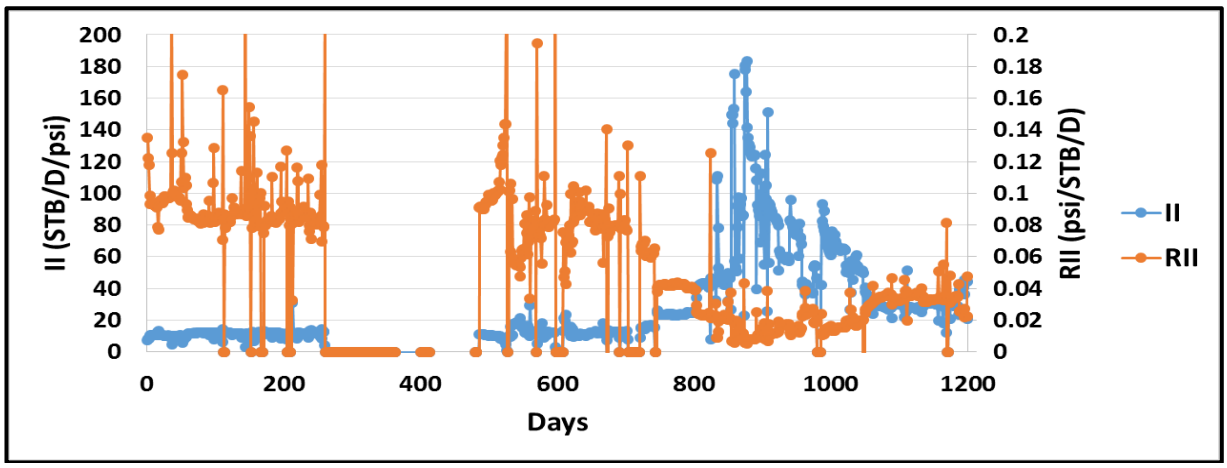

Figure 4-23: II and RII for for injector NI6

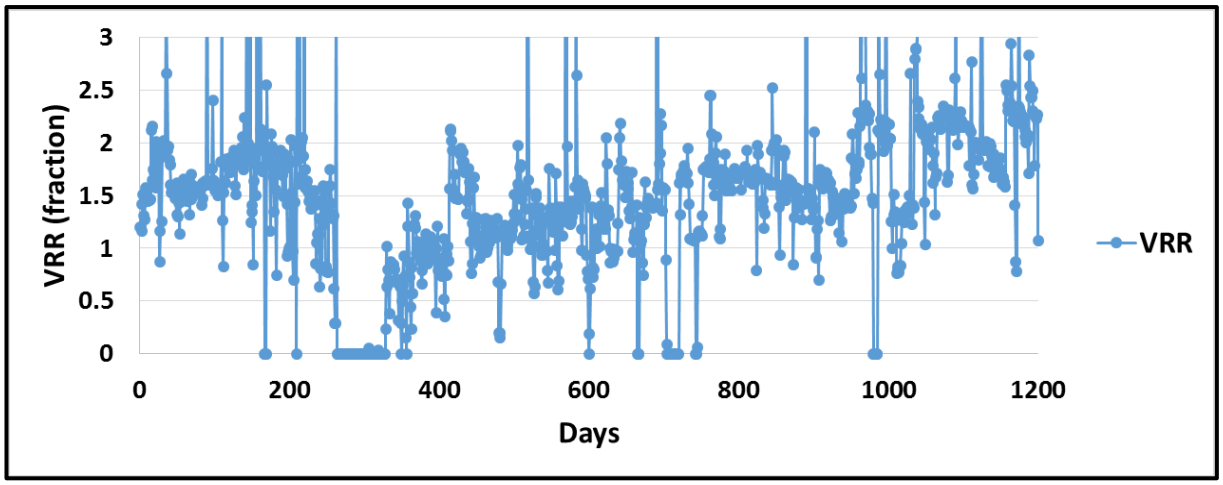

Figure 4-24: Voidage Replacement Ratio (VRR) for the selected sector reservoir

The Figure 4-1 workflow was applied to the history data of injection well NI6. MHI analysis (Figure 4-25) showed that there is a downward separation of derivatives, an indication of TIF, after 4.8 MM bbls of water had been injected. This corresponds to an injection period of 690 days. The TIF continued propagating until 6.8 MM bbls of water had been injected (870 days). TIF propagation then ceased until the injection volume reached 10.5 MM bbls (or 1185 days); after which TIF propagation recommenced.

The MHI analysis has thus not only successfully identified TIF initiation, but also identified periods when the TIF was actively growing and when it remained static. The same conclusions can be drawn from analysing the change in injection well NI6's skin with time (Figure 4-25).

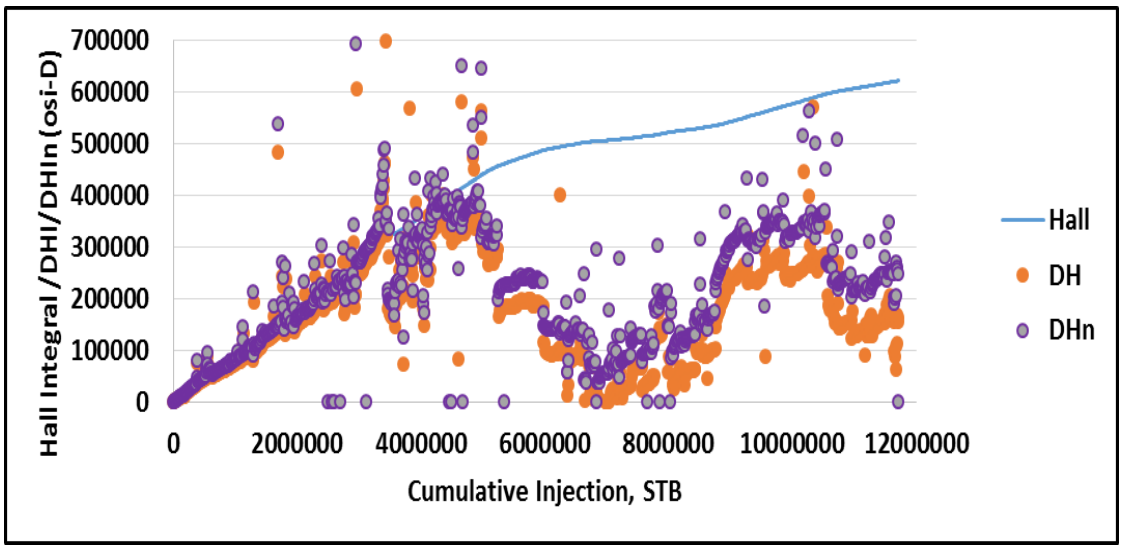

Figure 4-25: MHI plot for Injector NI6 shows a downward separation of derivatives implying TIF

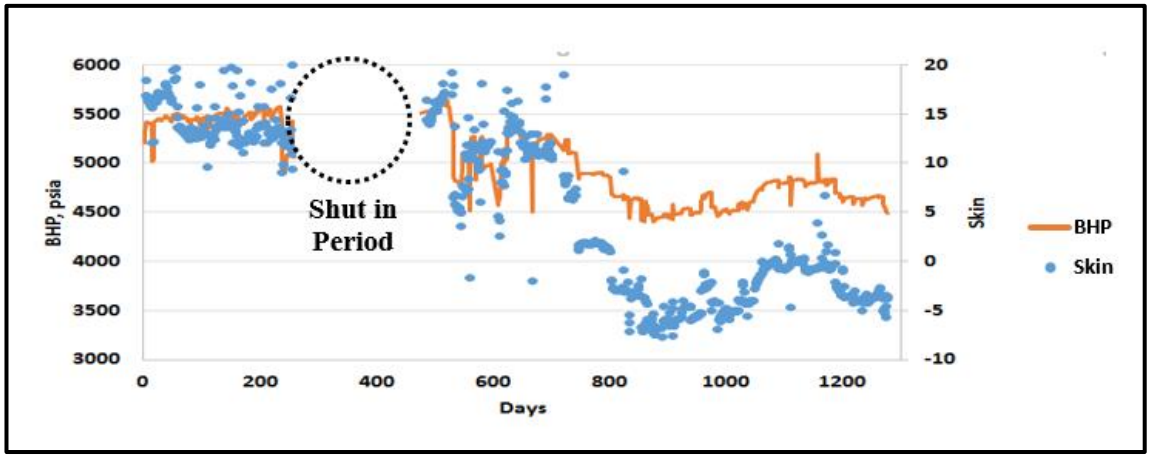

Figure 4-26: Well NI6's Skin value significantly reduces after 690 days and increases between 870 and 1185 days

FI and II analysis for injector NI6 (Figure 4-27) confirms TIF onset at an injection volume of 4.8 MM bbls (~ 690 days), prior to triangle 1 which identifies the further TIF growth starting at 10.5 MM bbls (~1185 days) where the FI and II data points follow the diagnostic triangle. Figure 4-28 records the advance of the water front and the corresponding water/oil interface pressure. A period of increasing P_e is observed (point 1) after the onset of the TIF at the injection volume of 4.8 MM bbls (690 days). A second period (point 2) of increasing Pe is observed starting at 10.5 MMbbl, the point at which TIF growth restarted.

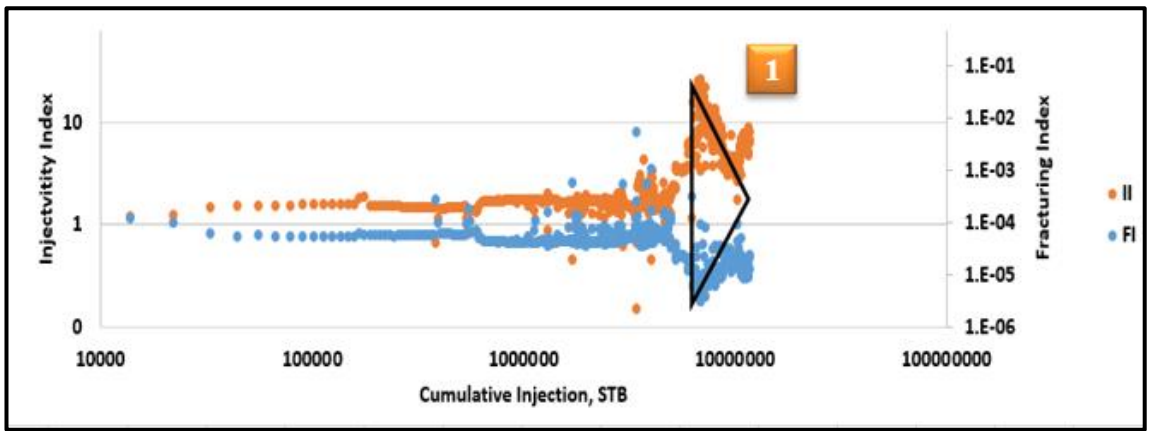

Figure 4-27: Log-log plot of FI and II of Injection Well NI6 confirms TIF Initiation and Propagation

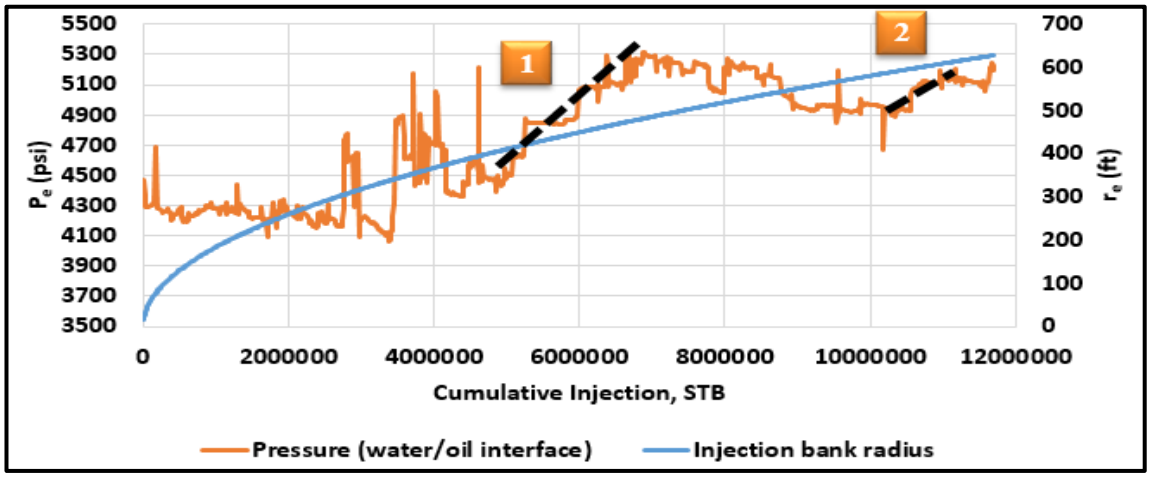

Figure 4-28: Advance of Water Bank and Pressure of Water/Oil Interface for Injector NI6

Semi-analytical model i.e. CRM is then applied for injector NI6 to support the findings of MHI, FI and PSS analysis using the Figure 4-1 workflow. The CRMIP solution reduced the complexity of the problem, as described previously, with the data from the time-interval before 200 days being used for the Pre-TIF period. The Post-TIF data was selected as the period between 870 and 1185 days; i.e. when the TIF had seemingly stopped propagating after its initial growth. Figure 4-29 presents the connectivity between well NP4 with the NI6 (f_{64}) and NI5 (f_{54}) injection wells in the Pre- and Post-TIF time intervals. f_{64} is significantly smaller in the Post-TIF period, implying the pressure support to NP4 by NI6 has considerably decreased even though the total volume of water injected has increased, as clearly shown by Figure 4-32.

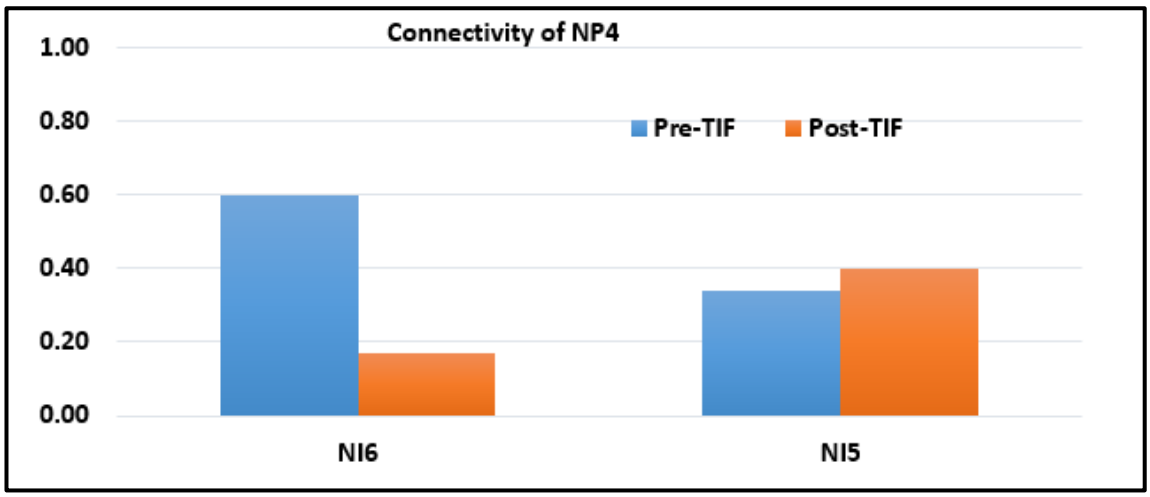

Figure 4-29: Pre- and Post-TIF Connectivity of Well NP4 with NI6 and NI5

The Post-TIF reduction in connectivity implies that the NI6 TIF propagated away from NP4 in an East-Westerly direction (Figure 4-30). This conclusion is supported by direction of tensile fractures observed by the Formation Micro Imager (FMI) log recorded after drilling another well in the same field (Figure 4-31). The NI6 TIF is thus expected to propagate approximately parallel to NP4's well path (Figure 4-30), the direction of the reservoirs maximum horizontal stress.

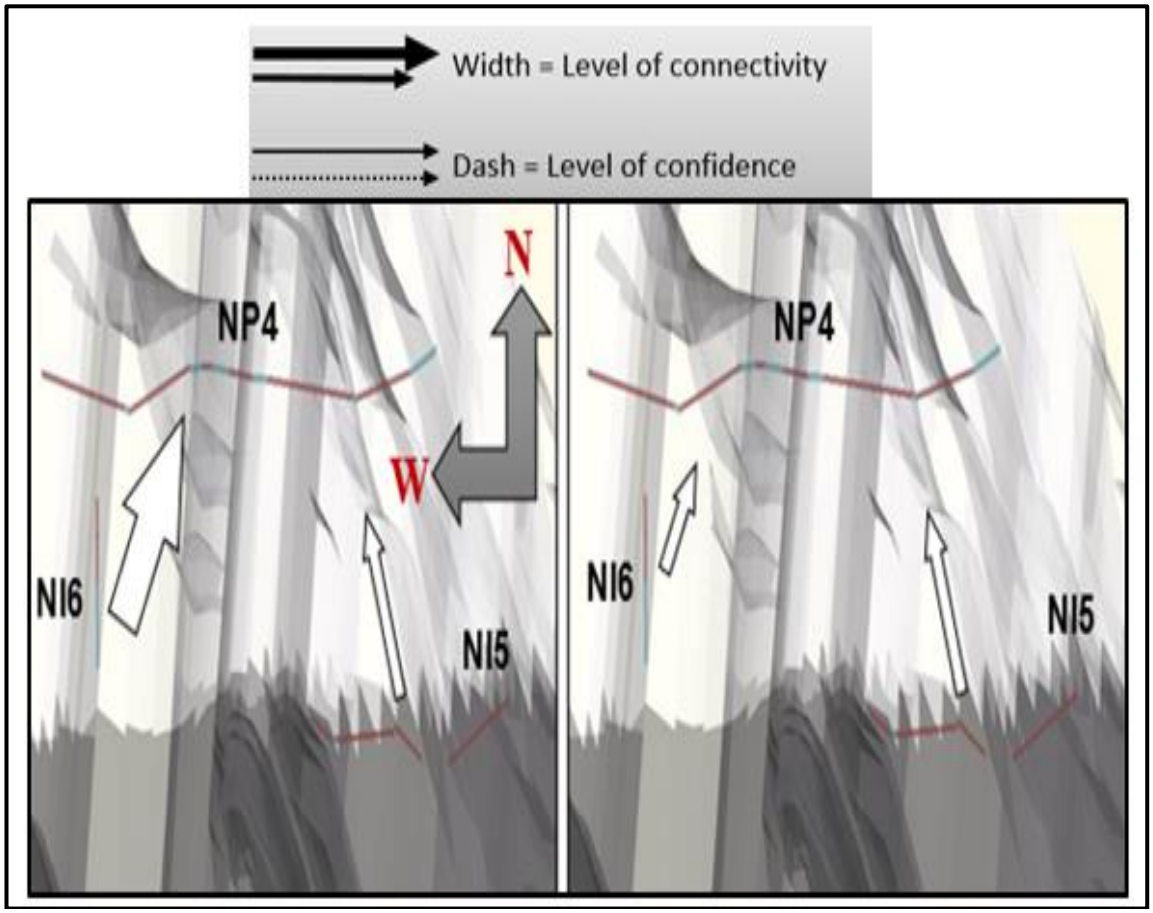

Figure 4-30: left: connectivity pre-TIF, right: connectivity post-TIF

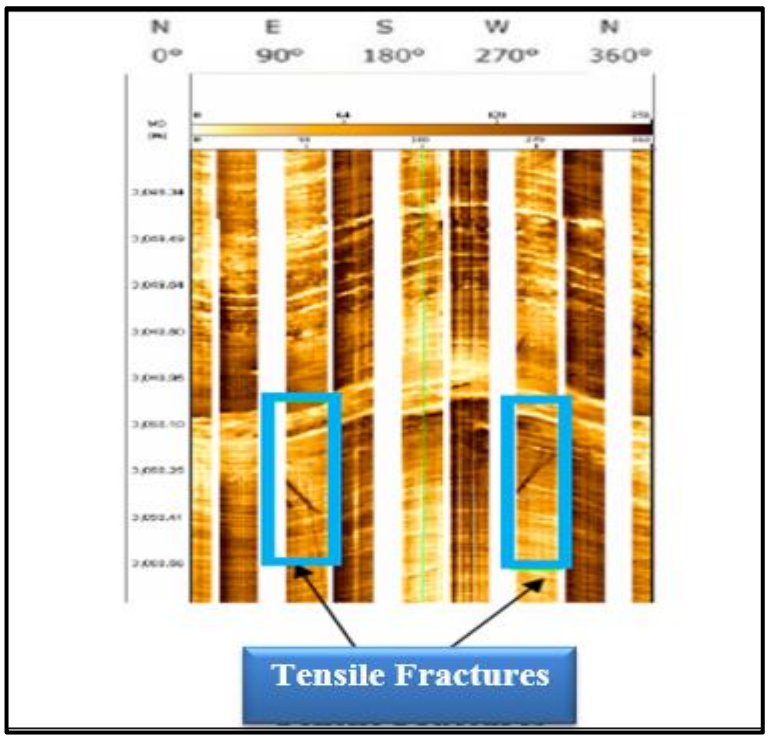

Figure 4-31:FMI image from one of well in the field with tensile fractures (supplied by the operator)

The CRM findings regarding a zone of reduced sweep efficiency between wells NI6 and NP4 were supported by Figure 4-32, a plot of the History Data for Injection Well NI6 and Production Well NP4. This figure shows that the injected and produced liquid volumes were reasonably similar before 690 days, the Pre-TIF time, but decreased thereafter, indicating TIF initiation and a reduced volumetric sweep efficiency between the well pair. The produced liquid also increased slightly when TIF propagation ceased between 870 and 1185 days (Figure 4-32). The flood front propagated in a more radial direction during this period, confirming TIF has a significant impact on the sweep efficiency.

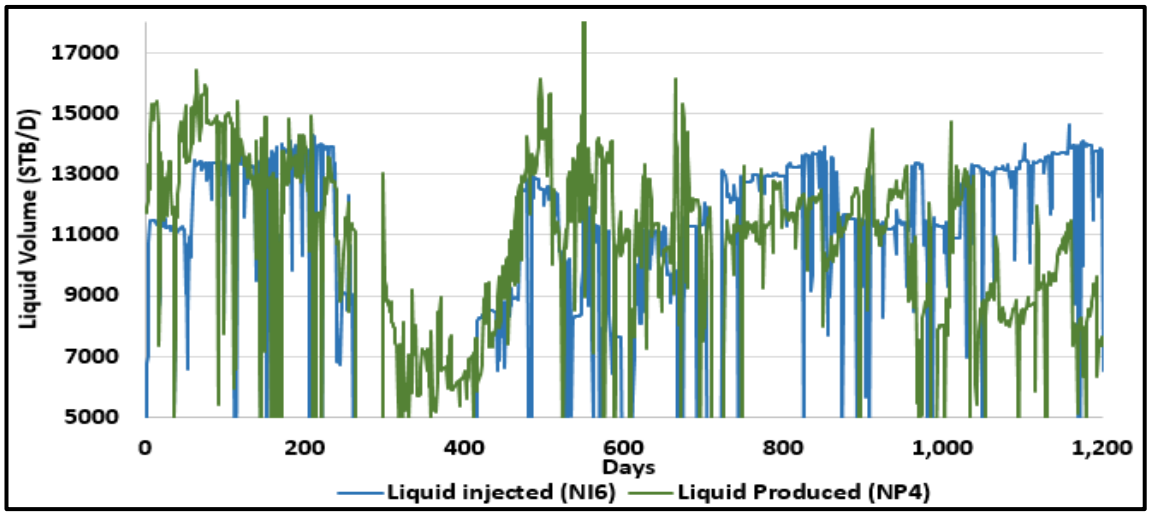

Figure 4-32: History Data for Injection Well NI6 and Production Well NP4

Improved pressure support due to an increase in the well injectivity index is the benefit of a TIF being formed due to the injection of cold water. This benefit is accompanied by the potential negative effect of the resulting loss in conformance control and a decrease in the waterflood's performance due to the more rapid advance of the flood front in the direction of TIF propagation. The above analysis of the injection history data from the N reservoir sector has illustrated the robustness of the proposed workflow for recognising when the injection wells performance changes from matrix to fracture injection due to TIF. This workflow also provides information on the subsequent development of the TIF, providing an alert that further studies may be required for reservoir management. This particularly true for decisions such as the design and placement of new injection or production wells as well as the need for remedial treatments to the existing well stock.

4.8 Summary

Following conclusions are drawn from this chapter, supported by the synthetic and real data analyses:

I. Analytical and semi-analytical modelling descriptions of a water injection reservoir's performance have been combined into a workflow employing routinely gathered injection and production well data to give insights into the performance of a water-flooded reservoir.

II. The workflow is shown to be robust for both Matrix and Hydraulic or Thermally Induced Fracture (TIF) injection Wells. Recourse to complex, geo-mechanical reservoir modelling was not required for this semi-qualitative analysis.

III. The Modified Hall Integral (MHI) model provided unambiguous clues about TIF onset and its subsequent propagation.

IV. The Fracturing Index and Injectivity Index models identifies TIF initiation, TIF growth periods and the TIF's properties. This model can be used to support the MHI findings.

V. Pseudo Steady State formulation allows the flood front radius (r_e) and water/oil flood front's pressure (P_e) to be evaluated. It forms the basis for a real-time, monitoring tool.

VI. Comparison of the Pre- and Post-TIF inter-well connectivity results using the Capacitive Resistance Model provided a probable direction of TIF propagation

and a qualitative evaluation of the sweep efficiency between an injection and production well pair.

VII. The practicality of the proposed workflow was tested with synthetic data and its robustness confirmed with the analysis of data from a real field.

Chapter 5 History Matching a Sector Model of (N) Field Using Reservoir Simulation Coupled with Thermally Induced Fracturing and Geomechanical Models

5.1 Introduction

History matching involves adjusting a reservoir model until it reproduces the history behaviour of the reservoir. The variations between simulated and observed values in the reservoir are analysed and the model parameters are changed to obtain a good match. History matching is very common in the oil and gas industry in order to obtain a reasonable, reservoir model for production forecasts. There are two approaches that are normally used in the history matching process. The first approach is the manual method which has the following features [128]

I. Running simulation for the historical period.
II. Comparing the results to the actual field data.
III. Adjusting the simulation input to improve the match.
IV. Further analysis and verification of input data based on knowledge and experience.

The second approach is the automatic method which involves the following additional features as it:

I. Minimizes the objective function; i.e. the difference between observed reservoir performance and simulation results.
II. Excludes human knowledge/experience factor, thus the results could be unrealistic.

Figure 5-1 summarises the general strategy used for history matching process.

A different history matching procedure is investigated in this chapter. The static reservoir parameters e.g. porosity, directional permeability, NTG, transmissibility, etc., are kept constant as they are in this case better understood and measured, and also history matched to the pre-TIF history. It is indeed the rock mechanical parameters, thermal properties, and stress gradients that are modified to obtain the final match since a fracture mechanics problem is investigated (TIF). Modifying the above parameters changes the TIF dimensions. This results in changes to the reservoir transmissibility which is adjusted until the good data match is obtained. TIF is a dynamic complex problem that relates the fracture mechanics to geomechanics and fluid flow. This manual approach is used to obtain the final match to the sector model of the (N) field provided by an operator (E).

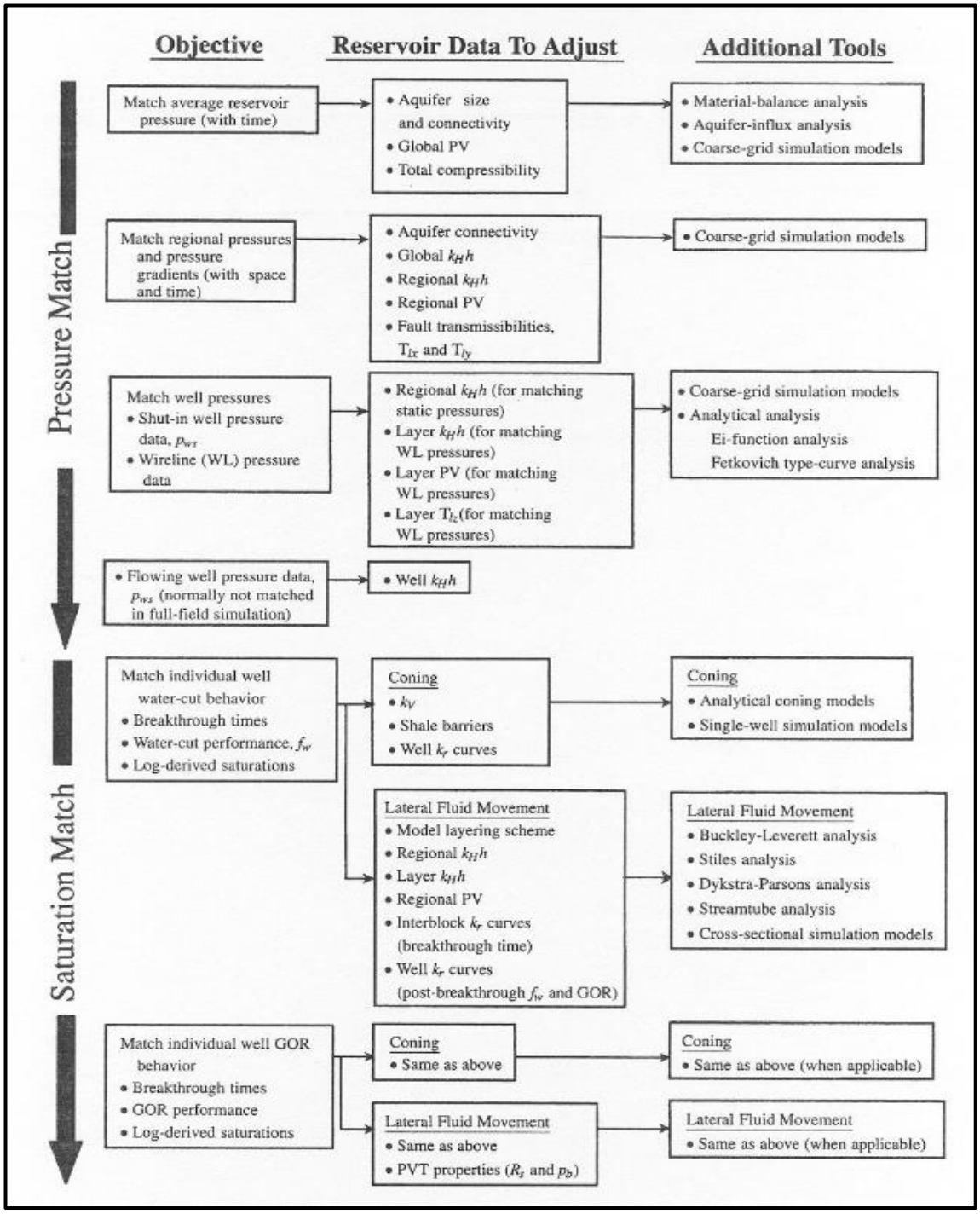

Figure 5-1: General history matching strategy [128]

5.2 Problem Statement and Solution Approach

Chapter 4 investigated TIF development in a real field case i.e. "N" field using a workflow that combined analytical and semi-analytical methods. The workflow used the gathered injection and production well data to give insights into the onset and propagation of TIF in one of the injectors i.e. NI6. The sector reservoir model received from the

operator was already history matched by the operator with respect to the static reservoir parameters. The objectives of history matching in this chapter are to:

I. Develop workflows that consider the dynamic nature of the TIF problem
II. Improve and validate the reservoir and geomechanical models
III. Identify and confirm the observed TIF onset and propagation periods
IV. Provide a history matched sector model with rock mechanical and thermal properties and stress gradients that can be used with confidence for subsequent studies

This chapter uses a 3D reservoir simulator coupled with a 3D finite element TIF model and geomechanical model to manually history match injector NI6 in the "N" field sector reservoir model where TIF was observed. A similar history matching study could not be found in the literature.

5.3 Previously Reported History Matching Studies with Thermally Induced Fracturing

Detienne et al [9] employed the history matching of an injection well with TIF in order to validate their analytical TIF model. They used a 2D hydraulic fracturing model to predict the TIF length and width. Thermo-elastic stress and poro-elastic effects are considered in the model using the solution given by Perkins and Gonzalez [23]. The TIF in the injectivity equation is represented by an equivalent radius.

Reference [9] described an offshore field in West Africa with ten injection wells that had been injecting water for a period of 3 to 5 years. WHP remained fairly constant at 100 to 120 bar during this time. It was observed that there had been a factor of 1.5 to 2 increase in the injectivity indices of seven wells due to TI, while on three wells, the injectivity index increased by a factor of 10 indicating a larger effect of TIF development. WHP history matching of one of these three wells (Well A) with a radial flow model showed a good match during the first 30 days (Figure 5-2). The injection rate was constant at approximately 200 m^3/d.

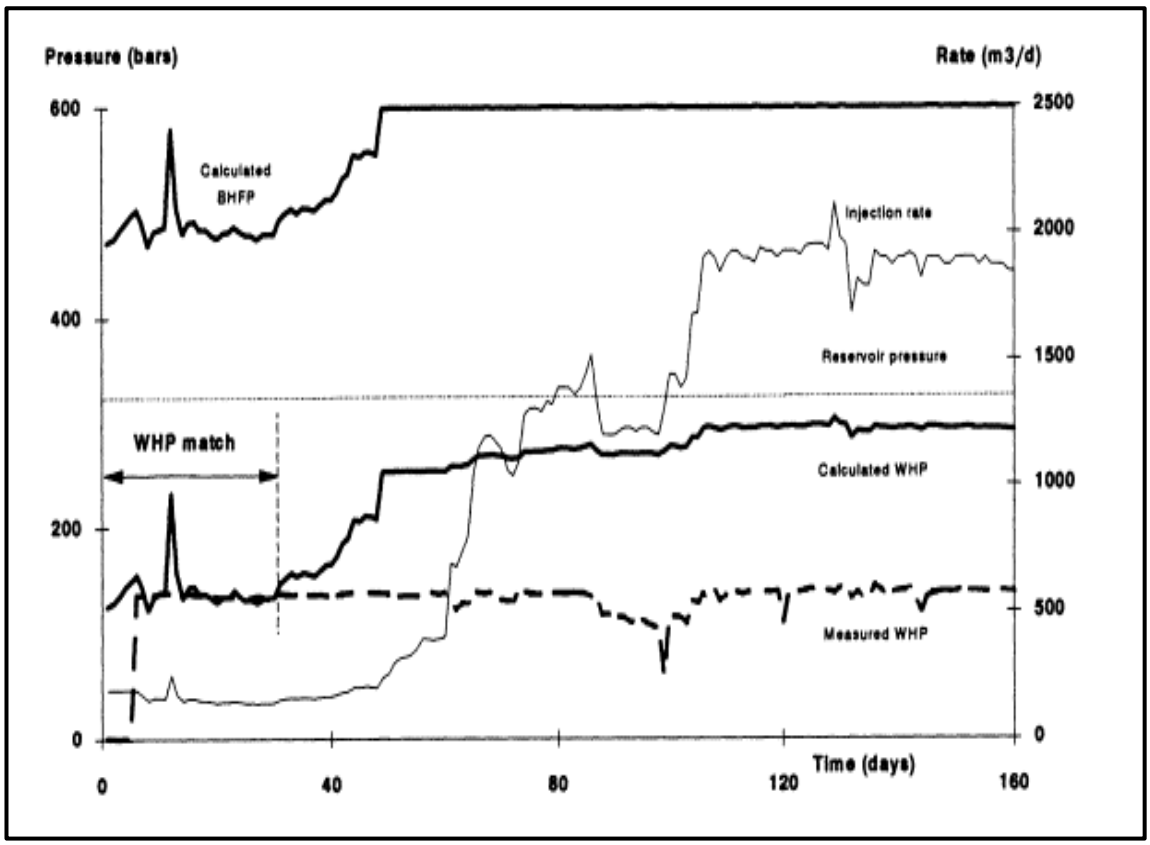

Figure 5-2:History match assuming radial flow for well A [9]

The injection rate suddenly started to increase from 200 m3/d after 30 days; reaching 2000 m3/d, after 120 days for well A. Initiating a modelled TIF that was vertically confined to the height of the reservoir was found to give a good history match for the period between 30 days and 60 days (Figure 5-3). However, the injectivity increased suddenly again after 60 days. It was found to be impossible to match the well history after 60 days if a reasonable set of reservoir parameters was employed.

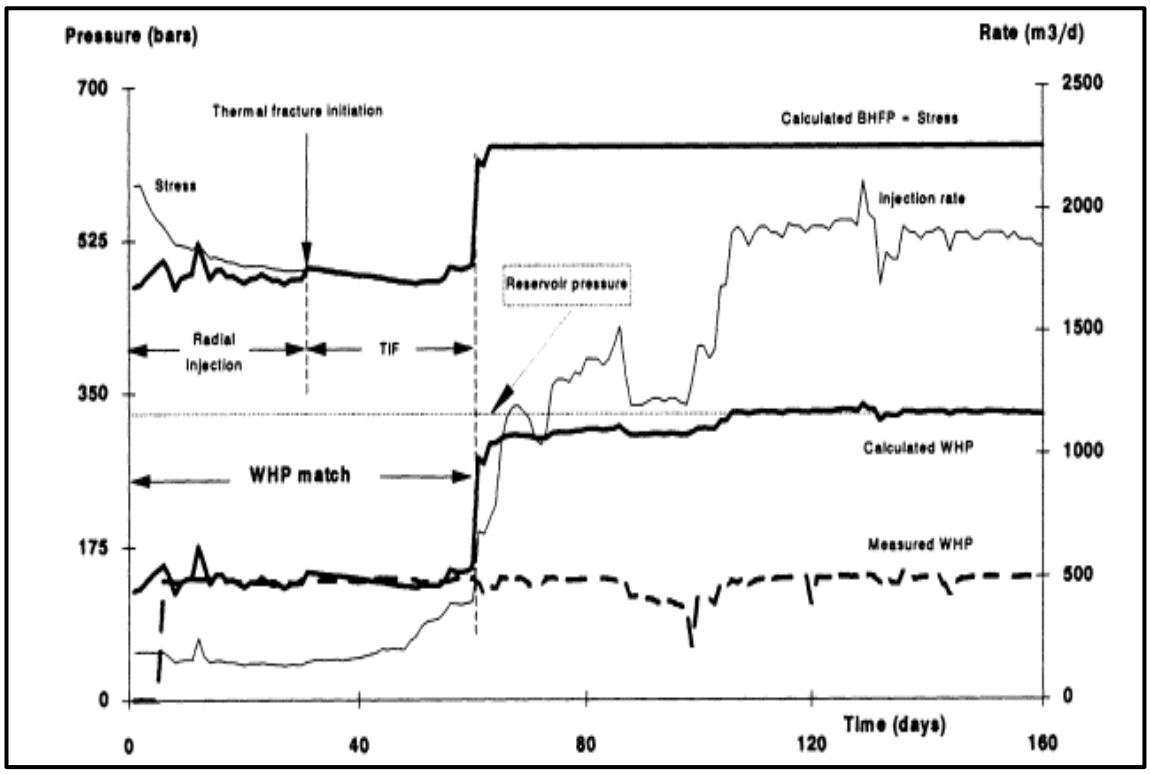

Figure 5-3: History match improves assuming a vertically confined TIF between 30 and 60 days for well A [9]

The TIF height and reservoir permeability must be increased in order to match the injection history after 60 days. The height of the TIF was increased from 20 m to 120 m and later back to 80 m (Figure 5-4). The complete injection history could now be matched by the model (Figure 5-5). The history matching workflow used in the case study has the following disadvantages:

I. The combination of varying TIF height and reservoir permeability makes it possible to match almost any possible change in flow rate and WHP, without proper checks of the physics of the model.
II. The 2D model used was not dynamic i.e. the matching had to be performed at different steps for different regimes.
III. The history matching was performed in an uncoupled manner.
IV. Changes to the geomechanical and rock mechanical were not considered.

A 3D reservoir model coupled to geomechanical model and a TIF model is required to simulate the dynamic TIF as required to overcome the above simplifications. Change to the rocks mechanical, thermal properties values as well as the stress all need to be considered for accurately modelling of the TIF's dimensions.

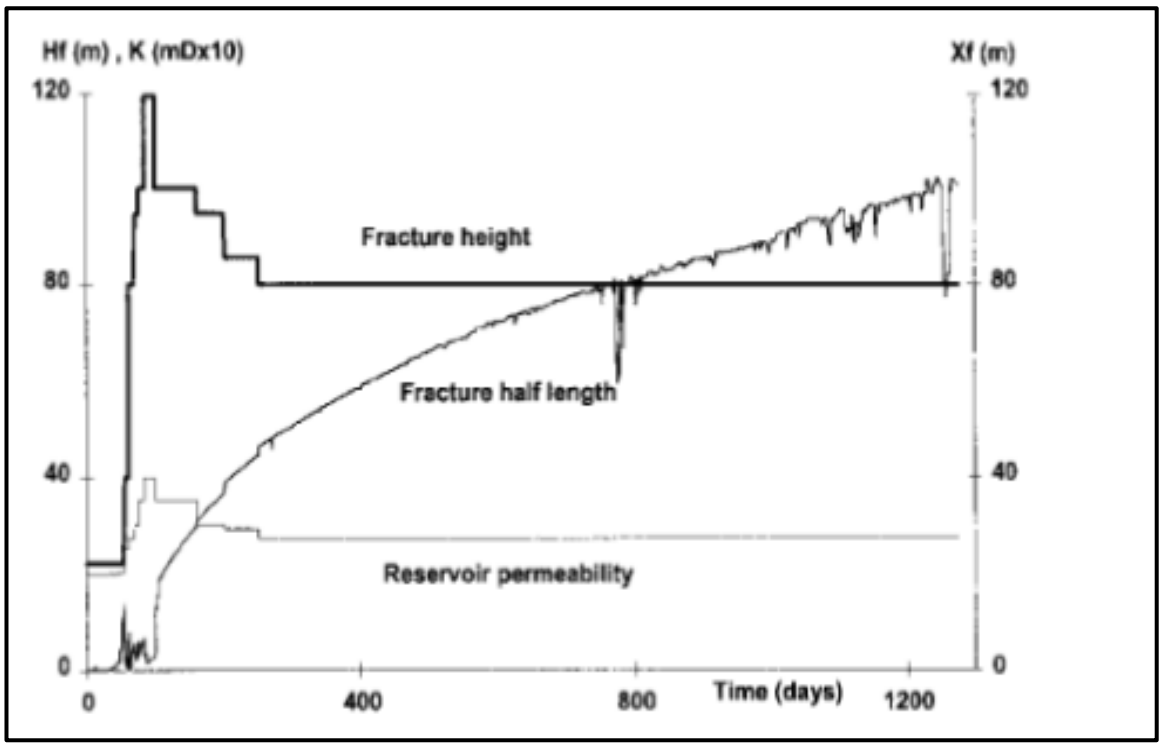

Figure 5-4: TIF dimensions and reservoir permeability in the final history match for well A [9]

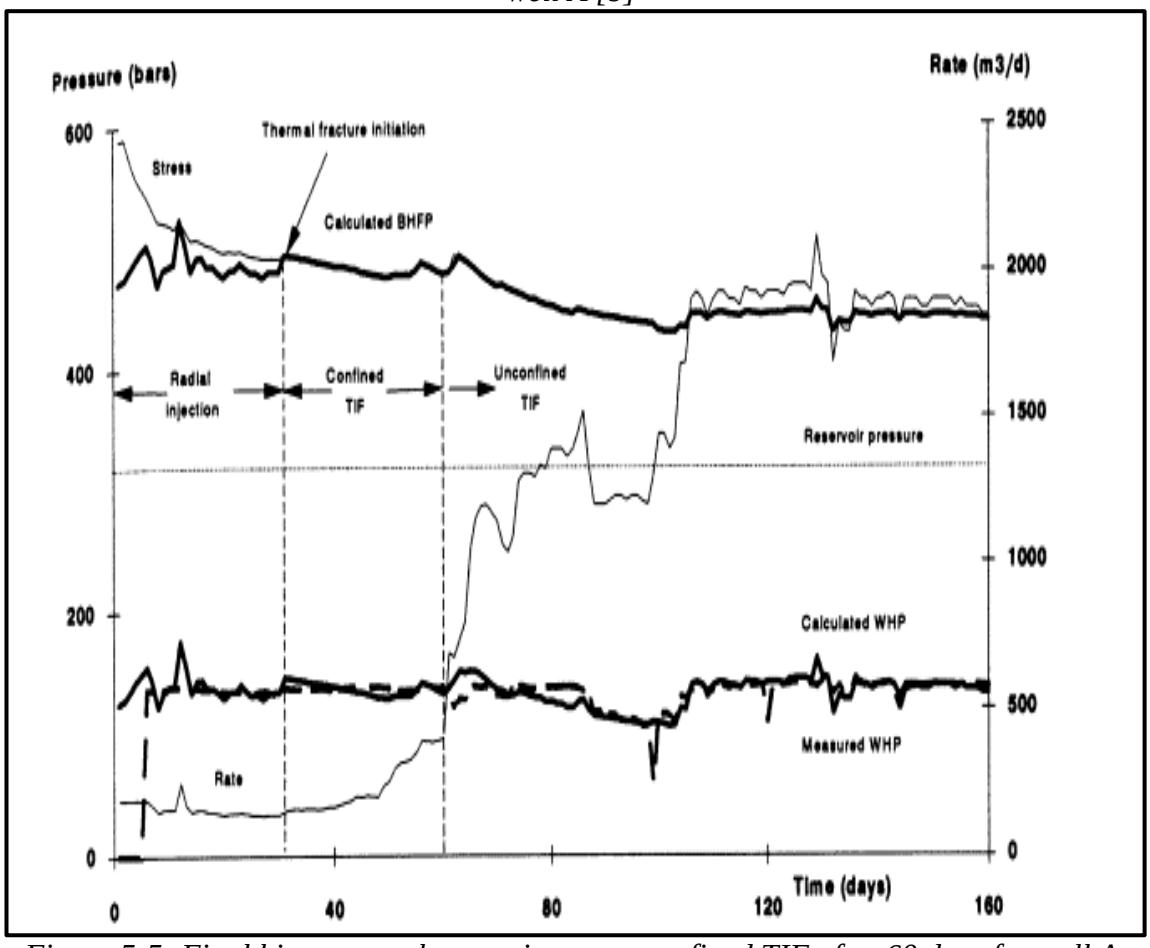

Figure 5-5: Final history match assuming an unconfined TIF after 60 days for well A [9]

5.4 Methodology

The starting point for the proposed workflow was an Eclipse sector reservoir simulation model. This Eclipse model must first be imported into the REVEAL reservoir simulator so that a TIF model can be used in the latter. The aim is to provide a history matched sector model that can be used with confidence for the remaining objectives of this thesis. The following stages in the workflow are described in this chapter:

I. The Eclipse sector model was imported into the REVEAL simulator using the provided "wizard". The validity of the obtained model was checked by comparing results of equivalent runs of the Eclipse and REVEAL models. This first step is important as it builds confidence in the REVEAL model.

II. The REVEAL model is converted from an isothermal to a thermal model. The PVT properties imported from Eclipse were defined at a single temperature. It is necessary to define the fluid PVT properties over the full range of temperatures encountered during the injection of cold water into the reservoir.

III. The simulation is run without TIF modelling and compared to the history data. This step is to study the performance of the injector "NI6" before modelling TIF. The calculated values for the reservoir pressure around well NI6 and NI6 BHIP were not matched at this stage to reliable data.

IV. In situ stresses for the "N" field were estimated from the data from offset wells that were supplied by the operator. This includes the estimation of the vertical stress, the orientation of the minimum horizontal stress and the estimation of the magnitude of minimum and the maximum horizontal stresses.

V. Dynamic rock mechanical properties such Young's Modulus, Poisson's Ratio, critical stress intensity factor (rock toughness), and Biot's coefficient were determined using either compressional and shear velocities from acoustic log data provided by the operator or, where necessary, by using published correlations.

VI. A TIF is then modelled to assess the uncertainties and data reliability as well as to investigate the possibility of TIF initiation and propagation using parameters obtained in steps "IV" and "V". The results were compared to the history data.

VII. History matching is then finalised after rectifying uncertain parameters e.g. reservoir pressure and BHP. Workflows at different levels of the history matching are used.

5.5 Sector Model Description, Import, and Verification

5.5.1 "N" Field Sector Model Description

The dimensions of the N field sector model are 7874 ft x 6758.53 ft with a thickness of 903.8 ft. The 3D sector model grid system (Figure 5-6) consists of 26 x 22 x 474 cells giving the average size of 307 x 307.4 ft and a (fine) vertical thickness of 2 ft. The histograms for the porosity and permeability distribution of the cells are shown in Figure 5-7 and Figure 5-8.

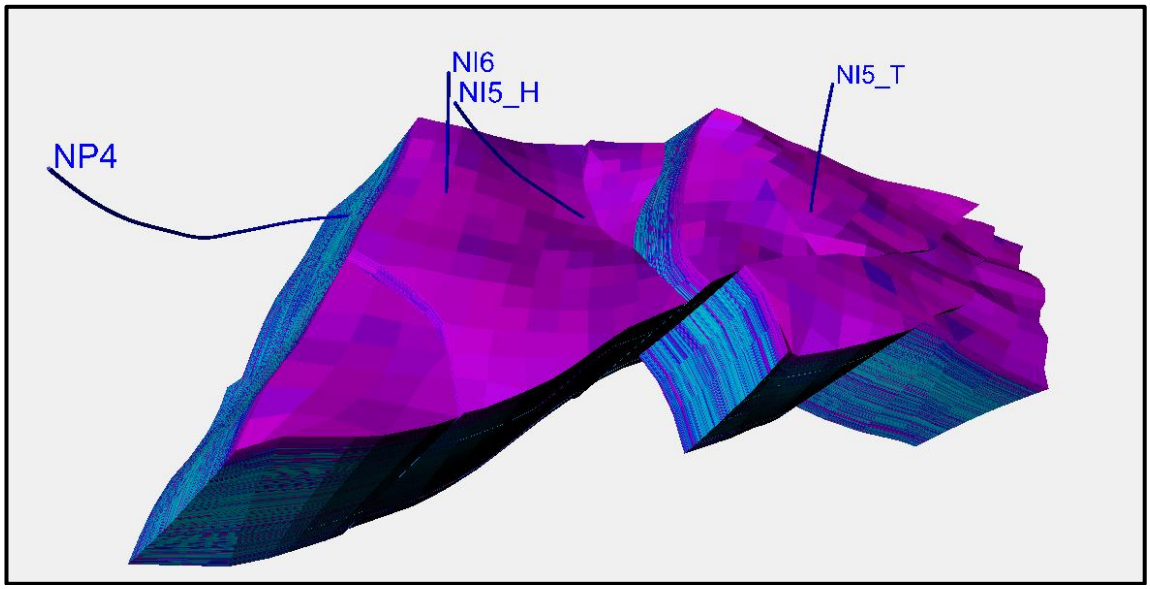

Figure 5-6: he 3D reservoir grids system for the "N"field sector model and the well locations

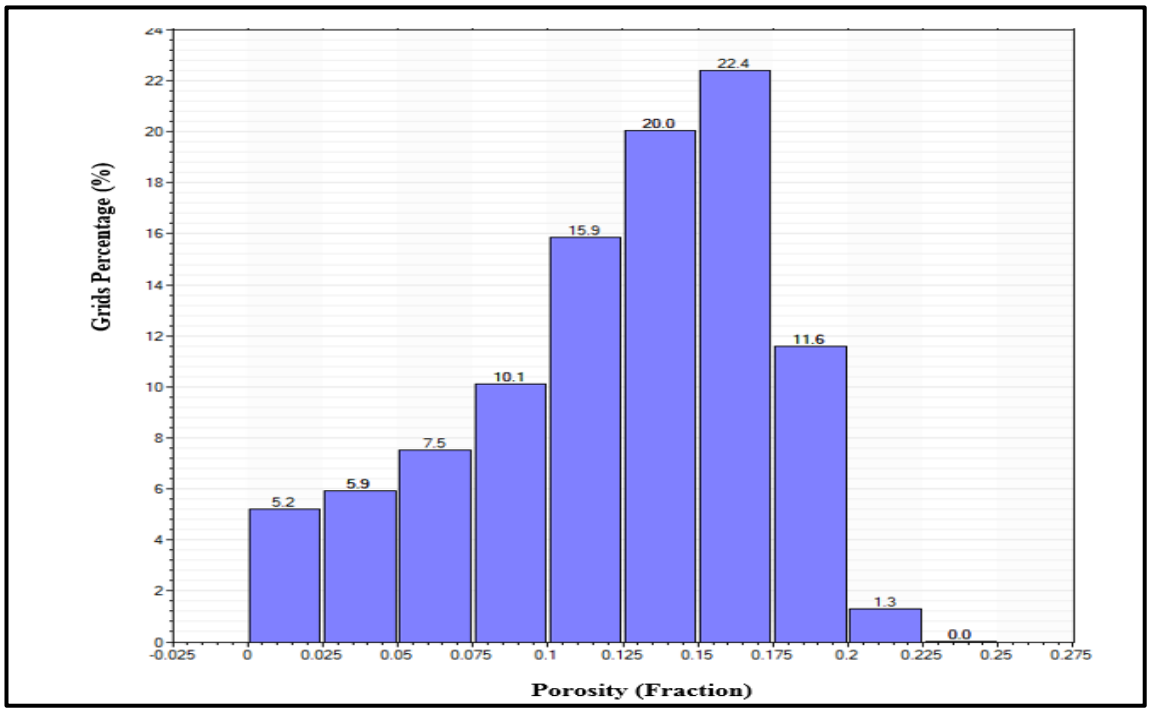

Figure 5-7: Porosity distribution histogram for the "N" field sector reservoir model

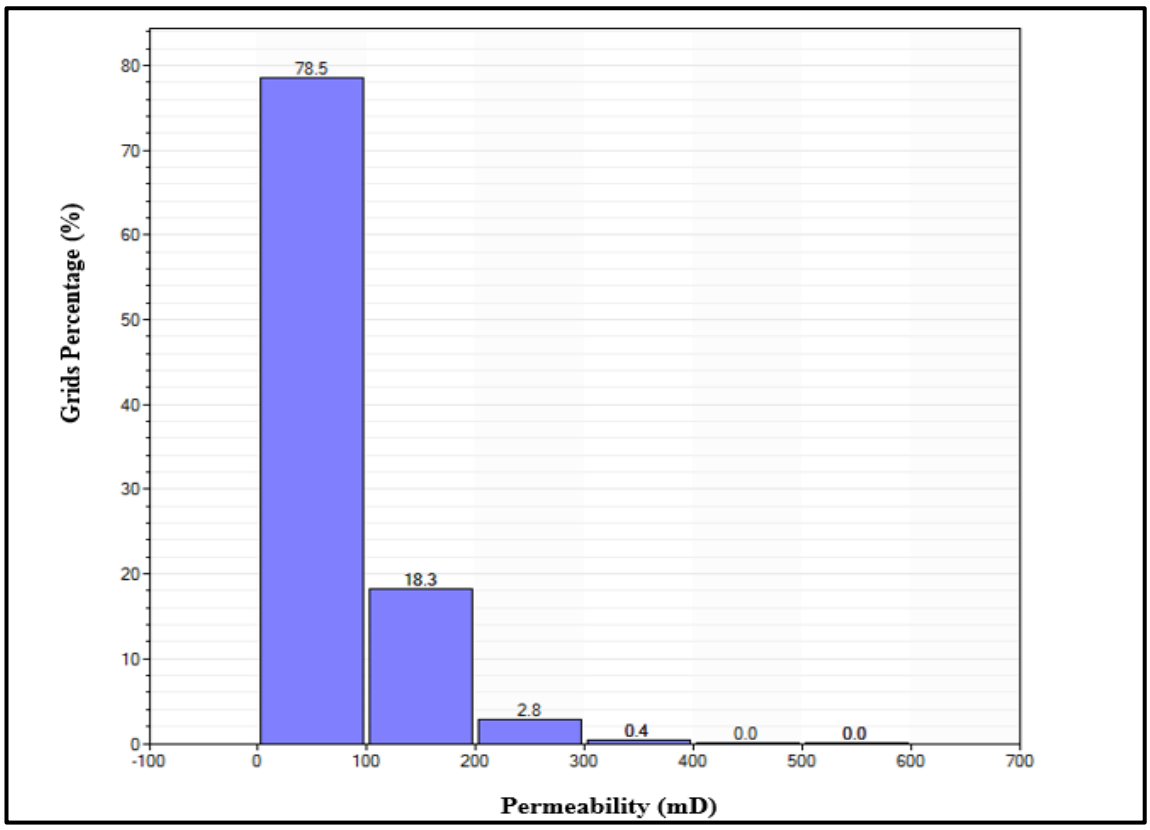

Figure 5-8: Horzointal permeablitiy distribution forthe "N" field sector reservoir model

The sector model has a total of 4 wells (Figure 5-6). There are three horizontal wells i.e. Producer "NP4", injector "NI5_T" and injector "NI5_H" and one vertical well (injector "NI6"). Producer NP4 and injector NI6 are completed within the oil column while injectors NI5_T and NI5_H are completed within the (weak) aquifer that is partially masked by a shale layer. The reservoir also has a small gas cap. The vertical saturation map is shown in Figure 5-9.

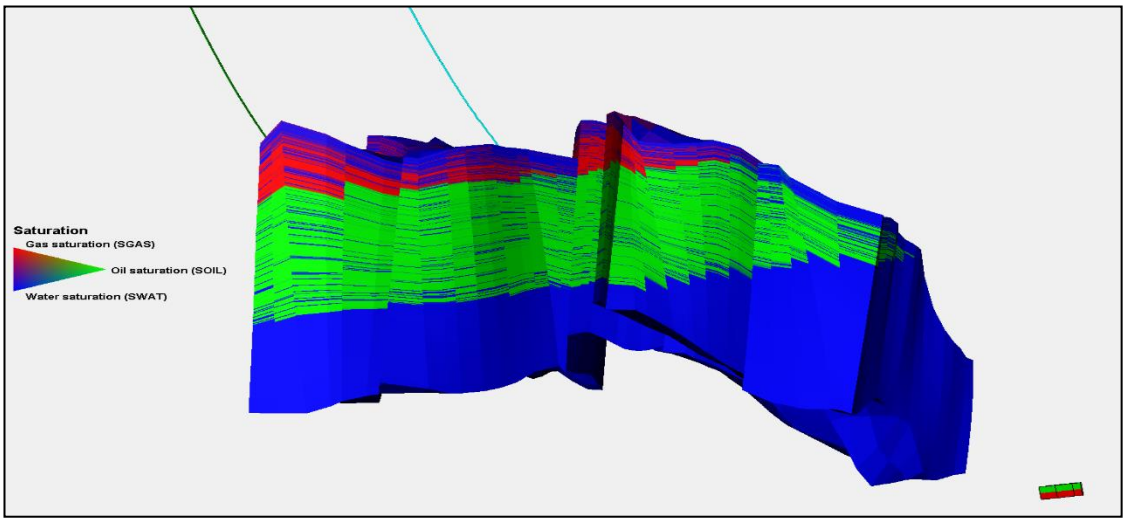

Figure 5-9: The vertical saturation map of the "N" field reservoir (at the start of production)

5.5.2 Importing the Eclipse Model into REVEAL Reservoir Simulator

The import process from Eclipse to REVEAL reservoir simulator can be done via a workflow that is incorporated into REVEAL. Geometry, reservoir properties, rock and regional data, relative permeabilities data, PVT tables and non-neighbour connections are all imported by the built in workflow. Well data i.e. locations and completions must be imported manually into REVEAL. Figure 5-10 shows the imported REVEAL model.

The imported Eclipse model is isothermal with PVT properties at one temperature i.e. reservoir temperature. However, REVEAL (w/o TIF option i.e. isothermal) should reproduce the Eclipse results under the same conditions before performing a TIF modelling.

5.5.3 Imported Model Verification

Data from only three wells (NP4, NI6, and NI5_H) in the "N" field sector model were available for the history matching analysis. The location of injectors NI6, NI5_H, and NI5_T with respect to the producer NP4 is shown in Figure 5-10. Injector NI5_H is located approximately 1230 ft below the producer "NP4" whereas injector "NI6" is located approximately 721.8 ft away from the heel of producer "NP4".

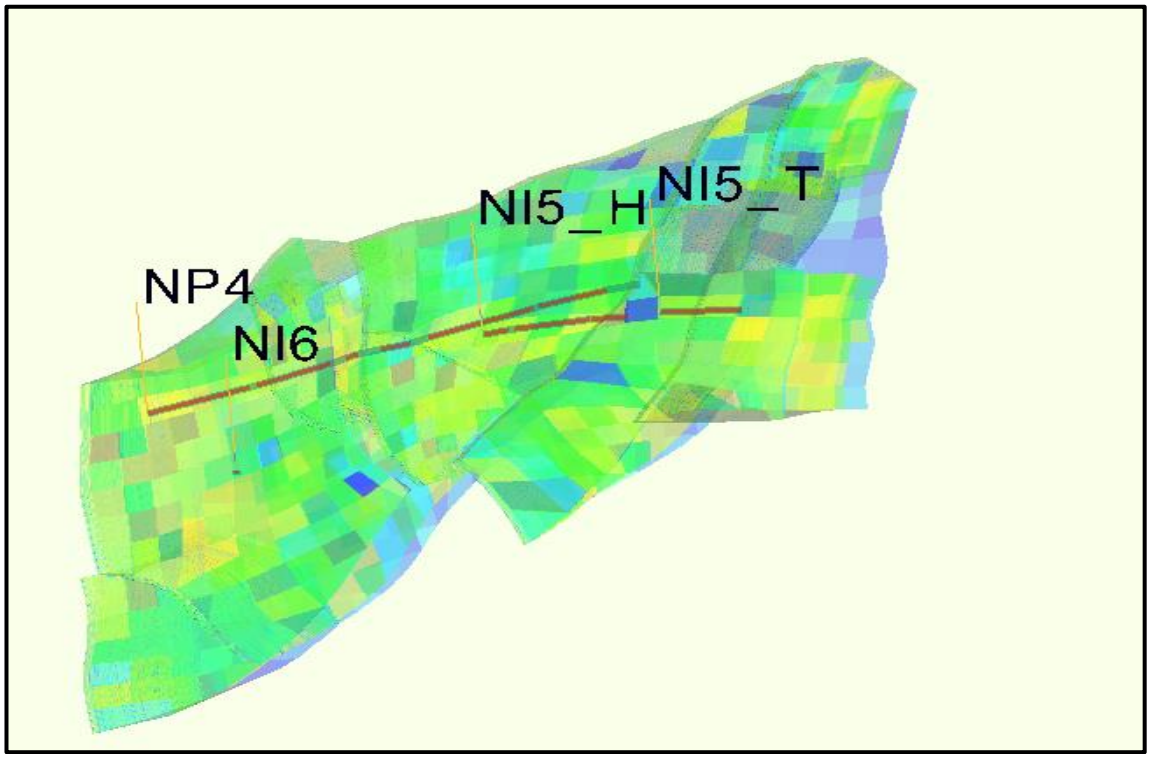

Figure 5-10: Locations of injectors NI6, NI5_H, and NI5_T with respect to producer NP4

A simulation case was run to compare the performance of Eclipse and REVEAL models of the three wells, i.e. the "NP4" producer, the "NI6" injector, and the NI5_H

injector. This step is important to build confidence in the imported sector model for the rest of the analysis. Well rates were fixed at 12580 STB/d for both NP4 and NI6 and 6290 STB/d for NI5_H. The REVEAL and Eclipse BHP results were comparable after matching the PVT tables and the relative permeability curves (Figure 5-11, Figure 5-12, and Figure 5-13). The difference were 1.4%, 1.2, and 0.5% for NP4, NI6, and NI5_H respectively. The REVEAL model can thus be used with confidence for the TIF modelling analysis.

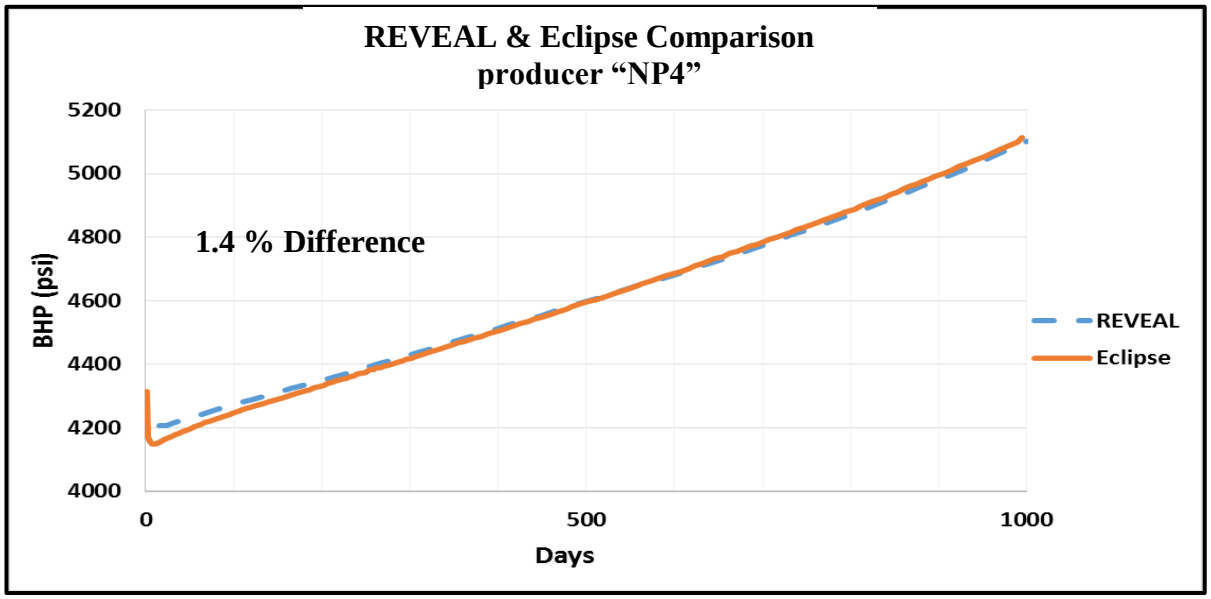

Figure 5-11: REVEAL and Eclipse model predictions for producer "NP4" BHP

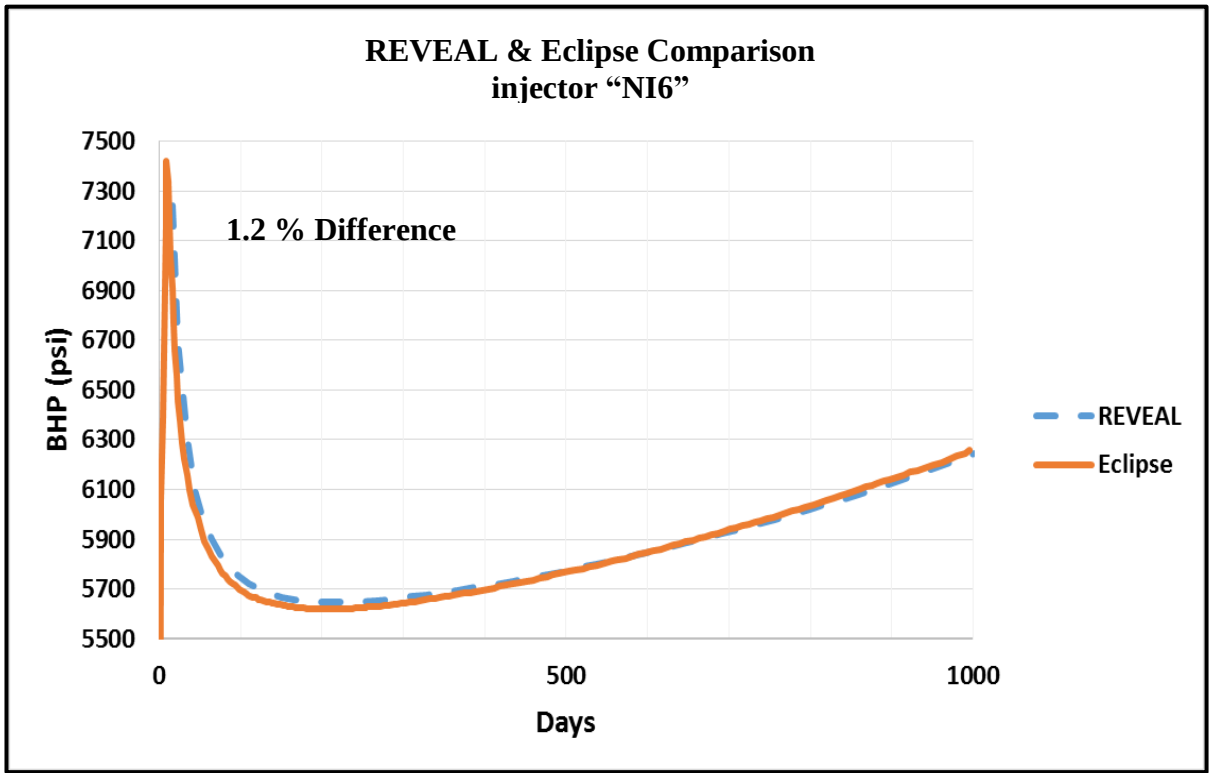

Figure 5-12: REVEAL and Eclipse model predictions for injector "NI6" BHP

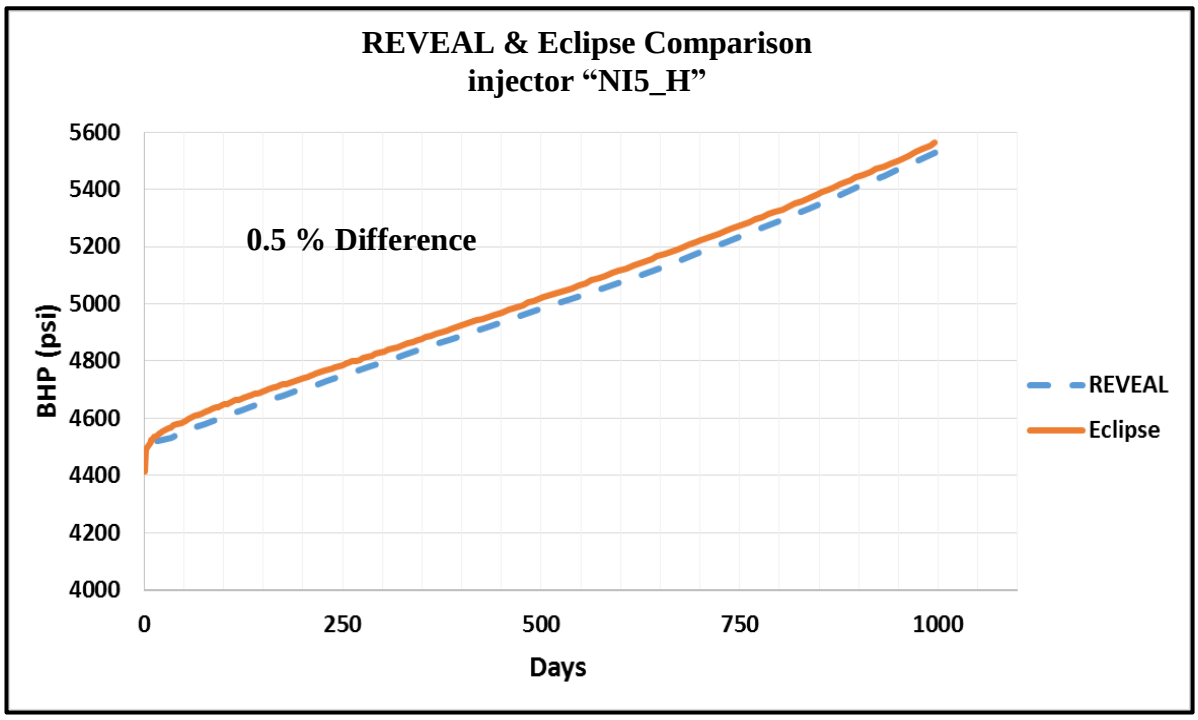

Figure 5-13: REVEAL and Eclipse model predictions for injector "NI5_H" BHP

5.6 Converting the Isothermal Reservoir Model to the Thermal One

The Eclipse isothermal model provided fluid PVT properties at a range of pressures and a single (reservoir) temperature of 224.6^{o} F (Table 5-2). Extension of the fluid PVT properties to different temperatures is required to account for the temperature and pressure variations that will be encountered during the productive life of the reservoir due to injection of surface temperature water in the reservoir.

The methodology used here is to match Table 5-2 to different correlations. Glaso, Standing, Lasater, Vazques-Beggs, and Petrosky correlations for Bubble point pressure, Gas Oil Ratio (GOR), and oil Formation Volume Factor (FVF) are compared. Beal et al, Beggs et al, Petrosky, and Bergman-Sutton correlations for oil viscosity are also compared. After checking match statistics for all correlations, Vazques-Beggs and Beggs et al correlations are selected.

The Vazques-Beggs correlations ([129] and Table 5-1) contain equations for solution GOR, oil FVF, and bubble point pressure. They were developed from data obtained from over 600 laboratory PVT analyses gathered from different fields all over the world. This data covered a wide range of pressure, temperature, and oil properties. The bubble point pressure equation is expressed as:

$$p_b = \left(\frac{R_s}{C_1 \gamma_g e^{\left(C_3\left(\frac{\gamma_o}{T+459.67}\right)\right)}} \right)^{\frac{1}{C_2}}$$ Equation 5-1

The Solution Gas Oil Ratio equation is expressed as:

$$R_S = C_1 \gamma_g P^{C_2} e^{\left(C_3\left(\frac{\gamma_o}{T+459.67}\right)\right)}$$ Equation 5-2

The Oil FVF – Saturated equation is expressed as:

$$B_O = 1 + A_1 R_S + A_2 (T - 60)\left(\frac{\gamma_o}{\gamma_g}\right) + A_3 R_S (T - 60) + \left(\frac{\gamma_o}{\gamma_g}\right)$$ Equation 5-3

The Oil FVF – Undersaturated equation is expressed as:

$$B_O = B_{ob} e^{\left(C_0 (P_b - P)\right)}$$ Equation 5-4

Where

Table 5-1: Coefficients for the Vazques-Beggs correlations [129]

Coefficient	***$\gamma_o \leq 30^o$ API***	***$\gamma_o \geq 30^o$ API***
A_1	*0.0362*	*0.0178*
A_2	*1.0937*	*1.187*
A_3	*25.724*	*23.931*
C_1	*4.68E-04*	*4.67E-04*
C_2	*1.75E-05*	*1.10E-05*
C_3	*-1.81E-08*	*1.38E-09*

Where

B_O = Oil formation volume factor (FVF)

B_{ob} = Bubble point oil FVF

R_s = The solution Gas Oil Ratio (GOR)

γ_o = The oil gravity, ^{0}API

γ_g = The gas gravity, (air =1)

p_b = The bubble point pressure.

Beggs et al [130] developed an empirical correlation to estimate the oil viscosity that was developed by analysing viscosity measurements of 460 dead oil samples covering the range of 16°API to 58°API and 70°F to 295°F [130]. The resulting equation for the oil viscosity is:

$$\mu_{od} = 10^{x} - 1 \qquad \text{Equation 5-5}$$

Where

$$X = yT^{-1.163} = 10^{Z} \qquad \text{Equation 5-6}$$

$$y = 10^{Z} \qquad \text{Equation 5-7}$$

$$Z = 3.0324 - 0.02023\, SG_O \qquad \text{Equation 5-8}$$

PVT tables were calculated from the above two correlations in Appendix F

Table 5-2: The isothermal fluid PVT properties

Temperature = 224.6 F								
Pressure (psi)	Bubble Point (psi)	Gas Oil Ratio (scf/STB)	Oil FVF RB/STB	Oil Viscosity cp	Gas FVF (RB/Mscf)	Gas Viscosity (cp)	Water FVF RB/STB	Water Viscosity (cp)
7251.89	738.415	1380.21	1.75093	0.283276	0.561812	0.033579	1.02306	0.32758
6890.03	738.415	1298.85	1.71203	0.292091	0.575612	0.032602	1.02428	0.32758
6528.16	738.415	1218.28	1.67351	0.303124	0.591175	0.031596	1.02551	0.32758
6166.31	738.415	1138.54	1.6354	0.316543	0.608871	0.030559	1.02673	0.32758
5804.45	738.415	1059.68	1.59769	0.332554	0.629183	0.029492	1.02795	0.32758
5442.58	738.415	981.727	1.56043	0.351413	0.652742	0.028393	1.02918	0.32758
5080.73	738.415	904.74	1.52362	0.37342	0.680391	0.027263	1.0304	0.32758
4718.88	738.415	828.775	1.4873	0.39893	0.71327	0.026103	1.03162	0.32758
4357.01	738.415	753.888	1.4515	0.428355	0.752957	0.024915	1.03284	0.32758
3995.15	738.415	680.158	1.41625	0.462165	0.801682	0.023706	1.03407	0.32758
3633.29	738.415	607.668	1.3816	0.500895	0.862681	0.022481	1.03529	0.32758
3271.43	738.415	536.518	1.34758	0.545137	0.940758	0.021254	1.03651	0.32758
2909.57	738.415	466.826	1.31427	0.59555	1.0433	0.020038	1.03774	0.32758
2547.71	738.415	398.739	1.28172	0.652833	1.18201	0.018856	1.03896	0.32758
2185.85	738.415	332.446	1.25002	0.717708	1.37632	0.017734	1.04018	0.32758
1823.99	738.415	268.179	1.2193	0.790879	1.66066	0.016701	1.0414	0.32758
1462.13	738.415	206.266	1.1897	0.872922	2.10233	0.015784	1.04263	0.32758
1100.27	738.415	147.181	1.16145	0.964077	2.85516	0.015003	1.04385	0.32758
738.415	738.415	91.6773	1.13492	1.06374	4.37215	0.014371	1.04507	0.32758
376.556	738.415	41.2191	1.1108	1.16895	8.84523	0.013896	1.04629	0.32758

5.7 History Matching the REVEAL "N" Field Sector Model without TIF

The "N" field REVEAL model after conversion into a thermal model was run and compared to history data from injector NI6. Injection well NI6, being the point of interest of this study, was set to operate under THP control using the provided (THP) history data. Producer NP4 and injector NI5_H control were set to rate control using the history data. The injection rate of well NI6 was matched based on unreliable (estimated) reservoir pressure and BHP data. Any mismatch will be rectified later after analysing these uncertainties. The current objective for running the simulation without modelling TIF here is to answer the following questions:

I. How does injector "NI6" perform during the entire period?

II. When does the deviation from the history data occur?

III. Does the deviation correspond to the observed TIF occurrence period?

The resulting simulation and the history data are shown in Figure 5-14. The injector NI6 simulation data shows a good match up to 520 days, after which increasingly large deviations from the history data occur. This deviation corresponds to TIF initiation period which is expected to take place in the period between 520 and 700 days i.e. between the dashed lines in Figure 5-14. The injection rate continued to increase during TIF initiation period, even though the BHP was still decreasing. This is especially clear after 700 days (the second dashed line in Figure 5-15). This is a clear indication of occurrence of TIF. Modelling the injection rate with a radial outflow equation does not match the reliable data after 520 days. It can be confidently concluded that TIF initiation occurred after 520 days (Figure 5-15). This will be discussed further in **Section 5.11.**

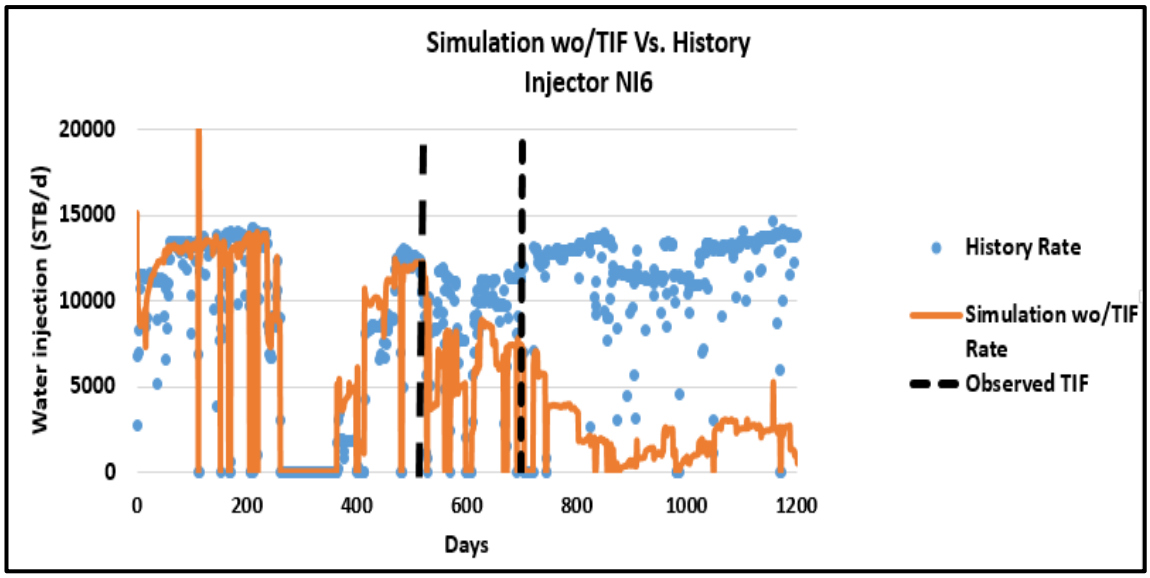

Figure 5-14: Simulation run versus the history for injector NI6

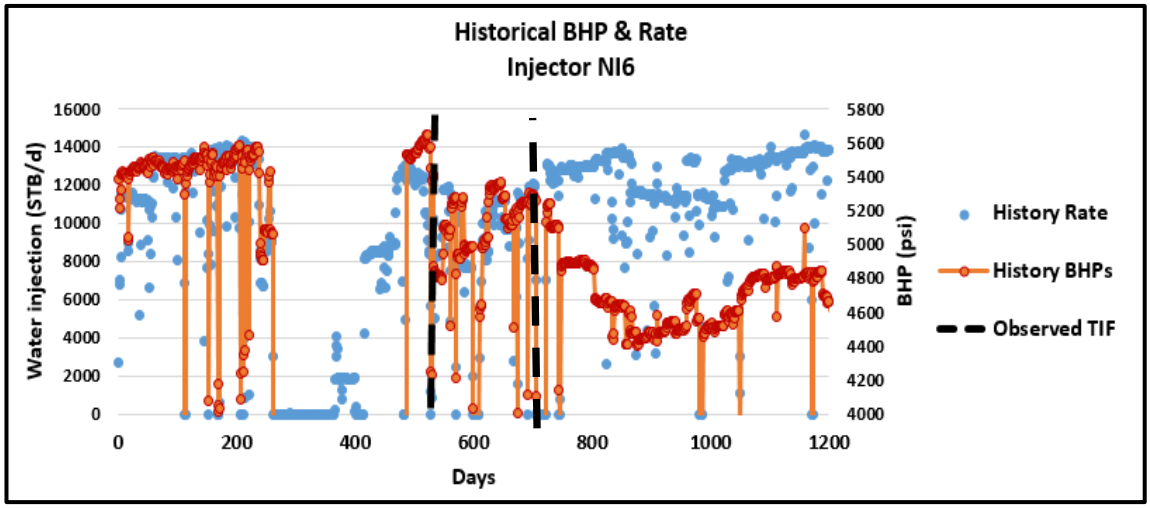

Figure 5-15: The historical injection rates and BHPs for injector NI6

5.8 In Situ Stress

The value of the in-situ stresses of the "N" field and the rock mechanical properties must be matched since they are one of the fundamental parameters that govern TIF occurrence. TIF initiation and growth, as observed in well "NI6" above and, by analogy, probably takes place in other "N" field injectors. Well test and well log were available from well N-8. The relative location of well N-8 to injector NI6 is shown in Figure 5-16. The following assumption were made:

I. It is assumed that the direction of the principal in-situ stress in the "N" field is vertical

II. The stress regime is normal faulting: $\boldsymbol{\sigma}_v > \boldsymbol{\sigma}_{Hmax} > \boldsymbol{\sigma}_{hmin}$

III. All measurements and estimations of in-situ stress and rock mechanical properties for well N-8 are assumed to apply to injector NI6.

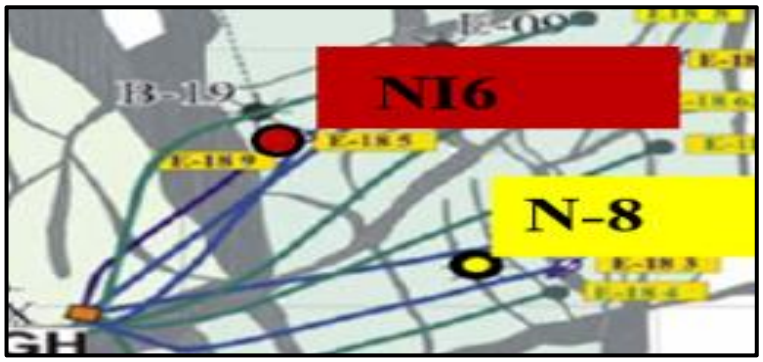

Figure 5-16: Well N-8 relative location to injector NI6 (supplied by the operator)

5.8.1 Estimation of the Vertical Stress

The magnitude of the vertical stress σ_v, equal to the weight of the overburden was calculated from the integrated bulk density log for well N-8. Figure 5-17 shows the bulk density (ρ_b) from the top of the logged interval to the top of the formation. The weight of the overburden for N-8 will be calculated down to depth of 2970 m (9744 ft) i.e. the perforated interval in well NI6. Average densities of different rocks at different depths is shown in Figure 5-17. These values are in SI units and will be converted to Oilfield units for the model. They are 1000 kg/m^3 for 130 m i.e. seawater, 1850 kg/m^3 down to 1000 m, 2400 kg/m^3 down to 2300 m , and 2700 kg/m^3 down to 2970 m . These values will be used to estimate the vertical stress σ_v:

$$\sigma_v = \int_0^z \rho(z) g \, dz \qquad \text{Equation 5-9}$$

$$\sigma_v = \text{Weight of Sea Water} + \text{Weight of Rocks} \qquad \text{Equation 5-10}$$

$$\sigma_v = 9.83\,[(1 * 130) + (1850 * 870) + (2400 * 1300) + (2700 * 670)]$$

$\sigma_v = 6.56 \times 10^7$ Pa = 9514 psi

A vertical stress value of 9514 psi was calculated transforming it into a stress gradient of 0.97 psi/ft. Hence, this vertical stress gradient will be used for the calculation of the vertical stress during the modelling of TIF in the rest of the analysis.

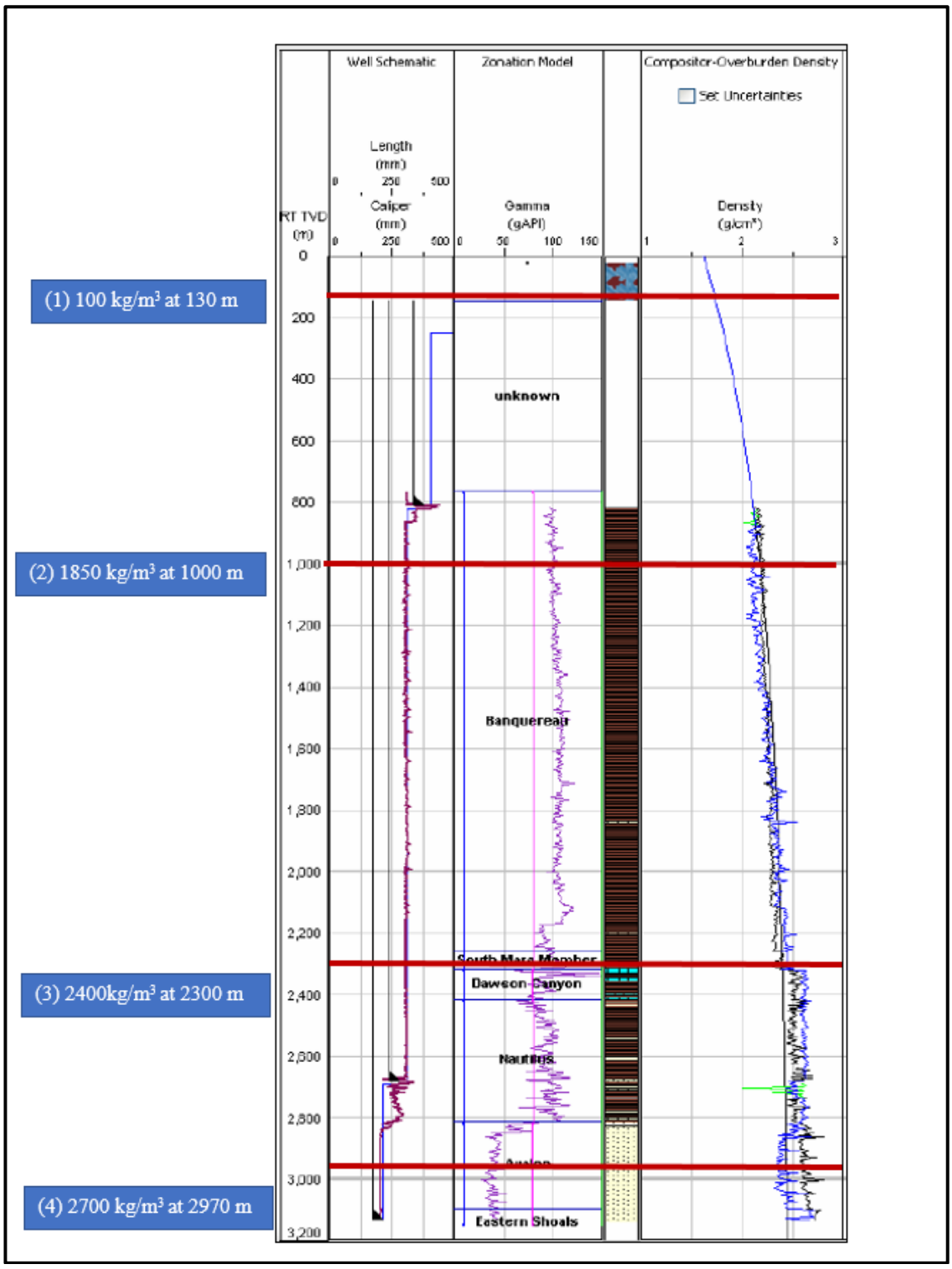

Figure 5-17:The bulk density (ρb) recorded by the log of Well N-8 (Blue Line) (supplied by the operator)

5.8.2 Magnitude of the Minimum Horizontal Stress

One of the most common method in the literature to determine the magnitude of the minimum horizontal stress is to use leak off tests (LOTs). Oyeneyin [44] has indicated that LOTs method is not the most accurate method since these tests are not performed in the reservoir intervals and they can only indicate a stress between the vertical stress and

the minimum horizontal stress. However, the best measurement available was LOTs performed on well N-8 at two different intervals (824 m and 2678 m) which are being used in this study.

The LOT at of 824 m TVD in Figure 5-18 shows an equivalent mud weight of 13.5 ppg (or 0.7 psi/ft) at the leak off pressure. A higher LOT value 14.56 ppg (or 0.76 psi/ft) was recorded at 2678 m TVD (Figure 5-19). The average (0.73 psi/ft) of these two values was used as the starting point in the history matching analysis.

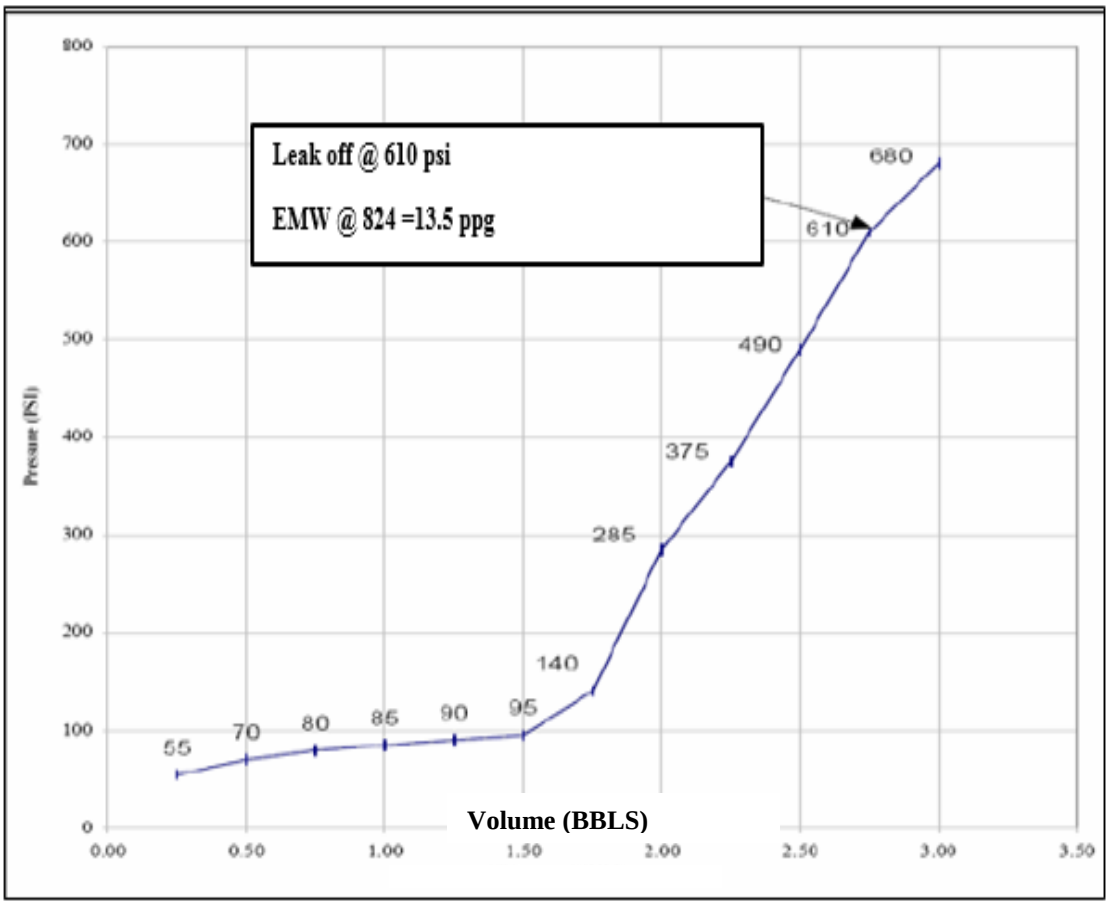

Figure 5-18: Leak off test at 824 m TVD for well N-8 (supplied by the operator)

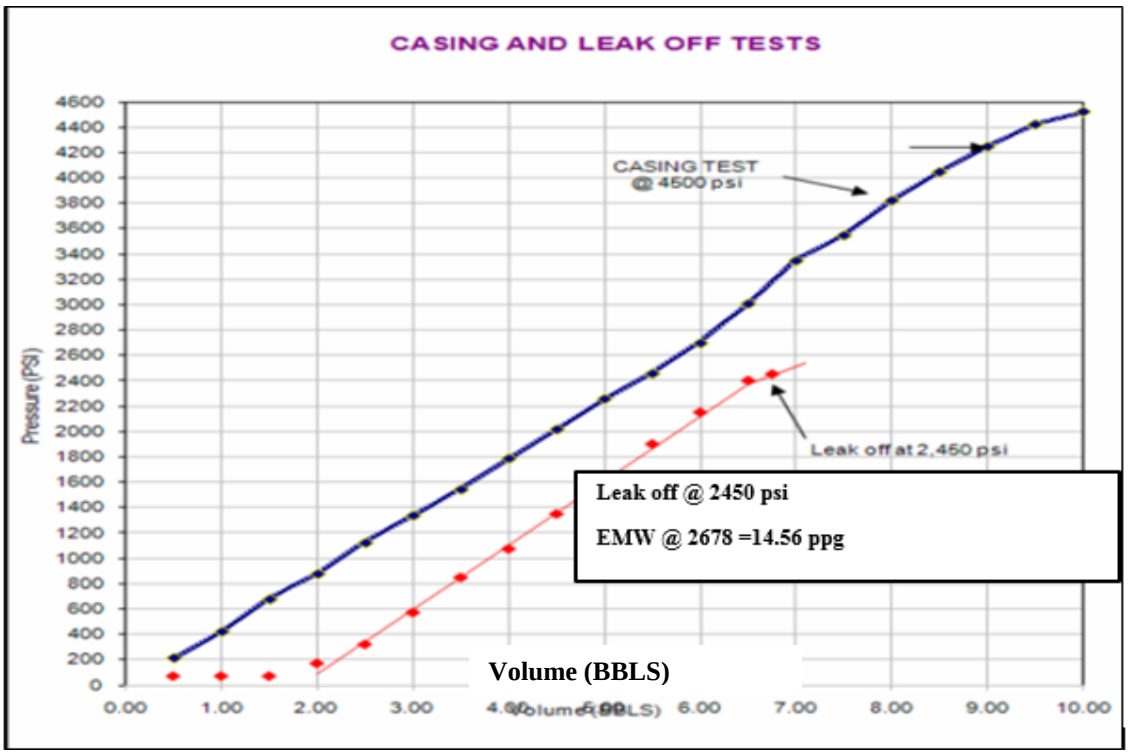

Figure 5-19: Leak off test at 2678 m TVD for well N-8 (supplied by the operator)

5.8.3 Magnitude of the Maximum Horizontal Stress

The magnitude of the maximum horizontal stress (σH_{max}) is the most difficult stress to estimate. However, drilling experience and wellbore imaging can give important information on the magnitude and orientation of σ_{Hmax} [24]. An approximate value for σ_{Hmax} can be obtained using stress polygon if the stress regime, the vertical stress (from density log) and the minimum stress (from a LOT) are all known.

The stress polygon defines all possible maximum and minimum stress magnitudes according to Anderson's theory and Coulomb faulting theory [24].The limiting ratio of Maximum Princaple Effective stress and Minimum Principal Effective stress is given for Normal Faulting by:

$$\frac{\sigma_v - P_P}{\sigma_{hmin} - P_P} \leq [(\mu^2 + 1)^{\frac{1}{2}} + \mu)]^2 \qquad \text{Equation 5-11}$$

μ, the coefficient of friction is assumed to be 0.6 and Pp, the pore pressure, is assumed to be a gradient of 0.433 psi/ft. Figure 5-20 is the resulting stress polygon at depth of 8786 ft, the LOT depth.

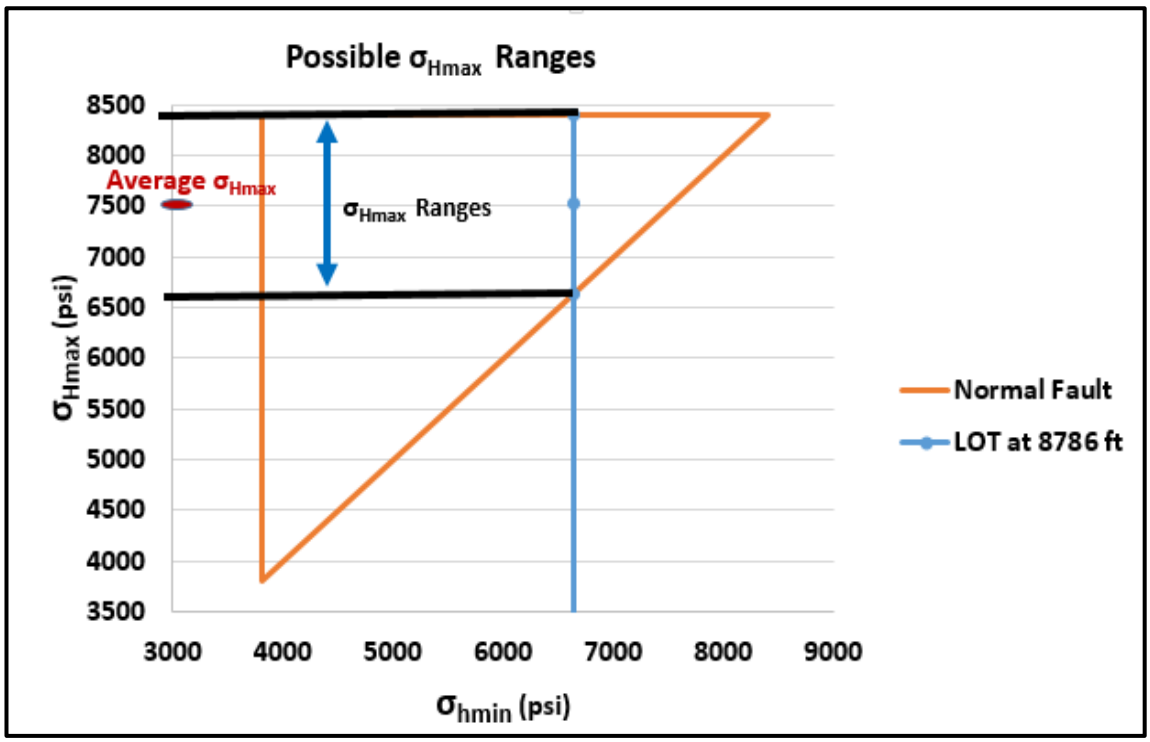

Figure 5-20: Possible range of σ_{Hmax} for normal faulting regime at depth of 2678 m (8786 ft) TVD

The Figure 5-20 stress polygon permits, in principle, a wide range of (σH_{max}) values at a depth of 8786 ft TVD. The regional stress regime is normal faulting which, when combined with the deep LOT, gives a narrower range of possible stress values. The average value (7513 psi or 0.86 psi/ft) was chosen as the starting point in the history matching analysis.

5.8.4 Orientation of the Minimum Horizontal Stress

A TIF propagates perpendicular to the direction of minimum horizontal stress (σh_{min}). The Formation Micro Imager (FMI) log often provides information on the stress direction. Well N-8's FMI did not show any failure features that could have been caused by drilling. However, well N-20's FMI (Figure 5-21) clearly showed tensile fractures propagating in an E-W direction; hence σH_{min} has a N-S orientation.

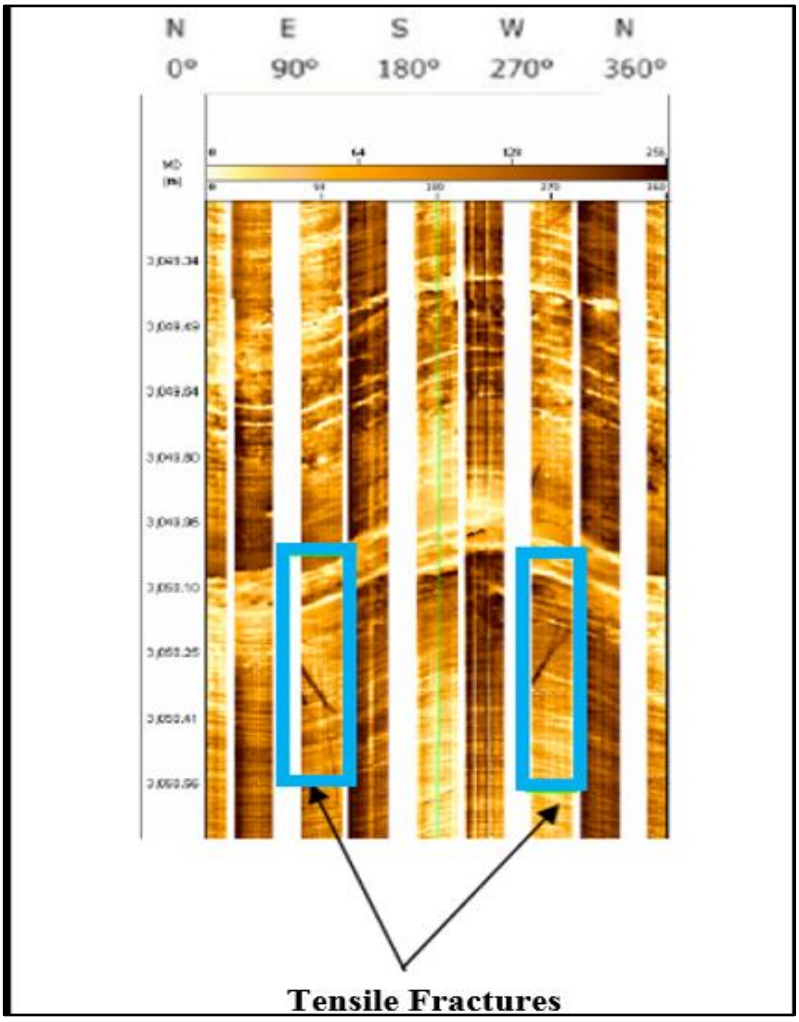

Figure 5-21: FMI image from Well N-20 with tensile fractures

5.9 Rock Mechanical Properties

An estimate of the rock mechanical properties for the reservoir are required for TIF modelling. The sonic log for well N-8 was used to derive the Young's Modulus and the Poisson's Ratio since no measurements were made on core samples. Fracture toughness and Biot's coefficient were estimated from published correlations.

5.9.1 Young's Modulus & Poisson's Ratio

The dynamic Young's Modulus (E) and Poisson's ratio (v) were derived from the log based compressional V_p and shear wave V_S velocities [131]:

$$v = \frac{\frac{1}{2}\left(\frac{V_p}{V_S}\right)^2 - 1}{\left(\frac{V_p}{V_S}\right)^2 - 1} \qquad \text{Equation 5-12}$$

$$E = \rho \times {V_S}^2 [\frac{3{V_P}^2 - 4{V_S}^2}{{V_P}^2 - 4{V_S}^2}$$ Equation 5-13

Compressional V_p and shear wave V_S velocities were estimated using well N-8 log measurements (Figure 5-22). Compressional V_p and shear wave V_S velocities were estimated to be 4545 m/s and 2702 m/s respectively. The Young's Modulus (E) was determined to be 47.04 GMPa (6.82×10^6 psi) and the Poisson's ratio (v) to be 0.23. These values were used as a starting point in the initial history matching analysis.

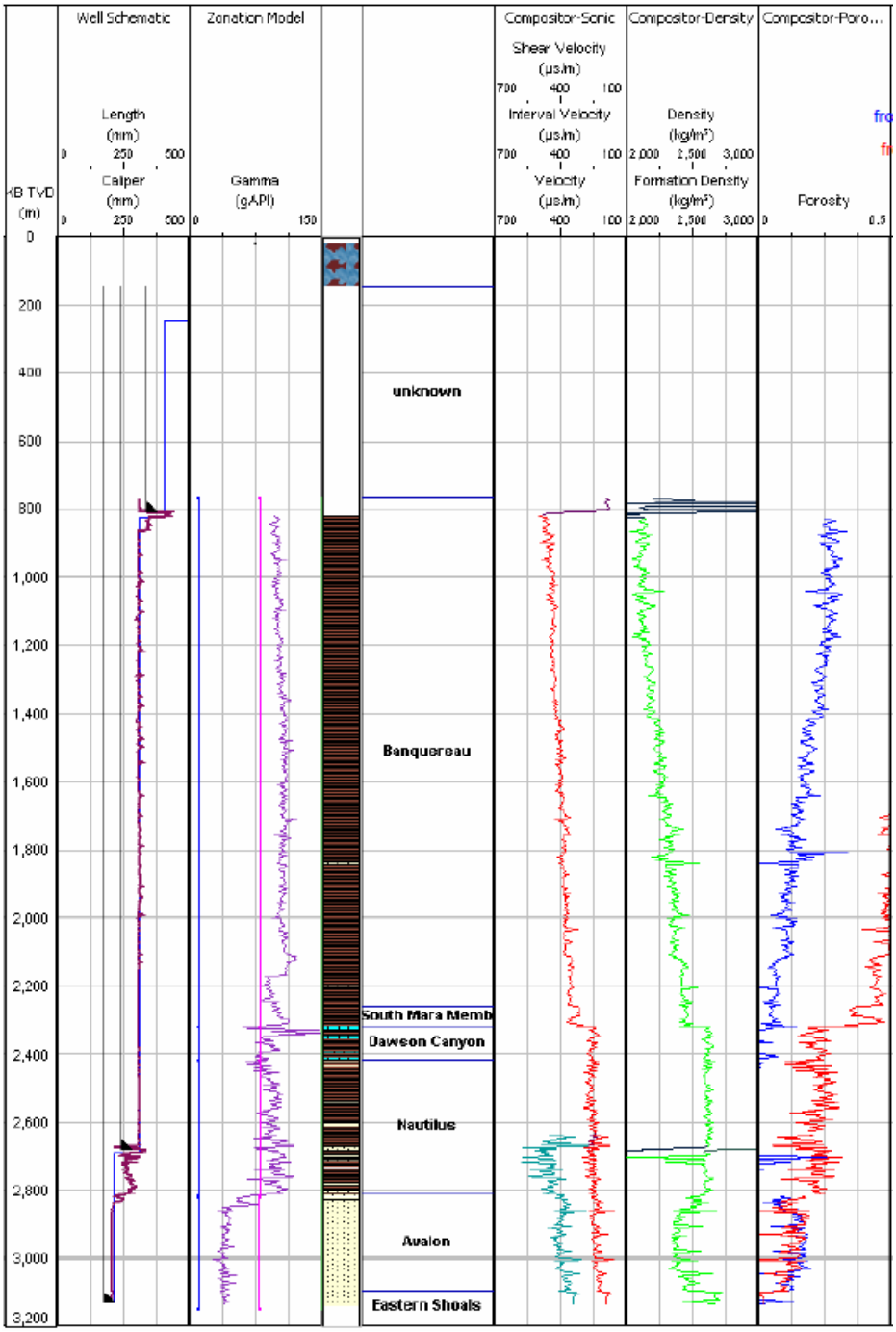

Figure 5-22: Well N-8 Compressional (Vp) and Shear Wave (Vs) Velocities

5.9.2 Fracture toughness

TIF propagation criterion employed in this thesis is the fracture toughness (K_{IC}) as a measure of the rock's resistance to fracturing. A fracture will propagate once the stress intensity factor of a type 1 fracture (K_I) is sufficiently larger than K_{IC} [132]:

$$K_I \geq K_{IC} \qquad \text{Equation 5-14}$$

K_{IC} can be measured by a laboratory experiment or by a field scale, fracture test. A statistical relationship between K_{IC} and the dynamic Young's Modulus (E) for sandstone developed by Zhix [132] was used since core measurments data was not available:

$$K_{IC} = 0.0215\ E + 0.2468 \qquad \text{Equation 5-15}$$

Equation 5-15 gives a fracture toughness of 1.26 MPa/$\sqrt{m}$ (330 psi/$\sqrt{ft}$). This value again will be used as a starting point in the history matching analysis.

5.9.3 Biot's coefficient

Biot's coefficient is used to estimate the reduction in total stress due to reservoir cooling by the cold injection water. The Wu empirical correlation for consolidated sediments was used in this thesis [131]:

$$\alpha = 1 - (1 - \emptyset)^{3.8} \qquad \text{Equation 5-16}$$

Where

α = Biot's coefficient

$\emptyset$ = The porosity

The perforated formation's porosity (Figure 5-22) is 0.18 at of 9744 ft, giving an estimated Biot's coefficient of 0.53.

5.10 Uncertainty Analysis

The initial estimates of the NI6 well data discussed above were used for the initial TIF performance modelling. It is recognised that these estimates have a large uncertainty. This section aims to assess these uncertainties that related to the NI6 reservoir pressure. TIF growth will also be evaluated. The in-situ stresses and rock mechanical data were input into the reservoir simulator coupled to geomechanical solution and TIF model. Injector well NI6 was operated under THP control using the history data while producer NP4, injector NI5 were rate controlled to reproduce the field history data. The average surface temperature of the NI6 injection water during the history period was 70^{o} F. The simulated "with TIF" and "no TIF" results were in good agreement, (Figure 5-23) up to 520 days. N.B. section 5-7 showed that TIF initiation occurred between 570 and 700 days

The "with" TIF simulation predicted that TIF initiation occurred at 620 days. The TIF initially delivered an injection rate that exceeded the history data, but it rapidly

decreases to much lower w/o TIF rate after ~ 750 days. This divergence from the simulated and history data might be due to use of incorrect values for the reservoir pressure, the injected water temperature or the thermal and geomechanical rock properties. This will be evaluated in the following sections.

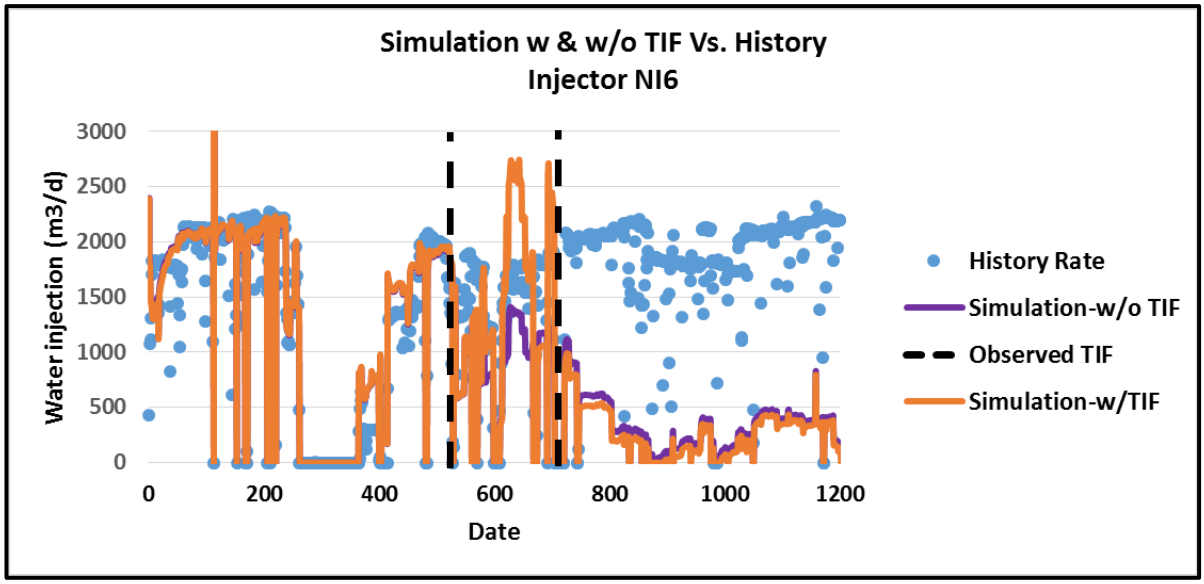

Figure 5-23: Simulation run with & without TIF modelled versus injector CW6 history data

5.10.1 Reservoir Pressure

Average reservoir pressure data for well NI6 was measured by long-term fall off tests during the period 2009 – 2012 (Table 5-3). Figure 5-24 shows that the (+TIF) simulated reservoir pressure around well NI6 did not match these fall off test measurements. The simulation overestimated the actual reservoir pressure by 100 psi initially, increasing to > 400 psi after 4 years. Section 5.11.1 describes how the simulated reservoir pressure was matched to reproduce the above fall off tests that measured the actual reservoir pressure.

Table 5-3: Average reservoir pressure measured by long-term fall off tests for well NI6

Well NI6 Shutdowns		***Average Regional Pressure (psi)***
After 266 days	*Jul-09*	*4480.5*
After 702 days	*Oct-10*	*4524*
After 1277 days	*May-12*	*4263*

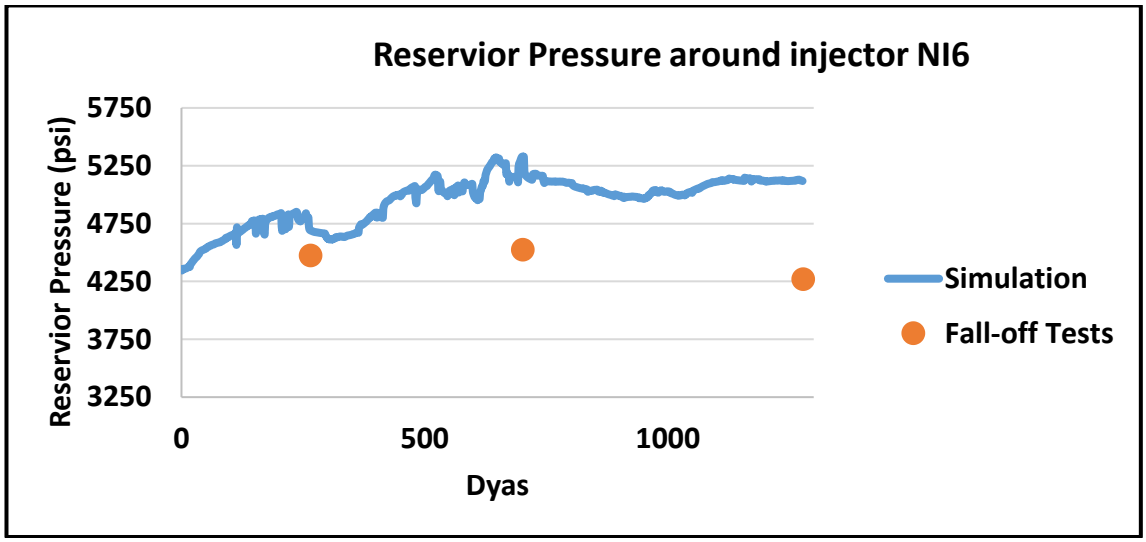

Figure 5-24: Calculated vs. fall off reservoir pressure around well NI6

5.10.2 Wellbore Modelling

Figure 5-25 shows that the NI6 wellbore model did not match the history data when the well was controlled by the wellhead pressure. Section 5.11.2 describes the calibration of the wellbore model to reproduce the BHP history.

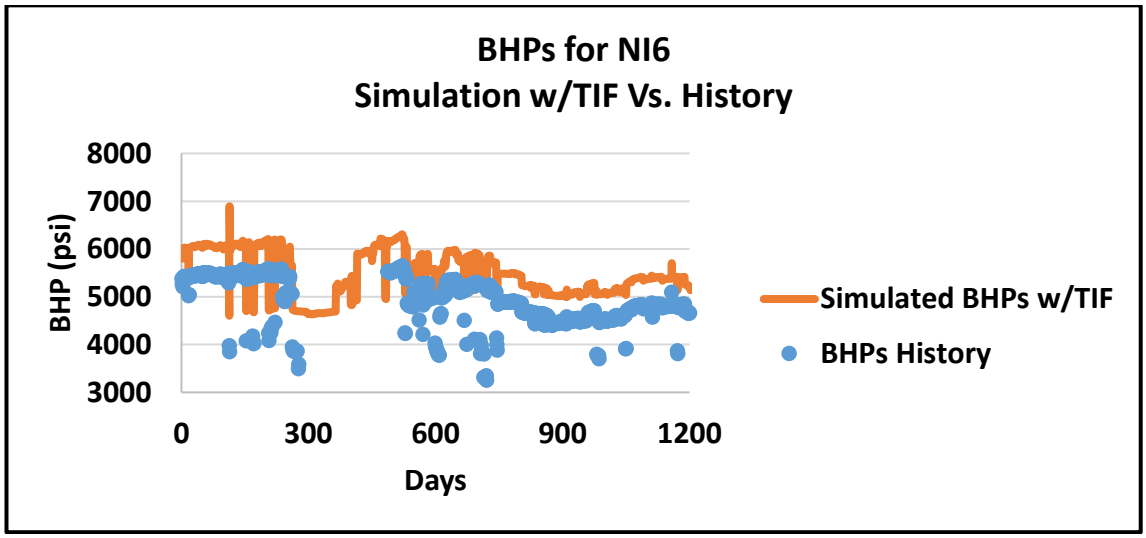

Figure 5-25: Well NI6 calculated (+TIF) simulated reservoir vs history data

5.10.3 Type and Surface Temperature of the Injection Water

The injected water's temperature at the surface as well as its type (or properties) is an important aspect of TIF modelling. The history data for the surface water temperature for injection well NI6 (Figure 5-26) shows a variation between 60° and 90°F that is difficult to properly include in the reservoir simulator. Knowledge of the injection water type and properties is required in addition to its temperature. Clean (low solids) sea water typically has a low temperature and creates a high conductivity TIF while (higher solids content) produced water leading to a TIF with a lower conductivity and a higher propagation pressure.

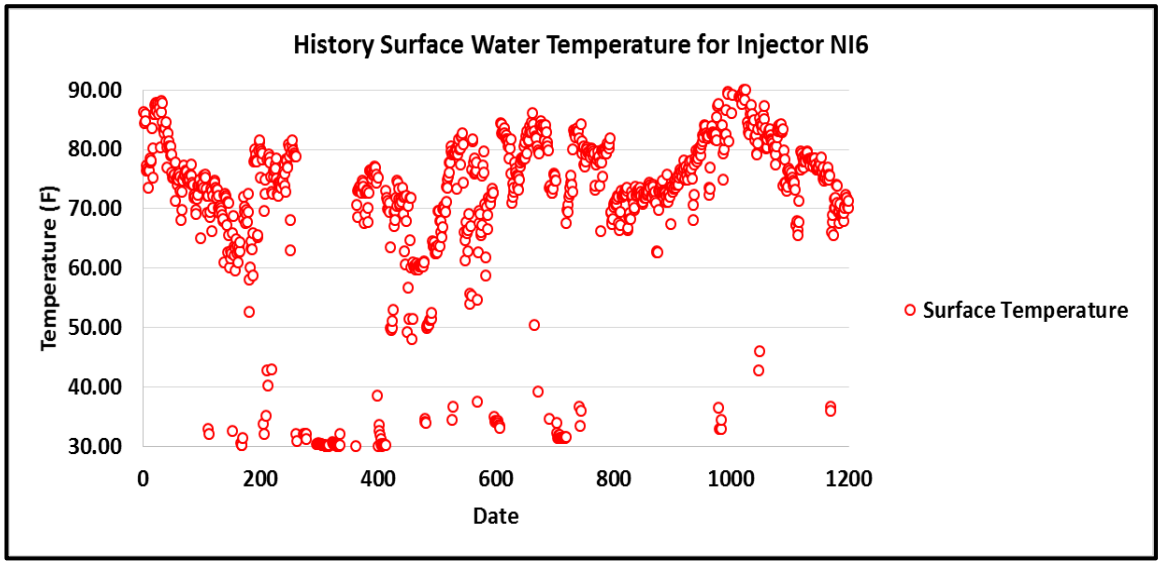

Figure 5-26: Surface water temperature for injector NI6

5.11 History Matching with TIF Modelling Workflow

The objective here is to match the history of a key well i.e.NI6 that showed a clear indication of TIF. The history matching with TIF modelling is a time consuming process for two primary reasons. First, the history matching is performed manually due to the dynamic nature of TIF and persistent transmissibility changes with time. Second, history matching involves geomechanical aspects i.e. in-situ stresses and rock mechanical properties in addition to reservoir properties and wellbore modelling. This complex history matching problem was divided into a two-step process:

1. **Figure 5-27**: This workflow is used to achieve a good match of the no-TIF simulation to the history data. Injection rate of well NI6 is not matched at this stage. This workflow is discussed further in section **5.11.1 and 5.11.2.**

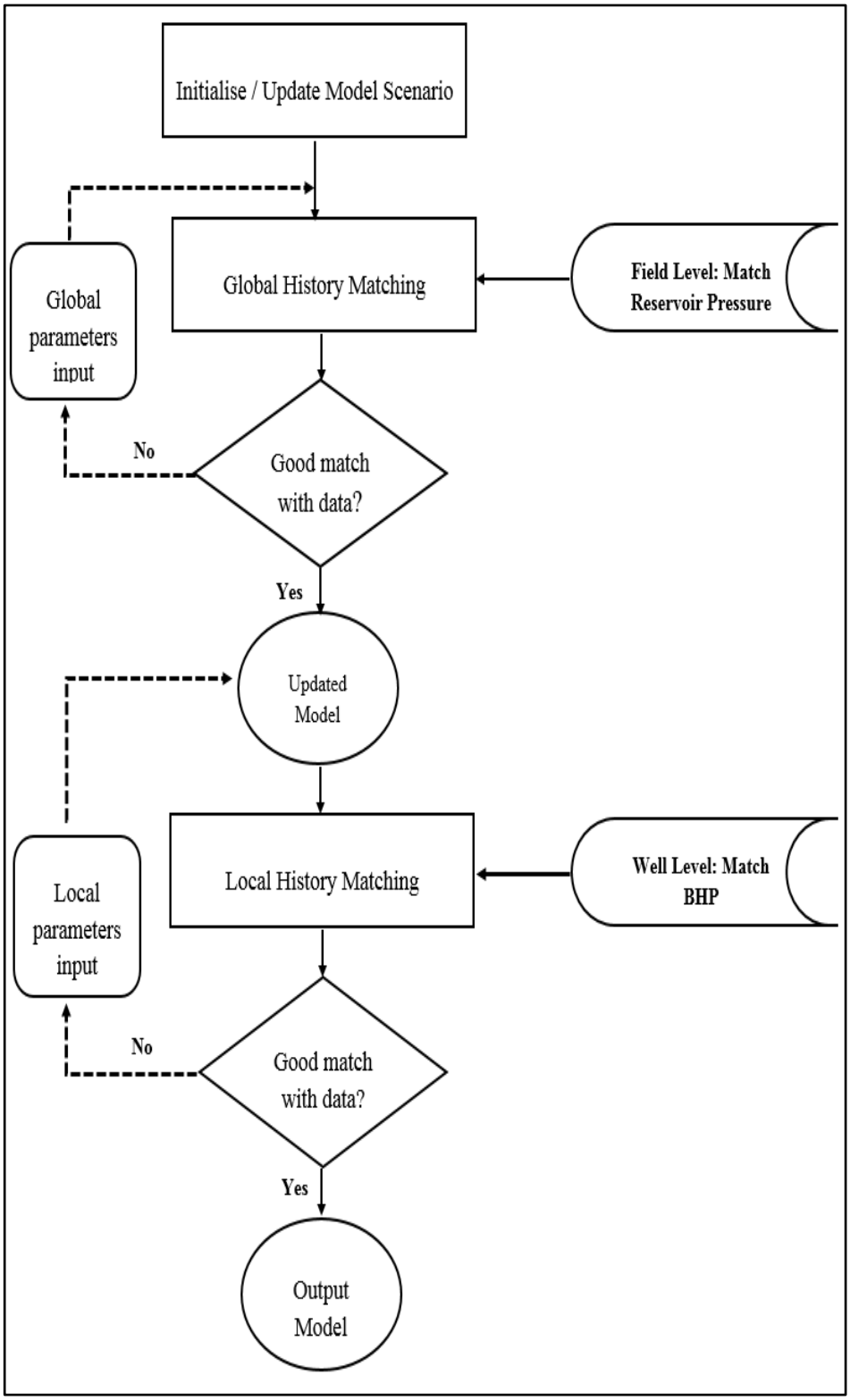

Figure 5-27: History matching workflow without TIF modelling

2. **Figure 5-28**: This workflow is used to obtain a good history match after TIF has occurred. The in-situ stresses and rock mechanical properties are matched here. A good match to the injection rate of NI6 is the ultimate goal at this stage. This workflow is discussed further in section **5.12.**

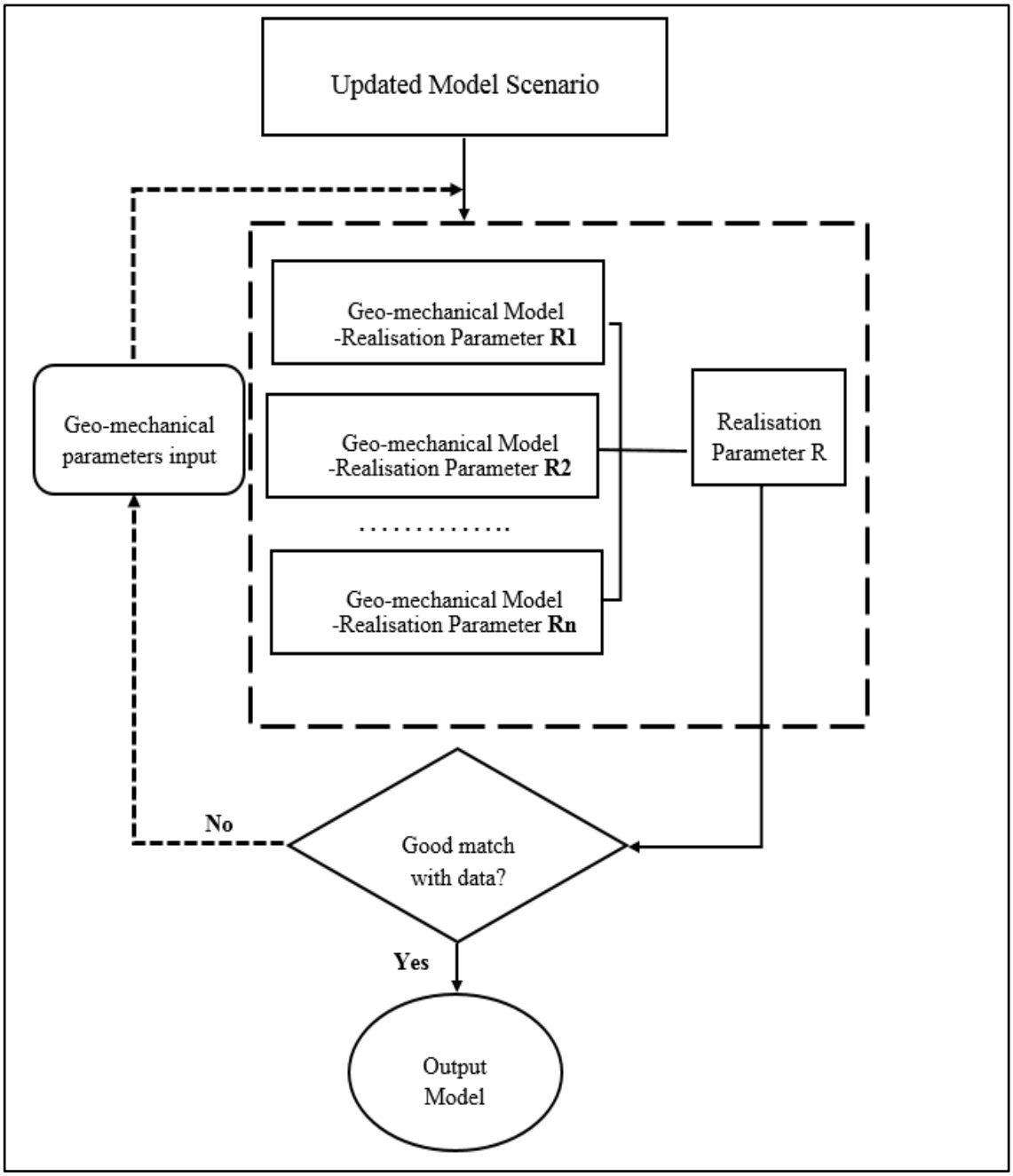

Figure 5-28: History matching workflow with TIF modelling

5.11.1 Global History matching

There are multiple parameters to be matched. A top down approach from the field level to the well level was adopted to minimise the effort obtaining the final history match.

5.11.1.1 *Well NI5 status*

Well NI5 was modelled as two wells separated by a sealing fault (see Figure 5-11) i.e. NI5_H and NI5_T. The history data was initially provided only for one of these "pseudo" wells i.e. NI5_H. The existence of these two "pseudo" wells has an important impact on the voidage replacement and reservoir support effects, and hence TIF growth,

for the nearby well NI6. Hence, the history data for the other well i.e. NI5_T was required and later provided by the operator.

Constant liquid rate control was modelled for both wells since they were not the "item of interest" in this thesis. This modelling approval is valid as the NI5 injects into two, separated reservoir zones that support different producers.

5.11.1.2 *Regional Reservoir Pressure*

Table 5-3 provides 3 data points for matching well NI6's regional reservoir pressure. Reservoir pore volume and compressibility were modified at this stage to match the simulated reservoir pressure to the Table 5-3 pressure fall-off data (Figure 5-29).

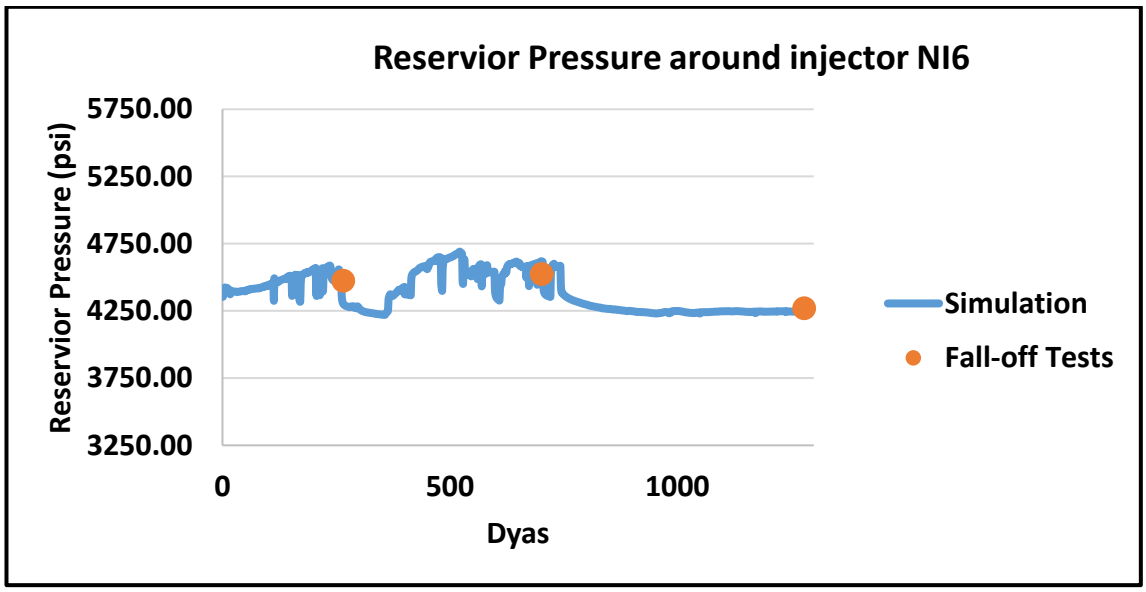

Figure 5-29: Matching simulated reservoir pressure to fall-off tests around well NI6

5.11.2 Local History matching

5.11.2.1 *Well NI6 Bottomhole Pressure*

A detailed wellbore model was built in PROSPER™ based on the well's completion schematic (Figure 5-30), survey, BHP measurements during an injection test, etc. These data were used to construct a wellbore model in PROSPER which was calibrated with the measured data. The following workflow was applied:

I. Critical review of the raw well test data (Figure 5-31). This review addressed how reliable are the measurements and how the test data compared to historical trends.

II. Three test points from injection test (Figure 5-31) were selected for further analysis

III. All VLP correlations in PROPSER were compared and Petroleum Experts 2 correlation was selected since it reproduced each well test with reasonable accuracy (Table 5-4).

IV. Finally, the simulated BHP successfully reproduced the history BHP (Figure 5-32).

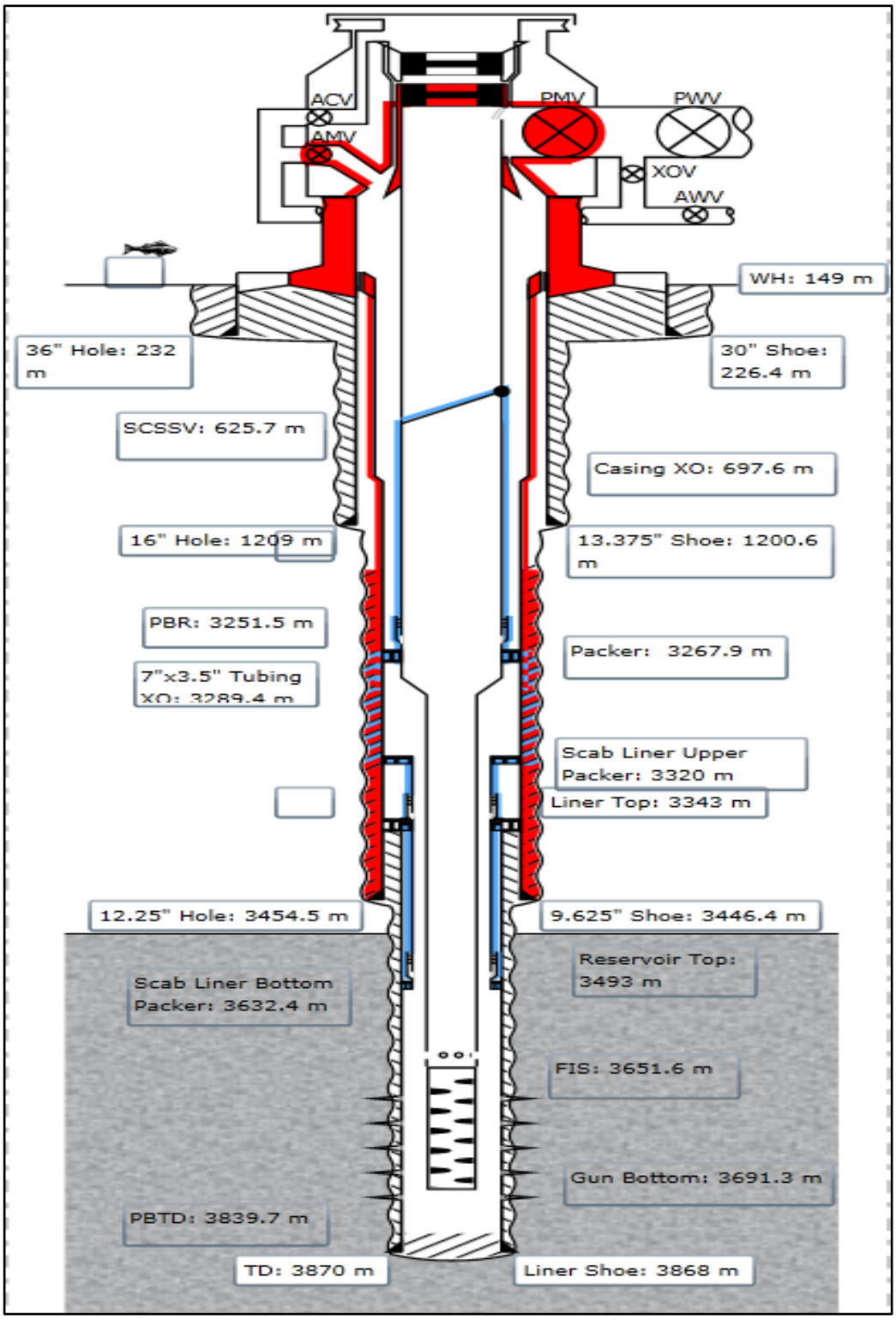

Figure 5-30: Well NI6 Completion Schematic

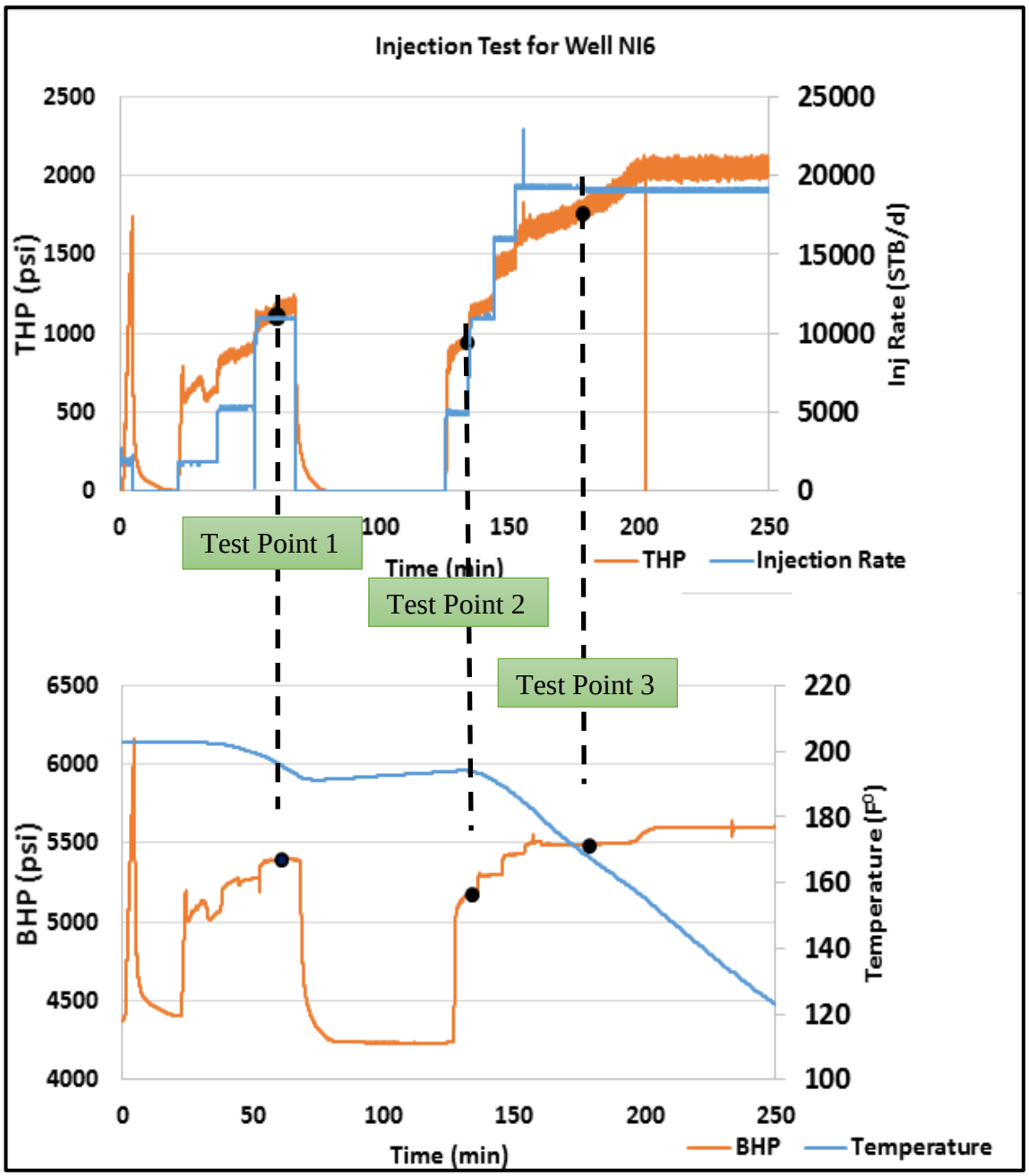

Figure 5-31: Injection test for well NI6

Table 5-4: Difference between measured test data and calculated values using PROSPER

	LIQUID RATE (STB/D)			
	Time (min)	*Measured Values*	*Calculated Values*	*% Difference*
POINT 1	*60.3*	*10860*	*10409*	*-4.33*
POINT 2	*133.6*	*5013*	*5045*	*0.63*
POINT 3	*178.2*	*19215*	*17968*	*-6.94*

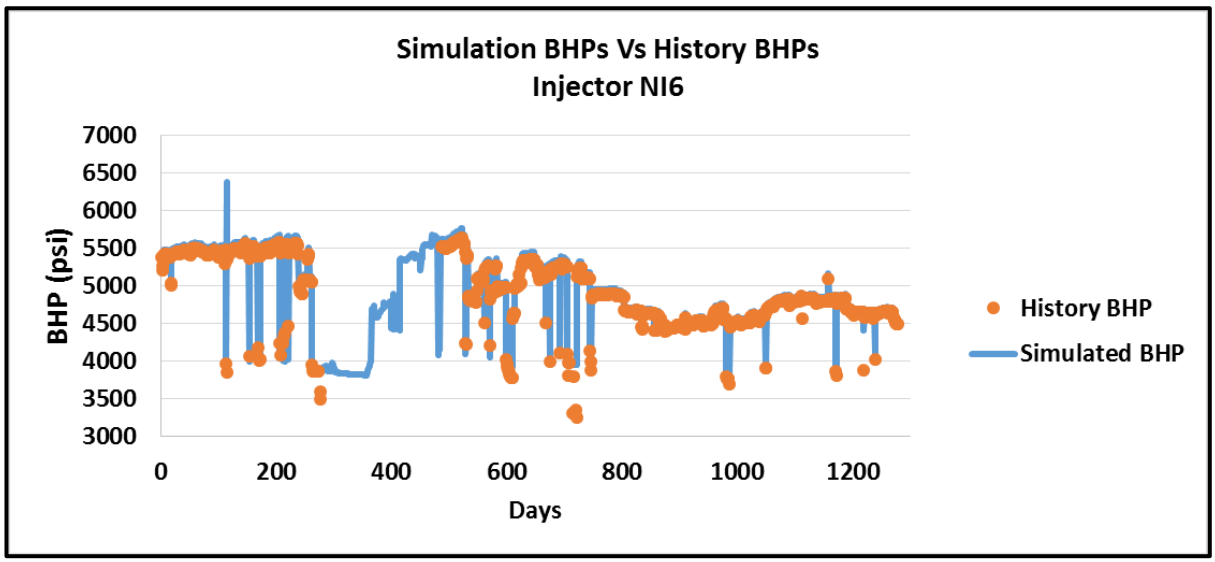

Figure 5-32: Simulated and History matched BHP for well NI6

5.12 Final Matching with TIF modelling

Reservoir pressure and BHPs related to well NI6 have now been matched. The focus is now directed to the thermal and geomechanical properties. The injection rate of well NI6 can now be matched with the well history by following the workflow in Figure 5-28.

5.12.1 Injected water temperature

Before going into details of modifying geomechanical and thermal properties, it is important to discuss other uncertainties e.g. water temperature and type. The operator confirmed that only sea water (SW) had been the source of the injected water. Produced water reinjection (PW) had not been injecting. The field is located nearby deep water and distant from the coast. The field data does show as a clear correlation between the injection temperature, the injection rate and TIF after 690 days (Figure 5-33). The injection of colder water has been found to improve the well's injectivity index in several, published field histories [5, 29, 7]. Further theory supports that cooling the formation will affect the TIF dynamics by encouraging TIF growth and greater TIF conductivity. However, average water injection temperature of 70^{o} F had to be assumed due to technical limitations with the geomechanical simulator. The TIF was assumed to have an infinite conductivity based on the above assumption that water quality is not an issue for the "N" field.

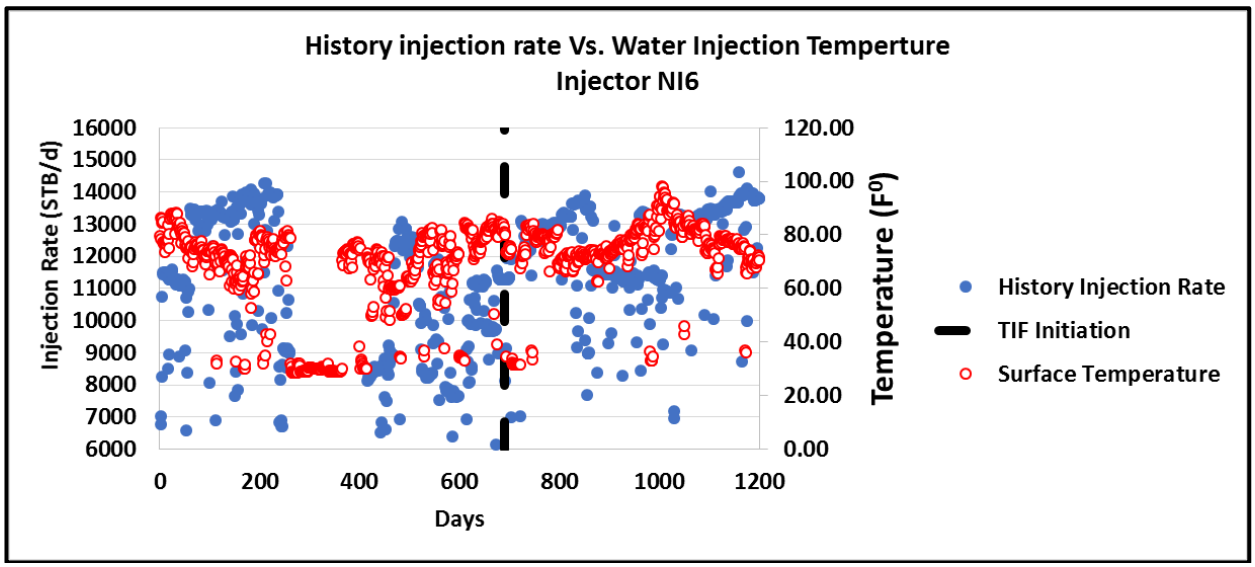

Figure 5-33: Surface water injection temperature and injection rate are correlated after 690 days

5.12.2 Geomechanical and thermal properties

History matching of the injection rate without TIF after correcting the reservoir pressure for well NI6 is shown in Figure 5-34. It can be noted that the simulation deviates from the history data after 690 days. In situ stresses, rock mechanical properties, and thermal properties were then modified from values determined in section 5-8 and 5-9 in order to match rate injection history using the workflow in Figure 5-28. The final history matching with TIF modelling is shown in Figure 5-35.

Matched geomechanical and thermal properties are shown in Table 5-5.The most uncertain parameters based on Table 5-5 are the Young's Modulus, Poisson's Ratio, Fracture toughness, and the Minimum Horizontal Stress. The matched Poisson's ratio was higher than the original, estimated values (section 5.9) whereas the final Young's Modulus was lower than the calculated value. These two elastic coefficients are used to calculate the stress reduction (or Thermoelastic stress) due to cold water injection. Therefore, these values calculate reduction in Minimum Horizontal Stress and, hence influence the initiation and propagation of the TIF. The initial Minimum Horizontal Stress value was reduced during the history matching process (i.e. it had been overestimated in section 5.8.2). It had been necessary to reduce this stress in order to obtain a good, final history match. Fracture Toughness was also reduced as well to a lower values since the initial estimate did not allow fracture initiation or/and propagation. The model can be finally used with confidence to test alternative development scenarios for the injection well completions which is the second objective of this research.

There are many sources of uncertainty in this study. Specific laboratory tests on core data were not available, hence generalised correlations were employed. These values are also assumed to be isotopic and homogenous which is far from reality in complex reservoirs. The geomechanical simulator was limited to a constant average value of the injected water temperature for the whole injection period.

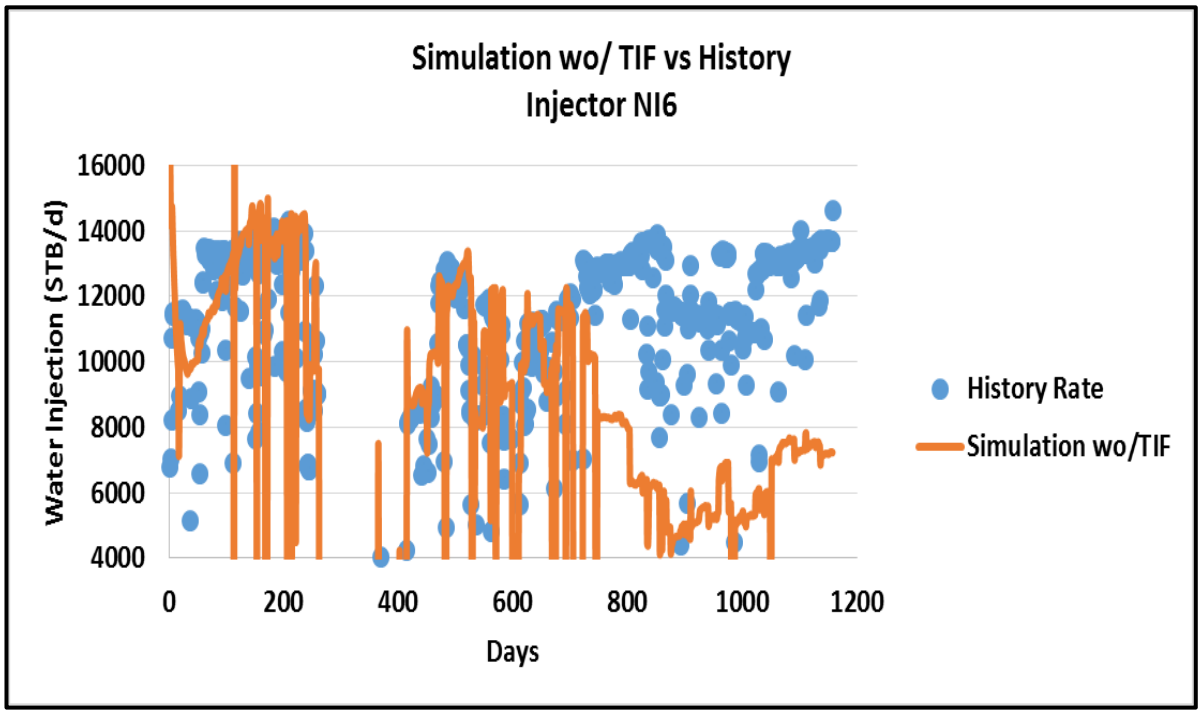

Figure 5-34: Simulated injection and history data without TIF after matching reservoir pressure and BHP to reliable data

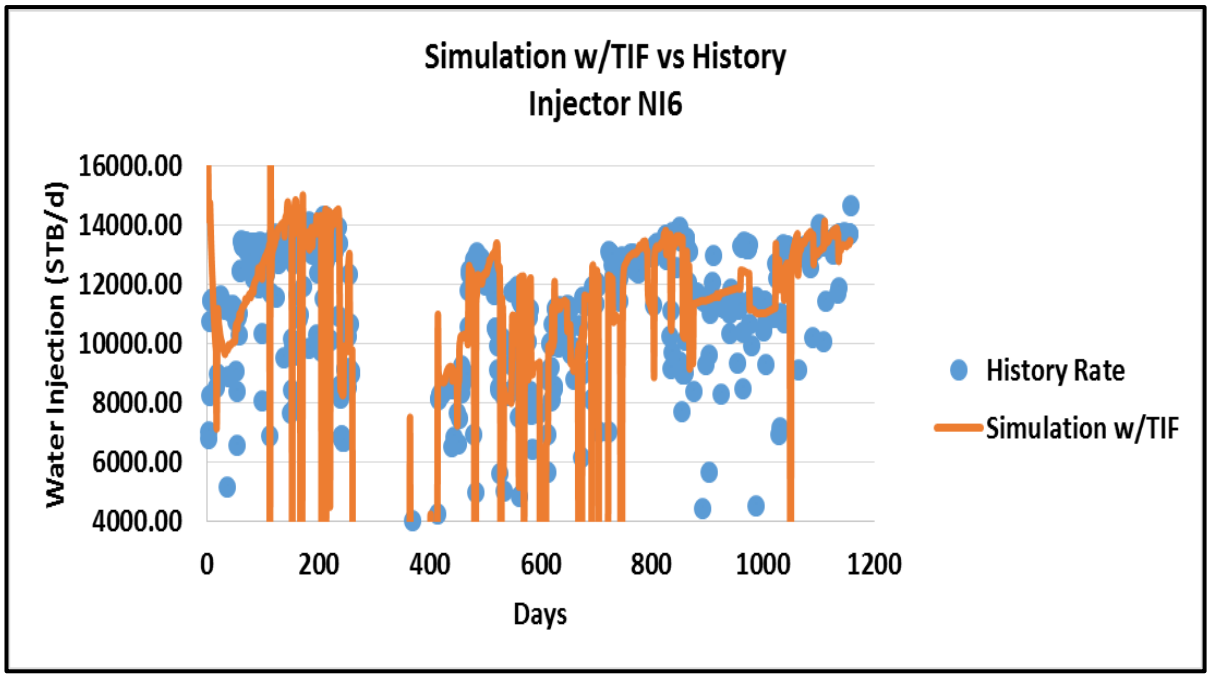

Figure 5-35: Final matched injection rate with TIF modelling after modifying geomechanical and thermal properties

Table 5-5: Initial and final matched Geomechanical and thermal properties

		Initial	***Matched***
Rock Mechanical Properties	Young's Modulus (MMpsi)	6.8	2
	Poisson's ratio	0.23	0.35
	Fracture toughness (psi/ft1/2)	330.48	150
	Biot's coefficient	0.53	0.67
In Situ Stresses	σ_v (psi/ft)	0.97	0.97
	σ_{Hmax} (psi/ft)	0.86	0.86
	σ_{hmin} (psi/ft)	0.73	0.65
Thermal Property	Rock thermal expansion coefficient ($1/F^0$)	3.20E-04	1.20E-05

5.12.3 TIF Growth Dynamics

TIF initiated and propagated based on the modelling analysis of the first 690 days and onward. This time corresponds to the observed sudden sharp decrease in well NI6 BHP history as shown in Figure 5-32 and confirmed by the monitoring workflow results in Chapter 4. It was also noted from the simulation (Figure 5-36) that TIF geometry propagated in both sides of NI6 and it is parallel to producer NP4 as expected form TIF direction analysis. Calculated TIF half-length increased sharply within few days as shown at point 1 in Figure 5-37 and then stabilised for some time. The TIF then propagated and increased after more cooling took place near TIF tip at point 2 in Figure 5-37. TIF half-length then slightly decreased at point 3 in Figure 5-37. This decrease is not supported by observed physical change and could be due to numerical error.

Even though TIF half-length cannot be correlated to injected water temperature since it was assumed as one value i.e. 70^o F, cooling effect can be clearly identified from Figure 5-37. TIF tip stopped propagating when the pressure inside the TIF was not large enough to propagate the TIF (point 1). After rocks were cooled further with time, TIF propagated until it reached hotter rocks (point 2). Even though TIF half-length is not certain and cannot be confirmed with data, it behaved physically as expected.

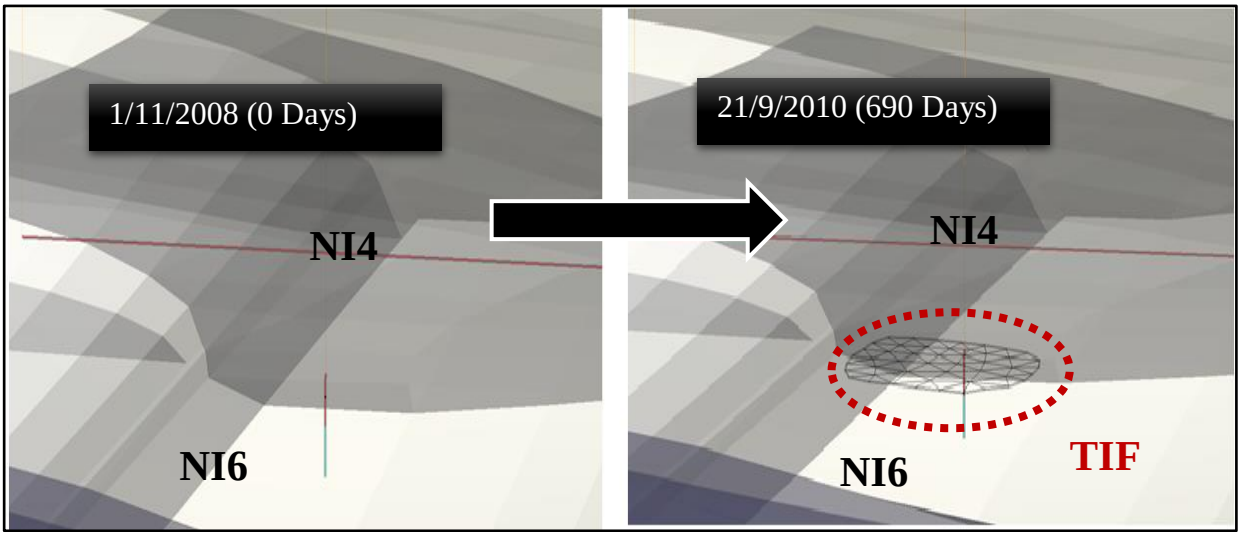

Figure 5-36: Geometry of TIF around Well NI6 after 690 days

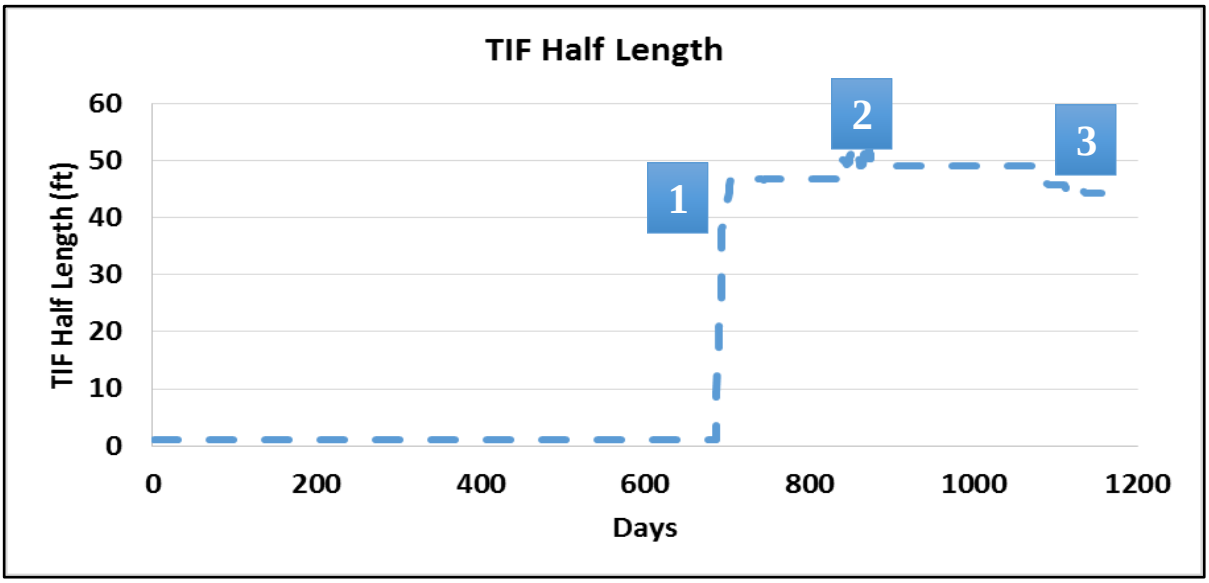

Figure 5-37: Evolving TIF half-length the whole injection period.

5.13 Summary

The Eclipse N field model was imported to REVEAL reservoir simulator. A test case confirmed that the two reservoir simulators gave similar results. The injector NI6 performance was modelled without TIF and history matched to the injection data. The magnitudes and orientations of the in-situ stresses were determined along with the rock mechanical properties based on provided data, well logs and published correlations. These geo-mechanical properties, together with upgrading to a thermal PVT model, allowed modelling and history matching of injector NI6's performance with TIF. It was concluded that:

I. The REVEAL and Eclipse reservoir models gave comparable results

II. The direction of maximum horizontal stress, and TIF propagation is most likely E-W with a normal faulting regime.

III. Inclusion of well NI5 in the model is important due to its impact on the dynamics of voidage replacement, pressure support, and hence TIF growth, of well NI6.

IV. The surface water temperature and both the volume of injected water and TIF propagation, are well correlated, especially after the onset of TIF at 690 days starting from 1/11/2008 (0 days).

V. The history matching with TIF modelling proved to be time consuming due to the dynamic nature of TIF and the presence of geomechanical uncertainties.

VI. Two workflows were developed for history matching of well NI6 data. The Reservoir and well parameters were first matched to the field data prior to TIF initiation at 690 days. The geomechanical properties were adjusted by history matching the subsequent field data to the TIF model.

VII. The model results without TIF was matched to the NI6 injection rate data before day 690. Inclusion of TIF, and suitable modification of the initially estimated values of the geomechanical properties, was required to obtain a comparable match after this date.

The resulting, history matched, N field sector model may be used in future studies of alternative, injection well completion scenarios.

Chapter 6 Evaluation of Inflow Control Device Effectiveness to Mitigate Thermally Induced Fractures in Water Injection Wells

6.1 Introduction

Inflow control devices (ICDs) have been employed by industry to increase the recovery. ICDs are well known for their ability to mitigate production challenges e.g. HTE and reservoir heterogeneity (Figure 6-1). Installation of ICDs creates a greater, extra pressure drop across the more productive, high permeablity zones and smaller pressure drop across low permeable zones; achieving more equalised inflow distrbuition. On the other hand, traditional injection wells regularly have two main challenges associated with them. The first challenge is the sand production during well shut in periods that requires the installation of a sand control completion. The second challenge is the uneven distribution of the injected fluid into the various zones along the wellbore.

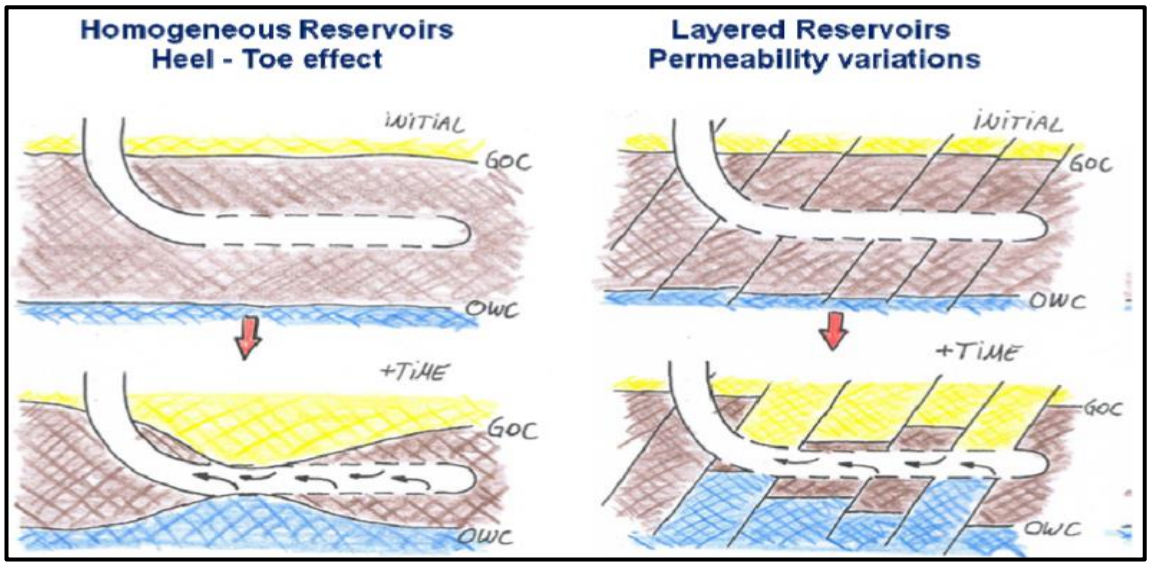

Figure 6-1: Examples of drainage challenges in horizontal wells [48]

Historically, sand control completions e.g. Stand-alone Screens (SAS) and open hole gravel packs have been used to alleviate the sanding problem. However, these completion do not provide equalisation of the injection profile. The simplest soultion for this problem is to install a SAS with an integrated ICD. The main managments goals of installing the special screens with integrated flow control devices for injection wells are to [84, 81] :

I. Optmise the pressure support and sweep effucency for different zones indepanedant of pearmbeality heterogeneities (Figure 6-2).

II. Delay early water breakthrough in high pearmblties zones connected to the production wells.

III. Avoid one, or more natural fractrures that would otherwise dominate the injection well's performance.

IV. Mitigate the occurance of wormhole channels that develop when heavy oil is produced simultaneously with sand until a communication path is established (Figure 6-3).

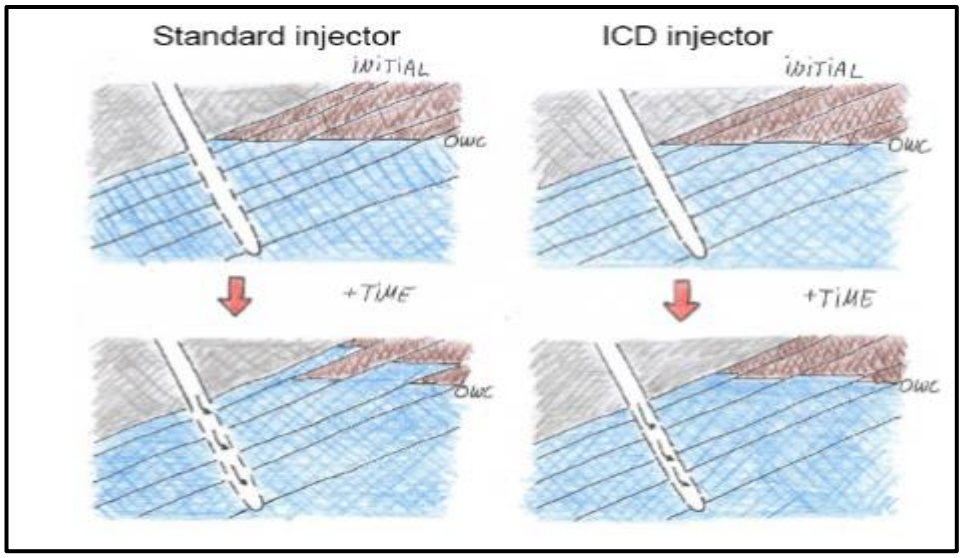

Figure 6-2: Conventional injector vs. ICD injector [81]

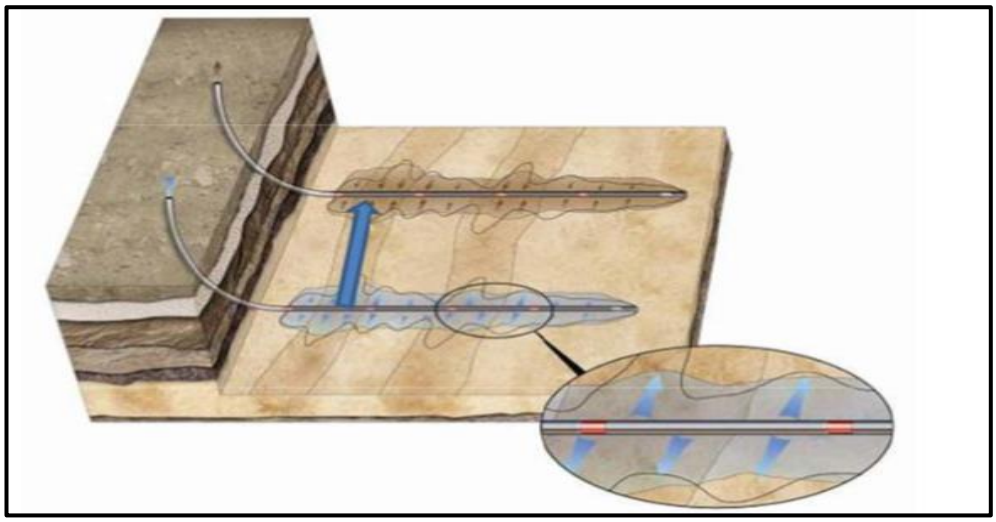

Figure 6-3: Wormhole channels formed between well pair due to sand mobilisation [84]

6.2 Problem Statement and Solution Approach

In this chapter, a different reservoir management challenge is investigated. TIF initiation and propagation due to injecting cold water can have a negative impact on the sweep efficiency and pressure support. If this phenomenon occurs, the majority of the

injected fluids will take the TIF path from the injector to the producer leaving the rest of the reservoir upswept. The application of ICD to mitigate the impact of TIF will be evaluated in this chapter.

Chapter 5 covered workflows developed to history matched the "N "field sector model that included an injection well NI6 with a TIF. The history matched sector model will now be used to investigate the performance of an ICD completion when TIFs are expected. The objectives of chapter 6 are to:

I. Understand the impact of available thermal and isothermal reservoir modelling options.
II. Appreciate the importance of taking TIF into consideration during field development planning by comparing SAS completion with and without TIF modelling.
III. Investigate the impact of installing different completions in the injection well (a.k.a. 'injector only' cases) or in both the injection and production wells.
IV. Study the impact of wells orientation with respect to that of the maximum horizontal stress on TIF initiation and propagation.

The previously used 3D reservoir simulator coupled with a 3D, finite element, TIF model and a geomechanical model will be used to evaluate the effectiveness of ICDs to mitigate TIF in Water Injection Wells

6.3 Methodology

Modelling TIF in reservoir simulation involves coupling reservoir flow to geomechanical properties/processes and fracture mechanics. Adding an Advanced Well Completion model (ICD in completion) adds complexity to the modelling process. A workflow has been developed not only to obtain a smooth and reasonable model of TIFs and of ICDs but also ensure that each step has been correctly implemented. The workflow was developed as follows:

I. The history matched sector model (from chapter 5) setup was modified by removing the existing wells and adding a new, horizontal, injector-producer pair.
II. Realistic well constraints and pair specifications were implemented in the history matched sector model.
III. Well completion types and designs were detailed. The Stand Alone Screen (SAS) completion was the base case with ICD strength, frequency, and annulus flow effect being added when appropriate.

IV. The performance of SAS and ICD completion without TIF modelling under isothermal and thermal conditions were compared. This is not only to ensure that temperature is modelled correctly but will also show the importance of taking temperature into consideration when modelling water injection wells.

V. The impact of different completions installed in the injection well with TIF modelling was investigated.

   a. A limited number of TIFs (10) were "seeded" along the horizontal injector. This limited number was found to be sufficient to perform the analysis without causing simulation convergence issues.

   b. The direction of the maximum horizontal stress and stress gradients were adjusted to produce two scenarios i.e. Transverse TIF (T-TIF) and Longitudinal TIF (L-TIF).

6.4 Model Setup

The history matched model was rectified based on the chapter 5 matched parameters. The existing wells were replaced by a new horizontal injector-producer pair (Figure 6-4).

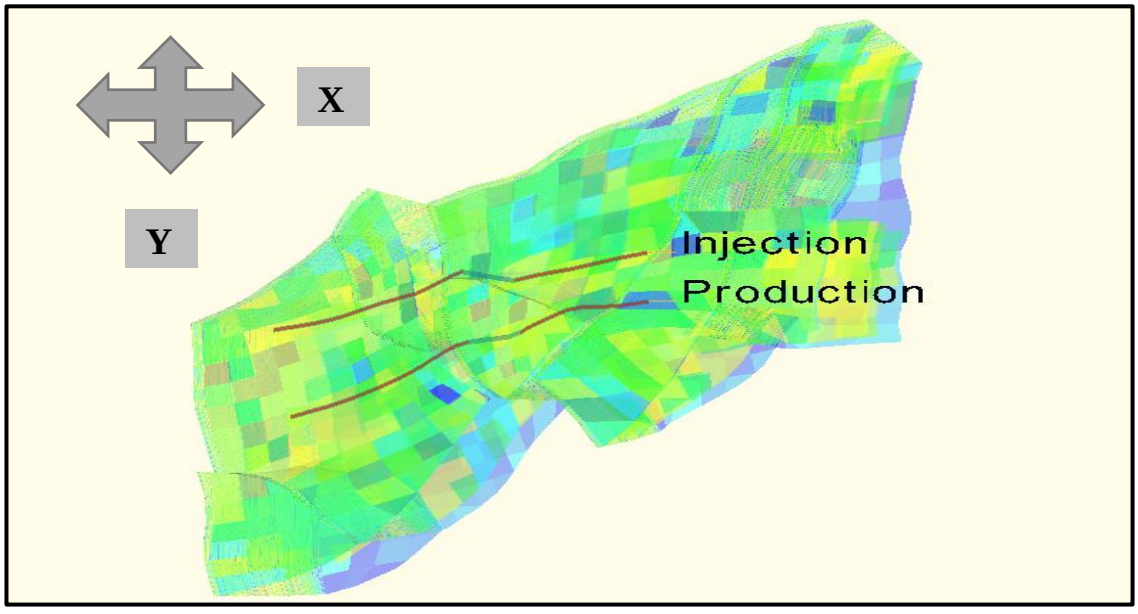

Figure 6-4: 4757 ft long injector and producer wells added to the history matched, "N" sector reservoir simulation model.

Two Scenarios were considered based on the orientation with respect to the preferred TIF direction. Different completion options were covered for each Scenario as follows:

I. The direction of Minimum Horizontal Stress was oriented along the axis of the wells; resulting in a Transverse TIF (T-TIF) which will propagate a plane

perpendicular to the injection wellbore axis (Figure 6-5). The performance of a Stand-Alone Screens (SAS) with Inflow Control Device (ICD) will be compared for:

a. SAS with and without TIF modelling (i.e. a comparison of thermal and isothermal simulation modelling).
b. ICD completion in injection well only.
c. ICD completion in both injection and production wells.

II. The direction of Maximum Horizontal Stress was initially oriented along the axis of the wells; resulting in an L-TIF which will propagate along the axis of the injection well (Figure 6-6). This represents the expected condition of the reservoir where the direction of Maximum Horizontal Stress is on x-axis as shown in Figure 6-4. The performance of Stand-Alone Screens (SAS) with Inflow Control Device (ICD) will be compared for the same combination of completion:

a. SAS with and without TIF modelling (i.e. a comparison of thermal and isothermal simulation modelling)
b. ICD completion in injection well only
c. ICD completion in both injection and production wells

The simulator requires that the number and location of potential TIFs initiation must be identified. 10 locations were chosen along the horizontal completion length, the maximum number that gave an adequate balance between avoiding excessive convergence problems while providing sufficient locations to differentiate between the performance of SAS and ICD completions. Generation of L-TIFs and T-TIFs are also expected to affect the sweep efficiency and the time of first water arrival at the production wells and hence the oil recovery. Chapter 3 showed that the TIF direction significantly affected the injection performance in the "N" field sector model and other synthetic models. Exchanging the direction of maximum and minimum stresses (Figure 6-5 and Figure 6-6) within the reservoir model allowed TIFs with different directions to be generated.

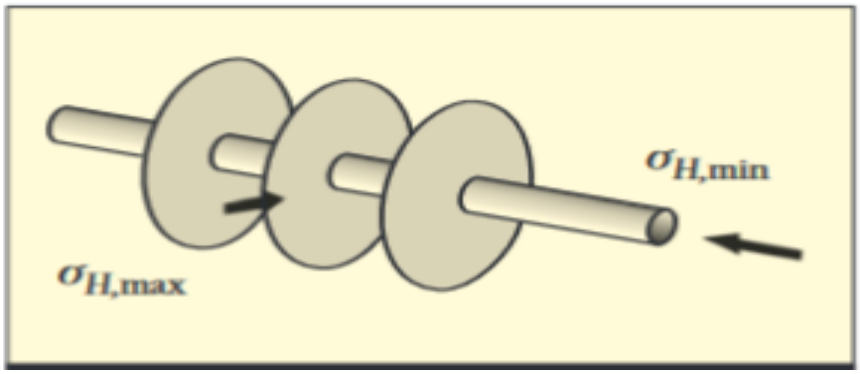

Figure 6-5: Transverse TIF configuration [133]

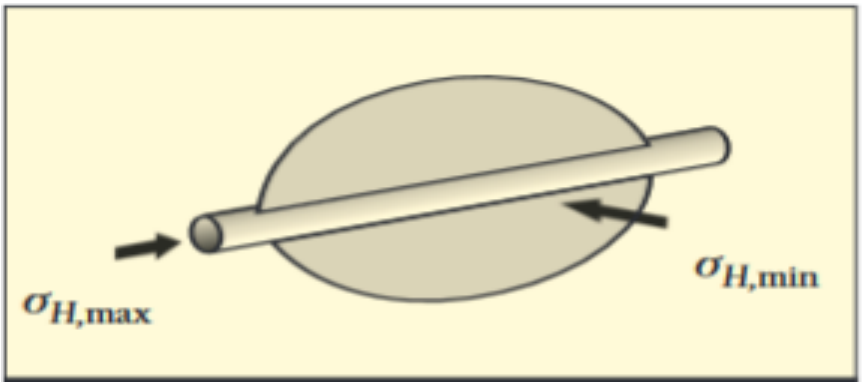

Figure 6-6: Longitudinal TIF configuration [133]

6.5 Well Constraints and Pair Specifications

Well production/injection constraints are applied during simulation of the operation of an oil field for operational reasons. For example, to: (1) honour the surface facilities limitations of maximum production or injection rate or pressure, (2) avoid the (hydraulic) fracturing of the formation for better sweep efficiency, (3) reduce sand production and ensure wellbore stability, (4) minimise pressure drops in the flowing system, and (5) respond to dynamic changes in the reservoir pressure. The following constraints, limitations and specifications were proposed by the operator and applied here:

I. Injection well THP between 1740 and 2900 psi.
II. Maximum water injection rate of 37,750 STB/d.
III. Production well BHP was between 1813 and 2900 psi.
IV. Injector and producer completion was 4757 ft long with a separation of 984 ft.

The well control for the injector was a THP of 1740 psi for all the cases. A constant THP is required by the simulator due to the iterative nature of TIF calculations. A maximum injection rate of 37,750 STB/d was applied to the injector, while the production well was controlled at a fixed rate of 15,725 STB/d. The fixed rate control was selected in order to improve the comparison and analysis of the various cases, while honouring the minimum

BHP of 1813 psi. The simulation time for all cases is 20 years. Note that the above well constraints resulted in both under or over injection i.e. the voidage replacement ratio was not controlled at 1.0.

6.6 Well Completion Types and Design

The main objective is to compare different completion scenarios and investigate their performance in water injection wells with existing TIF. The base case is the conventional, SAS (i.e. conventional, no flow control) completion. The SAS completion for both injector and producer has 29 compartments and a blank pipe across the fault. A sufficient number of packers were placed to ensure negligible annular flow (Figure 6-7). This ensures that an "apple-to-apple" comparison can be made when comparing the ICD completions. Removing annular flow effects also overcame some modelling issues, as will be discussed later.

A constant strength ICD completion design was employed; optimisation of the variable-strength is out of the scope of this thesis since optimisation problem requires more time and open resources. The ICD completion design (Figure 6-8) has 1 ICD per (41 ft long) joint with a nozzle diameter of 1.6 or 2.5 mm and 4 joints per compartment as discussed with the operator. Figure 6-8 is a conceptual representation of the completion design.

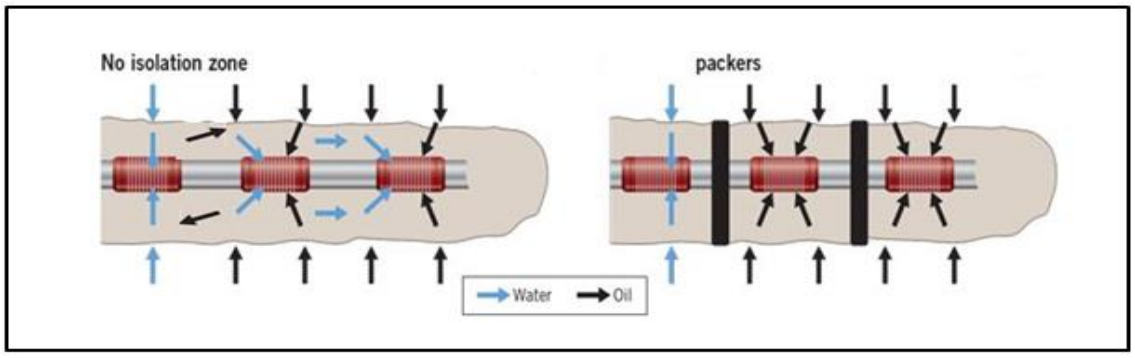

Figure 6-7: Prevention of cross flow in the annulus by packers

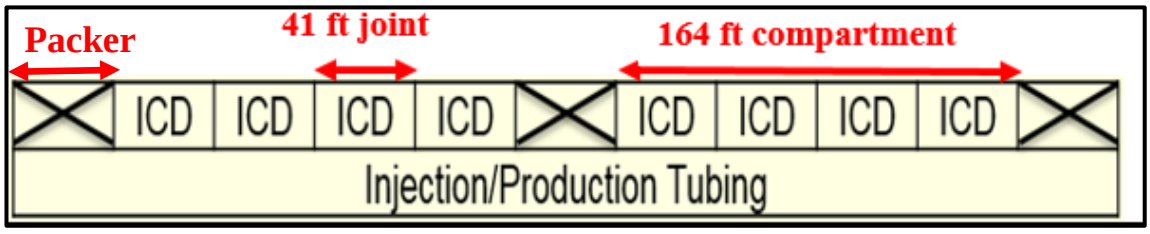

Figure 6-8: Conceptual ICD completion design with ICD/joint and 4 joints / compartment defined by the packers

6.7 ICD, wellbore, and annulus flow modelling options and related problems

A significant number of problems were faced when modelling ICD and annulus flow in conjunction with TIF modelling. These problems were not unexpected given the complexity of coupling geomechanics, wellbore, AWC and reservoir flow model. There were mainly two issues faced in this study:

6.7.1 Well Segmentation and reservoir gridding

Placing packers in the wellbore along with TIF modelling complicates the calculations. Convergence problems resulted when packers are placed between compartments. This is because the reservoir model's grid cells and those of the wellbore model are being asymmetrical and are not congruent i.e. the wellbore model's cell of the volume between two packers maybe superimposed on two reservoir grid cells (Figure 6-9). This caused the ICD completion to control two different cells with different properties. This is not possible in Eclipse, but can be dealt with in REVEAL. However, further complication of annulus flow and the cross flow together with TIF and geomechanical modelling caused convergence problems in the REVEAL simulator. Simultaneous cross flow and TIF models are not compatible. Different solutions to this problem are available, including placing packer between the cells as well as removing the effect of annulus flow. This difficulty was mitigated by modelling the water injection directly from the completion into the reservoir. This is equivalent of placing a packer between a 41 ft joint of the completion. The effect of annular flow and packers on TIF imitation and propagation could thus be the subject of further research.

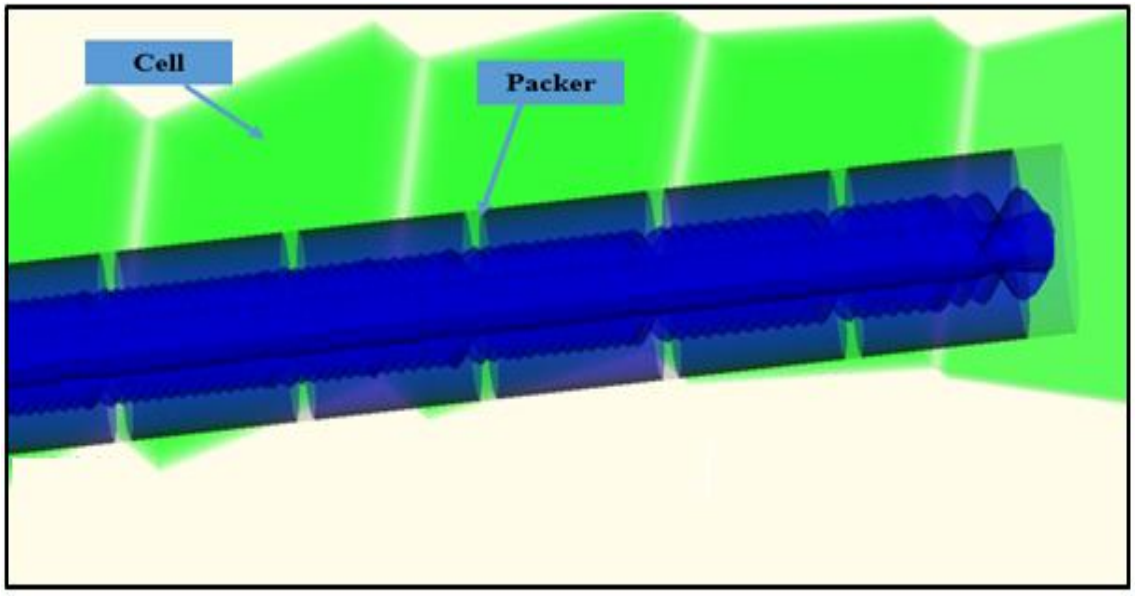

Figure 6-9: Reservoir grids and packer placement

6.7.2 Horizontal well trajectory

The sector reservoir model employed is a corner point grid with faults and tilted layers (Figure 6-4). The two horizontal wells initially were modelled as being perfectly horizontal i.e. 90^0 inclination to vertical (Figure 6-10). The Horizontal well partially crossed too many cells, due to the cell geometry and layer inclinations; resulting in unconverged solutions and interrupted simulations. The solution was to alter the well inclination degree to follow that of the formation layers (Figure 6-11).

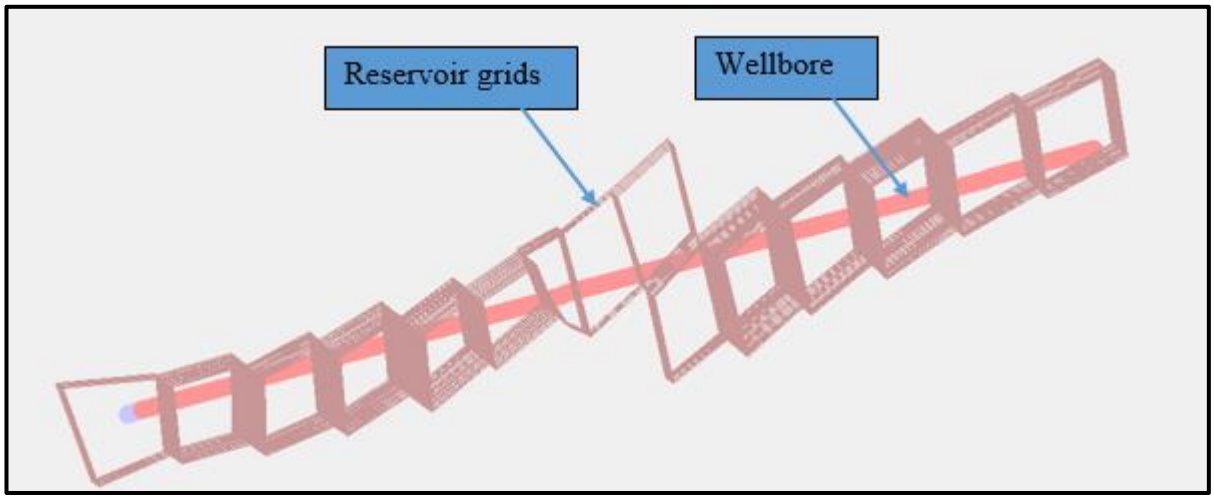

Figure 6-10: Visualisation of reservoir grids and well horizontal section as initially modelled

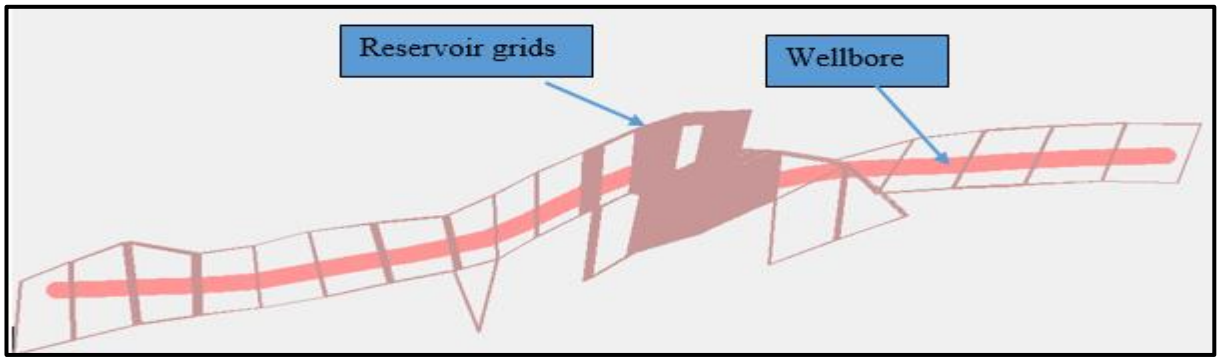

Figure 6-11: Visualisation of reservoir grids and well horizontal section as finally modelled

6.8 Isothermal and Thermal Models Comparison

It is important to understand the impact of thermal and isothermal reservoir modelling options with a simple completion (SAS) before going into details of modelling TIF and ICD. A constant liquid rate was employed for both the producer and the injector since TIF is not modelled here. The thermal modelling allows the temperature of the reservoir grids to be simulating the cooling. Figure 6-12A shows the temperature variation for a SAS completion in the thermal case due to injecting cold water. The temperature is cooler around the injector and gets hotter toward the producer. By contrast, the

temperature for the isothermal case is constant at all times and distances (Figure 6-12B). Variation in temperature in the thermal case caused the viscosity to increase to 5.5 cp because of the cooling of the reservoir, especially around the injector (Figure 6-13A). By contrast, oil viscosity in the isothermal case was < 0.5 cp at all locations (Figure 6-13B).

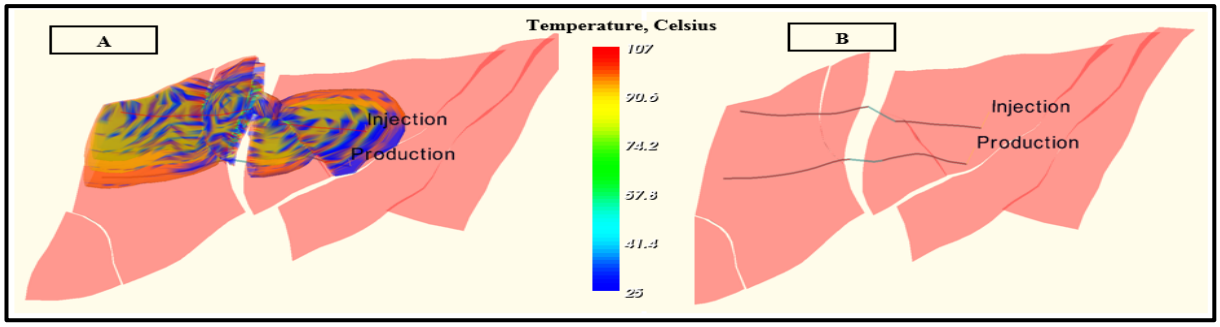

Figure 6-12: shows temperature variation after 3000 days of SAS completion; A) thermal case, B) isothermal case

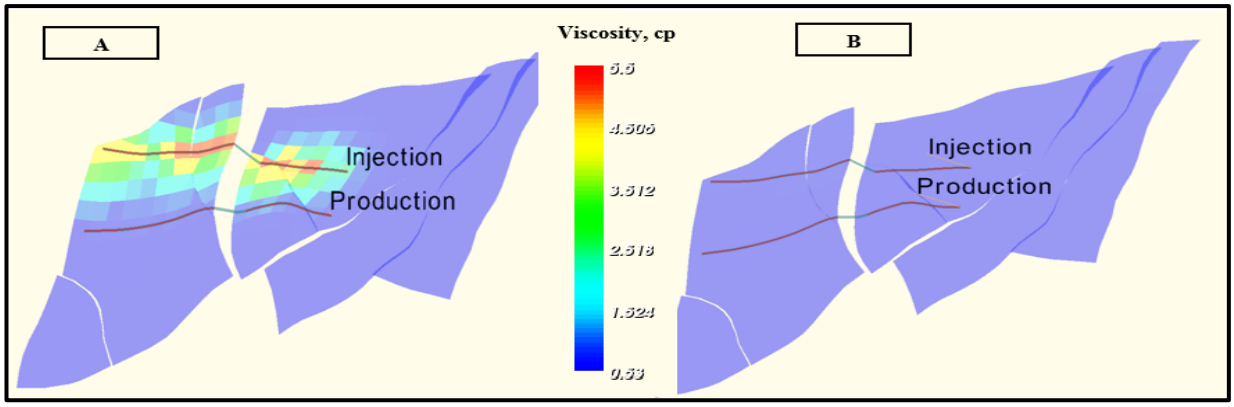

Figure 6-13: Viscosity variation for SAS completion after 3000 days; A) thermal case, B) isothermal case

This significant viscosity change, one order of magnitude from 0.5 to 5.5 cp, has a significant impact on both injection and production wells performance. The liquid injectivity index after 3000 days for the thermal case is 60% smaller in the thermal case due to this viscosity increase (Figure 6-14). Alternatively, a higher BHP to inject the same volume of water in the thermal case is required (Figure 6-15). **Isothermal modelling of water injection underestimates the actual BHP**. This effect will increase when simulating completions with added restrictions (ICDs).

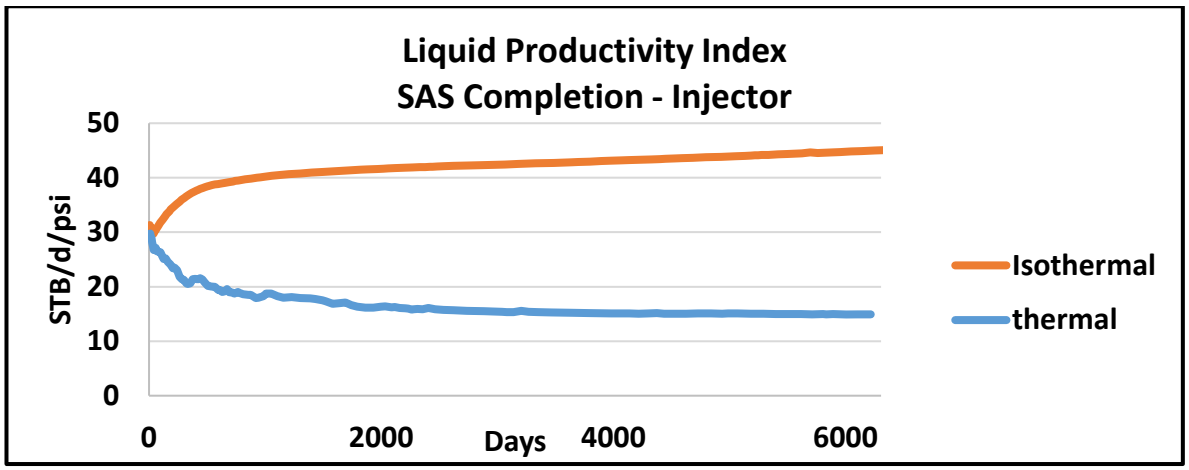

Figure 6-14: Injectivity index for both isothermal and thermal modelling of injector SAS completed well

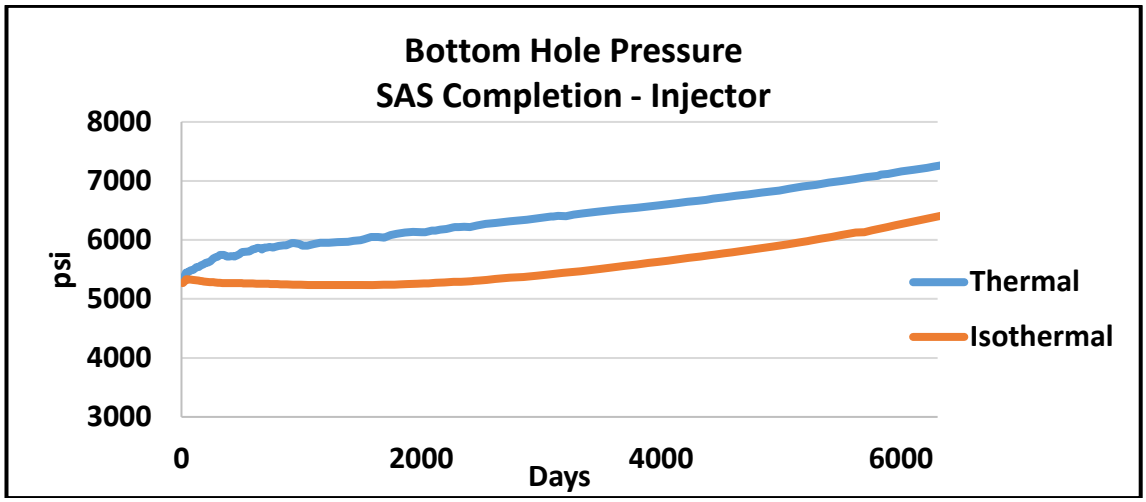

Figure 6-15: BHP required for both isothermal and thermal constant injection rate into SAS completed well

It is also important to note that the performance of injection and production wells differ once temperature changes are considered. Interestingly, at fixed rates, the increase in viscosity in the thermal case caused a more uniform sweep and hence higher oil recovery. The reserves for the field and/or well can be incorrectly estimated by isothermal modelling. Figure 6-16 shows 8% increase in the cumulative oil production after 6000 days for the thermal case. An ICD completion also increased the recovery once temperature is taken into account, but the advantage over SAS completion is smaller (Figure 6-17).

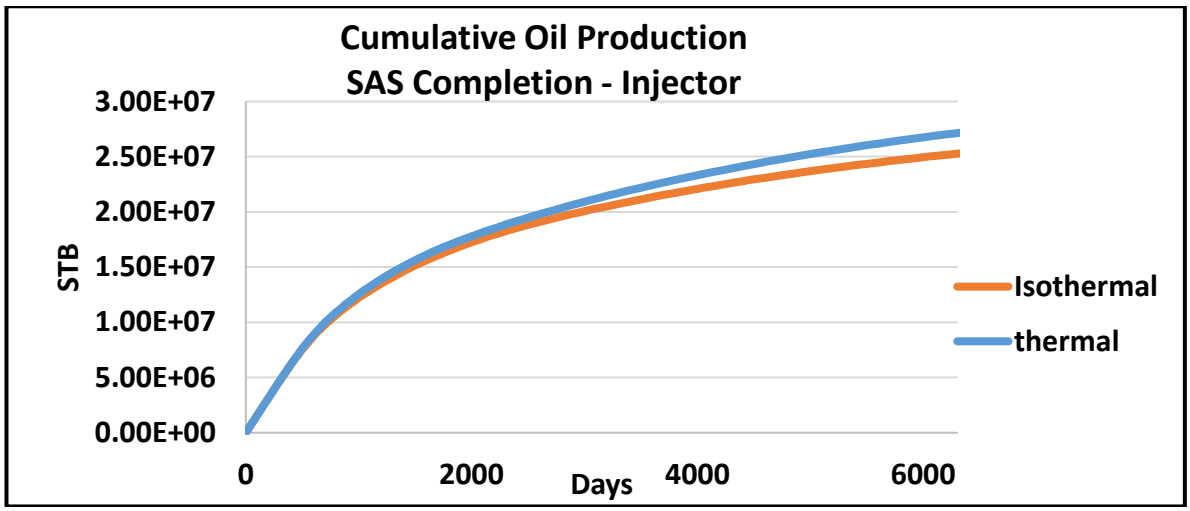

Figure 6-16: Cumulative oil production for both isothermal and thermal modelling of SAS completed wells

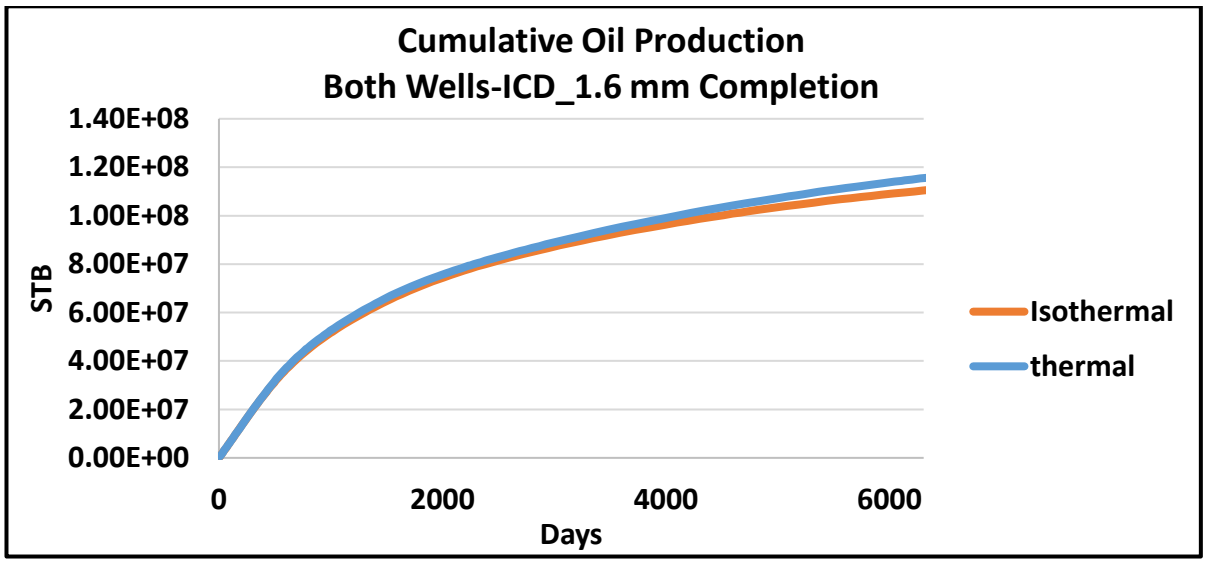

Figure 6-17: Cumulative oil production of both isothermal and thermal case for ICD completed wells

6.9 Impact of different completions installed in the injection well modelled with TIF

This section investigates the impact of TIF for SAS and ICD completions installed in the injector only (the producer is always completed with SAS). Two scenarios i.e. Transverse and Longitudinal TIFs, will be studied.

6.9.1 Transverse TIFs (T-TIF)

6.9.1.1 *SAS completion in injector with/without T-TIF*

The performance of a SAS completed injector with and without T-TIF modelling is compared in this section. Figure 6-18 shows the location and extent of the T-TIF in the SAS completed injector with reservoir region numbers i.e.R1, 2, 3, and 4. It can be noted

that TIFs propagated toward the producer with the T-TIFs in regions 1 and 2 (R1 and R2) being the longest. Modelling these T-TIFs has a large impact on the oil recovery and the injected and produced water. Figure 6-19 shows a 14% decrease in oil recovery when T-TIF is modelled. Figure 6-18 implies that regions 1 and 2 with long T-TIFs will experience a greater volume of injected water than the other regions. Oil recovery per each region (Figure 6-20) shows the impact of T-TIF on sweep efficiency. The reduction in oil recovery for SAS with T-TIF comes mainly from R3 and R4. These regions are being swept less efficiently since more water is injected into R1 and R2 by their dominant T-TIFs. The extra water injection into R1 and R2 has decreased the efficiency of the water flood.

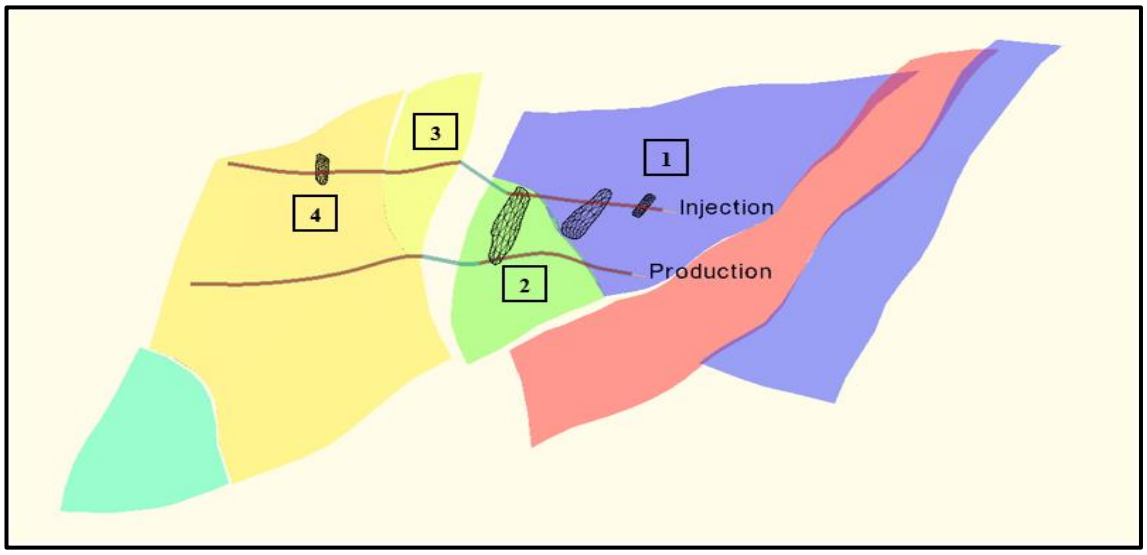

Figure 6-18: Extent of T-TIF propagation at last time step for SAS completed injector where coloring and numbers represent reservoir regions

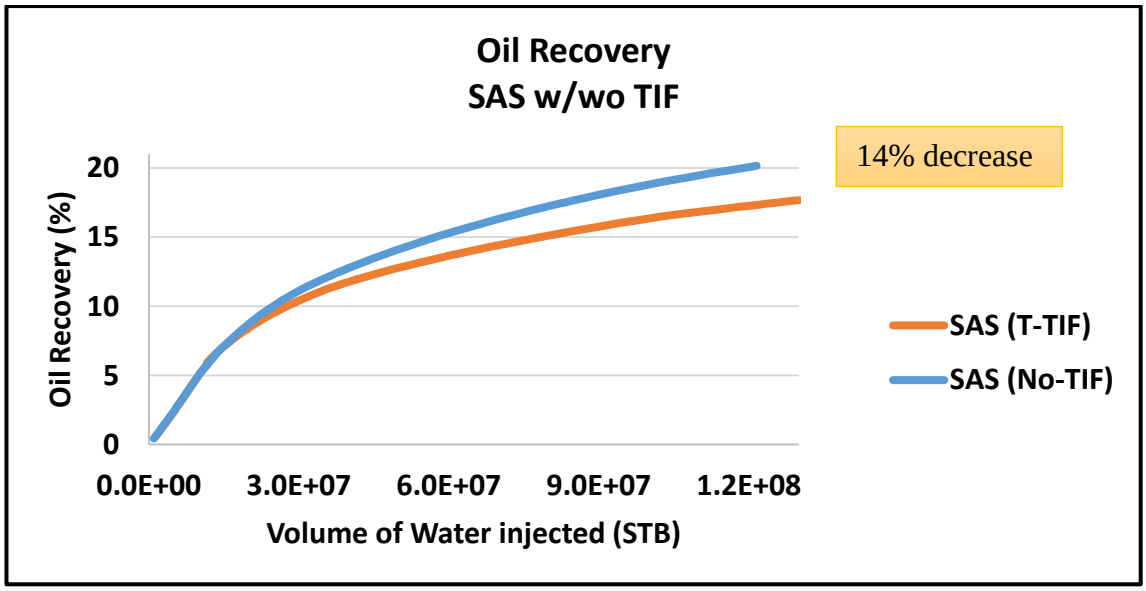

Figure 6-19: Oil Recovery for SAS with and without T-TIF

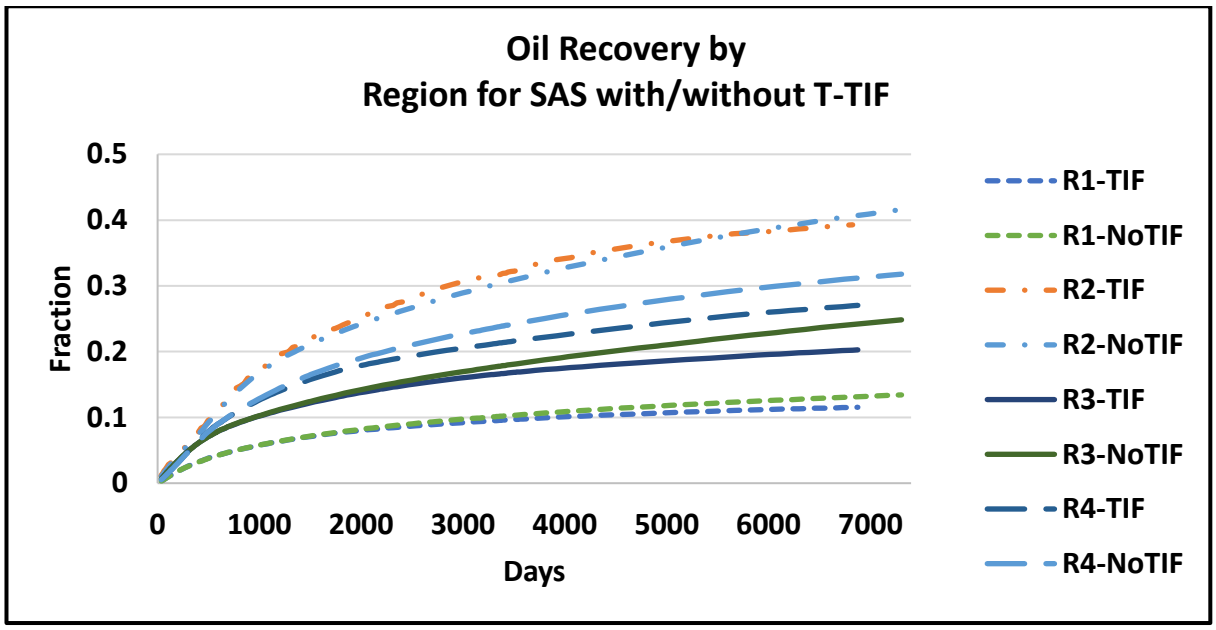

Figure 6-20: Oil recovery for different regions for SAS with and without T-TIF modelling

Another important note is that, not surprisingly, more water (up to 18870 STB/day) was injected with SAS with T-TIF (Figure 6-21) even though the BHP is similar with a maximum difference of 50 psi. This extra water injection, however, did not sweep more oil. This can be clearly shown by plotting the Injection Efficiency (IE) i.e. offset oil production divided by the water injected. Figure 6-22 shows that the SAS without TIF case has a higher IE values which indicate a more efficient flood from onset of the TIF and onward.

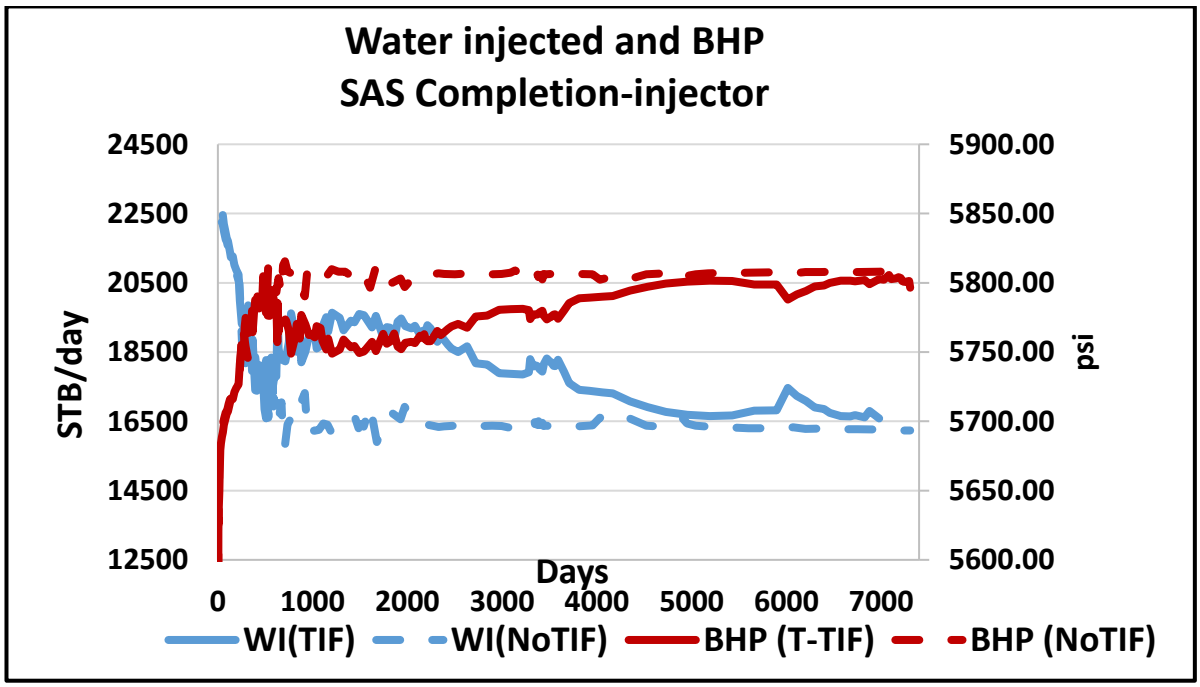

Figure 6-21: Water injected and BHP for both SAS with and without T-TIF

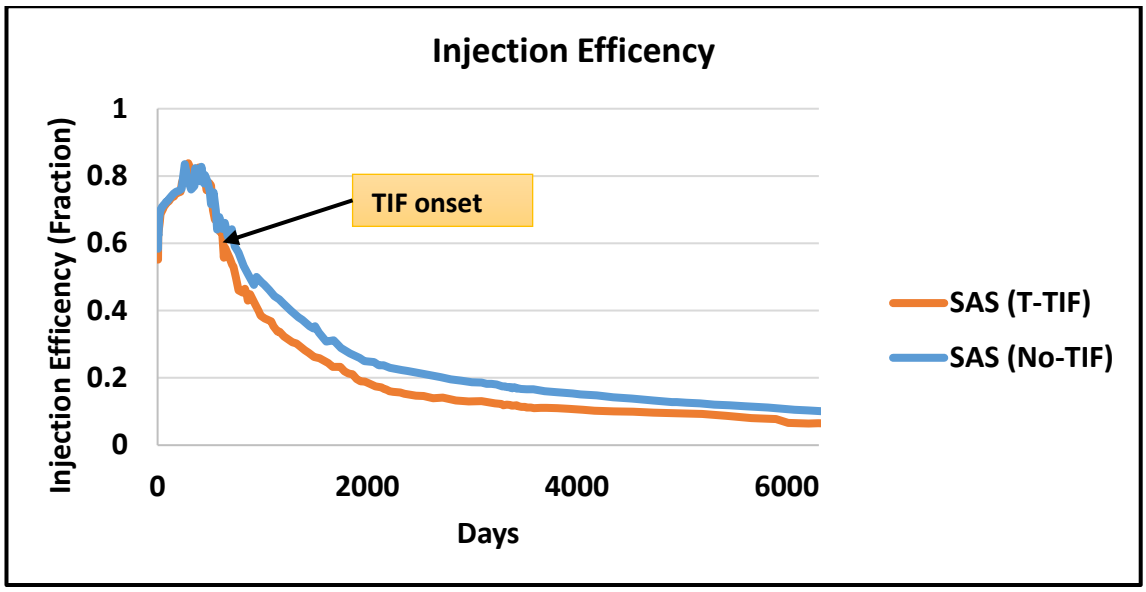

Figure 6-22: Injection Efficency for both SAS with and without T-TIF

6.9.1.2 *SAS and ICD completion in injector with T-TIF modelling*

This section evaluates the performance of the injection well being completed with SAS and ICDs equipped with a 1.6 mm and 2.5 mm diameter nozzle with T-TIF. Figure 6-23 confirmed that the ICD completions resulted in a more uniform water outflow. As expected, the smallest ICD diameter (i.e. the highest ICD strength) achieved the most uniform water injection outflow profile with smaller and more evenly distributed T-TIFs (Figure 6-24). Both ICD completions show a greater numbered T-TIFs, but these T-TIFs not only have a smaller length, but also propagate more slowly (Figure 6-25). The strongest ICD completion does not necessarily offer the best waterflood. A small ICD, such as 1.6 mm diameter also constrains the injection rate (Figure 6-29 early times), while the production rate is fixed. This faster reservoir pressure depletion giving poorer pressure support (Figure 6-26), results in later T-TIF initiation. This illustrates the importance of optimising the ICD diameter. The ICD size should control the T-TIF and achieve efficient waterflood performance for the given production/injection constraints .The selected ICD size should be neither too big (no control) nor too small (over-restriction of injection rate). Optimising ICD size in this manner requires both accurate modelling of the completion/reservoir interaction but also take into account the uncertainty in the reservoir model.

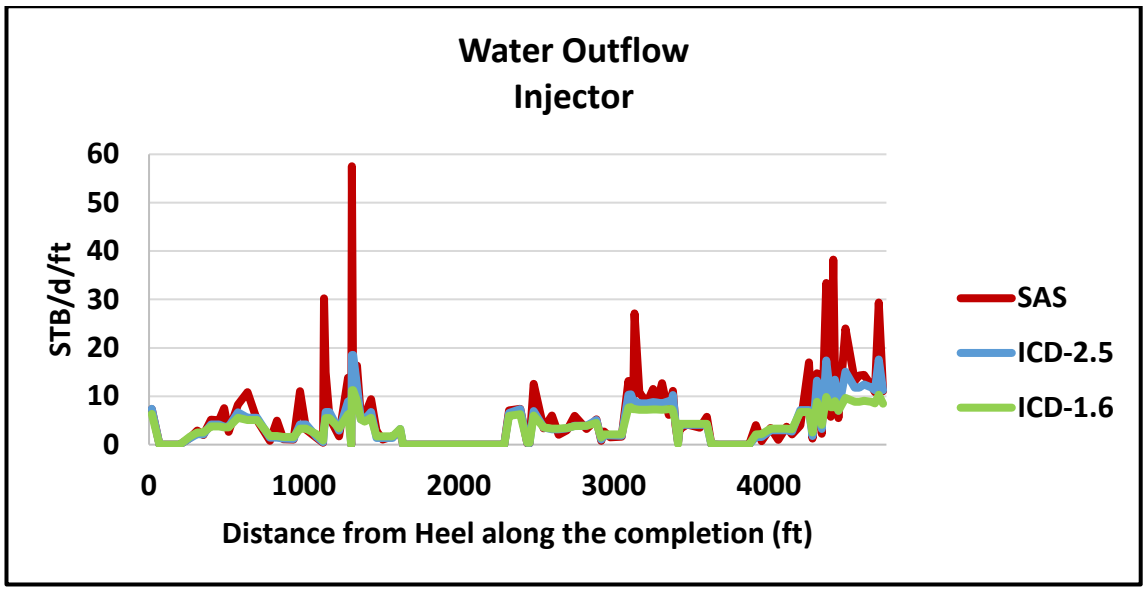

Figure 6-23: water outflow from the injector for SAS, ICD-2.5, and ICD-1.6 at early time step when T-TIF injection is not important

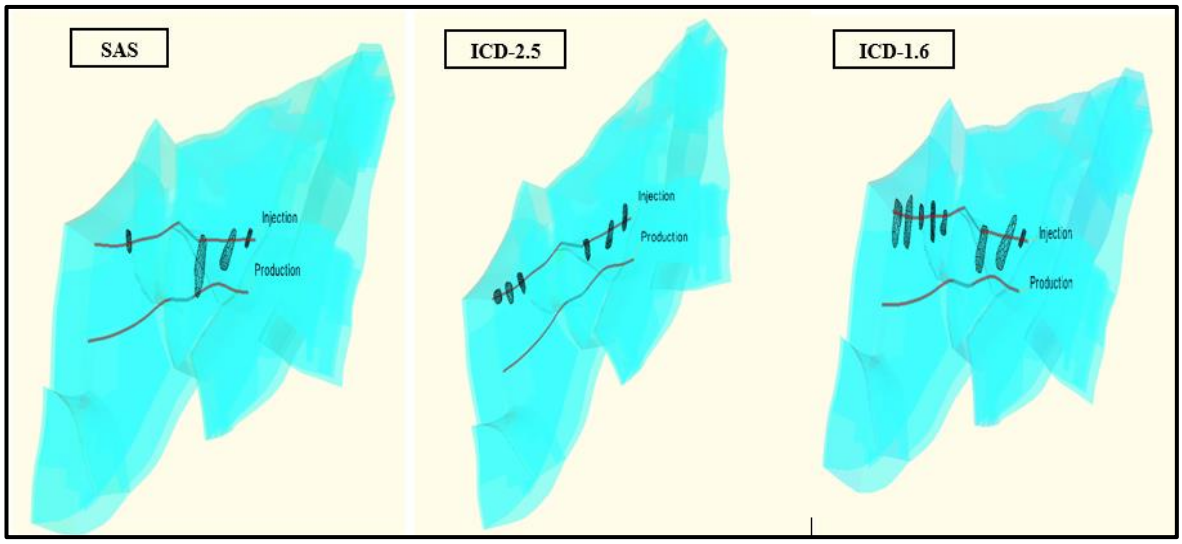

Figure 6-24: T-TIF frequency and length toward the producer for SAS, ICD-2.5, and ICD-1.6 at last time step

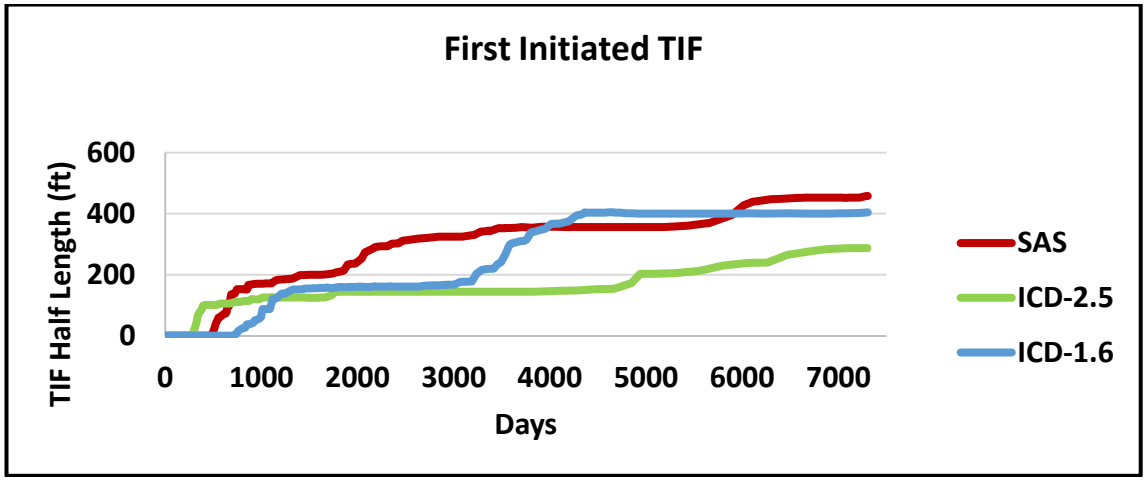

Figure 6-25: Half-length of first initiated T-TIFs for SAS, ICD-2.5, and ICD-1.6 at last time step

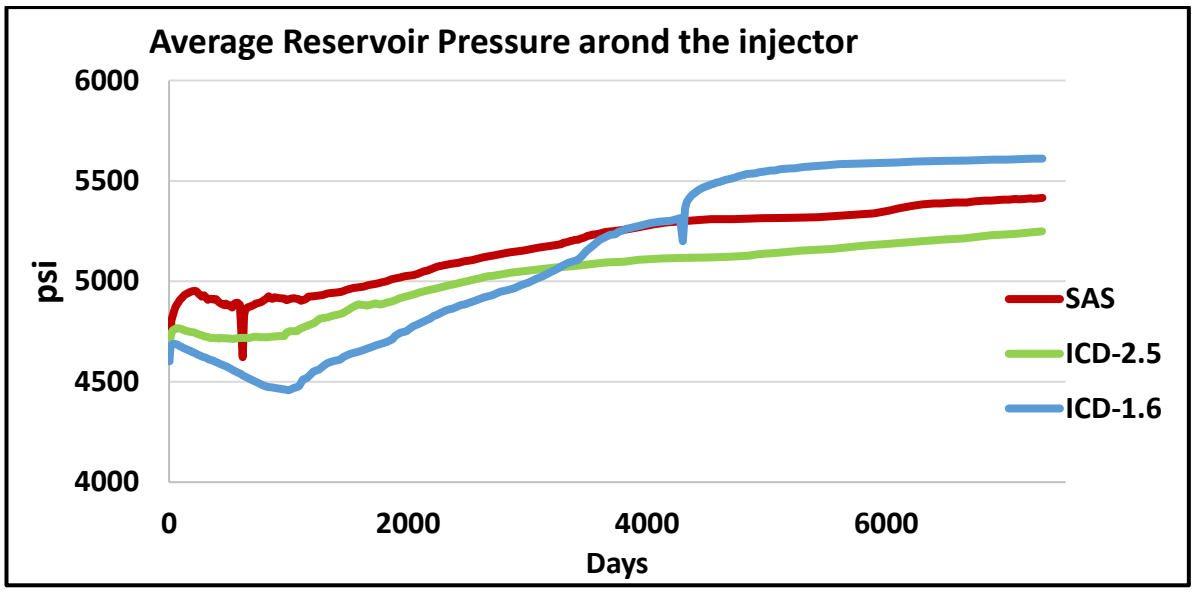

Figure 6-26: Average reservoir pressure around the injector for SAS, ICD-2.5, and ICD-1.6 mm

The ICD completion has improved the oil recovery because of the more equalised T-TIFs and more uniform water outflow as seen above. Figure 6-27 shows that both ICD completions achieved a higher oil recovery at all times compared to SAS completion. The smaller ICD diameter gave the best oil recovery up to 2000 days. This is because its larger number of T-TIFs eventually resulted in high water production (Figure 6-28). Figure 6-27 also shows that the 2.5 mm ICD gives the largest longer term (20 years) oil recovery i.e.8.5 % greater oil recovery compared to SAS. Both ICD completions delayed water breakthrough for 40 days compared to SAS (Figure 6-28). These findings illustrate the importance of ICD completions when T-TIFs have a negative impact.

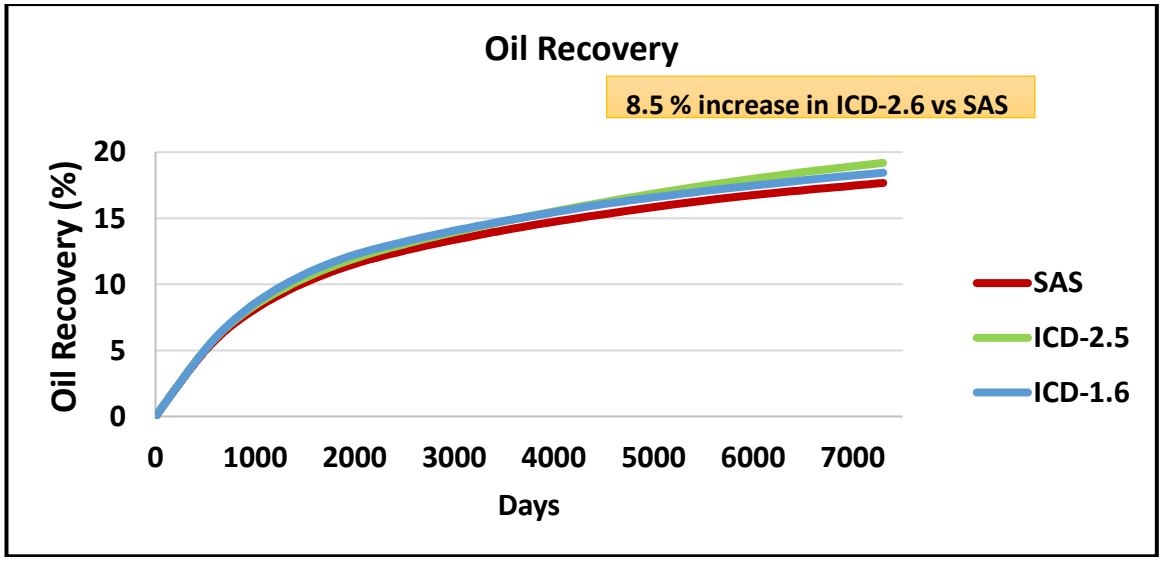

Figure 6-27: Oil Recovery for SAS, ICD-2.5, and ICD-1.6

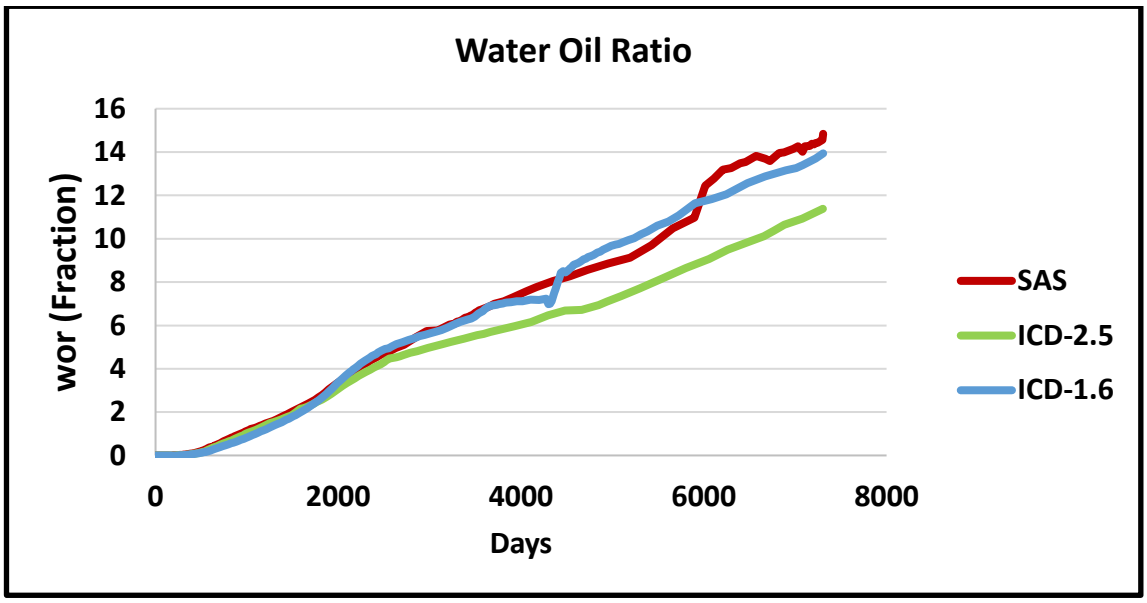

Figure 6-28: Water Oil Ratio for SAS, ICD-2.5, and ICD-1.6 completions for T-TIF

It was observed from this study that ICD and SAS completions behaved as expected at early times i.e. less injection rate and higher BHP for ICD completions compared to SAS as shown in Figure 6-29. However, this familiar performance was reversed after 1000 days (Figure 6-29). This change of performance is due to the timing of T-TIF propagation and the T-TIF performance subsequently becoming more dominant. It was observed that ICD-1.6 for instance has a higher injection rate and a lower BHP compared to SAS after 1000 days. This would not be expected without the existence of T-TIFs. This decrease in injection rate initially caused a decrease in the reservoir pressure (Figure 6-26) that contributed, along with the distributed cooling effect, to later initiation and propagation of T-TIFs. It was observed from Figure 6-30 that the ICD-2.5 completion has the most efficient flood in the long term while the ICD-1.6 has initially the most efficient flood and then decreased after initiation and propagation of T-TIFs

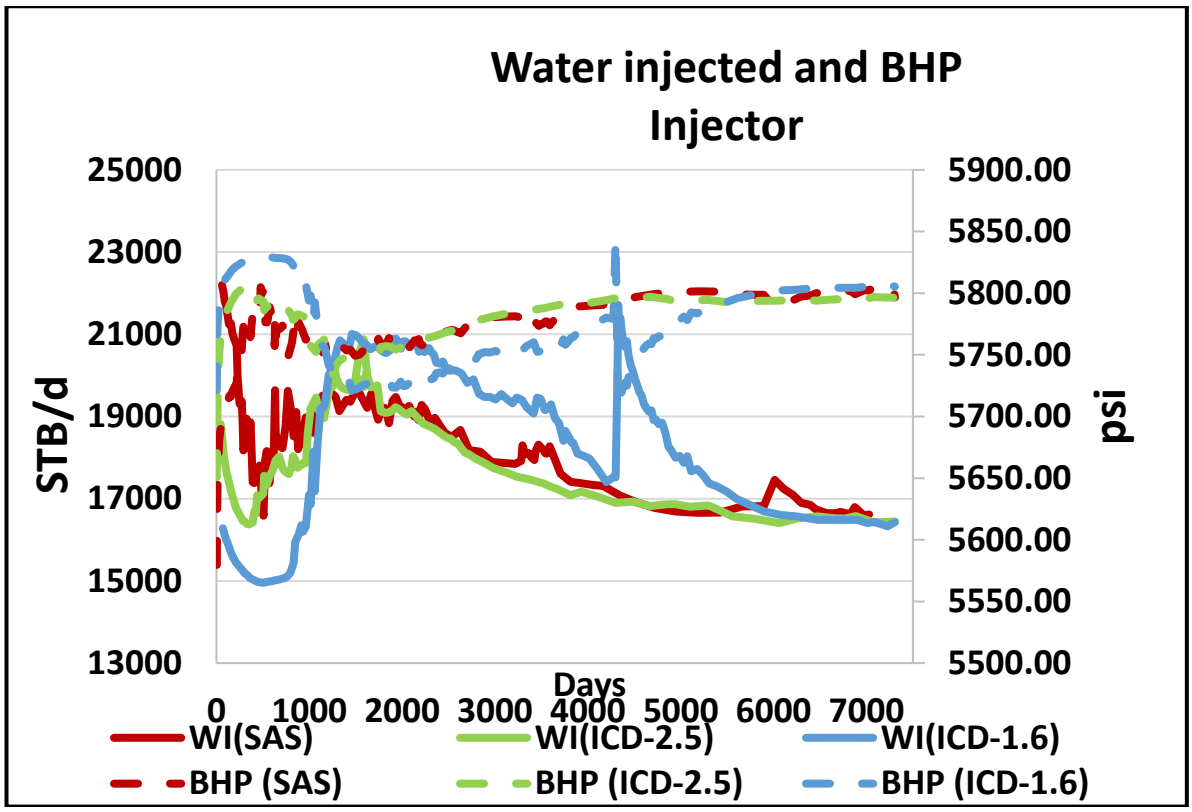

Figure 6-29: Water injection rate and BHP for SAS, ICD-2.5, and ICD-1.6 completions for T- TIF

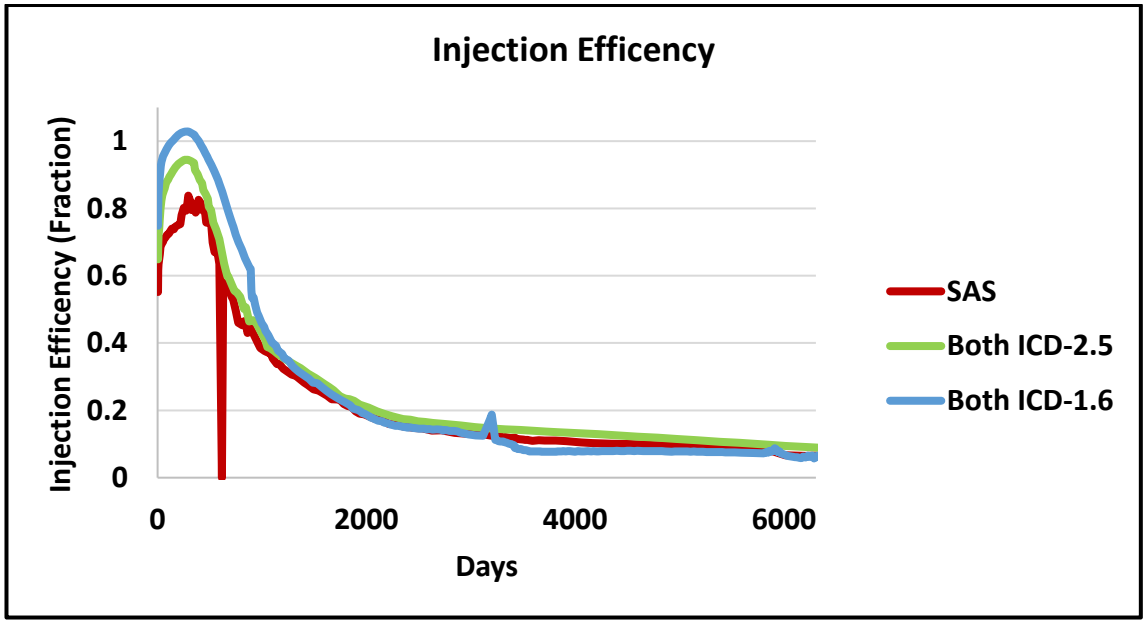

Figure 6-30: Injection efficency for SAS, ICD-2.5, and ICD-1.6 completions for T- TIF

6.9.1.3 *ICD completion in both injector and producer with T-TIF modelling*

The T-TIF impact now will be studied when both injector and producer are completed with ICD. This will then be compared to SAS completion in both injector and producer, as well as ICD in injector only and SAS in producer. T-TIF behaviour changed when both producer and injector are completed with ICD. Figure 6-31 shows that

completing a 1.6 mm ICD in both the injector and producer limited the length of the T-TIF and delayed the initiation of the final –TIF as well reducing the time period when T-TIFs were initiated. This can be explained by the more equalised oil inflow profile of the ICD completed producer compared to a SAS completion (Figure 6-32). The ICD-1.6 caused a more uniform drainage around both the injector and the producer when both are completed with ICD. This uniform distribution of reservoir cooling effect between the injection/production well pair limited the length of T-TIFs and changed the timing of T-TIF initiation.

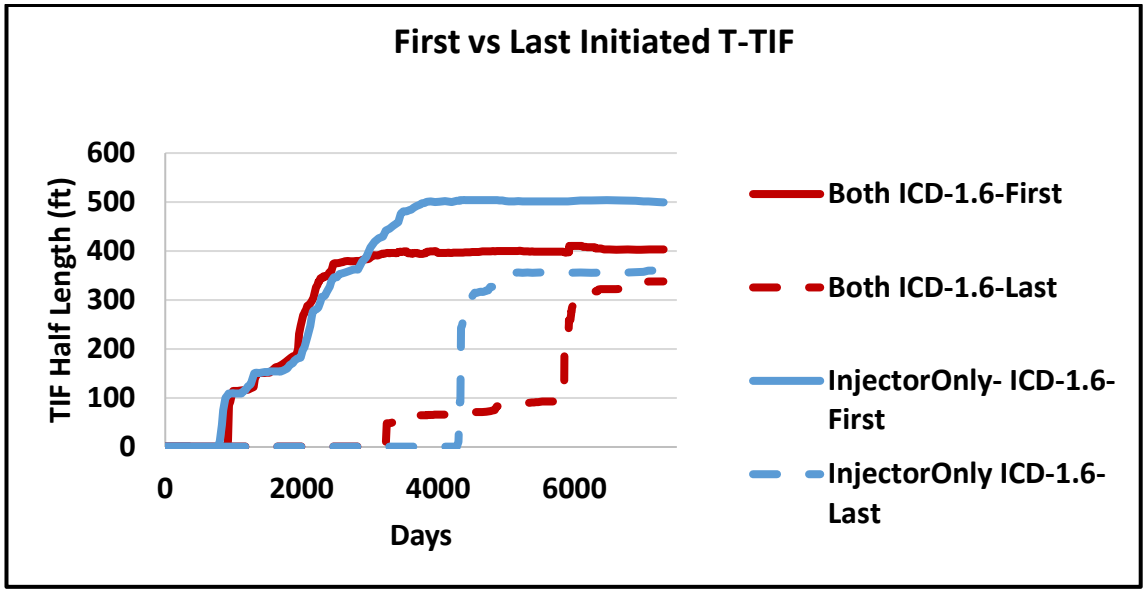

Figure 6-31: Time and half length of the first and last initiated T-TIFs for ICD-1.6 in both wells and in injector only

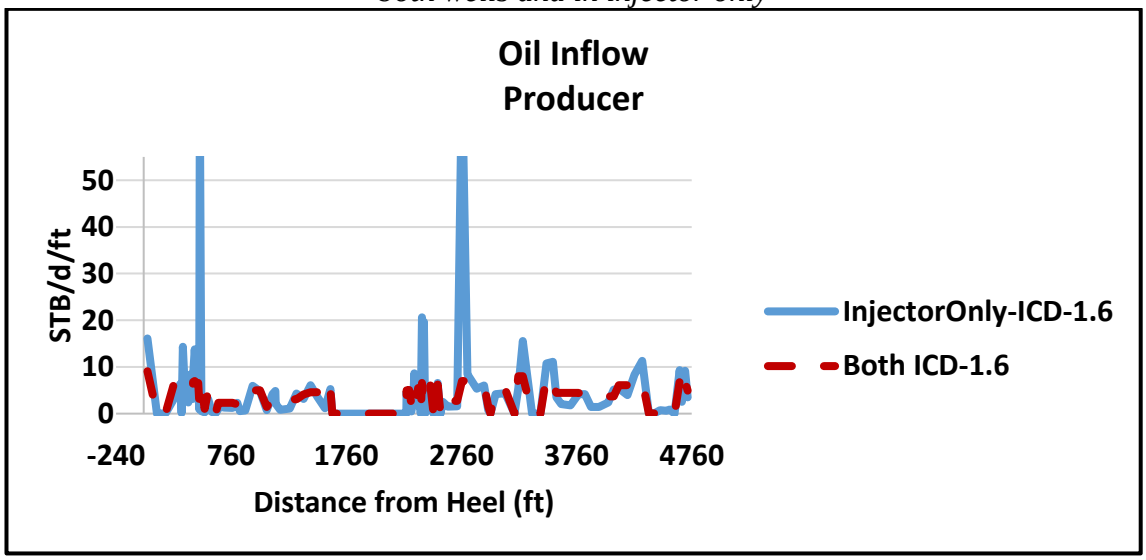

Figure 6-32: Oil inflow rate for ICD-1.6 in both wells and in injector only at early time step when T-TIFs are not important

The ICD completion in both injector and producer improved the oil recovery because of the more equalised T-TIFs and more equalised water outflow and oil inflow

as seen above. This completion gave the best oil recovery compared to SAS completion in the pair and ICD completed injector only, as shown in Figure 6-33 and Figure 6-34 for both ICD diameters. The ICD 1.6 gave a better oil recovery compared to SAS completion i.e. 5% increase on oil recovery with respect to SAS completion. Both ICD sizes achieved the best oil recovery when implemented in both wells. The smaller ICD diameter decreased the oil recovery after approximately 3200 days so that it eventually became similar to the 'injector only' ICD completed performance (Figure 6-33). This may be to do with the same effect of faster reservoir depletion as in the section above, only in this case this depletion rate was slightly better controlled due to the ICDs in the production well. By contrast, ICD-2.5 mm for both wells gave the best overall oil recovery with long term increase of 11% in oil recovery compared to 8% in ICD-2.5 completed injector only with respect to SAS completion in both wells. These ICD completions significantly improved the recovery compared to SAS from relatively early time, a factor which will be beneficial in NPV terms. Note that the smallest ICD diameter completion reached the minimum FBHP constraint and remained there for almost one year (Figure 6-36). This is attributed to the reduced pressure support at early times supplied by the 1.6 mm ICD completed injector (Figure 6-29).It shows once again the importance of designing and optimising ICD completion when evaluating such completions in a T-TIF prone environment.

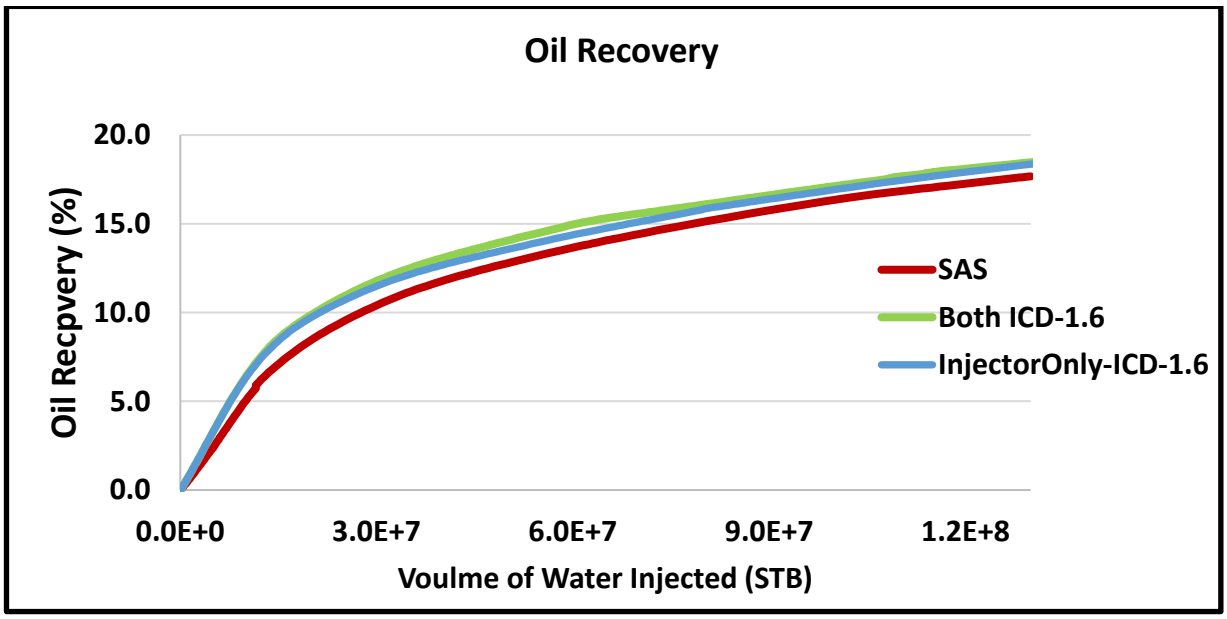

Figure 6-33: Oil Reovery for SAS, ICD-1.6 in both wells, and in injector only

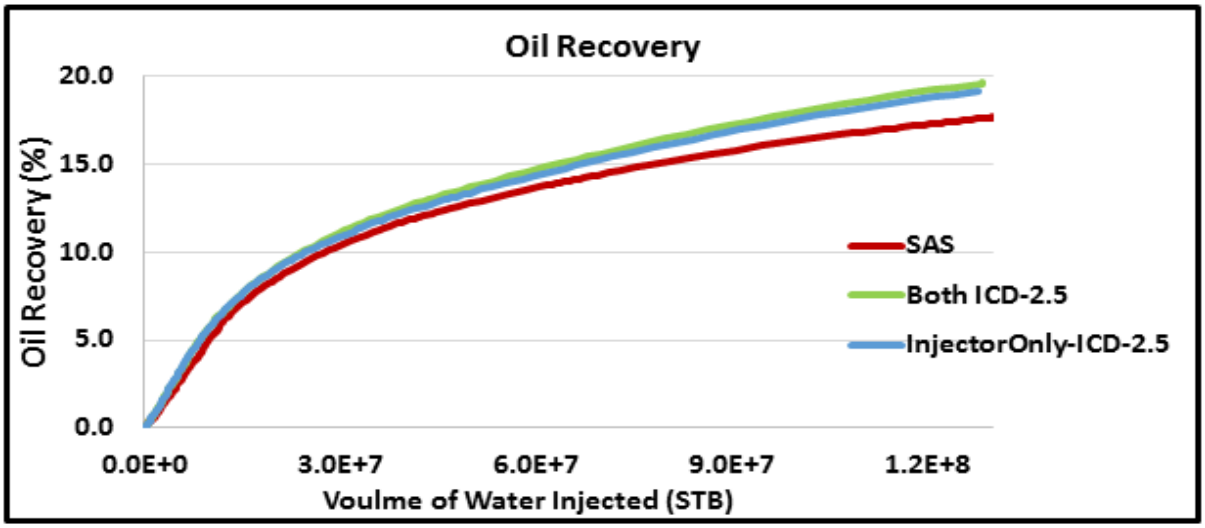

Figure 6-34: Oil Recovery for SAS, ICD-2.5 mm in both wells and in injector only

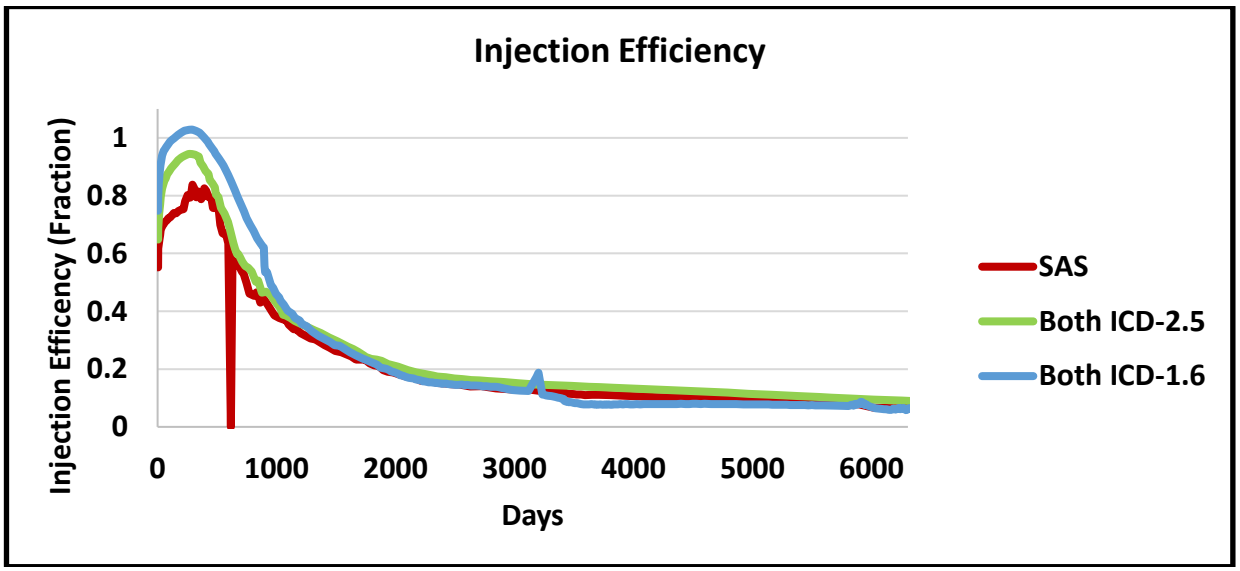

Figure 6-35: Injection efficiency for SAS, ICD-2.5 mm, and ICD-1.6 mm in both wells

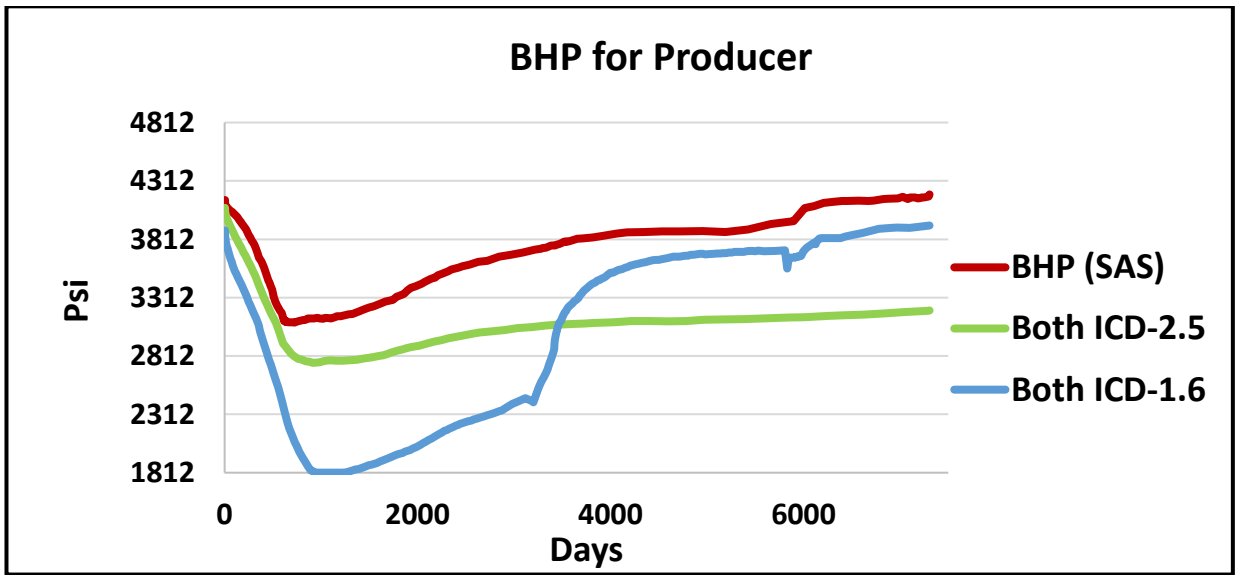

Figure 6-36: Production well FBHP for SAS, ICD-2.5 mm and ICD-1.6 mm in both wells

6.9.2 Longitudinal TIFs (L-TIF)

6.9.2.1 *SAS completion in injector with/without L-TIF*

This section studies a SAS completion with and without L-TIF. The impact of L-TIF will be compared to that of T-TIF to investigate the importance of TIF direction. Figure 6-37 shows the L-TIFs are propagating parallel to the SAS completed producer with two L-TIFs in R1 and R4.

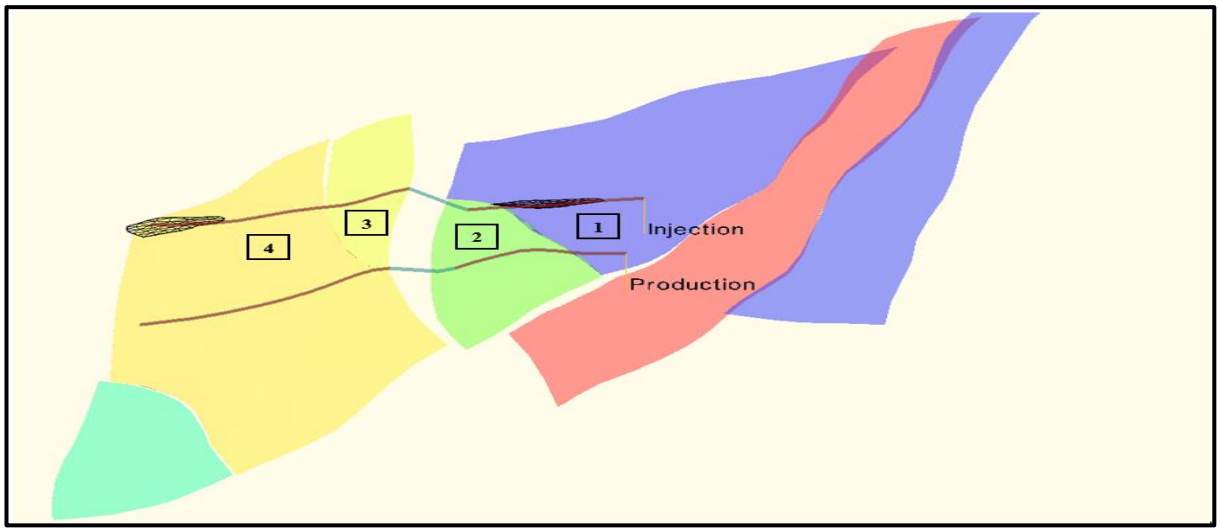

Figure 6-37: shows L-TIF propagation after 20 years for SAS completion

The Figure 6-38 oil recovery with L-TIF decreased 3% when compared to SAS without TIF, but also recovered more oil than SAS with-T-TIF. This was because that L-TIF, being parallel to the producer, increased the sweep efficiency (compared to T-TIF, but not to no-TIF) (Figure 6-39). It also decreased the volume of injected and produced water (Figure 6-39).

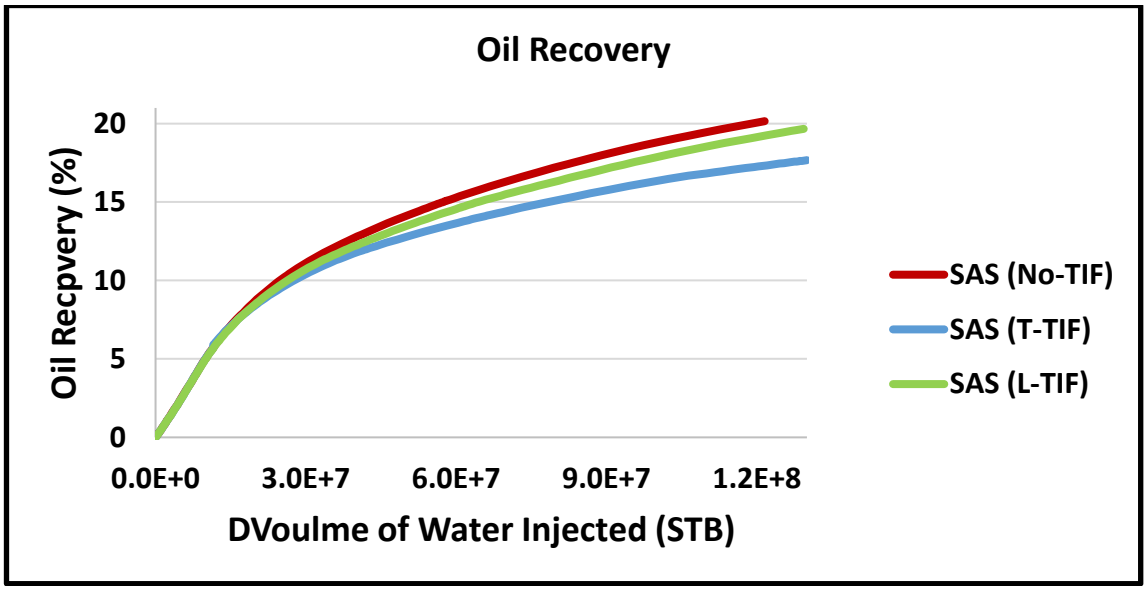

Figure 6-38: Oil Recovery for SAS with T-TIF, L-TIF and no-TIF

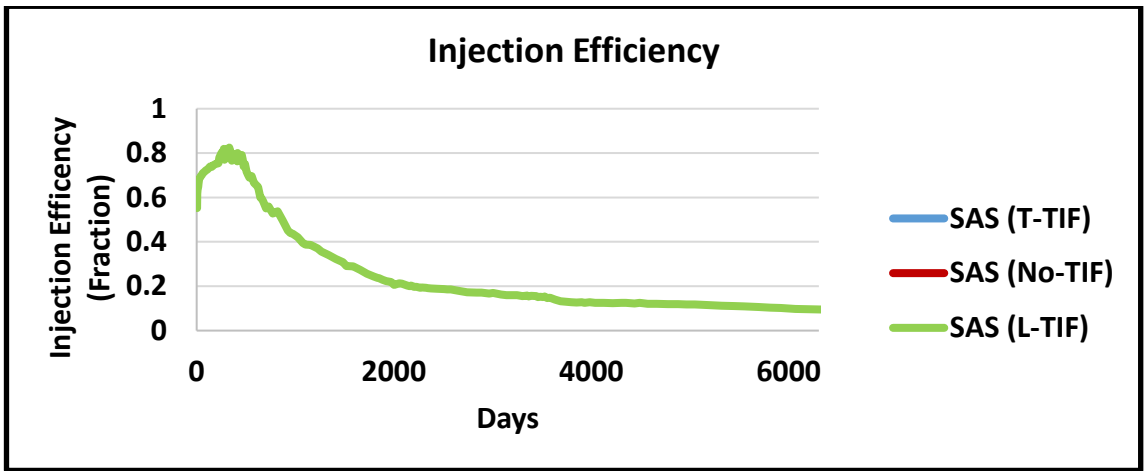

Figure 6-39: Injection Efficiency for SAS with T-TIF, L-TIF and no-TIF

Figure 6-40, oil recovery per region, shows the impact of L-TIF on sweep efficiency. The improved oil recovery for SAS without TIF comes from R3. More water is injected into R1 and R4 for SAS with L-TIF, leaving R3 relatively poorly swept. Region R2 in both scenarios i.e. L-TIF and T-TIF did not change much because only a small part of the water was injected into this region. The above clearly shows that TIF direction can have a big impact on the sweep efficiency and hence on oil recovery. SAS with L-TIF injected more water at almost the same BHP as SAS without TIF with a maximum difference of 30 psi, as shown in Figure 6-41. Both SAS with L-TIF and T-TIF behaved in a similar manner with respect to increased injected water and decreased oil recovery. However, SAS with L-TIF is favourable since it decreased the oil recovery by only 3% whereas SAS with T-TIF decreased the oil recovery by 12%. Orienting the well pair completed with SAS with the direction of the Maximum Horizontal Stress (L-TIF) achieved more oil recovery than these oriented with that of the Minimum Horizontal Stress (T-TIF).

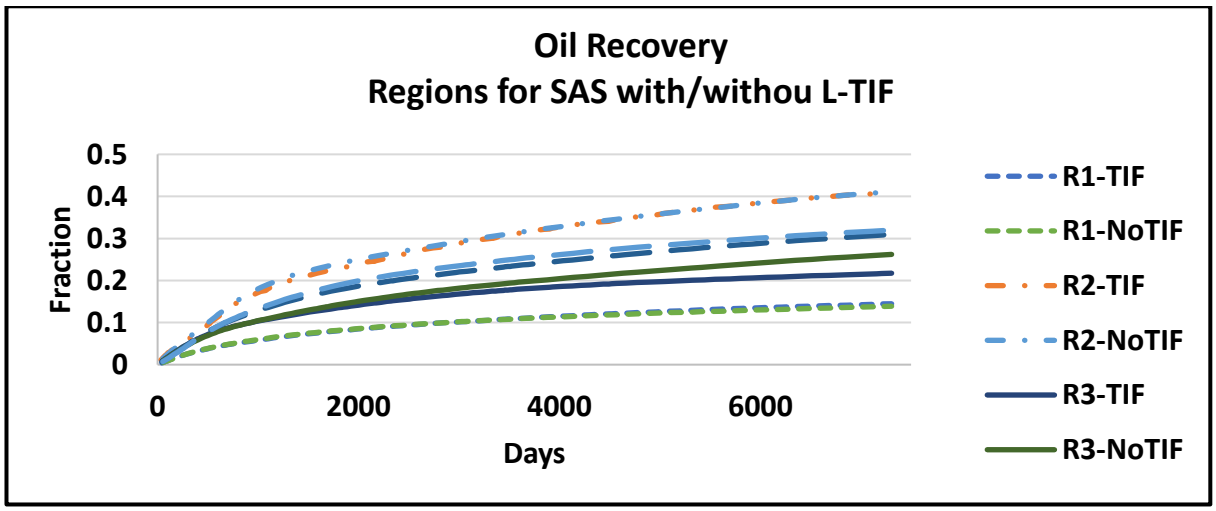

Figure 6-40: Oil recovery per region for SAS with and without L-TIF

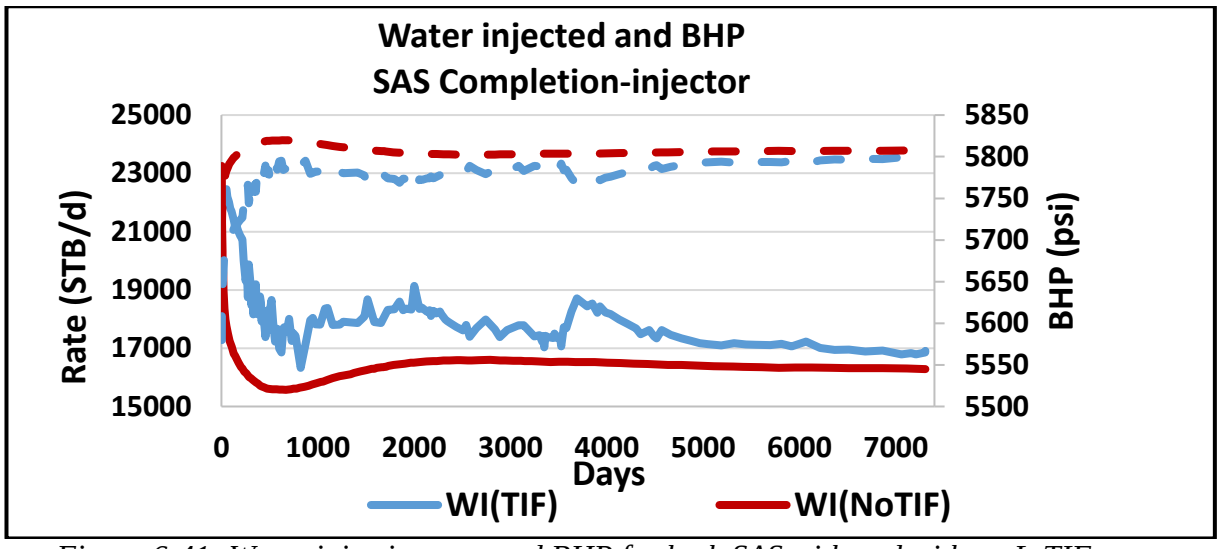

Figure 6-41: Water injection rate and BHP for both SAS with and without L-TIF

6.9.2.2 *SAS and ICD completion in injector only with L-TIF modelling*

This section considers the impact of L-TIF on SAS, a 1.6 mm and 2.5 mm diameter ICD completions. The ICD completions gave a more uniform water outflow and better distributed TIFs (Figure 6-42). ICD completions with L-TIF limited the TIFs length and slowed their propagation (Figure 6-43). These L-TIFs did not propagate after 2400 days, unlike their T-TIFs equivalent (Figure 6-25 and Figure 6-43). Figure 6-24 and Figure 6-42 show that ICD completions with T-TIF generate more TIFs than ICD completions with L-TIF. This is because water is being injected more toward the producer and hence the region between the producer and injector experience greater cooling in the case of ICD completions with T-TIF. Furthermore, once L-TIF has propagated, it dominates the other TIFs along the injector.

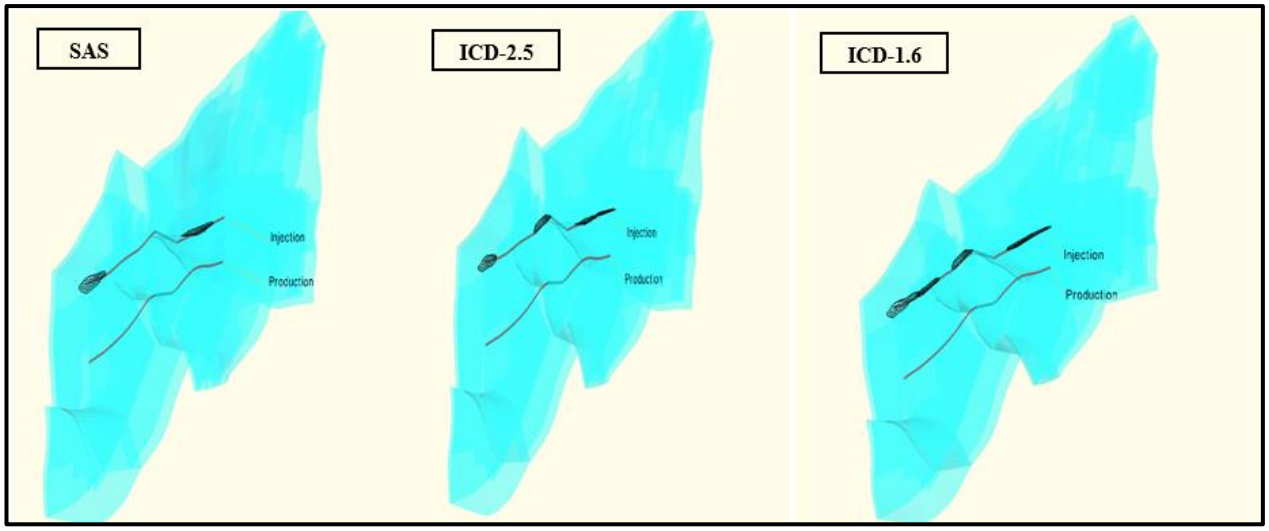

Figure 6-42: L-TIF frequency and distribution toward the producer for SAS, ICD-2.5, and ICD-1.6 mm completion in injection well after 20 years

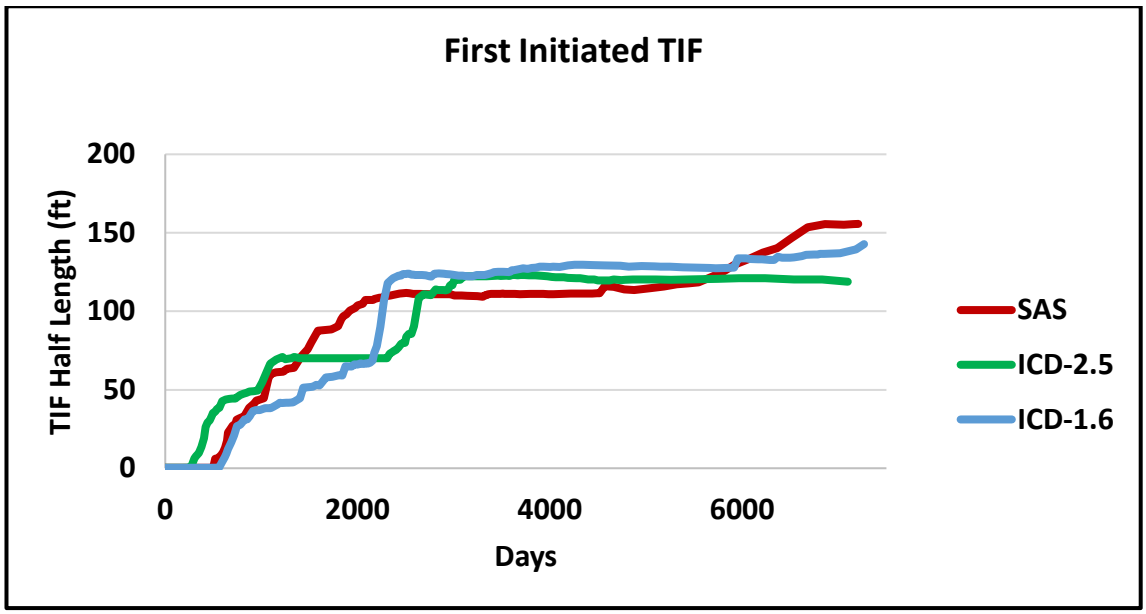

Figure 6-43: The time and half-length for the first initiated L-TIF for injection well for SAS, ICD-2.5, and ICD-1.6 mm

ICD completions with L-TIF improved the oil recovery up the injection volume of 73 MM STB i.e. 4000 days (Figure 6-44). ICD-2.5 completion continued to give a better oil recovery compared to SAS after 4000 days, whereas the oil recovery for the ICD-1.6 completion decreased compared to SAS completion after that time. This is because TIF initiation continued for the ICD-1.6 completion at later time compared to other completions. This generation of TIFs at later time results from a combination of the distribution of cooling effect as well as reduction of reservoir pressure. The small diameter ICD design did not give the best oil recovery at a longer term compared to SAS since a higher volume of water injected and water produced was observed from 2000 days and onward in ICD-1.6 completion (Figure 6-45 and Figure 6-46). These findings also confirm the importance of an ICD completion in injection wells when considering TIF propagation direction. The ICD-2.5 completion gave only a 1% increase on the oil recovery, a small increase in the added value.

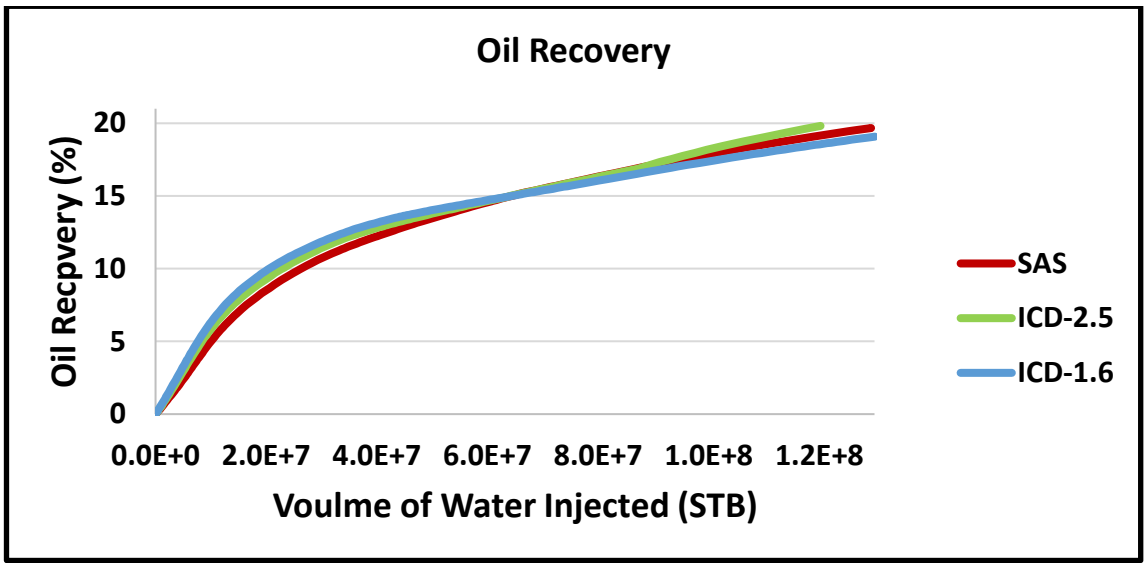

Figure 6-44: Oil Recovery SAS, ICD-2.5, and ICD-1.6 for L-TIF

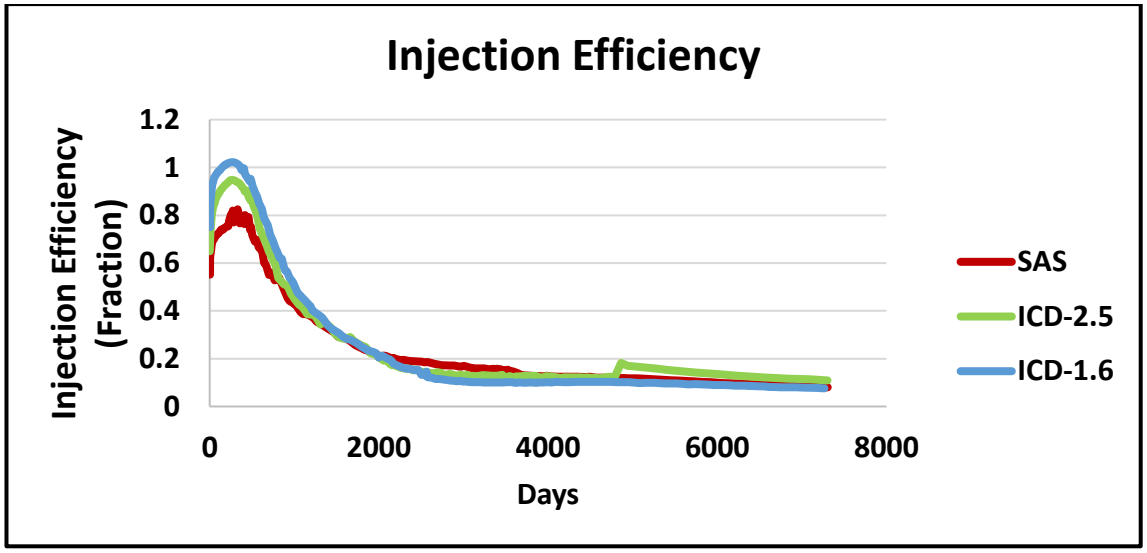

Figure 6-45: Injection Efficiency for SAS, ICD-2.5, and ICD-1.6 for L-TIF

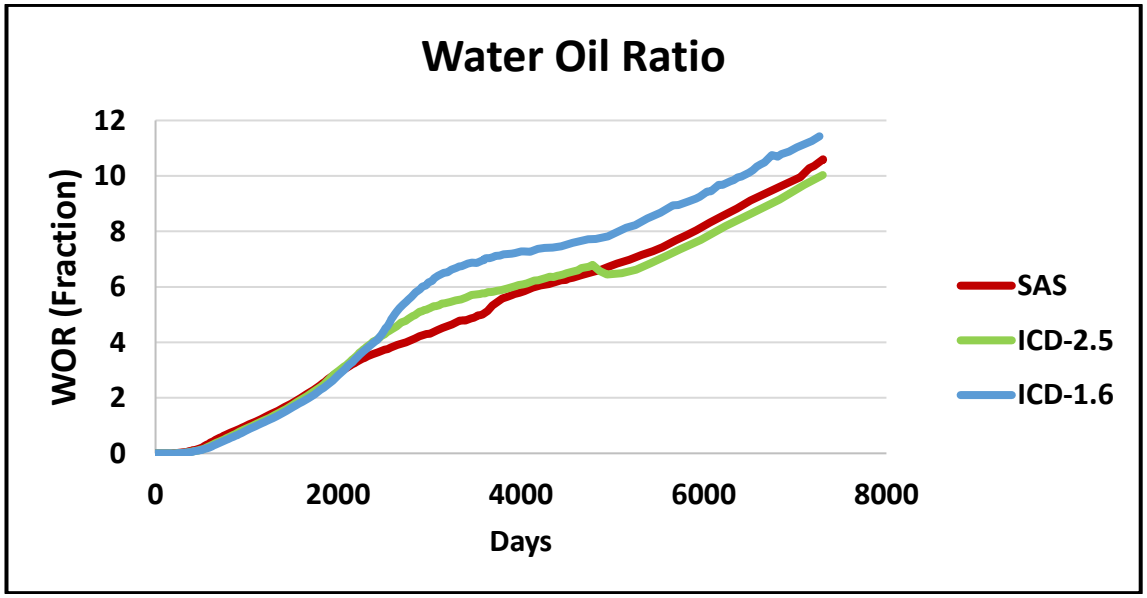

Figure 6-46: Producer water oil ratio for SAS, ICD-2.5, and ICD-1.6 for L-TIF

It was observed from this study that ICD and SAS completions behaved as expected at early times i.e. less injection rate and lower BHP for ICD completions compared to SAS (Figure 6-47). However, this familiar performance was reversed after 2000 days, as also shown in Figure 6-47. This change of performance is due to the L-TIF propagating and its performance becoming more dominant. It was observed that ICD-1.6 for instance has higher injection rate and lower BHP compared to SAS between 2000 and 6000 days in a manner that would not be expected without the existence of TIFs.

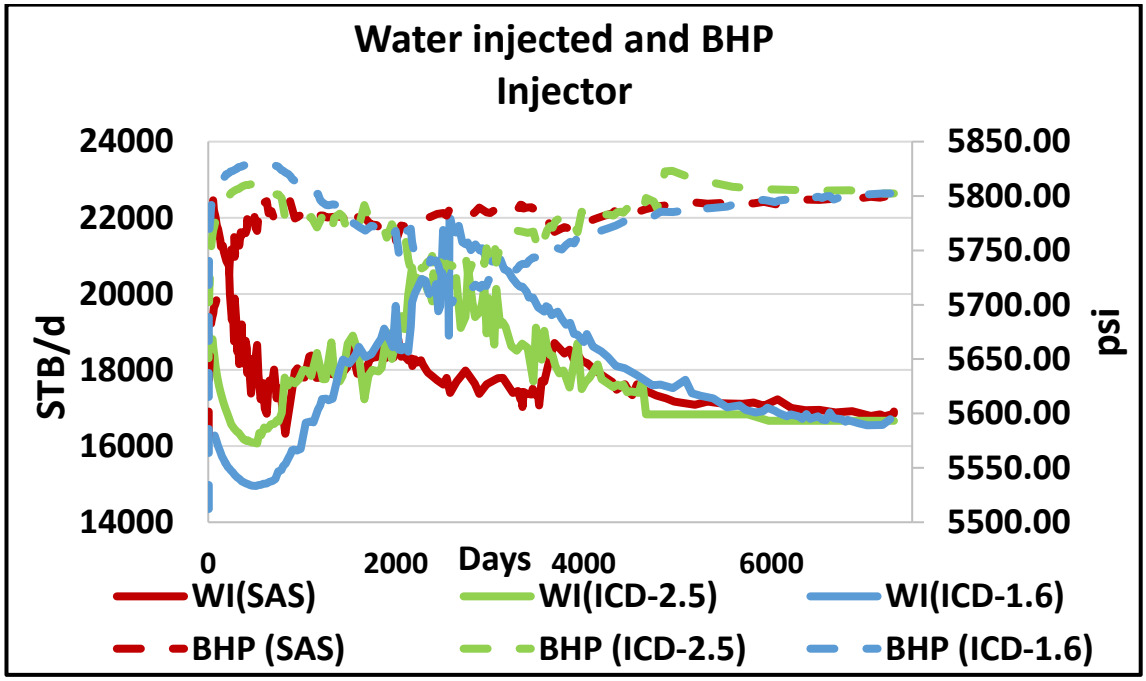

Figure 6-47: Water injection rate and BHP for SAS, ICD-2.5, and ICD-1.6 completions for L-TIF

6.9.2.3 *ICD completion in both injector and producer and L-TIF from injector*

In this section, L-TIF impact will be studied when both injector and producer are completed with ICD. This will then compared to a SAS completion in both injector and producer as well as ICD in injector only. It can be noted from Figure 6-48 that ICD in both injector and producer limited the length of L-TIF and initiated the last L-TIF earlier compared to ICD completion in injector only. This can be explained by the more equalised oil inflow in ICD completed producer compared to SAS completed producer with ICD in the injector only. It can also be observed from both Figure 6-48 and Figure 6-31 that the length of L-TIF was limited more significantly than for the length of T-TIF in both ICD completed wells. The more equalised oil and water inflow in the production well caused the L-TIF to be shorter than T-TIF.

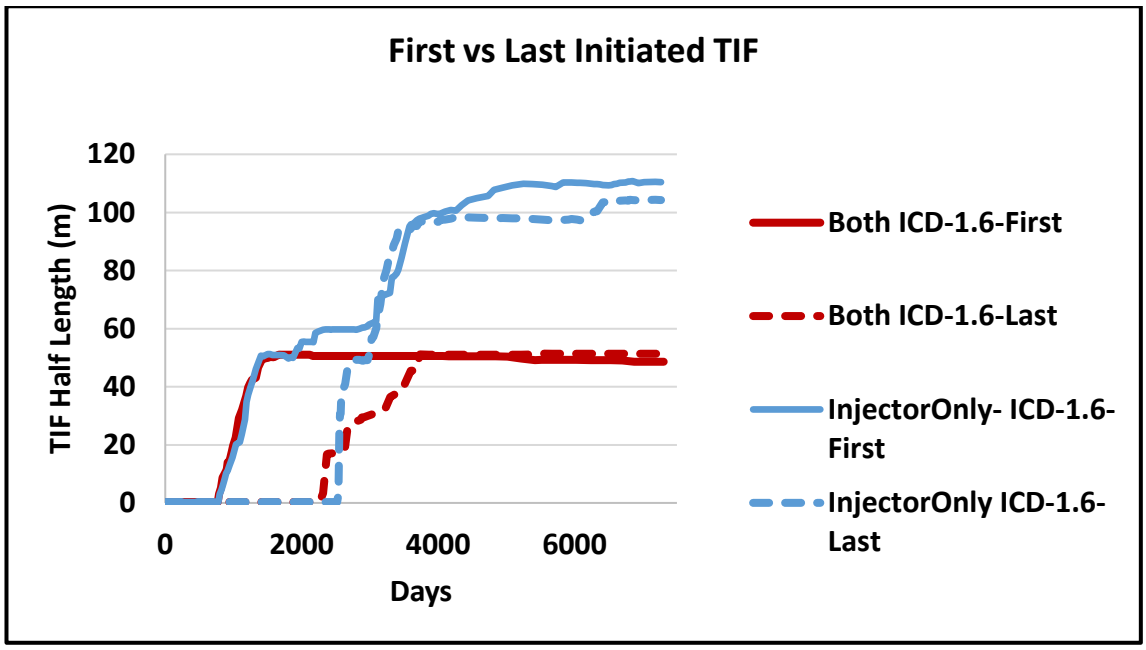

Figure 6-48: Growth of first and last initiated L-TIFs for both ICD-1.6 mm completed well and ICD completed injector only

The ICD completions in both injector and producer improved the oil recovery compared to ICD completed injector only and SAS completions (Figure 6-49 and Figure 6-50). An ICD completion in both injector and producer with the smallest ICD size in both gave the best oil recovery. Figure 6-49 shows a 4% increase, whereas an ICD completion in the injector only gave less oil recovery when compared to SAS. This is because ICD completion in both injector and producer limited the length of L-TIF, as can be seen in Figure 6-48, and restricted excessive water production. By contrast, ICD-2.5 for both injector and producer gave a small improvement on oil recovery i.e. 2 % compared to SAS completion. However, the smaller ICD diameter (or the highest strength) reached the minimum BHP constraint set for the producer and remained there after 1000 days (Figure 6-51). This highlights that advanced well completion, such as ICDs can add value to oil fields developed with long horizontal wells and water injection. However, it also shows that achieving the optimum added-value, requires realistic modelling, design and optimisation of ICD. The above shows that the value can be eroded by device of an inappropriate completion.

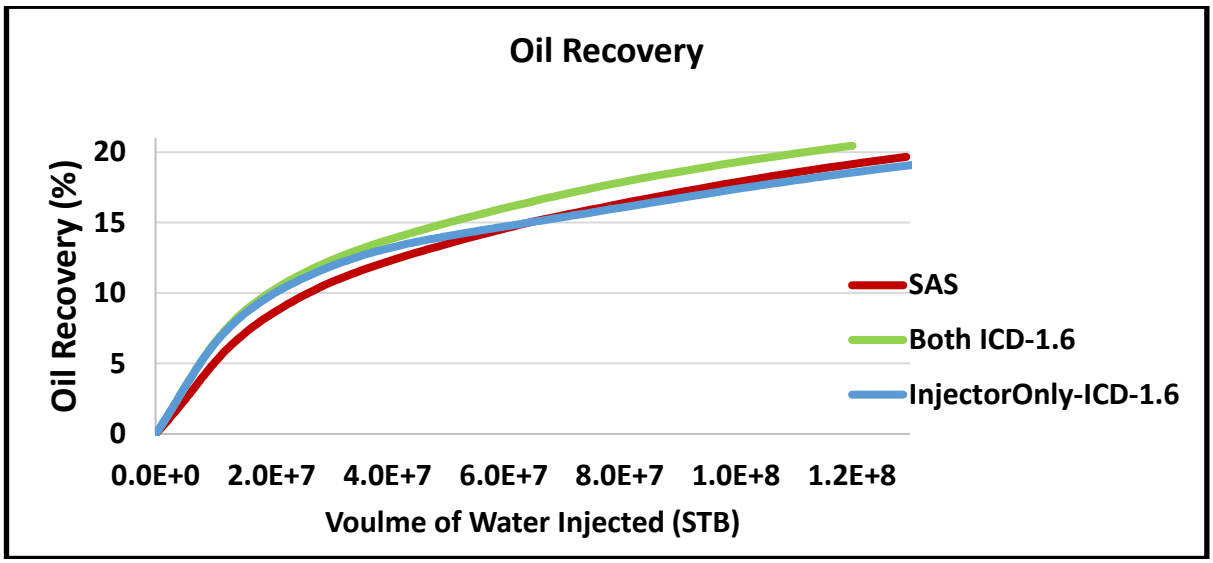

Figure 6-49: Oil Recovery for SAS, Both wells and injector only with ICD-1.6 mm

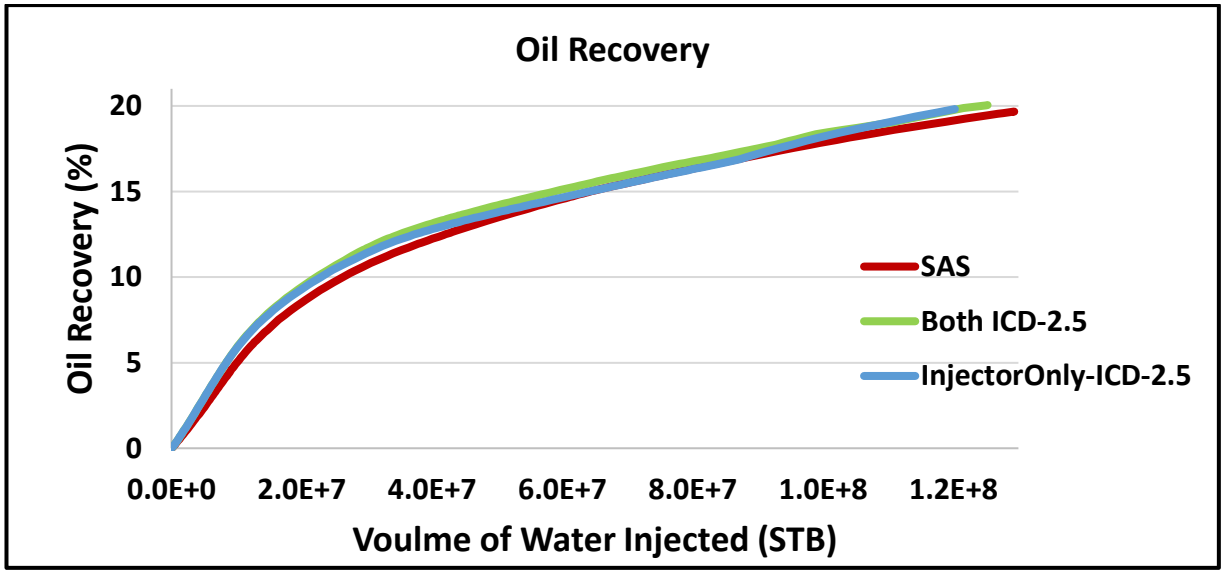

Figure 6-50: Oil Recovery for SAS, Both wells and injector only with ICD-2.5 mm

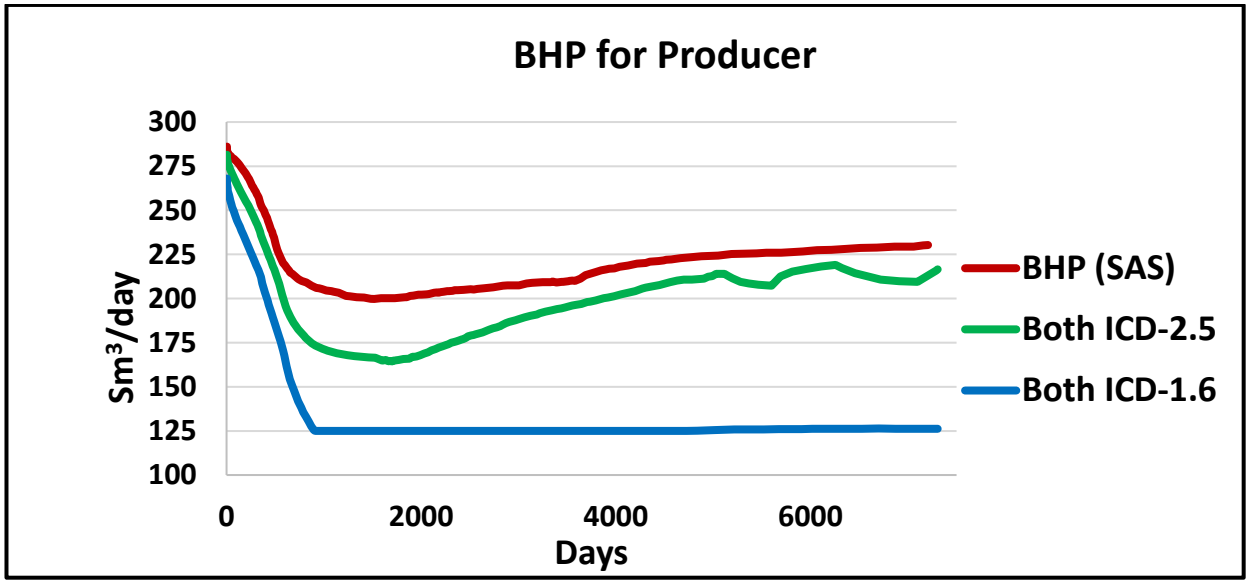

Figure 6-51: Producer's FBHP for Both wells SAS, ICD-2.5, and and 1.6 mm

6.10 Summary

The history matched model obtained from workflow in chapter 5 was set up and a new horizontal injector- producer pair was placed in the model. The well constraints and pair specifications were laid out and implemented in the new wells. The well completion types including ICD and SAS as well as annulus flow effect were detailed. The performance of ICD and SAS without modelling TIF were compared under isothermal and thermal conditions. Finally, the impact of different completions in injection well with TIF modelling under different scenarios were investigated.

The summary of findings and conclusions about all cases considered in this study can be found in Table 6-1, Table 6-2, Table 6-3, and Table 6-3.

It was concluded that:

I. Isothermal and thermal models comparisons (No- TIF Modelling):
    a. Modelling isothermal water injection can underestimate the actual BHP
    b. Oil recovery estimate can be incorrect if only isothermal water injection is considered.
    c. Thermal modelling for water injection is important for making accurate reservoir management decisions and future development plans.

II. SAS with/without (Longitudinal TIFs "L-TIF) and Transverse TIFs "T-TIF"):
    a. TIF impact is significant in waterflood operations
    b. TIF modelling should not be neglected in the modelling, designing and planning stages.
    c. Some regions on the TIF-affected waterflood will not be flooded more efficiently with SAS completion.
    d. Orienting the well pair completed with SAS with the direction of the Maximum Horizontal Stress (L-TIF) achieved more oil recovery than these oriented with that of the Minimum Horizontal Stress (T-TIF).

III. ICD in injector only vs. SAS (T-TIF and L-TIF)
    a. ICD completions distribute the cooling effect and create more TIFs.
    b. Smaller ICDs can have a negative impact on oil recovery at longer term.
    c. Designing ICD completion in injection wells when considering TIF propagation is critical.
    d. The expected performance of ICDs completions under normal injection conditions can be completely different when considering TIFs propagation

e. Restricting injection with smaller ICDs can promote TIFs at later time due to decreased reservoir pressure.
f. ICD completions with T-TIF has more TIFs than ICD completions with L-TIF.

IV. ICD in both wells vs. SAS (T-TIF and L-TIF)

a. Completing both wells with ICDs provides the most robust gain and reduces the production uncertainty associated with the reservoir description, TIF direction, etc.
b. Designing and optimisation ICD completion investigating more sophisticated completion combinations in injector-producer pair can have value.
c. Relation between the injection/production wells' performance, completions, and inter-well flow configuration is critical
d. ICD completion in the producer can have a limited value when indeed it is the TIF that needs control.
e. The length of L-TIF was limited more significant than length of T-TIF for both ICD completed wells.
f. TIF direction can have a big impact on the sweep efficiency and hence on oil recovery.

Table 6-1: Summary of isothermal and thermal modelling of SAS and 1.6 mm ICD (No-TIF)

	Cases	***Completion***		***Observations***
		Injector	*Producer*	
No-TIF	*Thermal vs Isothermal*	*1.6 mm ICD*	*SAS*	*1. Viscosity increases from 0.5 to 5.5 cp in cooled zone 2. The increased viscosity required higher BHP to inject the same volume of water in thermal modelling 3. oil recovery increase by (8%) in thermal modelling*
		1.6 mm ICD	*SAS*	*As above, but larger difference observed between thermal and isothermal modelled with ICDs*

Table 6-2: Summary of SAS and thermal modelling with/without L-TIF and T-TIF

Cases	Completion		TIF Orientation	Observations
	Injector	Producer		
SAS with/without TIF	SAS	SAS	Longitudinal TIF (L-TIF)	1. L-TIF decreased oil recovery after 20 years to 97% of SAS without TIF despite more water injection 2. Oil loss was even greater with T-TIF (88% of SAS without TIF at 20 years despite more water injection) 3. Oil displacement with L-TIF and T-TIF was poorer in some regions compared to SAS without TIF
	SAS	SAS	Transverse TIF (TIF)	

Table 6-3: Summary of ICD in injector only vs. SAS in producer (T-TIF and L-TIF)

Cases	Completion		TIF Orientation	Observations with respect to SAS completion
	Injector	Producer		
SAS vs ICD	1.6 and 2.5 mm ICD	SAS	Longitudinal TIF (L-TIF)	1. ICD completions achieved more uniform water injection profile 2. ICD completions reduce the number of L-TIFs and T-TIFs and reduce their length 3. ICD completions initially gave greater oil production while long term production depended on ICD restriction 4. ICD completions delayed water breakthrough 5. ICD completions injected more water at later time despite the additional pressure drop 6. ICD completions with T-TIF generate more TIFs than ICD completions with L-TIF 7. ICD completions with L-TIF gave greater oil production than ICD completions with T-TIF despite less water injection
	1.6 and 2.5 mm ICD	SAS	Transverse TIF (TIF)	

Table 6-4: Summary ICD in both wells vs. SAS with T-TIF and L-TIF

Cases	Completion		TIF Orientation	Observations with respect to SAS completion
	Injector	Producer		
SAS vs ICD	1.6 and 2.5 mm ICD	1.6 and 2.5 mm ICD	Longitudinal (L-TIF)	1. ICD completions in both wells gave the best performance compared to all cases 2. Smaller ICD completions in both wells resulted in FBHP being reduced to the minimum constraint 3. T-TIF are longer and more than L-TIF for ICD completions 4. ICD completions with L-TIF gave greater oil production than ICD completions with T-TIF despite less water injection

Chapter 7 Conclusions and Future work

7.1 Conclusion

One of the major challenges faced by injection wells during their injection lifetime is the existence of Thermally Induced Fractures. Reduced sweep efficiency, inefficient pressure support, and the possibility of TIFs propagating into caprock are all potential negative consequences of TIFs existence in the injection wells. Identifying and characterising dynamic TIF growth is thus a critical step when defining field development strategies and making day - to - day reservoir management decisions. Mitigating and controlling TIFs is another challenge in the oil industry. Advanced Well Completions (AWCs) employing Inflow Control Devices (ICDs) provide a practical solution to this challenge.

This thesis has provided a practical workflow that integrates recent analytical and semi-analytical models to identify the onset of TIF, its propagation properties, direction and impact during reservoir dynamic events occurring at different levels. The practicality of the proposed workflow was tested with synthetic data and its robustness confirmed with the analysis of data from a real field

History matching workflows that take the dynamic nature of the TIF problem, geomechanical, and thermal properties into consideration were developed. These workflows were applied in a real field reservoir sector model i.e. "N" field. The resulting, history matched, N field sector model was then used in comparative studies of alternative, injection well completion scenarios.

Finally, the impact of thermal and isothermal reservoir modelling options on injection wells was investigated. Furthermore, performance of different ICDs sizes in a horizontal injector-producer pair experiencing TIFs was evaluated and compared. The impact of well orientation with respect to the preferred TIF direction on TIF initiation and propagation was also studied.

The following conclusions can be drawn from this thesis:

1. TIFs existence in injection wells can cause non-uniform injection profile. This results in poor sweep efficiency, and non-uniform pressure support, and earlier than expected sand production during well shut-ins.
2. TIFs can have a positive impact in disposal wells by improving the injectivity and achieving the injection requirements. However, TIFs

propagating into caprrocks and contamination of fresh water remains a challenge.

3. Modelling of TIF requires a coupling of dynamic thermal reservoir Finite Difference model with a Finite element fracture mechanics and detailed wellbore system. The concept of coupling fracture mechanics to geomechanical analysis and reservoir simulation simultaneously is the only mean of modelling these complex phenomena in an accurate manner.
4. Analytical and semi-analytical modelling descriptions of a water injection reservoir performance have been combined into a workflow with routinely gathered injection and production well data to give insights into the performance of a water-flooded reservoir.
5. The Modified Hall Integral (MHI) employed multiple curves instead of restricting the analysis to a single curve. MHI did not only successfully identify TIF initiation, but also the periods when the TIF was actively growing and when it remained static.
6. The Fracturing Index and Injectivity Index models identified TIF initiation, TIF growth periods and the TIF's properties. This model was used to support the MHI findings.
7. Comparison of the Pre- and Post-TIF inter-well connectivity results for the Capacitive Resistance Model provided a probable direction of TIF propagation and a qualitative evaluation of the sweep efficiency between an injection and production well pair.
8. The Pseudo Steady State formulation allowed the flood front radius (r_e) and water/oil interface pressure (P_e) to be evaluated. It forms the basis for a real-time, monitoring tool.
9. The manual history matching approach was used to history match a real field sector model with an injector experiencing TIF. The manual approach was appropriate in this study because TIF is a coupled physics problem difficult to capture autonomously at the moment, as well as because the selection of input data is based on knowledge and experience.
10. The history matching with TIF modelling proved to be time consuming due to the dynamic nature of TIF and the presence of geomechanical uncertainties.

11. Inclusion of thermal modelling and dynamic TIF growth within the reservoir during modelling of a water injection project improves the accuracy of the predictions and the resulting reservoir management decisions and future development plans.
12. ICD completions added value based on the presented work due to their control of TIF initiation and propagation as well as production inflow performance.
13. Optimising the Design of the ICD completion in injection wells when considering TIF propagation is important. The selected ICD size should be neither too big (no control) nor too small (over-restriction of injection rate).
14. Both Wells i.e. injector and producer completed with ICDs provide the most robust gain and reduce the production uncertainty associated with the reservoir description, TIF direction, etc.
15. The horizontal well orientation and azimuth with respect to the direction of the preferred horizontal stress affect TIFs initiation, propagation, and dimensions and hence affect the oil recovery.

7.2 Future work

The area of Advanced Well Completions applications in wells with thermally induced fractures is rich in challenges and future areas for further research. Inflow Control Valves (ICVs) applications in injection wells with possible TIFs is a promising technology and hence an investigation of its design, optimisation, and added value forms a logical extension of this thesis. Based on the work presented in this thesis, the followings points for future work are recommended:

1. Investigate the effect of annulus flow on TIF initiation and propagation.
2. Development of the recommended ICD completion design optimisation workflow for an injector-producer pair. Uncertainty in the reservoir model should also be taken into account.
3. Uncertainty Analysis of Thermally Induced Fractures Initiation and Propagation under different reservoir, geomechanical, and well conditions. These uncertainties include:
    a) In Situ stress analysis (Analytical Methods, Mohr's Circle, and Dynamic Numerical Simulation).
    b) Rock mechanical sensitivities.
    c) Rock thermal properties sensitivities.

d) Other Sensitivities (surface injected water temperature, Tubing Head pressure, reservoir rressure at start of injection etc.).
e) Water quality.

4. Studying and comparing other Advanced well completions e.g. ICV in TIF affected waterflood environments.
5. Develop guidelines for reservoir simulation and well model gridding to allow accurate modelling of the annulus flow with different completions/ reservoir interaction in conjunction with TIF modelling. This makes the workflow applicable to an arbitrary well completion design.
6. Investigate the performance of ICDs with intermediate TIF direction i.e. when it's neither longitudinal nor transverse to the well trajectory.
7. Develop guidelines for TIF seeding and the minimising of required computational resources.
8. Develop guidelines for choice of the TIF permeability model at various production and geological conditions.

Appendices

Appendix A-Pseudo-Steady State approximation for Pressure inside a Water Bank

Izgec and Kabir [118] formulation of PSS starts with the radial diffusivity equation:

$$\frac{1}{\mathrm{r}}\frac{\partial}{\partial \mathrm{r}}\left(\mathrm{r}\frac{\partial \mathrm{P}}{\partial \mathrm{r}}\right)=\frac{\phi\mu \mathrm{c_t}}{\mathrm{k}}\frac{\partial \mathrm{P}}{\partial \mathrm{t}} \qquad \text{Equation A-1}$$

Assuming a constant injection rate for a small time increment, the change in pressure inside the waterbank with respect to time can be written as:

$$\frac{\partial \mathrm{P}}{\partial \mathrm{t}}=-\frac{\mathrm{i_w}B}{\pi h\phi(\mathrm{r_0^2}-\mathrm{r_w^2})} \qquad \text{Equation A-2}$$

Incorporating Eq. A-1 and Eq. A-2 and assuming steady state flow, we get the following expression:

$$\frac{1}{\mathrm{r}}\frac{\partial}{\partial \mathrm{r}}\left(\mathrm{r}\frac{\partial \mathrm{P}}{\partial \mathrm{r}}\right)=\frac{\phi\mu \mathrm{c_t}}{\mathrm{k}}\left(-\frac{\mathrm{i_w}B}{\pi h\phi(\mathrm{r_0^2}-\mathrm{r_w^2})}\right) \qquad \text{Equation A-3}$$

Using the procedure that authors provided, the final form of the equation for pressure inside the bank is the following:

$$P_e=P_{wf}-\frac{\mathrm{i_w}B\mu}{2\pi kh}\left[\frac{\mathrm{r_0^2}}{(\mathrm{r_0^2}-\mathrm{r_w^2})}ln\left(\frac{r_e}{r_w}\right)-\frac{1}{2}\frac{(\mathrm{r_e^2}-\mathrm{r_w^2})}{(\mathrm{r_0^2}-\mathrm{r_w^2})}+s^*\right] \qquad \text{Equation A-4}$$

$\mathrm{P_e}$ can be updated every time step with changing $\mathrm{r_e}$ and $\mathrm{s^*}$

Appendix B- Evaluation of Pseudoskin

Following the methodology outlined by Izgec and Kabir (2009) [9], the line source solution for transient flow during injection is:

$$\frac{P_e - P_{wf}}{\mathrm{i_n}} = m\sum_{\mathrm{j=1}}^{\mathrm{n}} \frac{(\mathrm{i_j} - \mathrm{i_{j-1}})}{\mathrm{i_n}} \log(\mathrm{t_j} - \mathrm{t_{j-1}}) + \mathrm{m}\left[\log\left(\frac{\mathrm{k}}{\emptyset \mu \mathrm{c_t r_w^2}}\right) - 3.23 + 0.868\mathrm{S}^*\right] \quad \text{Equation B-1}$$

Where

$$\mathrm{m} = \frac{141.2B\mu}{kh} \quad \text{Equation B -2}$$

$$\mathrm{b} = \left[\log\left(\frac{\mathrm{k}}{\emptyset \mu \mathrm{c_t r_w^2}}\right) - 3.23 + 0.868\mathrm{S}^*\right] \quad \text{Equation B -3}$$

and

$$\Delta \mathrm{t_{sup}} = \sum_{\mathrm{j=1}}^{\mathrm{n}} \frac{(\mathrm{i_j} - \mathrm{i_{j-1}})}{\mathrm{i_n}} \log(\mathrm{t_j} - \mathrm{t_{j-1}}) \quad \text{Equation B -4}$$

Replacing Eq. B-2, Eq. B-3, and Eq. B-4 with the right hand side in Eq. B-1

$$\frac{P_e - P_{wf}}{\mathrm{i_n}} = \mathrm{m}\Delta \mathrm{t_{sup}} + \mathrm{b} \quad \text{Equation B -5}$$

Parameter b can be updated every time step during injection as follows:

$$\mathrm{b} = \frac{P_e - P_{wf}}{\mathrm{i_n}} - \mathrm{m}\Delta \mathrm{t_{sup}} \quad \text{Equation B -6}$$

Then, pseudoskin can be updated continuously with the following equation

$$\mathrm{S}^* = \frac{1}{0.868}\left[\frac{\mathrm{b}}{\mathrm{m}} - \log\left(\frac{\mathrm{k}}{\emptyset \mu \mathrm{c_t r_w^2}}\right) + 3.23\right] \quad \text{Equation B -7}$$

Appendix C-Methods using the Analytic and Numeric Derivative of Hall Integral

Izgec [118]and Kabir presented MHI formulation using the analytic and numeric derivative.

They started with pseudo steady-state equation:

$$P_{wf} - P_e = \frac{141.2\mathrm{i_w}\, B\mu}{\mathrm{kh}}\left[ln\left(\frac{r_e}{r_w}\right) - 0.5 + s^*\right] \quad \text{Equation C-1}$$

Integrating both sides with respect to time

$$\int \left(P_{wf} - P_e\right) \mathrm{dt} \quad \text{Equation C -2}$$

$$= \frac{141.2\, W_i\, B\mu}{\mathrm{kh}}\left[ln\left(\frac{r_e}{r_w}\right) - 0.5 + s^*\right]$$

The derivative term can be obtained by differentiating the integral with respect to natural logarithm of the cumulative injection. This can be written as:

$$D_{HI} = \frac{\mathrm{d}\int \left(P_{wf} - P_e\right) \mathrm{dt}}{\mathrm{dln}\,(W_i)} \quad \text{Equation C -3}$$

By replacing the term in the parenthesis with the right hand side and defining the parameters:

Where

$$\alpha_1 = \frac{141.2B\mu}{kh} \quad \text{Equation C -4}$$

$$r_e = \left(\frac{5.615W_i\, B}{\pi h\phi(1 - S_{or})}\right)^{\frac{1}{2}} \quad \text{Equation C -5}$$

And

$$\alpha_2 = \left(\frac{5.615B}{\pi h \emptyset (1 - S_{or})}\right)^{\frac{1}{2}}$$ Equation C -6

Combining Egs. C-3 through C-6, the following Equation is obtained:

$$D_{HI} = \frac{\mathrm{d}\left[W_i \alpha_1 \left(ln\left(W_i^{\frac{1}{2}} \alpha_2\right) - 0.5 - S^*\right)\right]}{\mathrm{d}\ln(W_i)}$$ Equation C -7

Expanding the terms in Eq. C-7 yields:

$$D_{HI} = \frac{\mathrm{d}[0.5 W_i \alpha_1 ln(W_i) + W_i \alpha_1 ln(\alpha_2) - S^* W_i \alpha_1]}{\mathrm{d}\ln(W_i)}$$ Equation C -8

By use of the following relation:

$$\frac{d(x)}{d(lnx)} = e^{Inx}$$ Equation C-9

The final form of the analytic derivative is obtained as:

$$D_{HI} = \frac{W_i \alpha_1}{2} + e^{\ln(W_i)}\left(\frac{\alpha_1 \ln(W_i)}{2} + \alpha_1 In(\alpha_2) + S^* \alpha_1\right)$$ Equation C -10

Upon manipulation, one obtains:

$$D_{HI} = \frac{W_i \alpha_1}{2} + \alpha_1 W_i \left\{\frac{\ln(W_i)}{2} + In(\alpha_2) - \frac{1}{2} + S^*\right\}$$ Equation C -11

Final form can be obtained:

$$D_{HI} = \alpha_1 W_i \left(ln \frac{r_e}{r_w} + s^* \right)$$ Equation C -12

In this case, the numeric derivative of Hall integral can be easily taken by using the following expression:

$$D_{HIn} = \frac{\mathrm{d}\int\left(P_{wf} - P_e\right)\mathrm{dt}}{\mathrm{dln}\,(W_i)} = \left(\frac{I_{\mathrm{H}}^{\mathrm{n+1}} - I_{\mathrm{H}}^{\mathrm{n}}}{\ln\,(W_i)^{\mathrm{n+1}} - \ln\,(W_i)^{\mathrm{n}}}\right)$$ Equation C -13

Where

$$I_H = \int\left(P_{wf} - P_e\right)\mathrm{dt}$$ Equation C-14

Appendix D- Capacitance Resistance Model for Injector and Producer (CRMIP)

CRM is developed as differential equation from mass conservative. Lake et al [124] presented the equation following:

$$\frac{\partial \mathrm{q_{ij}(t)}}{\partial \mathrm{t}} + \frac{1}{\tau_{\mathrm{ij}}}\mathrm{q_{ij}}(t) = \frac{1}{\tau_{\mathrm{ij}}}\mathrm{f_{ij}i_i(t)} - \mathrm{J_{ij}}\frac{\partial \mathrm{p_{wf,j}}}{\partial \mathrm{t}} \qquad \text{Equation D-1}$$

For τ_{ij}, time storage (capacitance) is function of drainage volume (V_p), compressibility(C_t), and productivity index(J). This parameter explained the fluid storage between injector i and producer j pair.

$$\tau_{ij} = \left(\frac{C_t V_p}{J}\right)_{ij} \qquad \text{Equation D-2}$$

And f_{ij}, connectivity is fraction of steady-state rate of injector i to producer$j$.

$$f_{ij} = \frac{q_{ij}(t)}{i_i(t)} \qquad \text{Equation D-3}$$

For fixed injection rate $i(\Delta t_k) = I_i^{(k)}$ and linear BHP variation during interval Δt_k, the general solution for equation C-1 can be expressed as:

$$q_j(t_n) = \sum_{i=1}^{N} q_{ij}(t_0) e^{\frac{-(t_n - t_0)}{\tau_{ij}}} + \sum_{i=1}^{n} \left\{ \sum_{k=1}^{n} \left[\left(f_{ij} I_i^k - J_{ij}\tau_{ij}\frac{\Delta P_{wf}}{\Delta t_k} \right) \left(1 - e^{\frac{-\Delta t_k}{\tau_{ij}}} \right) e^{\frac{-(t_n - t_k)}{\tau_{ij}}} \right] \right\} \qquad \text{Equation D-4}$$

If we use the production history for each time $q_{ij}(t_{k-1})$ step thus replacing $q_{ij}(t_o)$ and $e^{\frac{-(t_n - t_0)}{\tau_{ij}}}$

$$q_{ij}(t_n) = q_{ij}(t_{n-1}) e^{\frac{-(\Delta t_n)}{\tau_{ij}}} + \left(1 - e^{\frac{-\Delta t_n}{\tau_{ij}}} \right) \left(f_{ij} I_i\,(t_n) - J_{ij}\tau_{ij}\frac{\Delta P_{wf},\, j(t_n)}{\Delta t_n} \right) \qquad \text{Equation D-5}$$

Objective function for nonlinear regression:

$$Obj.function = \min \sum_{n}^{N_n} \left(q_{real,j}^{n} - q_{CRMIP,j}^{n} \right)^2$$

Constraints for nonlinear regression:

$$\sum_{i=1}^{N_i} f_{ij}, \tau_{ij} \geq 0 \text{ And } \sum_{i=1}^{N_i} f_{ij} \leq 1$$

(j = 1, 2,..., Np)

Appendix E- Synthetic Case 2 Figures

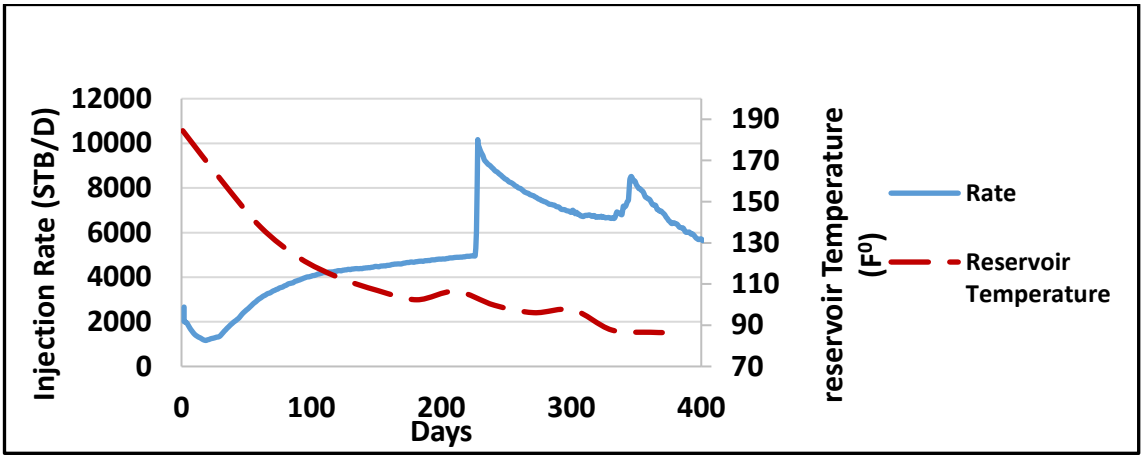

Figure E- 1: Case 2: Cold Water injection reduces the reservoir temperature

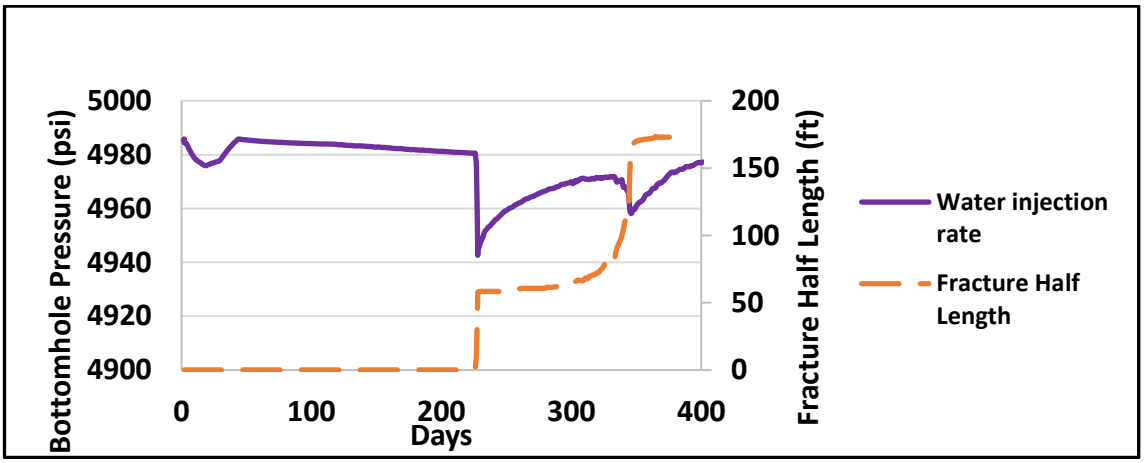

Figure E- 2: Case 2: BHP and Fracture length vs. time

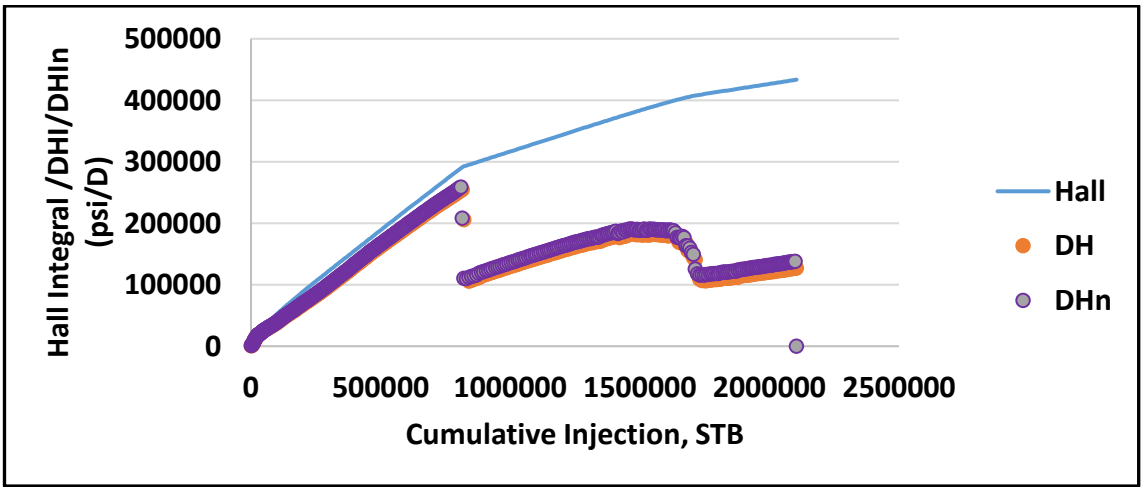

Figure E- 3: Case 2: MHI plot for Injector I1 shows downward separation of derivatives implying TIF.

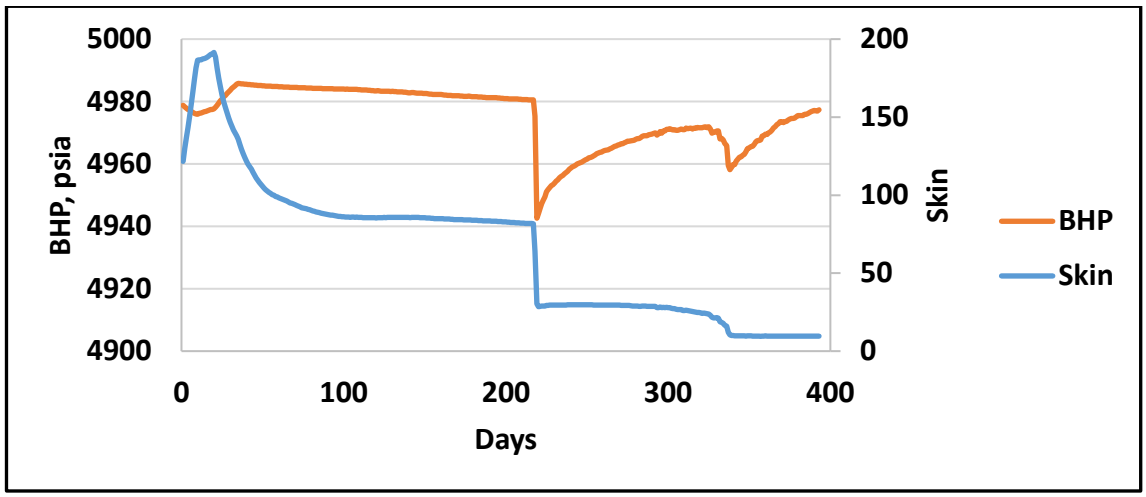

Figure E- 4: Case 2: Skin value decreases after 155 days

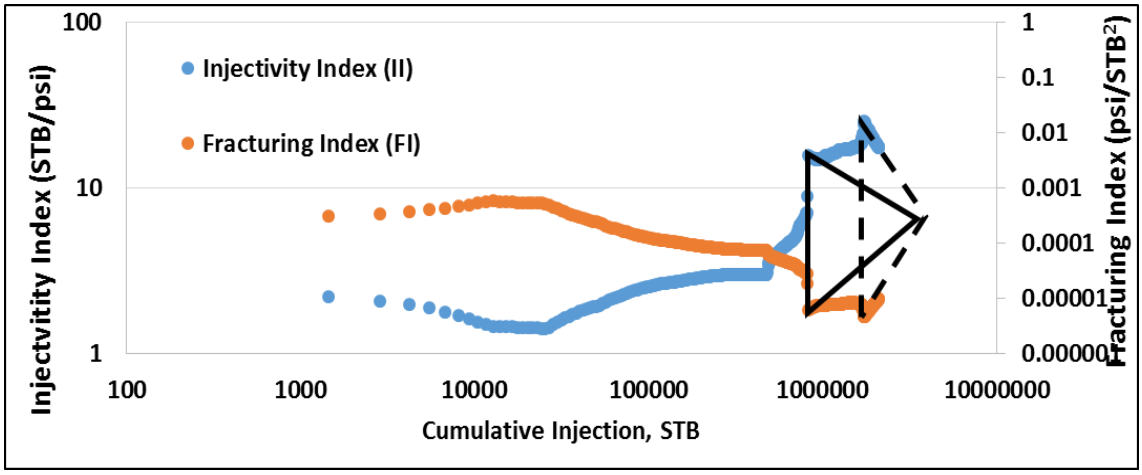

Figure E- 5: Case 2: log-log plot of FI and II indicates the onset of TIF and subsequent propagation

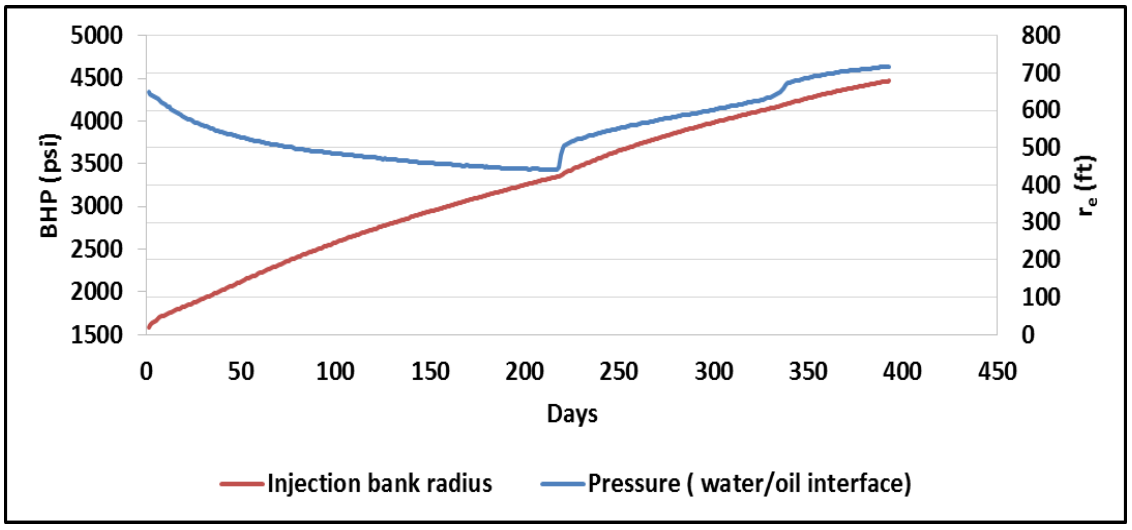

Figure E- 6: Case 2: P_e increase after TIF at 155 days indicates more efficient voidage replacement

Appendix F- PVT Tables for Thermal Model

Table F-1 : PVT properties at 200 F

Temperature = 200 F								
Pressure (psi)	*Bubble Point (psi)*	*Gas Oil Ratio (scf/STB)*	*Oil FVF RB/STB*	*Oil Viscosity cp*	*Gas FVF (RB/Mscf)*	*Gas Viscosity (cp)*	*Water FVF RB/STB*	*Water Viscosity (cp)*
7251.89	*738.415*	*1440.14*	*1.76358*	*0.323065*	*0.541712*	*0.0347134*	*1.01363*	*0.385872*
6890.03	*738.415*	*1355.25*	*1.72314*	*0.332854*	*0.554152*	*0.0337032*	*1.01479*	*0.385872*
6528.16	*738.415*	*1271.18*	*1.68309*	*0.345409*	*0.56817*	*0.0326593*	*1.01594*	*0.385872*
6166.31	*738.415*	*1187.99*	*1.64345*	*0.360948*	*0.584105*	*0.0315799*	*1.0171*	*0.385872*
5804.45	*738.415*	*1105.69*	*1.60425*	*0.379753*	*0.602395*	*0.0304631*	*1.01826*	*0.385872*
5442.58	*738.415*	*1024.36*	*1.5655*	*0.402172*	*0.623621*	*0.0293072*	*1.01942*	*0.385872*
5080.73	*738.415*	*944.029*	*1.52723*	*0.428631*	*0.64856*	*0.0281115*	*1.02058*	*0.385872*
4718.88	*738.415*	*864.763*	*1.48946*	*0.459644*	*0.678268*	*0.026876*	*1.02174*	*0.385872*
4357.01	*738.415*	*786.625*	*1.45224*	*0.495816*	*0.714225*	*0.0256024*	*1.0229*	*0.385872*
3995.15	*738.415*	*709.69*	*1.41559*	*0.537869*	*0.758529*	*0.0242948*	*1.02406*	*0.385872*
3633.29	*738.415*	*634.051*	*1.37955*	*0.586643*	*0.814251*	*0.0229603*	*1.02521*	*0.385872*
3271.43	*738.415*	*559.815*	*1.34418*	*0.643115*	*0.885996*	*0.021611*	*1.02637*	*0.385872*
2909.57	*738.415*	*487.097*	*1.30954*	*0.70842*	*0.980903*	*0.0202646*	*1.02753*	*0.385872*
2547.71	*738.415*	*416.054*	*1.27569*	*0.783847*	*1.11039*	*0.0189464*	*1.02869*	*0.385872*
2185.85	*738.415*	*346.882*	*1.24274*	*0.870853*	*1.29349*	*0.0176894*	*1.02985*	*0.385872*
1823.99	*738.415*	*279.824*	*1.21079*	*0.971055*	*1.56384*	*0.0165314*	*1.03101*	*0.385872*
1462.13	*738.415*	*215.222*	*1.18001*	*1.08614*	*1.98678*	*0.0155082*	*1.03217*	*0.385872*
1100.27	*738.415*	*153.572*	*1.15064*	*1.21767*	*2.71092*	*0.0146453*	*1.03333*	*0.385872*
738.415	*738.415*	*95.6586*	*1.12305*	*1.36632*	*4.17292*	*0.0139545*	*1.03449*	*0.385872*
376.556	*738.415*	*43.009*	*1.09797*	*1.52938*	*8.48563*	*0.0134408*	*1.03564*	*0.385872*

Table F-2 : PVT properties at 160 F

Temperature = 160 F								
Pressure (psi)	Bubble Point (psi)	Gas Oil Ratio (scf/STB)	Oil FVF RB/STB	Oil Viscosity cp	Gas FVF (RB/Mscf)	Gas Viscosity (cp)	Water FVF RB/STB	Water Viscosity (cp)
7251.89	738.415	1554.35	1.79168	0.383065	0.510262	0.0370349	1.00017	0.445872
6890.03	738.415	1462.73	1.74827	0.392854	0.520536	0.0359781	1.00126	0.445872
6528.16	738.415	1371.99	1.70529	0.405409	0.53208	0.0348808	1.00234	0.445872
6166.31	738.415	1282.2	1.66275	0.420948	0.545171	0.0337392	1.00343	0.445872
5804.45	738.415	1193.38	1.62068	0.439753	0.560171	0.0325496	1.00451	0.445872
5442.58	738.415	1105.59	1.57909	0.462172	0.577559	0.0313077	1.0056	0.445872
5080.73	738.415	1018.89	1.53802	0.488631	0.59799	0.0300097	1.00668	0.445872
4718.88	738.415	933.341	1.49749	0.519644	0.622365	0.0286523	1.00777	0.445872
4357.01	738.415	849.007	1.45754	0.555816	0.65196	0.0272331	1.00886	0.445872
3995.15	738.415	765.976	1.4182	0.597869	0.688622	0.0257524	1.00994	0.445872
3633.29	738.415	684.339	1.37953	0.646643	0.735094	0.0242142	1.01103	0.445872
3271.43	738.415	604.211	1.34157	0.703115	0.795582	0.0226291	1.01211	0.445872
2909.57	738.415	525.726	1.30439	0.76842	0.876744	0.0210164	1.0132	0.445872
2547.71	738.415	449.049	1.26807	0.843847	0.989484	0.0194088	1.01428	0.445872
2185.85	738.415	374.391	1.2327	0.930853	1.15229	0.017854	1.01537	0.445872
1823.99	738.415	302.015	1.19841	1.03106	1.39796	0.0164135	1.01645	0.445872
1462.13	738.415	232.291	1.16538	1.14614	1.78928	0.0151494	1.01754	0.445872
1100.27	738.415	165.751	1.13386	1.27767	2.46659	0.0141042	1.01863	0.445872
738.415	738.415	103.244	1.10425	1.42632	3.83983	0.0132894	1.01971	0.445872
376.556	738.415	46.4198	1.07733	1.58938	7.89285	0.0126981	1.0208	0.445872

Table F-3 : PVT properties at 100 F

Temperature = 100 F								
Pressure (psi)	Bubble Point (psi)	Gas Oil Ratio (scf/STB)	Oil FVF RB/STB	Oil Viscosity cp	Gas FVF (RB/Mscf)	Gas Viscosity (cp)	Water FVF RB/STB	Water Viscosity (cp)
7251.89	738.415	1778.87	1.85765	0.443065	0.466801	0.0419478	0.98456	0.505872
6890.03	738.415	1674.01	1.8084	0.452854	0.474114	0.0408453	0.985617	0.505872
6528.16	738.415	1570.17	1.75963	0.465409	0.482251	0.039696	0.986674	0.505872
6166.31	738.415	1467.4	1.71136	0.480948	0.491384	0.0384941	0.987732	0.505872
5804.45	738.415	1365.76	1.66362	0.499753	0.501744	0.0372327	0.988789	0.505872
5442.58	738.415	1265.29	1.61643	0.522172	0.513639	0.0359036	0.989846	0.505872
5080.73	738.415	1166.07	1.56983	0.548631	0.527494	0.0344971	0.990903	0.505872
4718.88	738.415	1068.15	1.52384	0.579644	0.543904	0.0330019	0.991961	0.505872
4357.01	738.415	971.642	1.47851	0.615816	0.563736	0.0314047	0.993018	0.505872
3995.15	738.415	876.614	1.43387	0.657869	0.588294	0.0296912	0.994075	0.505872
3633.29	738.415	783.187	1.38999	0.706643	0.619589	0.0278469	0.995132	0.505872
3271.43	738.415	691.485	1.34692	0.763115	0.660867	0.0258612	0.996189	0.505872
2909.57	738.415	601.665	1.30473	0.82842	0.71758	0.0237346	0.997247	0.505872
2547.71	738.415	513.912	1.26352	0.903847	0.799251	0.0214918	0.998304	0.505872
2185.85	738.415	428.47	1.22338	0.990853	0.923274	0.0191999	0.999361	0.505872
1823.99	738.415	345.64	1.18448	1.09106	1.12244	0.0169865	1.00042	0.505872
1462.13	738.415	265.844	1.147	1.20614	1.45951	0.01503	1.00148	0.505872
1100.27	738.415	189.693	1.11123	1.33767	2.06563	0.0134766	1.00253	0.505872
738.415	738.415	118.158	1.07763	1.48632	3.30934	0.0123491	1.00359	0.505872
376.556	738.415	53.1249	1.04709	1.64938	6.97785	0.0115842	1.00465	0.505872

Table F-4 : PVT properties at 60 F

Temperature = 60 F								
Pressure (psi)	Bubble Point (psi)	Gas Oil Ratio (scf/STB)	Oil FVF RB/STB	Oil Viscosity cp	Gas FVF (RB/Mscf)	Gas Viscosity (cp)	Water FVF RB/STB	Water Viscosity (cp)
7251.89	738.415	1976.74	1.9232	0.533065	0.44059	0.0464462	0.977331	0.595872
6890.03	738.415	1860.21	1.86879	0.542854	0.446223	0.0453275	0.978429	0.595872
6528.16	738.415	1744.82	1.8149	0.555409	0.452422	0.0441619	0.979526	0.595872
6166.31	738.415	1630.63	1.76156	0.570948	0.459302	0.0429434	0.980625	0.595872
5804.45	738.415	1517.67	1.70881	0.589753	0.467007	0.0416641	0.981721	0.595872
5442.58	738.415	1406.03	1.65666	0.612172	0.475734	0.0403147	0.982818	0.595872
5080.73	738.415	1295.77	1.60517	0.638631	0.485747	0.0388834	0.983917	0.595872
4718.88	738.415	1186.97	1.55436	0.669644	0.497419	0.0373553	0.985013	0.595872
4357.01	738.415	1079.71	1.50427	0.705816	0.511304	0.0357113	0.986112	0.595872
3995.15	738.415	974.12	1.45496	0.747869	0.528228	0.0339266	0.987209	0.595872
3633.29	738.415	870.298	1.40645	0.796643	0.549515	0.0319688	0.988307	0.595872
3271.43	738.415	768.398	1.35888	0.853115	0.577382	0.029798	0.989404	0.595872
2909.57	738.415	668.583	1.31225	0.91842	0.615803	0.0273679	0.990503	0.595872
2547.71	738.415	571.075	1.26671	0.993847	0.67232	0.0246424	0.991599	0.595872
2185.85	738.415	476.13	1.22237	1.08085	0.762122	0.0216381	0.992698	0.595872
1823.99	738.415	384.086	1.17937	1.18106	0.917317	0.0185031	0.993795	0.595872
1462.13	738.415	295.415	1.13797	1.29614	1.20562	0.0155876	0.994893	0.595872
1100.27	738.415	210.792	1.09844	1.42767	1.76154	0.0133162	0.99599	0.595872
738.415	738.415	131.301	1.06132	1.57632	2.92463	0.0117981	0.997087	0.595872
376.556	738.415	59.0339	1.02757	1.73938	6.34382	0.0108503	0.998182	0.595872

References

1. The University of Kansas. Petroleum: a primer for Kansas, [cited 02 October 2018; Available from: http://www.kgs.ku.edu/Publications/Oil/primer13.html.
2. Eltaher, E., "Modelling and Applications of Autonomous Flow Control Devices," PhD thesis, Heriot-Watt University, Edinburgh, UK, 2017.
3. Wormholes.Purpose of Inflow Control Systems (ICD), [cited 3 October 2017; Available from: http://www.wormholes.su/ICDdevices_en.htm.
4. Muggeridge, A., Cockin, A., Webb, K., Frampton, H., Collins, I., Moulds, T., and Salino, P., "Recovery rates, enhanced oil recovery and technological limits", Philosophical Transactions A: Mathematical, Physical and Engineering Sciences Journal, Vol. 372, No. 2014, 2 December 2013.
5. Charlez, P., Lemonnier, P., Ruffet, C., Bouteca, M. J., and Tan, C., "Thermally Induced Fracturing: Analysis of a Field Case in North Sea," SPE 36916 presented at European Petroleum Conference, Milan, Italy, 22-24 October 1996.
6. Suri, A. and Sharma, M. M., "Fracture Growth in Horizontal Injectors," paper SPE 119379 presented at SPE Hydraulic Fracturing Technology Conference, The Woodlands, Texas, 19-21 January 2009.
7. Svendson, A. P., Wright, M. S., Clifford, P. J., and Berry, P. J., "Thermally Induced Fracturing of Ula Water Injectors," paper SPE 20898, SPE Production Journal, Vol. 6, No. 4, November 1991.
8. Petroleum Experts IPM 9.0, REVEAL Online Manual.
9. Detienne, J. L., Creusot, M., Kessler, N., Sahuquet, B., and Bergerot, J. L., "Thermally Induced Fractures: A Field-Proven Analytical Model", paper SPE 30777 , SPE Production & Operations Journal, Vol. 1, No. 01, February 1998.
10. Settari, A. and Warren, G. M., "Simulation and field analysis of waterflood induced fracturing," paper SPE 28081 presented at Rock Mechanics in Petroleum Engineering, Delft, Netherlands, 29-31 August 1994.
11. Williams, D. B., Sherrard, D. W., and Lin, C. Y., "The Impacts on Waterflood Management of Inducing Fractures in Injection Wells in the Prudhoe Bay Oil Field," paper SPE 16358 presented at SPE California Regional Meeting, Ventura, California, 8-10 April 1987.
12. Garon, A. M., Lin, C. Y., and Dunayevsky, V. A., "Simulation of Thermally Induced Waterflood Fracturing in Prudhoe Bay," paper SPE 17417 presented at SPE California Regional Meeting, Long Beach, California , USA, 23-25 March 1988.

.

13. Al-Abdulmohsin, Y. A., Al-Mosa, M., Al-jandal, A. A., Al Ghafli, H. A., Al-Mulhim, A. A., Kamal, R. M., and El-Tonsy, M. M., "A Successful Trial of Special Downhole Completion for Optimizing Injection Profile in a Highly Fractured Horizontal Well," paper SPE 166141 presented at the 2013 SPE Annual Technical Conference and Exhibition, New Orleans, Louisiana, USA, 30 September-2 October 2013.
14. Nondestructive Testing .Materials and Processes, [cited 12 October 2017; Available from:https://www.nde-ed.org/EducationResources/CommunityCollege/Materials/Mechanical/StressStrain.htm.
15. Elastic and plastic/ductile behaviour .[cited 21 Feburary 2018; Available from http://www.uio.no/studier/emner/matnat/geofag/GEO1011/h05/undervisningsmateriale/forelesninger/Duktildef.pdf.
16. Felippa, C., "Stress-Strain Material Laws", presentation delivered at University of Colorado at Boulder, Accessed on 24 October 2017.
17. Amadei, B. and Stephansson, O., "Rock Stress and Its Measurement", Springer Netherlands Publishing,1997, ISBN: 978-0-412-44700-6, pp. 258-259.
18. Eberhardt, E., "Rock EngineeringPractice & Design", presentation delivered at International Society for Rock Mechanics and Rock Engineering, Accessed on 24 October 2017.
19. Petroleum Geology of the Western Weald and South Downs, [cited 22/02/2018]; Available from: http://www.southampton.ac.uk/~imw/Petroleum-Geology-Weald-Shale.htm.
20. Simpson, A. J. and Paige, R. W., "Advances in Forties Field Water Injection," paper SPE 23140 presented at Offshore Europe, Aberdeen, United Kingdom, 3-6 September 1991.
21. Stevens, D. G., Murray, L. R., and Shah, P. C., "Predicting Multiple Thermal Fractures in Horizontal Injection Wells; Coupling of a Wellbore and a Reservoir Simulator," paper SPE 59354 presented at SPE/DOE Improved Oil Recovery Symposium, Tulsa, Oklahoma, 3-5 April 2000.
22. Koning, E. J. L., "Fractured Water Injection Wells - Analytical Modelling Of Fracture Propagation," paper SPE 14684, SPE Technical Journal, 1985.
23. Perkins, T. K. and Gonzalez, J. A., "Changes in Earth Stresses Around a Wellbore Caused by Radially Symmetrical Pressure and Temperature Gradients," paper SPE 10080, Society of Petroleum Engineers Journal, Vol. 24, No. 02, April 1984.
24. Zoback, M. D., Barton, C. A., Brudy, M., Castillo, D. A., Finkbeiner, T., Grollimund, B. R., Moos, D. B., Peska, P., Ward, C. D., and

Wiprut, D. J., “Determination of stress orientation and magnitude in deep wells”, International Journal of Rock Mechanics and Mining Sciences, Vol. 40, No. 7, October 2003, pp. 1049-1076.
25. Gudmundsson, A., “Rock Fractures in Geological Processes”, Cambridge University Press, 2011, ISBN: 9780511975684. .
26. Abdalkadeer, K. M., Dunn-Norman, S., Senturk, E., Rivera, N., Prada, M., and Goodman, H. E., “Changes in Near Wellbore Stress and Fracture Gradient Due to Cold Water Injection in a Sirte Basin Field, Libya,” paper SPE 125310 presented at SPE/EAGE Reservoir Characterization and Simulation Conference, Abu Dhabi, UAE, 19-21 October 2009.
27. Andrade, A., Correa, R., Vaca, S., and Chango, M., “Thermal Induced Fracture Effect with a Lower Cool down Reduction - Case Studies for Ecuador; Villano and CPF Water Disposal Wells”, paper SPE 177155 presented at SPE Latin American and Caribbean Petroleum Engineering Conference, Quito, Ecuador, 18-20 November 2015.
28. Williams, B. D., Sherrard, D. W., and Lin, C. Y., "Impact of Inducing Fractures at Prudhoe Bay," paper SPE 16358, SPE Journal of Petroleum Technology, Vol. 14, No. 10, October 1989.
29. Martins, J. P., Murray, L. R., Clifford, P. J., McLelland, W. G., Hanna, M. F., and Sharp, J. W., Jr., "Produced-Water Reinjection and Fracturing in Prudhoe Bay," paper SPE 28936 , SPE Reservoir Engineering Journal, Vol. 10, No. 3, August 1995.
30. Navarro, W., "Produced Water Reinjection in Mature Field With High Water Cut," paper SPE 108050 presented at Latin American & Caribbean Petroleum Engineering Conference, Buenos Aires, Argentina, 15-18 April 2007.
31. Sequestration – Geologic Research and Assessments. [cited 28/8/2017; Available from: https://energy.usgs.gov/EnvironmentalAspects/EnvironmentalAspectsofEnergyProductionandUse/GeologicCO2Sequestration.aspx#3776287-overviewCarbon.
32. Kim, S. and Hosseini, S. a., “Above-zone pressure monitoring and geomechanical analyses for a field-scale CO2 injection project in Cranfield, MS”, Energy Procedia, Vol. 114, July 2017, pp. 81-98. Vol. 4. 2014.
33. Wu, Y., Taylor, J. M., Frei-Pearson, A., and Bryant, S. L., "Injection Induced Fracturing As a Necessary Evil in Geologic CO2 Sequestration," paper ARMA 444 presented at 49th U.S. Rock Mechanics/Geomechanics Symposium, San Francisco, California, 28 June-1 July 2015.
34. Goodarzi, S., Settari, A., Zoback, M. D., and Keith, D., "Thermal Aspects of Geomechanics and Induced Fracturing in CO2 Injection With Application to CO2 Sequestration in Ohio River Valley," SPE

139706 presented at SPE International Conference on CO2 Capture, Storage, and Utilization, New Orleans, Louisiana, USA, 10-12 November 210.
35. Oyeneyin, B. M., Moriwawon, B., Oluyemi, G. F., and Chris Macleod, J. O., ’Real-Time Evaluation of Sanding Potential’’, Journal of Advanced Materials Research, vol 18-19, pp293-300, 2007.
36. Papamichos, E. and Malmanger, E. M., "A Sand-Erosion Model for Volumetric Sand Predictions in a North Sea Reservoir," paper SPE 69841, SPE Reservoir Evaluation & Engineering, Vol. 4, No. 1, February 2001. 10.2118/69841-PA.
37. Risnes, R., Bratli, R. K., and Horsrud, P., “Sand Stresses Around a Wellbore”, paper SPE-9650-PA, SPE Society of Petroleum Engineers Journal, Vol. 22, No.6 , December 1982.
38. Vaziri, H., Allam, R., Kidd, G., Bennett, C., Grose, T., Robinson, P., and Malyn, J., "Sanding: A Rigorous Examination of the Interplay Between Drawdown, Depletion, Start-up Frequency and Water Cut," SPE paper 89895 presented at SPE Annual Technical Conference and Exhibition,Houston, Texas, USA, 26-29 September 2004.
39. Veeken, C. A. M., Davies, D. R., Kenter, C. J., and Kooijman, A. P., “Sand Production Prediction Review: Developing an Integrated Approach”, paper SPE SPE-22792 presented atSPE Annual Technical Conference and Exhibition held in Dallas, Texas, 6-9 October 1991.
40. Morita, N., Davis, E., and Whitebay, L., "Guidelines for Solving Sand Problems in Water Injection Wells," paper SPE 39436 presented at SPE Formation Damage Control Conference, Lafayette, Louisiana,USA, 18-19 February 1998.
41. Norman, W. D. and McCarty, R. A., "The Resiliency of Frac-Packed Subsea Injection Wells," paper SPE 102990 presented at SPE Annual Technical Conference and Exhibition, San Antonio, Texas, USA, 24-27 September 2006.
42. Santarelli, F. J., Skomedal, E., Markestad, P., Berge, H. I., and Nasvig, H., “Sand Production on Water Injectors: How Bad Can It Get?”, paper SPE 64297, SPE Drilling & Completion Journal, Vol. 15, No. 02, June 2000. 10.2118/64297-PA.
43. Tovar, J. J. and Navarro, W., "The Impact of sandstone strength's behaviour as a result of temperature changes in Water Injectors," paper SPE 113825 presented at Europec/EAGE Conference and Exhibition, Rome, Italy, 9-12 June 2008.
44. Oyeneyin, B., “Integrated Sand Management For Effective Hydrocarbon Flow Assurance”, Elsevier Science & Technology Books,2015, ISBN:9780444626370, pp. 133-160.
45. Fisher, E. K. and French, M. R., "Drilling the First Horizontal Well in the Gulf of Mexico: A Case History of East Cameron Block 278 Well

B-12," paper SPE 22545, SPE Drilling Engineering Journal, Vol. 7, No. 02, June 1992.
46. Joshi, S. D., "Cost/Benefits of Horizontal Wells," SPE 83621 presented at SPE Western Regional/AAPG Pacific Section Joint Meeting, Long Beach, California, 19-24 May 2003.
47. Salamy, S. P., Al-Mubarak, H. K., Al-Ghamdi, M. S., and Hembling, D. E., "Maximum-Reservoir-Contact-Wells Performance Update: Shaybah Field, Saudi Arabia," paper SPE 105141, SPE Production & Operations Journal, Vol. 23, No. 4, November 2008.
48. Vela, I., Viloria-gomez, L. A., Caicedo, R., and Porturas, F., "Well Production Enhancement Results with Inflow Control Device (ICD) Completions in Horizontal Wells in Ecuador," paper SPE 143431 presented at SPE EUROPEC/EAGE Annual Conference and Exhibition, Vienna, Austria, 23-26 May 2011.
49. Al-Khelaiwi, F. T., "A Comprehensive Approach to the Design of Advanced Well Completions", PhD thesis, Heriot-Watt University, Edinburgh, UK, 2010.
50. Edohamen and Awannegbe, P., "Characterization of flow regime of highly viscous oils using conventional ICD and BECH AICD", MSc Thesis, University of Stavanger,Stavanger, Norway, 2014.
51. Bringedal, B. O., Storkaas, E., Aarset, M. F., With, H. M., and Dalsmo, M., "Recent Developments in Control and Monitoring of Remote Subsea Fields," SPE 128657 presented at SPE Intelligent Energy Conference and Exhibition, Utrecht, The Netherlands, 23-25 March 2010.
52. Hembling, D. E., Sunbul, A. H., and Salerno, G., "Advanced Well Completions Result in Enhanced Well Productivity," SPE 108877 presented at Asia Pacific Oil and Gas Conference and Exhibition, Jakarta, Indonesia, 30 October-1 November 2007.
53. Awad, M. O., Al Ajmi, M. F., Safar, A., and Rajagopalan, V. S., "Advanced ICD Application Alleviating Well Intervention Challenges," paper SPE 175204 presented at SPE Kuwait Oil and Gas Show and Conference, Mishref, Kuwait, 11-14 October 2015.
54. Davila, E., Almeida, R., Paz, F., Vela, I., Pazos, J., Proano, G., Diaz, M., Santa Cruz, R., Vega, C., Humbert, O., Chillenato, F., and Porturas, F., "First Applications of Inflow Control Devices (ICD) in Open Hole Horizontal Wells in Block 15, Ecuador," SPE 123008 presented at Latin American and Caribbean Petroleum Engineering Conference, Cartagena de Indias, Colombia, 31 May-3 June 2009.
55. Edmonstone, G., Kofoed, C. W., Jackson, A. M., Parihar, S., Alvarez, A., Mumtaz, S., Abdouche, G., Shuchart, C. E., Mayer, C. S. J., and Troshko, A., "ICD Well History and Future Use in Giant Offshore Oilfield, Abu Dhabi,"SPE 171836 presented at Abu Dhabi

International Petroleum Exhibition and Conference, Abu Dhabi, UAE, 10-13 November 2014.
56. Lee, B. O., Al-Fassam, F. S., Galimzyanov, A., Faizal, S. A., and Vicario, R., "ICD Evaluation Study Using Numerous PLT Runs to Optimise Design Practice and Maximise ICD Value," paper IPTC 1788 presented at International Petroleum Technology Conference, Kuala Lumpur, Malaysia, 10-12 December 2014.
57. Brekke, K. and Lien, S. C., "New and Simple Completion Methods for Horizontal Wells Improve the Production Performance in High-Permeability, Thin Oil Zones", paper SPE 24762, SPE Drilling & Completion Journal, Vol. 9, No. 03, September 1994. 1994. 10.2118/24762-PA.
58. Lien, S. C., Seines, K., Havig, S. O., and Kydland, T., "The First Long-Term Horizontal-Well Test in the Troll Thin Oil Zone," paper SPE 20715 , SPE Journal of Petroleum Technology, Vol. 43, No. 8, August 1991.
59. Al-Khelaiwi, F. T. and Davies, D. R., "Inflow Control Devices: Application and Value Quantification of a Developing Technology", paper SPE 108700 presented at the First International Oil Conference and Exhibition in Mexico, held in Veracruz, Mexico, 27-30 June 2007.
60. Augustine, J. R., "An Investigation of the Economic Benefit of Inflow Control Devices on Horizontal Well Completions Using a Reservoir-Wellbore Coupled Model", paper SPE 78293 presented at the 2002 European Petroleum Conference held in Aberdeen, Scotland, U. K., 29 – 31 October 2002.
61. Henriksen, K. H., Gule, E. I., and Augustine, J. R., "Case Study: The Application of Inflow Control Devices in the Troll Field," SPE 100308 presented at SPE Europec/EAGE Annual Conference and Exhibition, Vienna, Austria, 12-15 June 2006.
62. Coronado, M. P., Garcia, L., Russell, R., Garcia, G. A., and Peterson, E. R., "New Inflow Control Device Reduces Fluid Viscosity Sensitivity and Maintains Erosion Resistance," paper OTC 19811presented at Offshore Technology Conference, Houston, Texas, 4-7 May 2009.
63. Haeberle, D., Nwankwo, A. S., McDermott, J., Gosavi, S. V., Duffy, B., and Grubert, M., "Application of Flow-Control Devices for Water Injection in the Erha Field," SPE 112726 presented at IADC/SPE Drilling Conference, Orlando, Florida, USA, 4-6 March 2008.
64. Prakasa, B., Muradov, K., and Davies, D., "Rapid Design of an Inflow Control Device Completion in Heterogeneous Clastic Reservoirs Using Type Curves," paper SPE 175448 presented at SPE Offshore Europe Conference and Exhibition, Aberdeen, Scotland, UK, 8-11 September 2015.

65. Aadnoy, B. S. and Hareland, G., "Analysis of Inflow Control Devices," paper SPE 122824 presented at Offshore Europe 2009, Aberdeen, Scotland, UK, 8-11 September 2009.
66. Jain, R., Long, T. A., Dickson, J., Brown, S. V., and Shtepani, E., "Experimental Investigation of Pressure-Drop/Flow-Rate Relationship for Small-Aperture Holes for High-Viscosity Fluids," SPE 36916 presented at SPE Annual Technical Conference and Exhibition, San Antonio, Texas, USA, 8-10 October 2012. .
67. Mayer, C. S. J., Spiecker, M., Shuchart, C. E., Burkey, R. C., Ufford, A., and Brysch, J., "Multiphase Flow Performance of Inflow Control Devices - Characterizing Downhole Flow Behavior in Lab Experiments," paper SPE 171890 presented at Abu Dhabi International Petroleum Exhibition and Conference, Abu Dhabi, UAE, 10-13 Novembe 2014.
68. Rahman, J. U., Allen, C., and Bhat, G., "Second Generation Interval Control Valve (ICV) Improves Operational Efficiency and Inflow Performance in Intelligent Completions," paper SPE 150850 presented at North Africa Technical Conference and Exhibition, Cairo, Egypt, 20-22 February 2012.
69. Ebadi, F. and Davies, D. R., "Should "Proactive" or "Reactive" Control be Chosen for Intelligent Well Management?," SPE 36916 presented at Intelligent Energy Conference and Exhibition, Amsterdam, The Netherlands,11-13 April 2006.
70. Al-Khelaiwi, F. T., Birchenko, V. M., Konopczynski, M. R., and Davies, D., "Advanced Wells: A Comprehensive Approach to the Selection between Passive and Active Inflow Control Completions", paper SPE 132976, SPE Production & Operations Journal, Vol. 25, No. 3, August 2010, pp. 305 – 326.
71. Gimre, J., "Efficiency of ICV/ICD systems," MSc Thesis,University of Stavang, Stavanger, Norway, 2012.
72. Least, B., Bonner, A. J., Regulacion, R. E., Pe??aranda, R., Sampedro, T. F., and Coloma Guti??rrez, F., "Autonomous ICD Installation Success in Ecuador Heavy Oil: A Case Study," paper SPE 166495 presented at SPE Annual Technical Conference and Exhibition, New Orleans, Louisiana, USA, 30 September-2 October 2013.
73. Halliburton. EquiFlow Autonomous Inflow Control Device. 2017 [cited 17 Septmber 2017; Available from: http://www.halliburton.com/en-US/ps/completions/sand-control/screens/inflow-control/equiflow-autonomous-inflow-control-device.page?node-id=hfqel9w4. [cited 2017 7/9/2017].
74. Bailin Pei, W. L. B. C., Songmei Zhang Jianwei Di "ICD-packer completion reduces water in China's Jidong oil field" article at Oil & Gas Journal, 10 March 2016. .

75. MoradiDowlatabad, M., Muradov, K. M., and Davies, D., "Novel Workflow to Optimise Annular Flow Isolation in Advanced Wells" paper IPTC 17716 presented at the International Petroleum Technology Conference, Kuala Lumpur, Malaysia, 10-12 December 2014.
76. Augustine, J. R., Mathis, S. P., Nguyen, H. T., Gann, C. L., and Gill, J., "World's First Gravel-Packed Inflow-Control Completion", paper SPE 103195, SPE Drilling & Completion Journal, Vol. 23, No. 01, March 2008.
77. Augustine, J. R., McIntyre, A., Adam, R. J., and Laidlaw, D., " Increasing Oil Recovery by Preventing Early Water and Gas Breakthrough in a West Brae Horizontal Well: A Case History," paper SPE 99718 presented at the 2006 SPE/DOE Symposium on Improved Oil Recovery, Tulsa, Oklahoma, U.S.A., 22-26 April 2006.
78. Augustine, J. R. and Ratterman, E. E., "Advanced Completion Technology Creates a New Reality for Common Oilfield Myths", paper SPE 100316 presented at the SPE Europec/EAGE Annual Conference and Exhibition held in Vienna, Austria, 12 – 15 June 2006.
79. Henriksen, K. H., Augustine, J. R., and Wood, E. T., "Integration of New Open Hole Zonal Isolation Technology Contributes to Improved Reserve Recovery and Revision in Industry Best Practices," SPE 97614 presented at SPE International Improved Oil Recovery Conference in Asia Pacific, Kuala Lumpur, Malaysia, 5-6 December 2005.
80. Ratterman, E. E., Augustine, J. R., and Voll, B. A., "New Technology Applications to Increase Oil Recovery by Creating Uniform Flow Profiles in Horizontal Wells: Case Studies and Technology Overview," paper IPTC 10177 presented at International Petroleum Technology Conference, Doha, Qatar, 21-23 November 2005.
81. Raffn, A. G., Hundsnes, S., Kvernstuen, S., and Moen, T., "ICD Screen Technology Used To Optimize Waterflooding in Injector Well," paper SPE 106018 presented at Production and Operations Symposium, Oklahoma City, Oklahoma, U.S.A, 31 March-3 AprIL 2007.
82. Amaral, A. D. S., Augustine, J. R., Henriksen, K. H., Rodrigues, V. F., Steagall, D. E., Paixao, L. C., and Barbosa, V. P., "Equalization of the Water Injection Profile in a Subsea Horizontal Well: A Case History", paper SPE 112283 presented at the SPE international Symposium and Exhibition on Formation Damage Control, Lafayette, Louisiana, U.S.A., 13-15 February 2008.
83. Kvernstuen, S., Dowling, K. R., Graham, J. S., Chechin, A. V., Porturas, F., and Wibawa, S., "ICD Screen Technology in Stag Field to Control Sand and Increase Recovery by Avoiding Wormhole Effect," paper IPTC 12385 presented at International Petroleum

Technology Conference, Kuala Lumpur, Malaysia, 3-5 December 2008.
84. Kuck, M. D., Holderman, L., Brown, D., Thornton, K. V., and Kuo, N., "Enhancing the Effectiveness of Long Horizontal Water Injection Wells with ICD/SSD Technology - Design, Simulation and Installation," SPE paper 160159 presented at SPE Annual Technical Conference and Exhibition, San Antonio, Texas, USA,8-10 October 2012.
85. Haeberle, D., Nwankwo, A. S., McDermott, J., Gosavi, S. V., Duffy, B., and Grubert, M., "Application of Flow-Control Devices for Water Injection in the Erha Field," SPE 112726 presented at IADC/SPE Drilling Conference, Orlando, Florida, USA, 4-6 March 2008.
86. Kvernstuen, S., Dowling, K. R., Graham, J. S., Chechin, A. V., Porturas, F., and Wibawa, S., ICD Screen Technology in Stag Field to Control Sand and Increase Recovery by Avoiding Wormhole Effect. International Petroleum Technology Conference.
87. Gibson, D., Medd, D. M., McCarthy, T., Toldo, B., Moselely, P., and Pudin, V., "Controlled Multi-zone Water Injection: The Enfield ENC05 story," SPE paper 136539 presented at SPE Asia Pacific Oil and Gas Conference and Exhibition, Brisbane, Queensland, Australia,18-20 October 2010.
88. Khalil, A. K., Elasmar, M., and Shafie, S. H., "Optimizing Injection Wells through Innovative Completion," SPE paper 137057 presented at Abu Dhabi International Petroleum Exhibition and Conference, Abu Dhabi, UAE,1-4 November 2010.
89. Channa, Z., Khan, M. N., Iwama, H., Husain, A., Al-blooshi, J. R., El-Sayed, H. S., Nofal, S. F., Al-feky, M. H., and Ahmed, F., "The Performance of Water Injection Wells Equipped with ICD Completions in One of the Giant Offshore Field, Abu Dhabi," paper SPE 183476 presented at Abu Dhabi International Petroleum Exhibition & Conference, Abu Dhabi, UAE, , 7-10 November 2016.
90. Becerra, O., Kearl, B., and Sanwoolu, A., "A Systematic Approach for Inflow Control Devices Testing in Mackay River SAGD Wells", paper SPE 170055 presented at SPE Heavy Oil Conference-Canada, Calgary, Alberta, Canada, 10-12 June 2014.
91. McChesney, R. and Edlebeck, J., "Design, Testing, and Field Performance of Steam-Injection Flow-Control Devices for Use in SAGD Oil Recovery," paper SPE 174490 presented at SPE Canada Heavy Oil Technical Conference,Calgary, Alberta, Canada, 9-11 June 2015.
92. Medina, M., "Design and Field Evaluation of Tubing Deployed Passive Outflow Control Devices in SAGD Injection Wells," paper SPE 165563 presented at SPE Heavy Oil Conference-Canada, Calgary, Alberta, Canada, 11-13 June 2013.

93. Luo, Z., “Modeling Injection Induced Fractures and Their Impact in CO2 Geological Storage ”, PhD Thesis, Texas A&M University, Houston, TX, USA, August 2013.
94. Hagoort, J., Weatherill, B. D., and Settari, A., "Modeling the Propagation of Waterflood-Induced Hydraulic Fractures," paper SPE 7412, SPE Journal, Vol. 20, No. 04, August 1980. 10.2118/7412-PA.
95. Koning, E. J. L., "Waterflood under Fracturing Conditions", PhD thesis, Technical University of Delft, Delft, Netherlands, 1988.
96. Yang, M., “Hydraulic Fracture Optimization with a Pseudo-3d Model in Multi-Layered Lithology”, MSc Thesis, Texas A&M University, Houston, TX, USA, August 2011.
97. Perkins, T. K. and Gonzalez, J. A., "The Effect of Thermoelastic Stresses on Injection Well Fracturing," paper SPE 11332, Society of Petroleum Engineers Journal, Vol. 25, No. 01, February 1985.
98. Dikken, B. J. and Niko, H., "Waterflood-Induced Fractures: A Simulation Study Of Their Propagation And Effects On Waterflood Sweep Efficiency," paper SPE 16551 presented at Offshore Europe, Aberdeen, United Kingdom, 8-11 September 1987.
99. Clifford, P. J., Berry, P. J., and Gu, H., "Modeling the Vertical Confinement of Injection-well Thermal Fractures," paper SPE 20741 , SPE Production Engineering Journal, Vol. 6, No. 4, November 199. 10.2118/20741-PA.
100. Hustedt, B., Zwarts, D., Bjoerndal, H.-P., Al-Masfry, R. A., and van den Hoek, P. J., "Induced Fracturing in Reservoir Simulations: Application of a New Coupled Simulator to a Waterflooding Field Example," ", paper SPE 102467, SPE Reservoir Evaluation & Engineering Journal, Vol. 11, No. 3, June 2008.
101. Ji, L., Settari, A., and Sullivan, R. B., "A Novel Hydraulic Fracturing Model Fully Coupled with Geomechanics and Reservoir Simulator," paper SPE 110845 presented at SPE Annual Technical Conference and Exhibition, Anaheim, California, U.S.A. , 11-14 November 2007.
102. Chin, L. Y., Raghavan, R., and Thomas, L. K., "Fully Coupled Geomechanics and Fluid-Flow Analysis of Wells With Stress-Dependent Permeability," paper SPE 58968 , SPE Journal, Vol. 5, No. 01, March 2000.
103. Longuemare, P., Detienne, J. L., Lemonnier, P., Bouteca, M., and Onaisi, A., "Numerical Modeling of Fracture Propagation Induced by Water Injection/Re-Injection," paper SPE 68974 presented at SPE European Formation Damage Conference, The Hague, Netherlands, 21-22 May 2001.
104. Dontsov, E. V. and Peirce, A. P., "An enhanced pseudo-3D model for hydraulic fracturing accounting for viscous height growth, non-local elasticity, and lateral toughness," Energy Journal, Vol. 80, February 2015, pp. 116-139. 2015.

105. Settari, A. and Cleary, M. P., "Development and Testing of a Pseudo-Three-Dimensional Model of Hydraulic Fracture Geometry," paper SPE 132976, SPE Production Engineering Journal, Vol. 1, No. 6, November 1986.
106. van den Hoek, P. J., Matsuura, T., de Kroon, M., and Gheissary, G., "Simulation of Produced Water Reinjection Under Fracturing Conditions," paper SPE 57385, SPE Production & Facilities Journal, Vol. 25, No. 3, August 2010, pp. 305 – 326.
107. Yew, C. H. and Weng, X., "Mechanics of Hydraulic Fracturing", Elsevier Science & Technology, 1997, ISBN: 978-0-12-420003-6, pp. 30-34.
108. Clifton, R. J. and Wang, J. J., "Multiple Fluids, Proppant Transport, and Thermal Effects in Three-Dimensional Simulation of Hydraulic Fracturing," paper SPE 18198 presented at SPE Annual Technical Conference and Exhibition, Houston, Texas, USA, , 2-5 October 1988.
109. Clifton, R. J. and Abou-Sayed, A. S., "On The Computation Of The Three-Dimensional Geometry Of Hydraulic Fractures," paper SPE 7943 presented at Symposium on Low Permeability Gas Reservoirs, Denver, Colorado, USA, 20-22 May 1979.
110. Clifton, R. J. and Abou-Sayed, A. S., "A Variational Approach To The Prediction Of The Three-Dimensional Geometry Of Hydraulic Fractures," paper SPE 9879 presented at SPE/DOE Low Permeability Gas Reservoirs Symposium, Denver, Colorado, USA, 27-29 May 1981.
111. Hsiao, C. and El Rabaa, A. W., "Fracture Toughness Testing Of Rock Cores," paper ARMA 0141 presented at The 28th U.S. Symposium on Rock Mechanics (USRMS), Tucson, Arizona, USA, , 29 June-1 July 1987. .
112. Roegiers, J.-C. and Zhao, X. L., "The Measurement of Fracture Toughness of Rocks Under Simulated Downhole Conditions," paper ISRM 120 presented at 7th ISRM Congress, Aachen, Germany, 16-20 September 1991.
113. Makris, C., Arogundade, O., and Zhiyenkulov, M., "Impact of Thermal Effect on the Fracture Plane and Formation Integrity During Cold Water Injection," paper SPE 180132 presented at SPE Europec featured at 78th EAGE Conference and Exhibition, Vienna, Austria, 30 May-2 June 2016.
114. Kabir, C. S. and Izgec, B., "Identification and Characterization of High-Conductive Layers in Waterfloods," paper SPE 123930 presented at SPE Annual Technical Conference and Exhibition, New Orleans, Louisiana, USA, 4-7 October 2009.
115. Fekete. Surveillance Analysis Theory 2017 [cited 19 Septmber 2017; Available from: http://www.fekete.com/SAN/WebHelp/FeketeHarmony/Harmony_

WebHelp/Content/HTML_Files/Reference_Material/Analysis_Method_Theory/Surveillance_Theory.htm.
116. Nwokolo, C., "Application of Novel Techniques to Fractured Injection Diagnostics in Waterflood Developments," paper SPE 167564 presented at SPE Nigeria Annual International Conference and Exhibition, Lagos, Nigeria,5-7 August 2013.
117. Advntk. Applications of the Hall Plot Method For Monitoring and Prediction of PWRI Performance, [cited 19 Septmber 2017; Available from: http://www.advntk.com/pwrijip2003/pwri/final_reports/task_1/hall_plots/hall_plot_method_2.htm.
118. Izgec, B. and Kabir, C. S., "Real-Time Performance Analysis of Water-Injection Wells," paper SPE 109876 presented at SPE Annual Technical Conference and Exhibition, Anaheim, California, U.S.A, 11-14 November 2007.
119. Slevinsky, B. A., "A Model for Analysis of Injection-Well Thermal Fractures," paper SPE 77568 presented at SPE Annual Technical Conference and Exhibition, San Antonio, Texas , USA,, 29 September-2 October 2002.
120. Geertsma, J. and De Klerk, F., "A Rapid Method of Predicting Width and Extent of Hydraulically Induced Fractures," paper SPE 2458, SPE Journal of Petroleum Technology, Vol. 21, No. 12, December 1969.
121. Williams, B. B., "Fluid Loss from Hydraulically Induced Fractures," paper SPE 2769, SPE Journal of Petroleum Technology, Vol. 22, No. 7, July 1970.
122. Zhu, D. and Hill, A. D., "Field Results Demonstrate Enhanced Matrix Acidizing Through Real-Time Monitoring," paper SPE 52400, SPE Production & Facilities Journal, Vol. 13, No. 4, Nuvember 1998.
123. Izgec, B., "Integrated Injection Modeling," paper SPE 174840 presented at SPE Annual Technical Conference and Exhibitior, Houston, Texas, USA, 28-30 September 2015.
124. Lake, L. W., Liang, X., Edgar, T. F., Al-Yousef, A., Sayarpour, M., and Weber, D., "Optimization Of Oil Production Based On A Capacitance Model Of Production And Injection Rates," paper SPE 107713 presented at Hydrocarbon Economics and Evaluation Symposium,Dallas, Texas, U.S.A, 1-3 April 2007.
125. Moreno, G. A. and Garriz, A. E., "Channelling Detection Using Data-Driven Models," paper SPE 177046 presented at SPE Latin American and Caribbean Petroleum Engineering Conference, Quito, Ecuador,, 18-20 November 2015.
126. Sayarpour, M., Kabir, C. S., and Lake, L. W., "Field Applications of Capacitance-Resistance Models in Waterfloods," paper SPE 114983, SPE Reservoir Evaluation & Engineering Journal, Vol. 25, No. 3, December 2009.

127. Holanda, R. W. d., Gildin, E., and Jensen, J. L., "Improved Waterflood Analysis Using the Capacitance-Resistance Model Within a Control Systems Framework," paper SPE 177106 presented at SPE Latin American and Caribbean Petroleum Engineering Conference, Quito, Ecuador, 18-20 November 2015.
128. History Matching/Prediction. [cited 19 April 2017; Presentations at New Mexico Institute of Mining and Technology]. Available from: http://infohost.nmt.edu/~petro/faculty/Engler571/HistoryMatching.pdf.
129. Vazquez, M. and Beggs, H. D., "Correlations for Fluid Physical Property Prediction," paper SPE 6719 , SPE Journal of Petroleum Technology, Vol. 32, No. 06, June 1980.
130. Beggs, H. D. and Robinson, J. R., "Estimating the Viscosity of Crude Oil Systems," paper SPE 5434, SPE Journal of Petroleum Technology, Vol. 27, No. 09, September 1975.
131. Luo, X., Were, P., Liu, J., and Hou, Z., "Estimation of Biot's effective stress coefficient from well logs," Environmental Earth Sciences Journal, Vol. 73, No. 11, June 2015, pp. 7019 – 7028.
132. Zhixi, C., Mian, C., Yan, J., and Rongzun, H., "Determination of rock fracture toughness and its relationship with acoustic velocity," International Journal of Rock Mechanics and Mining Sciences, Vol. 34, No. 3-4, April–June 1997.
133. staff, J. P. T., "Transverse Hydraulic Fractures From Horizontal Wellbores," paper SPE 0399-0043, SPE Journal of Petroleum Technology, Vol. 51, No. 3, March 1999.